Rab requirements in HOPS-mediated late endosome-lysosome tethering and dissection of fusion factor requirements in Ca^{2+}-dependent phagosome-lysosome fusion

Dissertation

zur

Erlangung des Doktorgrades (Dr. rer.nat.)

der

Mathematisch-Naturwissenschaftlichen Fakultät

der

Rheinischen Friedrich-Wilhelms-Universität Bonn

Vorgelegt von

Ariane Christina Schleinitz

aus

Düsseldorf

Bonn 2025

Angefertigt mit Genehmigung der Mathematisch-Naturwissenschaftlichen Fakultät der Rheinischen Friedrich-Wilhelms-Universität Bonn

Gutachter/Betreuer: Prof. Dr. Albert Haas

Gutachter: Prof. Dr. Dieter Fürst

Tag der Promotion: 20.02.2025

Erscheinungsjahr: 2025

Table of Contents

1 Summary

Cells are in constant contact with their environments via endocytic mechanisms, which serves to ensure cellular maintenance. Phagocytosis is a specialised form of endocytosis crucial for innate and adaptive immunity. Uptake of material from the extracellular space leads to the formation of a new endocytic compartment. Through sequential fusion with early- and late endosomes (EEs and LEs) and ultimately lysosomes (LYS), a degradative (endo-)lysosome ((E)LYS), or in the case of phagocytes, a phagolysosome is formed. Directionality of fusion is ensured by the action of Ras-like GTPases and their effector proteins, such as tethering proteins. In LE-LYS fusion, tethering is mediated by the HOPS complex and its interaction partners. The chronological order in which these proteins are recruited and act was not established. It is also unclear how HOPS is recruited and anchored to maturing LEs. Ferrofluid (FF)-labelled, purified late endocytic compartments (FFEs) from Arl8b, Arl8a/b, Rab7a, Vps41 (subunit of HOPS), and BORC subunits myrlysin and diaskedin KO cell lines were thoroughly characterised. The examined cells still contained functional (E)LYS, which were acidified and contained active Cath B. However, transport of endocytosed material to LYS was significantly delayed in cells lacking Arl8a/b, Rab7a, Vps41, myrlysin, or diaskedin. Thus, these proteins play a crucial role in transporting cargo to LYS. Kinetic assessment revealed that Rab7a and Vps41 were recruited to maturing endosomes simultaneously and before Arl8, lyspersin (BORC), and LAMP1. Arl8 and BORC subunit levels were reduced on FFEs from Rab7a and Vps41 KOs, indicating that both proteins are recruited first and act before Arl8 and BORC. Neither loss of Rab7a nor Vps41 displaced Arl8 from membranes, substantiating the conclusion that both act before Arl8. Vps41 (HOPS) being required before Arl8 raised the question of how HOPS was recruited to LEs. Assessment of Arl8 levels on FFEs from Rab7a and Vps41 KOs showed that Vps41 (HOPS) is indeed essential for acquiring Arl8 on FFEs, whereas Rab7a is not. This led to the hypothesis that although Rab7a and Vps41 are recruited simultaneously, they might not act together to mediate LE-LYS fusion. In support of this, KO of Rab7a did not affect the levels of Vps41 and Vps39 on FFEs. Rab2a was a good candidate for recruiting HOPS, as it binds to the Vps39 subunit of HOPS [1]. Kinetic assessment revealed that Rab2a was already present early in endosome maturation and could therefore possibly recruit HOPS. A new Rab2a KO HeLa cell line was established to characterise the effects of Rab2a loss on endosome maturation. The levels of Vps41 and Vps39 on FFEs were reduced, as were the levels of other lysosomal proteins (Arl8, mCath D, lyspersin), indicating a role for Rab2a in recruitment of HOPS. However, loss of Rab2a did not displace Vps41 from membranes to the cytosol. Thus, Rab2a

cannot be the main membrane anchor of HOPS. This study provides insight into the chronological sequence of recruitment and functional interdependence of proteins relevant for LE-LYS tethering and fusion. Rab2a is identified as recruiter of HOPS to LEs. Further studies are required to determine how HOPS is anchored to LE membranes.

In a cell-free fusion assay, requirements of ATP-and cytosol-dependent phagosome-with-LYS fusion (StaFu) can be bypassed by adding micromolar [Ca^{2+}] (CaFu). It was unclear whether CaFu required the action of SNARE proteins or NSF (N-ethylmaleimide [NEM] sensitive factor)-dependent priming during the reconstituted fusion reaction. Furthermore, it is unknown which protein(s) act as Ca^{2+}-sensor in CaFu. First, differences and similarities between the two *in vitro* fusion reactions were emphasised. StaFu and CaFu reactions were carried out in parallel in the presence or absence of ATP and cytosol. The effects of PI(3)P-, and PI(4)P-binders, and RabGDI were also tested. In contrast to StaFu, CaFu was unaffected by any treatment, suggesting that CaFu neither depends on ATP, cytosolic proteins, Ras-like GTPases, nor PI(3)P-and PI(4)P-binding proteins. An attachment assay revealed that attachment, besides fusion itself, is also a Ca^{2+}-dependent process with a higher Ca^{2+} requirement than fusion. NEM only had moderate inhibitory effects on CaFu, indicating independence of CaFu from NSF-dependent priming during the *in vitro* fusion reaction. CaFu was moderately inhibited by α-$SNAP^{L294A}$, a potent inhibitor of SNARE-dependent fusion. SNARE participation in CaFu was shown by the inhibitory effect of three preincubated soluble Q-SNAREs. Hence, CaFu depends on the action of SNARE proteins. It was hypothesised that Q-SNAREs may already be primed before purification of latex bead phagosomes (LBP) and LYS and held in a fusion-competent state by a Ca^{2+}-sensitive protein. To identify a Ca^{2+}-sensitive protein involved in CaFu, the already known ion spectrum for CaFu (Ca^{2+}, Ba^{2+}, Mn^{2+}) [2] was expanded by Sr^{2+}. This yielded cytosolic phospholipase A_2 ($cPLA_2$) as a possible candidate. Adding $cPLA_2$-inhibitor $AACOCF_3$ had no effect and was hence excluded as Ca^{2+}-sensor. Synaptotagmin-7 (Syt-7) and myoferlin, two Ca^{2+}-sensitive proteins implicated in plasma membrane (PM) repair, were excluded because they were not present on purified LYS. Annexin A7 (Anx A7), another membrane repair-related protein, whose activity is stimulated by adding GTPγS could also be excluded, as adding GTPγS had no effect. This study shows that CaFu likely depends on SNAREs already separated before purification of LBP and LYS. Attachment of LBP with LYS and fusion are Ca^{2+}-sensitive subreactions of CaFu. Further studies must uncover which protein(s) are involved in CaFu and which physiological function this putative shortcut reaction might serve *in vivo*.

2 Introduction

LYSs are the main catabolic compartments of eukaryotic cells that mediate a plethora of crucial cellular functions, such as degradation of cytosolic and extracellular proteins and macromolecules, lipid turnover, sensing of the cellular nutrient status, killing of microbes, and antigen presentation. Molecules destined for degradation can reach the LYS via endocytic, phagocytic, or autophagic pathways [3–6]. To ensure directionality of cargo transport to LYS, endocytic and phagocytic compartments undergo an elaborate maturation process, during which the maturing compartment fuses with vesicles or other organelles. These fusion processes are directed by concerted action of various proteins and lipids. Much of these interrelated actions of proteins of the fusion machinery are not yet fully understood. Temporal and functional hierarchy – especially regarding late endosome with LYS fusion – remain elusive [7–10]. In addition, a Ca^{2+}-dependent *in vitro* fusion reaction of late phagosomes with LYS has been described in recent years, which appears to be independent of the conventional fusion-mediating machinery. A physiological function and potential Ca^{2+}-sensing and fusion-promoting proteins are yet to be identified [2,11–13]. Maintaining the ability of LYSs to degrade macromolecules and kill pathogens is of utmost importance for higher organisms. Therefore, it is necessary to understand the mechanisms by which phagocytosed material reaches this compartment.

This study aims to shed some light on the fusion machinery needed for LE with LYS fusion and the Ca^{2+}-dependent fusion reaction of late phagosomes with LYS. The following is a brief introduction to the maturation of late endocytic/phagocytic compartments, emphasising molecular events that underlie late maturation stages and the role of Ca^{2+} and Ca^{2+}-dependent proteins in such processes.

2.1 Endocytosis and phagocytosis – key cellular functions

2.1.1 Endocytic routes to the cell's interior

Endocytosis is a process by which internal membranes are derived from invagination and inward budding of the PM bilayer, leading to internalisation of PM lipids, integral proteins, receptor-bound ligands, and extracellular fluids in the process [7]. There are multiple different mechanisms of endocytosis, of which only the most prominent ones will be discussed here (see Figure 1 A). Endocytosis plays a crucial role in regulating many intracellular signaling processes and is often exploited by pathogens to access the cell's interior [14–18]. By far the most

work has been dedicated to clathrin-mediated endocytosis (CME). Cargo molecules are recruited to the developing endocytic site, where the clathrin coat begins to nucleate. The coat comprises clathrin, adaptor, and scaffold proteins and binds to the cytosolic portions of various cargo molecules (e.g. Transferrin-receptor (TfR)), forming a clathrin-coated pit (CCP) [7,19–22]. Clathrin polymerizes into a curved lattice, helping to stabilize membrane deformation and constriction of the vesicle neck [23,24]. Membrane scission of the clathrin-coated vesicle (CCV) is mediated by the GTPase dynamin, which forms a helical polymer around the vesicle neck, pinching off the vesicle upon GTP hydrolysis [25] (Figure 1 A). Subsequently, the clathrin coat is released, and the naked vesicle undergoes further trafficking along the endocytic route [26,27].

Another far less understood mechanism of endocytosis is the uptake of extracellular material through caveolae (Figure 1 A). The main coat protein is caveolin1, along with various other proteins present at endocytic sites [28,29]. Caveolin1 can form oligomers, is palmitoylated, and binds to cholesterol. It is thought to be involved in intracellular lipid trafficking and metabolism [28,30,31]. It is not yet fully clear whether dynamin is involved in membrane scission of caveolae. However, it is known that caveolae can either be trafficked via the endocytic pathway or independently of that [28,32].

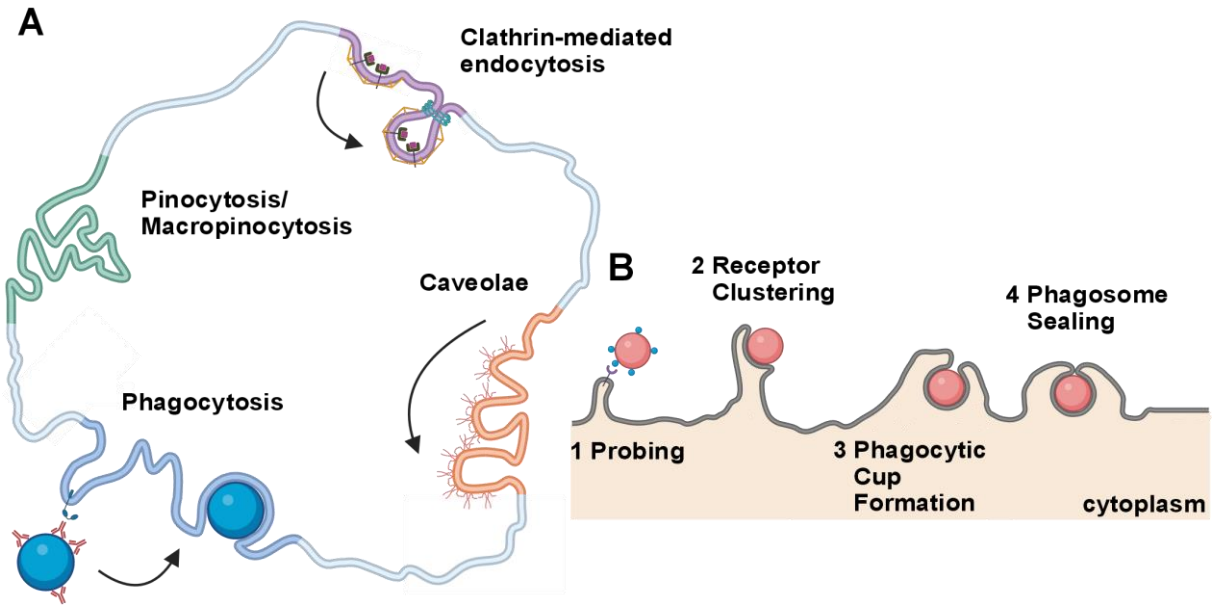

Figure 1: Schematic representation of different endocytic routes and phagocytosis. See next page for legend.

(**A**) The four main routes of endocytosis. (Purple) Clathrin nucleates on endocytic sites and recruits cargo molecules to the forming CCP. A vesicle containing receptor-bound cargoes, extracellular fluids, and PM is subsequentially pinched off by the action of the GTPase dynamin. (Orange) Caveolin1 forms hairpin structures embedded in the PM, generating cave-like pits. Caveolin1 and other proteins comprising the coat interact with cargo molecules to be internalised. (Blue) Phagocytosis is a specialised form of endocytosis mostly found in phagocytes. Opsonins, or surface molecules on large particles or pathogens, are recognised by receptors on the phagocytes' cell surface and initiate a signalling cascade, leading to internalisation of the particle. (Green) Macropinocytosis is an actin-dependent form of endocytosis commonly found in immune or cancer cells. Extracellular fluids and a portion of the PM are internalised in a non-specific manner. (**B**) Phagocytosis can be subdivided into several steps. 1) Probing – Immune cells continuously extend membrane protrusions to probe their surroundings for possible targets. 2) Recognition of particle – Once a particle has been recognised, a signalling cascade is activated, and the ingestion of the particle is initiated. 3) Phagocytic cup formation – Productive signalling leads to extensive remodelling of the actin cytoskeleton, forming protrusions that engulf the phagocytic particle. 4) Phagosome sealing – The membrane protrusions eventually seal off the particle from the extracellular space, forming a phagosome (created with BioRender.com).

Macropinocytosis is an actin-dependent but coat-protein- and dynamin-independent endocytic mechanism in which large intracellular vesicles containing a non-selective sampling of solute molecules are formed [33,34]. It is an important mechanism in immune cells (e.g. dendritic cells, macrophages) and tumor cells [34,35]. After the macropinosome is severed from the PM, regulatory proteins are recruited; the vesicle undergoes tubulation and eventually shrinks in size [34].

2.1.2 Phagocytosis – a specialised form of endocytosis

Phagocytosis is a specialised form of endocytosis and a key function of professional phagocytic cells of the innate immune system (e.g. macrophages, dendritic cells or neutrophils) to clear pathogens and apoptotic cells [36]. In the case of microbial pathogens, the antigenic molecules are transported to the cell surface and presented to cells of the adaptive immune system afterwards, creating an interface between innate and adaptive immune response [37].

Phagocytes recognise particles larger than 0.5 µm through an array of cell surface receptors. Either pattern recognition receptors (PRRs) on the cell surface bind to molecules not found in the organism (pathogen-associated molecular patterns – PAMPs) [38], or opsonic receptors bind to opsonins, such as IgGs or complement components [39–41]. Detection of a foreign particle leads to the offset of signaling cascades, activating the internalisation machinery of phagocytes. Extensive remodelling of lipids in the PM and the actin cytoskeleton leads to formation of pseudopods that gradually engulf the particle in the phagocytic cup [38,42–44] (Figure 1). After sealing off the particle from the extracellular space, a new intracellular compartment is formed – the phagosome [38,44]. The luminal contents of the newly formed phagosome closely resemble the composition of the extracellular space, whereas the membrane composition largely corresponds to the PM [45].

2.2 Endosome and phagosome maturation are intertwined yet distinct processes

In endocytosis and phagocytosis, new membrane-enclosed intracellular compartments are generated. Cells rely on endocytosis to interact with their exterior environment (i.e. uptake of nutrients, signal transduction, uptake of receptor-bound ligands, etc.) for degradation of macromolecules in LYS and termination of signalling processes [18,46–48]. The ultimate goal of phagocytosis is inactivation (i.e. killing of pathogens) and subsequent degradation of luminal phagosome contents [45]. To that end, the phagosome is gradually turned into a microbicidal and highly degradative compartment [44].

After their formation, both endocytic vesicles and phagosomes undergo elaborate and strictly regulated maturation processes, which are intimately interwoven. This transition is caused by numerous fusion events with other organelles and vesicles, leading to changes in membrane and protein composition, luminal contents, and pH. Although the transition from early to late endosomes and ultimately (E)LYS is gradual, distinct maturation stages can be classified by the presence of marker proteins on the cytosolic surface of the compartments. Due to the similarities in the maturation process, phagocytic compartments are termed in analogy to endocytic compartments [38,44,45]. Much knowledge about the maturation of phagosomes was derived from research dedicated to deciphering the maturation of endosomes, and both maturation processes seem to share molecular machinery [47,49–51]. Nonetheless, both processes are distinct, and despite all commonalities, there are differences in the modes of maturation [49]. For practical reasons, the discussion of the maturation processes will be centred around the maturation of endosomes. Caveats concerning phagosome maturation will be acknowledged when needed.

2.3 Maturation of endocytic compartments and phagosomes

2.3.1 Early maturation stages and recycling to the cell surface

After a newly formed endocytic vesicle buds from the membrane, it first interacts and fuses with EEs or sorting endosomes (SEs) [52,53]. EEs are the main sorting hub for incoming cargo. Their limiting membrane and luminal contents are mostly derived from primary endocytic vesicles that fuse with each other [47,54–56]. The luminal pH of EEs is only mildly acidic (pH 6.8-5.9) due to only few molecules of the proton pump v-ATPase present on the limiting membrane. Gradual acidification induces conformational changes in some of the cargo receptors to release their ligands [57–59]. Varying pH sensitivities of different receptors allow for differential release

of their respective ligands and, therefore, represent an additional mode for cargo sorting [59,60]. In these sorting hubs, the fate of internalised cargo is decided. Either cargo is rapidly recycled back from EEs to the PM (e.g. TfR; glycosphingolipids) or trafficked to recycling endosomes (REs) in tubules or vesicles that bud off the main EE vacuole [61–64]. Moreover, there is extensive traffic between EEs and the *trans*-Golgi network (TGN), not only at the stage of EEs but all maturation levels. Endosomal contents are transported to the TGN and lysosomal components, such as lysosome-associated membrane proteins (LAMPs); and acid hydrolases are transported from the TGN to endosomes – the latter as inactive zymogens which have to undergo further processing until their active forms eventually reach the LYS [47,65–67].

EEs display a complex morphology, with tubules emanating from the main vacuole. Most of the EE surface area is concentrated in these tubules, whereas the bulk of the volume is in the vacuolar portion. The tubular structures allow for the formation of a mosaic of functionally differing subdomains, facilitating the sorting of cargo [47,68,69]. On the cytosolic membrane of the EE, 'plaques' containing clathrin and endosomal sorting complexes required for transport (ESCRT) components can be observed. These promote the sorting of ubiquitinated membrane proteins into inward-budding vesicles, called intralumenal vesicles (ILVs) [70,71]. Sorting into ILVs increases accessibility of hydrolases and serves to inactivate signaling receptors [46,72]. Cargo that is not recycled to the PM or transported to the TGN is destined to be transported further along the endocytic pathway and eventually degraded in LYS [47].

Nascent phagosomes also initially interact with EEs [38,44,51]. They shrink (much like macropinosomes) and undergo outward tubulation and scission, as well as formation of ILVs to facilitate the maturation and ultimately degradation of internalised particles or pathogens [44,73].

2.3.2 LEs are generated from MVBs/ECVs and interact with maturing phagosomes

Cargo destined to be transported towards LYS is further trafficked from EEs through LEs before reaching the LYS for degradation. However, it is incompletely understood how cargo progresses from EEs to LEs [55]. It is consensus that LEs are formed from endosomal carrier vesicles (ECVs) and multivesicular bodies (MVBs), both generated from EEs. How exactly an ECV/MVB is formed and detached from an EE is poorly understood, but ECVs/MVBs are distinct from either EEs or LEs despite all three containing multivesicular regions [55,72,74]. Moreover, in contrast to EEs and LEs, ECVs/MVBs do not undergo homotypic fusion [75].

Conversely, early phagosomes seem to rather fuse with LEs than forming MVBs/ECVs, but still form tubules and ILVs [49,51,73]. Uribe-Querol and Rosales term the stage in which the phagosome extensively forms tubules and ILVs as intermediate phagosome in their 2017 review. This intermediate phagosome proceeds to mature into a late phagosome after all cargo to be recycled has been eliminated from the main vacuole [38].

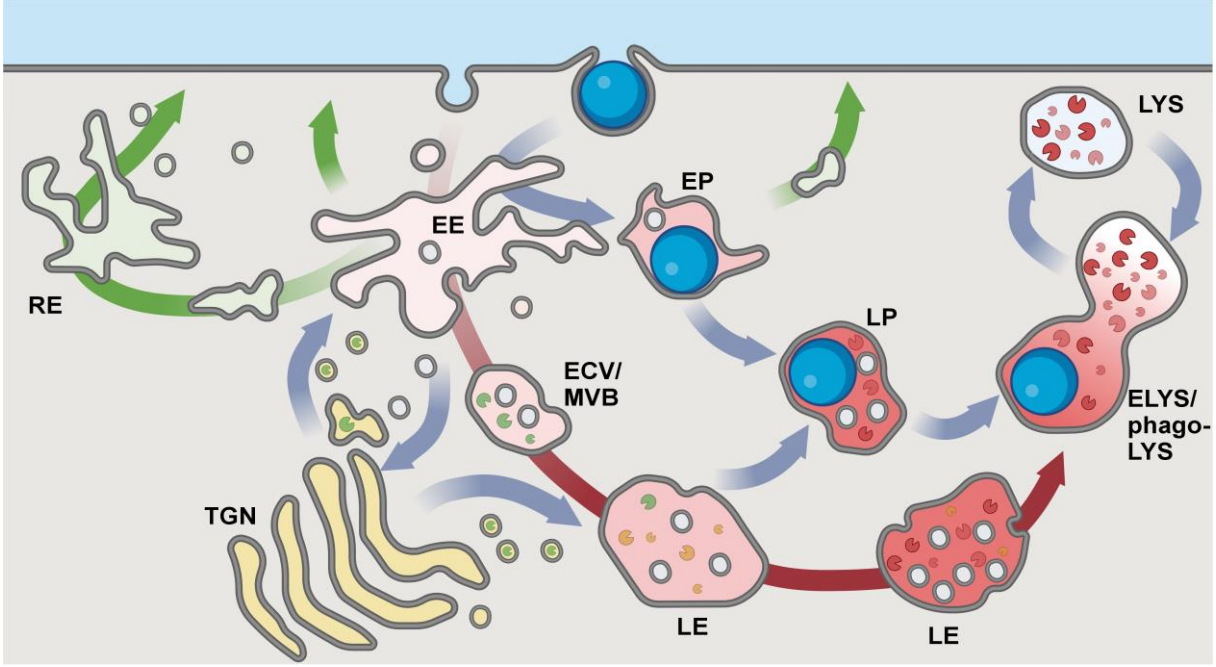

Figure 2: Schematic representation of different pathways for endocytosed or phagocytosed cargo. Recycling pathways are depicted using green arrows. Blue arrows represent general interactions between different intracellular compartments. The red arrow represents gradual acidification of endocytic compartments as they are trafficked towards LYSs. This acidification is also represented by a gradually intensifying red background in endocytic/phagocytic compartments. Gradual processing and activation of lysosomal acid hydrolases is also symbolized by gradual transition from green (inactive (pre)proenzyme) to red (mature). See text for details (created with BioRender.com).

During the transition from EE to LE, the luminal pH becomes more acidic as more copies of vATPase are recruited to the organelle membrane (pH 6.0-4.9). Numerous ILVs of 50-100 nm can be observed. LEs are typically spherical or oval, with diameters ranging from 250-1000 nm and are more closely related to LYS than EEs [38,47]. They also contain dynamic tubular regions similar to the ones found in EEs [72]. Besides endocytosed compartments and Golgi-derived vesicles, autophagosomes (not shown in Figure 2) enter the endosomal pathway at these later maturation stages and contribute to the complex morphology of LEs [72]. LEs move along microtubules from the cell periphery towards the perinuclear region, where they eventually encounter LYS and fuse [76–79]. The pathway that leads to fusion with LYS is a dead-end pathway for most macromolecules, except for proteins that contribute to the functional maintenance of LYS, such as hydrolases and heavily glycosylated membrane proteins [47,65,80,81]. LAMPs are

most abundant on LEs and LYS and, amongst other functions, may help to protect the limiting membrane from the degradative interior with their heavily glycosylated luminal portions [47,82–84]. Lysosomal hydrolytic enzymes (e.g. lipases, proteases, nucleases, glycosidases) are translated as inactive preproenzymes. After transfer to the Golgi apparatus, they are processed into proenzymes by proteolytic cleavage, disulfide bond formation and receive glycosylation. At this point, the hydrolases have little to no proteolytic activity to protect susceptible organelles from their degradative abilities [85]. Most lysosomal hydrolases are transported along the biosynthetic route and targeted to LYS via association with mannose-6-phosphate receptors (M6PRs), where they become fully activated. It was shown that M6PRs rapidly enter multivesicular endosomes and rapidly leave again without accumulating in pre-lysosomal compartments [85–87]. In the lumen of LEs, most ligands are now dissociated from their receptors, together with proteins and solutes internalised and destined for degradation. On the other hand, the receptors that deliver new lysosomal proteins are to be recycled back to the TGN [87]. As in endosome maturation, late phagosomes not only contain internalised foreign particles or pathogens but also slowly accumulate lysosomal proteins, which are indispensable to maintaining the functionality of LYS [38].

2.3.3 Endolysosomes are the primary sites of cargo degradation

Before finally fusing with a LYS, LEs either fuse with each other or undergo transient ‘kiss and run’ fusion events, where luminal contents are exchanged without a full merger event [4,88]. Furthermore, it was proposed that LEs fuse with so-called terminal storage LYS to form active, degrading ELYS [89,90]. In that model, acidic LEs containing molecules for degradation fuse with LYS that do not accumulate acidotropic probes and are hydrolase inactive but store fully functional hydrolases. LEs, ELYS, and LYS seem to exist in dynamic equilibrium and are difficult to distinguish biochemically. Fusion of a late phagosome with a LYS results in the formation of a phagolysosome [38].

Although discrimination at the molecular level remains a challenging objective, LEs, ELYS, and LYS vary in their morphology, electron density (electron microscopy), and buoyancy [47]. Due to the LE-LYS regeneration cycle, no known markers are exclusively attributable to LYS or ELYS [72,89,91]. Only now is there evidence that certain marker proteins are present on ELYS and LYS but not on LEs [10]. Conversely, cation-independent (CI)-M6PR is found in LEs but not in LYS [92]. LEs and LYS are not ‘consumed’ upon fusion but appear to be reformed from ELYS [89,93]. As phagosomes eventually fuse with LYS, the ingested particle is finally destroyed by the low pH, degradative enzymes, reactive oxygen species (ROS), and NO radicals [3,45,50].

2.4 SNARE-mediated fusion events in the endocytic pathway are coordinated by numerous proteins

2.4.1 Ras-like GTPases function as architects of membrane fusion sites

The maturation of endocytic and phagocytic compartments is a carefully regulated and complex process. Cargo must be sorted according to its destination, and the maturation process must be directional. Ras-like GTPases are the main proteins defining compartment identity and maturation status, and they coordinate membrane fusion in the endocytic pathway [69,94]. There are several families of Ras-like GTPases, of which the largest family are Rab proteins. Another related subfamily which regulates membrane fusion in the endocytic and biosynthetic pathway is the ADP-ribosylation factor (Arf)-family [95–97].

Ras-like GTPases act as molecular switches and cycle between an inactive GDP-bound state and an active GTP-bound state in which they turn on subsequent pathways. They recruit downstream effectors, which mediate a multitude of processes. Some of these processes are tethering, recruitment of GTPase-activating proteins (GAPs) and guanine nucleotide exchange factors (GEFs), and organelle motility [69,78,98–101]. Because Ras-like GTPases have low GTP-hydrolysing capabilities and bind GDP tightly, they need the assistance of GAPs and GEFs, which help stimulate GTP hydrolysis and exchange from GDP to GTP respectively. Many Ras-like GTPases also carry a farnesyl or geranylgeranyl anchor at their C-termini. GDP-bound Ras-like GTPases reside in the cytosol and are bound by guanine dissociation inhibitor (GDI) to shield these lipid groups from the aqueous environment. Upon nucleotide exchange, the lipid groups are released, facilitating membrane association of the activated GTPase [102].

2.4.2 Tethering proteins initiate first contacts

As described above, membrane-bound small GTPases recruit and bind to various proteins, including a group called tethers. Tethering proteins loosely and reversibly attach membranes to be fused by binding to both membranes. The specificity of the interaction is ensured by recognition of specific GTPases on either compartment surface [69,103].

There are three classes of tethering factors – long coiled-coil proteins, Complexes Associated with Tethering Containing Helical Rods (CATCHR), and class C Multisubunit Tethering Complexes (MTCs). Despite structural differences, subunit architecture, and interaction partners, all of them bind to Ras-like GTPases and add to the specificity of fusion events [103]. Tethering proteins and especially MTCs, such as Homotypic Fusion and Protein Sorting

(HOPS) complex, bind to Soluble N-ethylmaleimide-sensitive factor Attachment REceptors (SNAREs) and facilitate the formation of productive '*trans*'-SNARE complexes between membranes and in this way regulate membrane fusion [104–106].

2.4.3 Docking and fusion

After tethering proteins have established first contact between two membranes, tight contact (docking) and subsequent fusion are initiated by SNARE proteins present on both sides of the opposing membranes. SNAREs are essential for membrane fusion in endocytic, autophagic, and exocytic events and constitute the minimal machinery necessary for fusion in *in vitro* experiments [107,108]. It is worth noting that not all fusion events that can occur in cells rely on SNAREs as drivers of membrane fusion. For example, viruses have their own sets of fusion-promoting proteins [109], and the structure of the endoplasmic reticulum (ER) is maintained by a group of fusion-promoting GTPases called atlastins [110].

SNAREs are associated with and regulated by several other proteins, such as tethers, Sec1/Munc18 (SM) proteins, Synaptotagmins, N-ethylmaleimide Sensitive Factor (NSF/ Sec18p), and Soluble NSF-Attachment Proteins (SNAP/ Sec17p) [104,111–114]. SNAREs have about 60-70 amino acids and a common heptad-repeat SNARE-motif, which has no secondary structure unless it interacts with other SNARE-motifs to form a four-helix coiled coil bundle [115,116]. Based on a 1998 study of Fasshauer and colleagues, SNARE proteins were classified into Q- and R-SNAREs, depending on whether they contain a glutamine (Q) or arginine (R) residue in their central "0"-layer. Based on sequence homologies, Q-SNAREs can be further classified into Qa-, Qb-, or Qc-SNAREs. Usually, SNARE complexes comprise three Q-SNAREs of the composition QaQbQc and one R-SNARE [115,117]. In most fusion events, one R-SNARE is present on one membrane and a complex of three Q-SNAREs on the opposing membrane [118,119]. Almost all SNAREs also contain a C-terminal transmembrane domain (TMD), whereas other SNAREs are anchored to membranes with prenyl groups or a phosphoinositide-binding domain. At least one SNARE with a TMD must be present for productive fusion on either membrane. Furthermore, TMDs fulfil regulatory functions or aid in the supramolecular assembly of SNARE complexes [120–124]. Some SNARE proteins also contain cytosolic N-terminal domains that precede the heptad-repeats, which contribute to regulating SNARE complex formation [125,126].

After tethering, SNAREs become enriched in membrane microdomains that contain specific lipids with small headgroups that favour non-bilayer structures and fusion, and proteins that

regulate when and where *trans*-SNARE complexes are assembled (Q- and R-SNAREs present on opposing membranes) [111,119,127–129]. SM-proteins are the best-known regulators of SNARE complex assembly. They associate with SNARE proteins and may act as 'clasps', binding SNARE-motifs and possibly N-terminal domains of Q- and R-SNAREs, aiding in the orderly 'zippering' of *trans*-SNARE complexes. SM-proteins can also clamp Qa-SNAREs into a 'closed' conformation, inhibiting or delaying their assembly in *trans*- or *cis*-SNARE-complexes [119,127]. Furthermore, these fusion site microdomains may contain numerous other fusion-regulating proteins, such as lipid kinases, Ca^{2+}-sensitive proteins, and lipid-binding proteins [108].

Trans-SNAREs progressively zipper from their N-termini to their C-termini, drawing the two bound membranes in proximity. During this zippering process, the four SNARE domains can adopt a half-zippered intermediate conformation, which may be a potential target for regulation [130]. The force generated by the zippering process is transduced from the SNARE-motifs to the TMDs via the SNARE linker regions [131,132]. It exceeds the repelling force from the water shell surrounding the membranes, making direct contact between the two membranes possible [133,134]. It has become broadly accepted that all membrane fusion proceeds through the formation of a 'hemifusion' intermediate, where the outer membrane leaflets merge, and the distal lipid leaflets stay intact [123,135]. The transition of a hemifused state to full membrane merger and mixing of lipids might have a significantly higher energy barrier than the generation of the hemifused state [136]. After mixing the lipid bilayers, a fusion stalk is established, connecting the luminal contents of both vesicles and allowing for content mixing. The formation of such a fusion stalk or pore can lead to either transient 'kiss and run' or full membrane merger [137]. It is not yet apparent how exactly the fusion pore is widened. However, recent studies suggest that despite one single SNARE complex being sufficient for membrane fusion, fusion-stalk expansion is influenced by transducing mechanical force from zippering to SNARE TMDs [135,138,139].

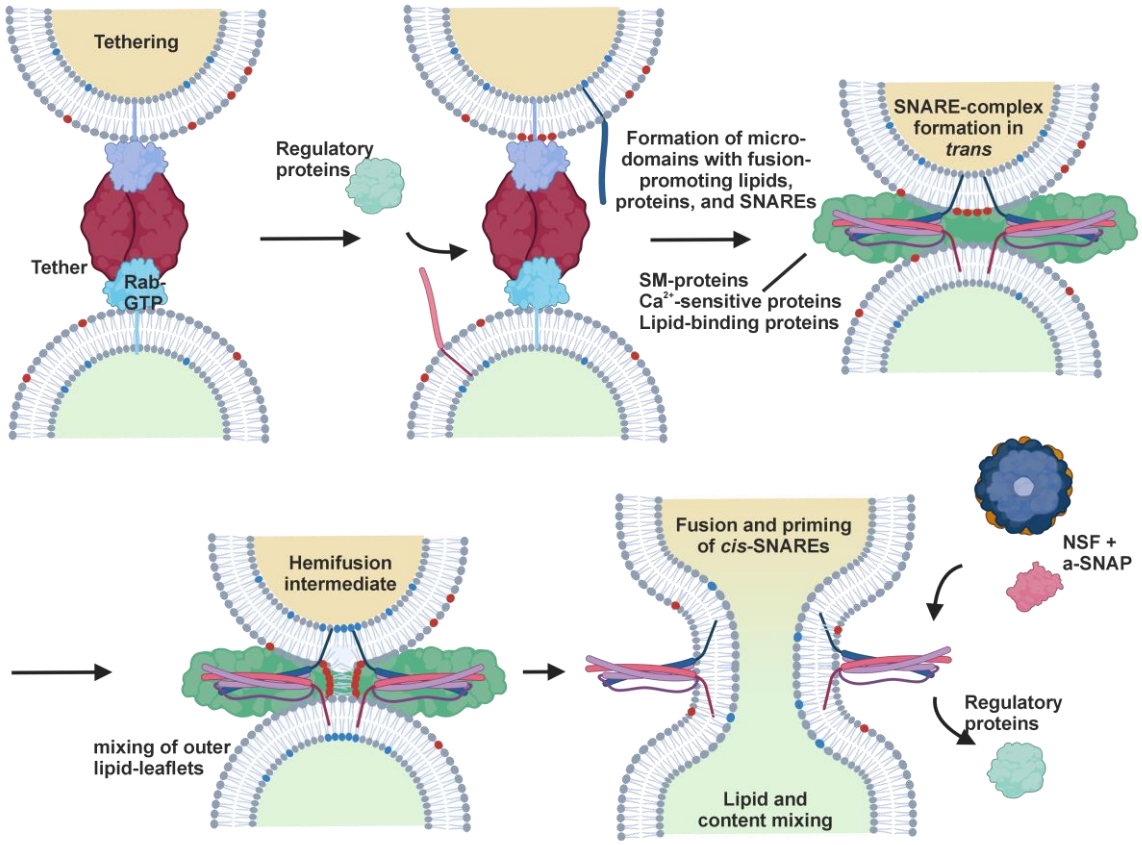

Figure 3: Schematic representation of membrane merger event in the endo-lysosomal route. (A) Lose contact between fusion partner is established through action of small GTPases and tethering-proteins. **(B)** SNAREs and fusion-promoting lipids are recruited to sites of tethering. **(C)** SNARE complex assembly in *trans* is chaperoned by accessory proteins (i.e SM-proteins, lipid-binding proteins). **(D)** Formation of a 'hemifusion' intermediate, with mixing of the outer lipid bilayer leaflets precede **(E)** full merger and content mixing. *cis*-SNARE complexes are separated by action of NSF and its cofactor α-SNAP. Illustration modelled after [108] (review). Created in BioRender. Schleinitz, A. (2024) BioRender.com/b23s074.

2.4.4 Priming of *cis*-SNARE complexes

After two membranes have fully merged, the assembled *cis*-SNARE complexes reside on the same membrane. The very stable four helix-coiled-coil complexes must be disassembled to make the individual SNARE proteins available for another round of fusion. Disassembly is ATP-dependent and catalysed by NSF and its cofactor α-SNAP [113,140,141]. SNAP is recruited to *cis*-SNARE complexes and attracts NSF, which binds and unwinds the *cis*-SNAREs upon ATP hydrolysis. This process is called priming [127].

2.4.5 Rab5 to Rab7 switch marks the transition from EEs to LEs

Characteristic of EEs is the presence of Rab5 and its effectors. Rab5 is needed for the fusion of EEs with phagosomes and the transition from EEs/ early phagosomes to LEs/ late phagosomes [38,142,143]. Rab22a recruits the Rab5 GEF Rabex-5. In turn, Rabex-5, together with Rab4, recruits Rabaptin-5, which enhances the nucleotide exchange activity of Rabex-5, creating a positive

feedback loop for Rab5 activation. Activated Rab5-GTP associates with EE membranes, from where it recruits downstream effector proteins [143–145]. Rabaptin-5 furthermore recruits the class III phosphatidylinositol-3 kinase Vps34, which creates the lipid phosphatidylinositol-3-phosphate (PI(3)P), in which EE membranes are enriched [146]. Rab5 recruits the coiled-coil tether EEA1, which binds to PI(3)P via its FYVE domain [147,148]. EEA1 promotes fusion by tethering EEs to incoming endocytic vesicles or phagosomes [149,150]. PI(3)P also serves as a binding site for class C core vacuole/endosome tethering (CORVET) complex, an MTC involved in EE fusion and recycling of a subset of EEs [151,152].

As phagosomes mature, PI(3)P-enriched early phagosomes interact with PI(4)P-enriched LEs or late phagosomes [51]. This is accompanied by a switch from Rab5 to Rab7, which is believed to occur on MVBs/ECVs in the endocytic pathway [153,154]. Rab7 is recruited to endosomal/phagosomal membranes by its GEF, the monensin sensitivity 1a/calcium caffeine zinc sensitivity 1 (Mon1a/Ccz1) complex [155]. Mon1a/Ccz1 – which needs active Rab5 to be recruited – displaces Rabex-5 from membranes and thus terminates the activation of Rab5 [101].

2.4.6 Rab7a and Arl8 mark the late stages of endosome maturation

Rab7 is one of the most investigated Rab GTPases to date. There is one conserved ortholog in yeast – Ypt7 – which is required to transfer cargo from LEs/MVBs to LYS [154]. Mammalian cells possess Rab7a and Rab7b, which are not considered to be isoforms since they only share 50 % of their amino acid sequence. In contrast to Rab7a, Rab7b is implicated in controlling transport between endosomes and the Golgi [156,157]. Rab7a has multiple upstream and downstream interaction partners and is involved in endosomal sorting, trafficking, and LYS biogenesis [158,159]. It is present primarily in a perinuclear pool of late endocytic compartments and colocalizes with lysosomal markers such as LAMP1 [160,161].

Arl8 is a small GTPase of the Arf-like protein family with two isoforms (Arl8a and Arl8b), which share 92 % of their amino acid sequence and have partially redundant functions [100,162,163]. In contrast to Rab7, Arl8 has no yeast ortholog. However, it is highly conserved in multicellular eukaryotes [162,164,165]. Interestingly, Arl8 is the only known GTP-binding protein that is present primarily on mature LYS, as it has been discussed to be present in compartments of later maturation stages than Rab7a [10,99,166]. Unlike other Arf or Arl proteins, Arl8 does not contain an N-terminal myristoylation site for membrane association. Instead, it relies on N-terminal acetylation of a methionine residue for lysosomal localisation [166].

2.4.7 Intracellular motility of LEs/ late phagosomes and LYS is mediated by Rab7 and Arl8

Rab7a is the defining Rab-protein for LEs/ late phagosomes and is involved in LE-LYS fusion. Furthermore, it mediates the retrograde transport of LEs/ late phagosomes towards the microtubule organising centre (MTOC) by recruiting the dynein-dynactin motor complex in concert with its effectors Rab-interacting lysosomal protein (RILP), which interacts with the $p150^{Glued}$ subunit of the dynein-dynactin complex. Dynein-dynactin recruitment is controlled by oxysterol-binding protein-related protein 1L (ORP1L) and VAP (VAMP [vesicle-associated membrane protein]-associated ER protein) [158,167]. Most LYS are present in the perinuclear region, near the MTOC, but some are also scattered throughout the cytoplasm [168,169]. For LEs to fuse with LYS, both compartments must be transported toward each other. Anterograde transport is mediated by the small GTPase Arl8, which recruits kinesin-1 via its effector Sif-A and kinesin interacting protein/Plekhm-2 (SKIP) [170]. Rab7a and Arl8 are locked in an antagonistic relationship, controlling the positioning of LEs and LYS, thereby facilitating their encounter and fusion [100,161].

2.4.8 The fusion machinery required for late endosome-lysosome fusion

Rab7a and Arl8 transport LEs and LYS along microtubule tracks and mediate LE with LYS fusion. Although much work has been dedicated to revealing the precise functions of both GTPases in this process, their exact roles, the order of their actions, and the topography of the machinery they assemble to promote LE-LYS fusion remain largely elusive [10].

Another protein complex integral for LE-LYS fusion is the HOPS complex [105]. HOPS is an MTC and consists of six subunits (Vps11, Vps16, Vps18, Vps33A, Vps39, Vps41), of which it shares four with the early endosomal MTC CORVET [152]. The Vps39 and Vps41 subunits are unique to the HOPS complex. Vps33A is a member of the SM protein family and facilitates *trans*-SNARE complex formation [104,106,171–173]. Vps16 and Vpss33A form a stable heterodimer located in the head region of HOPS, whereas Vps11-Vps18-Vps39 form a heterotrimer [174,175]. Both subcomplexes only assemble into the hexameric complex in the presence of Vps41 [175]. HOPS has many interaction partners, and it is not yet apparent how and when HOPS is recruited to late endosomal or lysosomal membranes or how exactly it is anchored [10].

In yeast, HOPS promotes fusion of LEs with vacuoles (yeast LYSs) by directly binding Ypt7, present on both membranes through its Vps39 and Vps41 subunits [176–178]. This is not the case in mammalian cells, as mammalian HOPS does not bind to Rab7a directly but to its effector

RILP [179,180]. Arl8b was identified as a critical regulator of cargo delivery to LYS and HOPS as one of its effectors [181]. Khatter and colleagues postulate that Arl8b is essential for membrane localisation of HOPS instead of Rab7a/RILP. In this model, Arl8b binds to the Vps41 subunit of HOPS via its WD40 domain and complex assembly is guided by subunit-subunit interactions. Furthermore, SKIP/Plekhm-2 binds to the Vps39 subunit of HOPS [182]. These conclusions are corroborated by the 2020 study of Jongsma et al., in which it is postulated that Rab7a and Arl8 can both be present on the membranes of a temporarily existing joint compartment. The Rab7a GAP TBC1D15 is recruited to SKIP via the HOPS complex, which eventually leads to inactivation of Rab7a and the formation of an Arl8-only compartment, a process that is suspected to be similar to the Rab5 to Rab7a handover from EEs to LEs [99]. However, these findings make SKIP an unlikely candidate for HOPS recruitment or anchoring on neighbouring membranes.

The Vp41 subunit of HOPS also binds to the dual Rab7a and Arl8 effector pleckstrin homology domain-containing protein family member 1 (Plekhm1) [183,184]. Plekhm1 is a multivalent endocytic adaptor protein involved in fusion of LEs or autophagosomes with LYS. It binds to Rab7a via its C-terminal pleckstrin homology (PH) domain as well as HOPS and Arl8 via its N-terminal RUN domain [184,185]. Contrary to the previously presented findings of an Arl8 involvement in HOPS recruitment/anchoring, there is also evidence that HOPS may be recruited by RILP and Plekhm1 [179,180,186].

Another possible interactor of HOPS could be BLOC-1 (biogenesis of lysosome-related organelle complex-1) -related complex (BORC) [187]. BORC is a heterooctameric complex (LOH12CR/myrlysin, C17orf59/lyspersin, C10orf32/diaskedin, KxDL1, MEF2BNB, BLOS1, BLOS2, and snapin) that shares BLOS1, 2, and snapin with BLOC-1. Membrane association of BORC is partially achieved through an N-terminal myristoyl group of myrlysin. Its main function seems to be the recruitment of Arl8 to LYS for which the lyspersin subunit is essential [169]. In BORC-deficient cells, LYS accumulate in the perinuclear region as they are unable to recruit Arl8, which is needed for anterograde transport of LYS [188,189].

As mentioned before, HOPS also binds to late endosomal SNARE proteins through its Vps33A subunit and aids in complex formation and zippering [104,106,171–173]. It was reported that yeast HOPS interacts with a number of different SNARE proteins and even has proofreading capabilities for mismatched SNAREs [190–192]. HOPS also possibly interacts with PIPs, which could serve as an additional putative anchoring point of the complex to membranes [9,193].

A more novel suspect for the recruitment and anchoring of HOPS is the small GTPase Rab2, primarily located at the Golgi. HOPS interacts with Rab2a and Rab2b [1,194]. Rab2a binds to HOPS via the Vps39 subunit. It was hypothesised by Lőrincz and colleagues that Rab2a-bound HOPS is delivered to late endosomal Rab7a-positive vesicles on Golgi-derived CVs. HOPS may then bind to other proteins like Plekhm1 to promote fusion. It is likely that Rab2a only remains active for short periods on late endosomal membranes and is lost quickly after fusion [1]. Such an interaction between Rab2a, HOPS and Rab7a effector is generally conceivable since Plekhm1 can interact with Vps39 and Vps41, respectively [184].

2.5 Ca^{2+} – a tightly regulated universal second messenger

Ca^{2+} is an essential cellular second messenger. Usually, Ca^{2+} resting concentrations in the cytosol are kept low and range around 50-200 nM [195,196] but can be raised quickly and dramatically as a reaction to incoming stimuli. Unsurprisingly, a plethora of well-characterised Ca^{2+}-sensitive proteins have been identified that partake in the regulation of critical cellular processes, such as cell membrane repair, neurotransmitter release, stress responses, and membrane fusion. Although many studies suggest a role for Ca^{2+} in phagocytosis and phagosome maturation/ fusion, the proteins involved and the exact role Ca^{2+} plays in these events are still being debated [197–203].

A transient elevation in cytosolic Ca^{2+} levels can be achieved in two different ways: by opening of Ca^{2+} channels at the plasma membrane or by releasing Ca^{2+} from intracellular stores. ER and LYS are the most prominent intracellular Ca^{2+} storage organelles [196,203]. Extracellular [Ca^{2+}] is much higher than resting cytosolic Ca^{2+} concentrations ($[Ca^{2+}]_{cyt}$) and ranges around 2 mM [204]. Multiple channels mediate Ca^{2+} influx into the cell, the driving force of which is the electrochemical potential across the membrane generated by the steep difference in Ca^{2+} concentrations [203,205]. To maintain low $[Ca^{2+}]_{cyt}$, Ca^{2+} must actively be pumped out of the cell. The two main channels responsible for this are the Plasma Membrane Ca^{2+} ATPase (PMCA) and the plasma membrane Na^+/Ca^{2+} exchanger (NCX) [206]. LYS are unique as Ca^{2+} storage organelles due to their acidic pH and are thought to release Ca^{2+} via two-pore channels (TPC) and transient receptor potential (TRP) mucolipin (TRPML) channels [207–209]. However, it is unclear how LYS accumulate Ca^{2+} [208].

Intracellular and extracellular Ca^{2+}-release pathways are interconnected [205]. Upon depletion of ER Ca^{2+} stores, the Ca^{2+}-sensing stromal interaction molecule (STIM) proteins – transmembrane proteins that occur as dimers – undergo conformational changes. This leads to

unfolding and extending of the C-terminal domain into the cytoplasm and the subsequent generation of junctions between the ER and PM. STIMs activate and interact with Ca^{2+} channels of the Orai family at the STIM-Orai activating region (SOAR). This coupling process generates high [Ca^{2+}] microdomains, which regulate multiple cellular functions and the refilling of ER Ca^{2+} stores. Ca^{2+} is actively pumped back into the ER lumen via sarcoplasmic/ER Ca^{2+} ATPase (SERCA). This pathway is called store-operated Ca^{2+} entry (SOCE) [210–212]. Ca^{2+} released from ER and/or LYSs could possibly play a role in phagosome maturation and/or fusion [203], which will be discussed below.

2.5.1 Role of Ca^{2+} in phagocytosis and phagosome maturation

In their 2019 review, Westman and colleagues summarise data regarding the involvement of Ca^{2+} in phagocytosis and phagosome maturation. Although much evidence points to Ca^{2+} requirement in both processes, the matter remains controversial. It is unclear how much Ca^{2+} is stored in phagosomes throughout their maturation, whether releasing Ca^{2+} from phagosomes is critical for fusion events with organelles of the endocytic pathway, and which proteins would be involved [203]. There are substantial technical issues which complicate research in the field even further; the most critical caveats probably being pH-sensitivity of Ca^{2+} probes, accurately measuring Ca^{2+} currents from organelles with a comparably small volume, interconnection of pathways, Ca^{2+} as a contaminant in commercial preparations, and experimental settings [203]. Despite all caveats hampering the measurement of [Ca^{2+}] in small organelles, there are reports of acidic compartments functioning as dynamic Ca^{2+}-stores [213].

According to the review, transient increases in $[Ca^{2+}]_{cyt}$ can be frequently measured during phagocytosis, but there are also studies in which no such Ca^{2+} transients are observed. Interestingly, phagocytosis in bone marrow-derived macrophages is inhibited when Ca^{2+} is chelated, but not in macrophages from Synaptotagmin-7-deficient mice [214]. Therefore, it is still a subject of debate whether Ca^{2+} is crucial for phagocytosis or not [203]. An earlier review proposed that Ca^{2+} influx, albeit an early event, may be necessary for regulating subsequent events in phagosome maturation [196]. One explanation for the ambiguous observations could be the vast number of different phagocytic mechanisms/receptors or cell lines used, some of which could require Ca^{2+}, whereas others do not. Furthermore, differences in Ca^{2+}-sensing efficiency for different detection systems should not be dismissed as a possible source of ambiguity (reviewed in[203]).

Ca^{2+} release from phagosomes was observed in numerous studies [215–217]. Early endosomes and phagosomes initially contain high intraluminal [Ca^{2+}], which, in the case of endosomes, is released within a few minutes after formation [218]. Such a release was also observed for phagosomes in neutrophils [215]. Similarly, Nunes and colleagues observed periphagosomal Ca^{2+} hotspots at phagosomes, colocalizing with STIM1 puncta, reflecting both Ca^{2+} release from ER and phagosomes. Depletion of STIM1 led to impaired fusion of phagosomes with endosomes and LYS. However, this is no direct evidence for a fusion-promoting role of Ca^{2+} [216,219]. An earlier study by Mayorga et al. reported Ca^{2+}-dependent homotypic fusion of early endosomes [220], and some studies attribute an arrest in phagosome maturation to inhibition of Ca^{2+} signaling by *Mycobacterium tuberculosis* [221–223].

Ligand-gated TRP and Orai channels (e.g. TRPV2, TRPM2, TRPML1, Orai 1, 2 & 3) have been found on phagosomes [219,224–227] and could function in Ca^{2+} efflux and phagosome maturation, with the caveat, that Orai channels are inhibited at pH < 6 [203,228]. Another Ca^{2+}-channel identified on LYS is P2X4. Even though it is not certain that P2X4 is active on LYS due to it being inhibited by acidic pH, it was reported to promote endolysosomal fusion in concert with calmodulin [229,230]. Since phagosome maturation is also intimately linked to the endocytic pathway, endocytic organelles could also be a source for Ca^{2+} fluxes that aid in phagosome maturation. In line with this, TRPML3 has been linked to endosome fusion. It stays active at mildly acidic pH, which is of great relevance regarding the gradual acidification of maturing phagosomes and endosomes alike [231,232].

There is also evidence that Ca^{2+} plays a role in phagosome-with-LYS fusion. For example, Ca^{2+} oscillations preceding phagosome with LYS fusion were observed in neutrophils [233]. Ca^{2+} transients have been attributed to ER and lysosomal origins [216,217,234], and some studies reported a secondary Ca^{2+} release from the ER after Ca^{2+} efflux from LYS [235,236]. Notably, many of these observations have been made in a wide variety of different cell types with specialised functions. Therefore, phagosome-LYS fusion may be a Ca^{2+}-dependent process in some, but not all, cell types. Zimmerli and colleagues observed phagosome with LYS fusion at nanomolar [Ca^{2+}] in macrophages, and therefore postulated that phagosome-LYS fusion was Ca^{2+}-independent in macrophages but not in other cell types [237]. In contrast, millimolar [Ca^{2+}] are sufficient to elicit fusion in *in vitro* fusion experiments with late latex bead-containing phagosomes and LYS derived from macrophages [2]. Furthermore, phagosome-LYS fusion in J774E macrophages and endosome-LYS fusion (rat hepatocyte) is inhibited by Ca^{2+}-chelator 1,2-bis (2-aminophenoxy) ethane-N ,N ,N -tetraacetate (BAPTA), pointing to an essential role of Ca^{2+} in late

phagocytic and endocytic fusion in J774E macrophages-like cells [2,238,239]. Dayam and colleagues also noticed that phagosomes from TRPML1-depleted cells docked to LYS but did not fuse. Similar effects were seen upon inhibition of PIKfyve, which implies TRPML1 participation since TRPML1 is a $PI(3,5)P_2$-gated Ca^{2+}-channel [224]. There are many additional studies regarding the role of Ca^{2+} in phagosome maturation and phagosome-LYS fusion, which are not considered here. However, an increasing amount of evidence favours Ca^{2+}-requirement in such processes.

2.5.2 Role of Ca^{2+} in membrane fusion events

Essential cellular functions such as cell membrane repair or synaptic vesicle fusion are Ca^{2+}-dependent processes, as well as the fusion of cortical vesicles (CV) in sea urchin eggs with the PM or with each other [197,240–242]. In membrane repair, four main mechanisms are widely accepted: exocytosis (of LYS), endocytosis, membrane patching, and membrane shedding [243–248]. The mechanism employed for resealing the membrane lesion may depend on the type of injury (i.e. mechanical injury, chemical, etc.) and size. Some injuries might also elicit combinations of different mechanisms to ensure quick membrane resealing [201,249]. All mechanisms depend on Ca^{2+}, which enters the cell rapidly and uncontrolled upon membrane rupture, but Ca^{2+} from intracellular Ca^{2+}-stores may also play a role in PM resealing [197]. Ca^{2+}-sensitive proteins from multiple different protein families are known to be involved in repair processes. Among them are Synaptotagmins (Syt), of which Syt-7 is the most prominent, annexins, dysferlin – a member of the ferlin family, and proteins of the ESCRT machinery [244,250–252].

Syts also play an essential role in neurotransmitter release. Once an action potential reaches the presynapse, Ca^{2+} channels open, allowing for a transient increase in $[Ca^{2+}]$. Syt I binds Ca^{2+} and displaces complexin. Complexin activates and clamps *trans*-SNARE complexes into a metastable fusion-ready state. Therefore, neurotransmitter vesicles are fixed in proximity to the presynaptic membrane. After displacement, rapid zippering of SNARE-domains into four helix bundles catalyses fusion. Syts not only interact with complexin but also with phospholipids and the SNAREs themselves [202,253]. The general function of Syts and complexins may be conserved in many Ca^{2+}-regulated secretion events, such as the sperm acrosome reaction [254].

CV exocytosis in sea urchin eggs is another Ca^{2+}-regulated exocytic process. Shortly after fertilisation, Ca^{2+} levels rise, triggering fusion with the PM of fully primed and docked CVs to prevent polyspermy. Studies show that CV exocytosis is independent of ATP and cytosolic

factors and does not depend on the action of NSF [255–257]. It was also postulated that low micromolar [Ca^{2+}] are the only requirement to elicit CV exocytosis [258,259]. Interestingly, different [Ca^{2+}] cause a graded response, where only subsets of the available vesicle population fuse. The respective subpopulation's size depends on the amount of Ca^{2+} present, suggesting a heterogeneous Ca^{2+}-sensitivity among exocytic vesicles [241]. CVs possess the complete fusion machinery necessary for fusion, enabling them to fuse [260,261].

2.6 Ca^{2+}-sensitive proteins in membrane fusion

Ca^{2+}-sensitive proteins serve as a link between Ca^{2+}-stimuli and cellular responses. Corresponding to the wide variety of Ca^{2+}-regulated processes in the cell, many Ca^{2+}-binding proteins are involved in generating and integrating Ca^{2+} signals and mediating appropriate responses [262]. To carry out their diverse functions, these proteins must harbour Ca^{2+}-binding domains, such as EF-hand motifs, C2 domains, and annexin Ca^{2+}-binding domains. The EF-hand motif is the most common Ca^{2+}-binding motif and is found in proteins such as calmodulin, parvalbumin, S100 proteins, myosin, calpain, troponin C, and calcineurin. The canonical EF-hand sequence is a short helix-loop-helix motif. 12 residues in a characteristic sequence (loop) are found to participate in metal coordination. The two helices are termed E and F and are linked by a loop. Once Ca^{2+} binds, helix F adopts an open conformation orthogonal to helix E [263].

Another group of common Ca^{2+}-binding motifs are C2-domains, which were originally identified in protein kinase C. They comprise approximately 130 amino acids and form an anti-parallel ß-sandwich with two four-stranded ß-sheets. C2 domain-containing proteins bind to various ligands, including lipids and other proteins and participate in numerous cellular events, such as membrane trafficking, activation of GTPases and control of protein phosphorylation. Variations in interconnecting loops fine-tune the ability of C2 domains to respond to different [Ca^{2+}] and lipids. There are also C2 domains that do not bind to Ca^{2+} and may act as a structural component in some proteins [264,265].

Syts belong to a C2 domain-containing family of proteins that in mammals (mouse and human) consists of sixteen isoforms, eight of which (Syt1, 2, 3, 5, 6, 7, 9, 10) bind to Ca^{2+} [266,267]. They have an N-terminal transmembrane domain, a variable length linker region, and two distinct C2 domains (C2A and C2B) arranged in tandem [267]. Syts, as many C2 domain proteins display variations in Ca^{2+}-sensitivity and binding-kinetics and may also be activated or bind to other divalent cations, such as Sr^{2+} and Ba^{2+} [268,269]. Syts have been implicated in fusion events, such as PM repair or neurotransmitter release [250,253,266] and bind to lipids, such as phosphatidylserine

(PS) and PIPs, which contributes to their function [268,270]. It has also been shown that Syts directly bind to SNAREs in a Ca^{2+}-dependent manner and take part in regulating SNARE-mediated fusion [111].

Ferlins are also a C2 domain containing protein family (dysferlin (Fer1L1), otoferlin (Fer1L2), myoferlin (Fer1L3), Fer1L4, Fer1L5, and Fer1L6). Ferlins are type II transmembrane proteins with a single transmembrane domain located at their C-terminus [271,272]. Myoferlin and dysferlin share the highest similarity within the ferlins, and both contain seven C2 domains, which can bind PS and PI [273]. Both are expressed in myoblasts, where they are most abundant at the PM; a small pool of myoferlin is also present at the nucleus. Defects in dysferlin and myoferlin are associated with muscle dystrophy [251,273,274]. Myoferlin might also play a critical role in endocytosis in endothelial cells, participates in membrane repair, and mediates lysosomal exocytosis in macrophages [275–277].

Phospholipase A_2 (PLA_2) enzymes are a somewhat peculiar group of proteins that may contribute to membrane trafficking or membrane fusion events. PLA_2 enzymes are a large and diverse superfamily of enzymes which hydrolyse membrane phospholipids to create a lyso-phospholipid (LPL) and a free fatty acid (FFA), which often is arachidonic acid (AA). AA is subsequently metabolised to eicosanoids (prostaglandins or leukotrienes) by cyclooxygenases or lipoxygenases [278,279]. There are Ca^{2+}-independent and Ca^{2+}-dependent PLA_2 enzymes. Some PLA_2 bind Ca^{2+} through neighbouring aspartate and histidine residues, and some as cytosolic phospholipase A_2 ($cPLA_2$) via C2 domains [278,280]. It has been reported that various PLA_2 are involved in mediating fusion events, such as exocytosis or endosomal fusion events in a Ca^{2+}-dependent manner. However, this function of PLA_2 enzymes is not well understood [279,281]. One way in which PLA_2 enzymes could promote fusion activity is by generation of LPL, which has an inverted-cone shape, favours the outward bending of the membrane and would therefore introduce fusion-favouring membrane curvature in vesicles [278]. Furthermore, $cPLA_2\alpha$ has been shown to induce membrane curvature by binding to and penetrating internal membranes [282].

Annexins are a multigene family of Ca^{2+}- and lipid-phospholipid binding proteins with twelve members. All annexins are structurally related and consist of a variable N-terminal domain, considered relevant for protein-specific functions and a conserved annexin core-domain at the carboxy terminus. Annexins have four to eight (Anx A6) highly conserved repeats for Ca^{2+}-coordination in their core domains. These repeats enable the interaction of annexins with negatively charged phospholipids. Annexins have differential sensitivity to $[Ca^{2+}]$, which for some annexins may be further modulated by phospholipids [201,283–285]. Under Ca^{2+} resting

conditions, most annexins are diffusely distributed in the cytosol. In response to Ca^{2+} binding, they are associated with membranes. The variable N-terminal domain of annexins allows for multiple different interactions with a broad range of different proteins, resulting in a diverse range of functions [283]. Many annexins (A1, A2, A4, A5, and A6) are most prominently known for their role in membrane repair. Moreover, annexins have a pivotal role in organising membrane domains, allowing them to participate in a wide array of events, such as cell motility, growth and cell death [201,283,286]. Some annexins have also been reported to have a role in exocytic fusion events [287–290]. They may facilitate exocytosis in multiple ways. Anx A2, for example, is recruited near SNAREs and is known to form lipid domains at exocytic sites, favouring fusion and possibly fusion pore expansion [288].

3 Aims of this study

LYS are the main catabolic compartments in eukaryotic cells. They fulfil multiple cellular functions which are essential to the cell's survival, such as degradation of cytosolic and extracellular proteins, macromolecules, lipid turnover, and sensing of the cellular nutrient status. For endocytosed cargo to reach LYS, endosomes run through an elaborate maturation sequence, which relies on multiple fusion events of endocytic vesicles. Fusion is mediated by the interdependent action of multiple proteins (i.e. Ras-like GTPases, tethering proteins, etc.) and lipids. Although the crucial proteins involved in LE-LYS fusion have been identified many, questions regarding their role in this process remain unanswered. This study aims to investigate the effects loss of either Rab7a, Arl8, Vps41 (HOPS), myrlysin, and diaskedin (BORC) have on delivery of endocytosed material to LYS. It is also known that all these proteins interact with each other directly or indirectly in multiple ways. However, the temporal sequence in which they appear on maturing endosomes is unknown. Understanding the chronological hierarchy of protein acquisition could be the key to a better understanding of the topography of the fusion apparatus required for LE-LYS fusion and will therefore also be investigated. The HOPS complex fulfils a critical role in mediating LE-LYS tethering and possibly also other roles related to this fusion event. There are many conflicting reports on how HOPS is recruited to endosomal membranes. This study also aims to address this issue and shed light on possible recruitment of HOPS to LEs via Rab2a.

Phagocytosis – a specialised form of endocytosis – is of utmost importance for killing of pathogens in phagocytes. Regular fusion between late phagosomes and LYS has been extensively investigated *in vitro*. An alternative fusion mechanism was identified that is solely dependent on micromolar Ca^{2+} concentrations. Firstly, the requirements of CaFu for various known StaFu regulators should be determined in parallel with StaFu. This serves to highlight any similarities and differences between the two reactions and to validate previous data. Beyond that previous data indicates that CaFu either requires multiple Ca^{2+}-dependent proteins or processes. A possible Ca^{2+}-dependency of attachment in addition to the fusion itself will be investigated. Typically, fusion in the endo-lysosomal pathway is mediated by the action of SNARE proteins, but their involvement in CaFu has not been established and will therefore be assessed. Lastly, an expanded ion-spectrum for the CaFu reactions may provide hints on proteins involved in CaFu and possibly a physiological function of CaFu. Therefore myoferlin, annexin A7, Synaptotagmin-7 and cytosolic phospholipase A_2 are tested for a possible role in mediating CaFu.

4 Material and Methods

4.1 Materials

4.1.1 Chemicals and Reagents

4.1.1.1 Chemicals

Compound	Manufacturer/Distributor
1, 4 dithiothreitol	Roth (6908.2)
1,10 phenanthroline monohydrate	Sigma-Aldrich (P-1294)
5(6)-carboxy-tetramethyl-rhodamine	Novabiochem (8.51030.8500)
AACOCF3	Chem Cruz (sc-201412C)
ADA Pufferan® ≥ 99 %	Roth (0250.2)
albumin fraction V	Roth (8076.3)
ampicillin sodium salt	Roth (K029.2)
ATP (adenosine triphosphate)	Roche (1275123)
ATTO 488 NHS ester	ATTO-TEC (AD 488-35)
$CaCl_2$, anhydrous	Sigma-Aldrich (C1016)
creatine phosphate	Roche (13810732)
D(+)-sucrose ≥ 99.5 %, p.a.	Roth (4621.3)
dextran, amino, 10,000 MW	Invitrogen (D1860)
EDAC (N-(3-Dimethylaminopropyl)-N'-ethylcarbodiimide hydrochloride)	Sigma-Aldrich (E6383)
EDTA (ethylenediaminetetraacetic acid)	Roth (8943.2)
EGTA (ethylene glycol bis(2-aminoethyl) tetraacetic acid)	Roth (3054.3)
GTPγS	Roche (10220647001)
HEPES Pufferan® ≥ 99.5 %, p.a.	Roth (9105.6)
Hoechst 33342	ImmunoChemistry Technologies
kanamycin sulphate 750 I.U/mg	Roth (T832.4)
LB (Lennox)	Roth (X964.4)
leupeptin hemisulfate salt	Sigma-Aldrich (L2884)
L-glutathione, reduced	Roth (6382.3)
Magnesium chloride, anhydrous	Roth (KK36.2)
Mowiol® 4-88	Sigma-Aldrich (81381)
NaCl	Roth (9265.2)
N-ethylmaleimide (NEM)	Sigma-Aldrich (E1271)
N-Hydroxysuccinimide	Fluka (56480)
Pefabloc® SC-protease-inhibitor	Roth (A154.3)
PEI MAX® transfecting grade linear polyethylenimine hydrochloride (MW 40,000)	Polysciences Inc. (24765-100)
pepstatin A	Sigma-Aldrich (H4502)
PMSF (phenylmethanesulfonyl fluoride)	Sigma-Aldrich (P7626)
Ponceau S (C.I. 27195)	Roth (5938.1)
powdered milk, low-fat	Roth (T145.2)
ROTIPHORESE®Gel 40 (37.5:1), 40 %	Roth (T802.1)
$SrCl_2$ hexahydrate	Roth (4473.1)
SYTO13™ (Green)	Invitrogen (S7575)
Tris-HCl (Tris(hydroxymethyl)-aminomethan) Pufferan®	Roth (9090.4)
Tween®20	Roth (9127.1)

4.1.1.2 Reagents, kits, miscellaneous items

Product name	Manufacturer/Distributor
10 x DNA Loading Buffer	Invitrogen
10 x FastDigest Green Buffer	Thermo Scientific
5 x FIREPol® Master Mix (12.5 mM $MgCl_2$)	Solis BioDyne (04-11-00125)
cOmplete	Roche (11697498001)
Glutathione Sepharose™ 4B	Cytiva (17075601)
LysoTracker™ Red DND-99	Invitrogen (L7528)
NucleoBond® Xtra Maxi EF	Macherey-Nagel (740424.50)
MagicRed ® Cathepsin-B Assay Kit	ImmunoChemistry Technologies (800-829-3194)
Midori Green Advance DNA stain	NIPPON Genetics Europe (MG04)
NucleoSpin®Gel and PCR Clean-up	Macherey-Nagel (740609.250)
NucleoSpin® Plasmid EasyPure	Macherey-Nagel (740727.250)
PageRuler™ Prestained Protein Ladder	Thermo Scientific (26616)
PageRuler™ Unstained Protein Ladder	Thermo Scientific (26614)
Polybead® carboxylate microspheres 1.00 µm	Polysciences Inc.
Protein Assay Dye Reagent Concentrate	Bio-Rad (5000114)
Protino® Ni-NTA Agarose	Macherey-Nagel
Quick-Load® 1 kb DNA Ladder	New England Biolabs Inc. (NO468S)
Quick-Load® 100 bp DNA Ladder	New England Biolabs Inc. (NO467S)
ROTI®NC, transfer membrane, roll	Roth (HP40.1)

4.1.1.3 Enzymes

Enzyme	Manufacturer/Distributor
creatine kinase	Roche (16166420)
proteinase K	Roth (7528.2)
SacII	NEB (R0157S)
T4-DNA ligase (200,000 CEU) 5 Weiss U/µL	Thermo Scientific
XhoI	NEB (R0146S)

4.1.1.4 Cell culture medium and solutions

Medium/Solution	Composition/other	Manufacturer
DMEM	3.7 g/L $NaHCO_3$, 4.5 g/L D-glucose, no additives, sterile filtrated	PAN Biotech
DMEM	4.5 g/L D-glucose, no additives, sterile filtrated	Gibco
Pen Strep	10,000 Units/mL penicillin, 10,000 µg/mL streptomycin	Gibco
sodium pyruvate	100 mM, sterile filtrated	PAN Biotech
stable glutamine	200 mM, sterile filtrated	PAN Biotech
trypsin/EDTA	0.25 % trypsin, 0.02 % EDTA in PBS, sterile filtrated	PAN Biotech
FBS	F7524, Lot. 035M3394, sterile	Sigma-Aldrich
FBS	P30-3306, Lot. P190702, sterile filtrated	PAN Biotech

4.1.2 Special devices

Device	Manufacturer
Apotome 2	Zeiss
Axio Observer.Z1 epifluorescence microscope	Zeiss
AxioPlan epifluorescence microscope	Zeiss
Dounce Dura-grind™ stainless steel homogenizer	Zinsser Analytic
Dynal™ magnetic rack	Invitrogen
Optima L-XP 80 ultracentrifuge	Beckman & Coulter
Optima Max Ultracentrifuge	Beckman & Coulter
SW40TI-40,000 RPM (Rotor)	Beckman
TLA 55K RPM S/N 19U1521 (Rotor)	Beckman & Coulter

4.1.3 Software

Programm	Publisher
BioRender	Science Suite Inc.
CorelDRAW	Corel Corporation
FIJI (Image J)	Open Source [291,292]; https://imagej.nih.gov/ij/
Image J plugin JACoP	[293]; https://imagej.nih.gov/ij/plugins/ track/jacop.html
Origin Pro 8G	OriginLab Corporation
MS Office	Microsoft
MS Excel	Microsoft
Zotero	Corporation for Digital Scholarship [294] https://www.zotero.org/support/credits_and_acknowledgments

All illustrations and schematics were created using BioRender.com, with a student plan. Figures were assembled in CorelDRAW with 600 dpi resolution. Bar plots and curve plots were generated in Origin Pro 8G, calculations were carried out in MS Excel. Quantifications of immunoblots were performed using FIJI. Quantifications of micrographs were carried out using FIJI and the JACoP plugin [291,293].

.

4.1.4 Antibodies

All antibodies used for immunoblotting were prepared in a solution of 2 % (w:v) powdered milk in PBS-T (140 mM NaCl, 10 mM Na_2HPO_4, 1.8 mM KH_2PO_4, 2.7 mM KCl, 0.05 % (v:v) Tween®20) and diluted as indicated below.

4.1.4.1 Primary antibodies

Antibody against	Host Species	Clonality	Manufacturer	Catalogue No	Dilution
lyspersin	rabbit	polyclonal	Abcam	ab247064	1:500
Arl8 a/b	mouse	monoclonal	Santa Cruz	sc-398635	1:500
Arl8b	rabbit	polyclonal	Proteintech	13049-1-AP	1:1000
cathepsin B	rabbit	polyclonal	Santa Cruz	sc-365558 (discontinued)	1:250
Cathepsin D	mouse	monoclonal	Santa Cruz	sc-377124	1:250
Cathepsin D	rabbit	polyclonal	Sigma-Aldrich	219361	1:250
TfR	mouse	monoclonal	Santa Cruz	sc-65882	1:500
EEA1	rabbit	monoclonal	Thermo Scientific	MA5-14794	1:500
LAMP1	mouse	monoclonal	Santa Cruz	sc-20011	1:500
LOH12CR1/myrlysin	rabbit	polyclonal	Proteintech	17169-1-AP	1:1000
Myoferlin	rabbit	polyclonal	Novus Biologicals	NBP1-84694	1:500
Rab2a	rabbit	polyclonal	Proteintech	15420-1-AP	1:1000
Rab7a	rabbit	polyclonal	T. Watts (University of Toronto, Toronto, ON, Canada) [295]		1:500
Synaptotagmin-7	rabbit	polyclonal	Synaptic Systems	105173	1:1000
Vps39	mouse	monoclonal	Santa Cruz	sc-514762	1:500
Vps41	mouse	monoclonal	Santa Cruz	sc-377118	1:500

4.1.4.2 Secondary antibodies

Species reactivity	Conjugate	Host species	Clonality	Specificity	Manufacturer	Dilution
rabbit	HRP-coupled	goat	polyclonal	IgG (H+L)	Jackson ImmunoResearch (115-035-062)	1:5000
mouse	HRP-coupled	goat	polyclonal	IgG (H+L)	Jackson ImmunoResearch (111-035-003)	1:5000

4.1.5 Plasmids and oligonucleotides

4.1.5.1 Bacterial expression plasmids

Name	Origin	Parental plasmid	Description	Source
pGEX-4T1 SidC P4C	*Legionella pneumophila*	pGEX-4T1	P4C fragment from SidC	provided by H. Hilbi [296](University Zurich)
pGEX-4T3-hArl8b	human	pGEX-4T3	hArl8b	[182]
pGEX-2xFYVE	mouse	pGEX-5X-3 (Pharmacia)	2xFYVE-GST	provided by W. Wickner [297] (Geisel School of Medicine, Dartmouth)
pGEX-4T1	*Schistosoma japonicum*	pGEX-4T-1	GST from Schistosoma japonicum	-
pRSET-RabGDI-His_6	cow	pRSET A (Invitrogen)	Bovine RabGDI (AA 1-407)	provided by O. Ullrich, [298] (Heidelberg University)
sol Syntaxin 8-His_6	rat	pET28a (Novagen)	Syntaxin 8 (AA 1-213)-His_6	provided by R. Jahn [299]
sol Vti1b-His_6	mouse	pET28a (Novagen)	Vti1b (AA 1-206)-His_6	R. Jahn [299]
Syntaxin7 Delta TM	rat	pGEX-4T2 (Amersham Bioscience)	Syntaxin 7 (AA 1-238)-GST	D. Langosch [122] (Technical University of Munich)
VAMP7-longin-His_6	human	pET15b	N-terminal ~120 AA of R-SNARE VAMP7/TI-VAMP	From T. Galli [300] (Institute of Psychiatrie and Neuroscience, Paris)
α-SNAP WT-His_6	Bovine/ human	pET28b (Novagen)	α-SNAP DNA (from pQE-9 α-SNAP) was cloned into NdeI/HindIII-digested pET28 [301]; pQE-9 sequence matched human α-SNAP [301]	Provided by Phyllis Hanson (University of Michigan)
α-$SNAP^{L294A}$-His_6	-	pET28b (Novagen)	dominant negative α-SNAP mutant, which fails to activate NSF ATP-hydrolase activity [302]	Provided by Phyllis Hanson (University of Michigan)

4.1.5.2 Mammalian expression plasmids

Name	Origin	Parental plasmid	Description	Source
hArl8b-pmCherry-N1	human	pmCherry-N1	hArl8b sequence was amplified from pGEX-4T3-hArl8b with restriction sites for Sac II and Xho I; mCherry tag is located at C-terminus	hArl8b insert was amplified from pGEX4T3-hArl8b [182]

4.1.5.3 Oligonucleotides

Designation	Sequence	Fragment size
hArl8b_fwd_XhoI	5'-TAAGCACTCGAGATGCTGGCGCTCATCTCC-3'	561 bp
hArl8b_rev_SacII	5'-TGCTTACCGCGGGCTTCTTCTAGATTTTGAATGCTGA-3'	

4.1.6 Mammalian cell lines

Designation	Cell line	Organism	Description
J774E	macrophage -like cells	murine	Established from tumour tissue of a female BALB7c mouse, high expression of mannose receptor [303,304], obtained from P.D. Stahl (Washington University, St. Louis, USA)
HeLa WT	HeLa	human	Parental wild type cell line, obtained from J. Bonifacino (National Institute of Child Health and Human Development, Bethesda, Maryland, USA)
Arl8b KO	HeLa	human	HeLa cells, deficient for Arl8b [189]
Arl8a/ Arl8b DKO	HeLa	human	HeLa cell line deficient for Arl8a/Arl8b [163]
Vps41 KO	HeLa	human	HeLa cell line deficient for Vps41 [305]
myrlysin KO	HeLa	human	HeLa cell line deficient for BORC subunit myrlysin[169]
diaskedin KO	HeLa	human	HeLa cell line deficient for BORC subunit diaskedin [187]
HeLa WT (Kiel)	HeLa	human	Parental wild type cell line of Rab7a KO, provided by P. Saftig (Biochemical Institute, University of Kiel, Kiel, Germany)
Rab7a KO	HeLa	human	Rab7a gene was inactivated using the CRISPR/Cas9 system. SgRNA sequence: UGAAUUUCUUAUUCACAUAC (Synthego), cells were provided by P. Saftig (Biochemical Institute, University of Kiel, Kiel, Germany)
Rab2a 1A12 KO	HeLa	human	sgRNA RAB2A + 60591915 GAAGCUUUUGCACGAGAACA sgRNA RAB2A - 60591929 AGAACAUGGACUCAUCUUCA mixed clones were provided by P. Saftig (Biochemical Institute, University of Kiel, Kiel, Germany) and selected by A. Schleinitz
Rab2a 1G6 KO	HeLa	human	sgRNA RAB2A + 60591915 GAAGCUUUUGCACGAGAACA sgRNA RAB2A - 60591929 AGAACAUGGACUCAUCUUCA mixed clones were provided by P. Saftig (Biochemical Institute, University of Kiel, Kiel, Germany) and selected by A. Schleinitz

Knockout of indicated genes was confirmed by immunoblotting.

4.1.7 Bacterial strains

Bacterial strains were either used for efficient protein expression of recombinant proteins or production of plasmid DNA.

Strain	Description	Manufacturer
E. coli BL21 (DE3)	T7 expression strain, deficient in proteases Lon and OmpT (C3010)	New England BioLabs Inc.
NEB® 5**α** Competent *E. coli* (high efficiency)	Cloning strain, derivative of DH5α (C2987)	New England BioLabs Inc.

4.2 Methods

4.2.1 Cell culture

4.2.1.1 Cultivation of mammalian cells

J774E macrophage-like cells were cultivated in DMEM/FBS containing 5 % (v:v) FBS, 1 % (v:v) stable glutamine, 1 % (v:v) Pen Strep and HeLa cells in DMEM/FBS containing 5 % (v:v) FBS, 1 % (v:v) stable glutamine, 1 % (v:v) Pen Strep, 1 % (v:v) sodium pyruvate at 37 °C in a humid atmosphere with 5 % CO_2. FBS was heat-inactivated for 1 h at 56 °C before use. Medium additives were sourced as indicated in Chapter 4.1.1.4. For simplicity, medium used for J774E cells or HeLa cells will be referred to as DMEM/FBS without further distinction.

4.2.1.2 Passaging of HeLa cells

To passage HeLa cells when confluence was achieved, the cell culture medium was removed and cells were washed once with phosphate buffered saline (PBS) (140 mM NaCl, 10 mM Na_2HPO_4, 1.8 mM KH_2PO_4, 2.7 mM KCl). To remove the adherently growing cells from the surface of a 10 cm cell culture dish, they were incubated in 1 mL trypsin (PAN Biotech) for 5 min. The cells were suspended in DMEM/FBS and diluted to the desired ratio (usually 1:4). 1 mL of the suspension was added to a new cell culture dish with 7 mL of fresh DMEM/FBS.

4.2.1.3 Passaging of J774E macrophage-like cells

The cell culture medium was discarded and 1 mL of fresh DMEM/FBS added to the cell culture dishes. The cells were removed from the dishes carefully, using a rubber policeman, collected in a 50 mL centrifugation tube and diluted in a 1:2 ratio. 1 mL of cell suspension was added to a new cell culture dish with 7 mL DMEM/FBS.

4.2.1.4 Cryoconservation of mammalian cells

For long term storage J774E and HeLa cells were kept at -80 °C. Cells were removed from the surface of cell culture dishes either by using a rubber policeman or trypsinisation. The cells were pooled in a 50 mL centrifugation tube and sedimented (440 rcf, 4 °C, 5 min). DMEM/FBS was discarded, and cells were resuspended in DMEM/FBS/10 % (v:v) DMSO (sterile) and transferred to cryo tubes.

4.2.2 Chemical methods

4.2.2.1 Coating of latex beads with BSA

Latex beads used for fusion assays were chemically conjugated with bovine serum albumin (BSA). All steps were performed at ambient temperature (AT). 320 µL of carboxylate latex bead suspension (Ø 1 µm, Polysciences) per aliquot were sedimented for 5 min at 17,000 rcf. The beads were washed thrice with 4-morpholinoethane sulfonic acid (MES) buffer (72.5 mM MES, pH 6.8) and spun down at full speed for 1 min after each washing step. Beads were resuspended in 220 µL MES buffer and 100 µL of a 1 mg/mL BSA/ddH_2O solution was added. The suspension was incubated for 15 min at ~ 700 rpm, on a rocker. 6.4 µL of a freshly prepared 10 mg/mL N-(3-Dimethylaminopropyl)-N'-ethylcarbodiimide hydrochloride (EDAC)/ ddH_2O solution was added and incubated at ~ 700 rpm. After 1 h another 6.4 µL of 10 mg/mL EDAC/ddH_2O were added and incubated for another hour. The reaction was stopped by adding 12.8 µL 1.5 M Tris-HCl, pH 6.8. The beads were washed thrice in PBS (17,000 rcf, 1 min) and stored in 10 mg/mL BSA/PBS, supplemented with 0.01 % sodium azide at 4 °C.

4.2.2.2 Preparation of fluorescently labelled BSA or dextran

5(6)-carboxy-tetramethyl-rhodamine-BSA was prepared as stated in Sydor et al., 2008. Alternatively, 5(6)-carboxy-tetramethyl-rhodamine-10 K dextran (TAMRA-dextran) was prepared, using amino dextran MW 10,000 instead of BSA.

ATTO488 10 K amino dextran (ATTO488-dextran) was prepared by dissolving 5 mg/mL amino dextran MW 10,000 and 0.1 M $NaHCO_3$ in ddH_2O. Once fully dissolved, 5 mg/mL ATTO 488-NHS/DMSO was added to a final concentration of 0.108 mg/mL. The mixture was incubated on a rocker for 3 h at AT. ATTO488-dextran was dialyzed against PBS in a ratio of 1:1000 for approximately 16 h at 4 °C.

4.2.3 Moleculargenetic methods

4.2.3.1 Purification of plasmid DNA from *E. coli* DH5α

Plasmid DNA was purified, using either Mini- or Maxi prep kits from Macherey-Nagel as specified in the user manual.

4.2.3.2 Cloning of pmCherry-N1-hArl8b construct

To visualize Arl8b in HeLa cells human Arl8b was cloned into the pmCherry-N1 plasmid, to generate an Arl8b-mCherry fusion protein. To not disturb the membrane interaction of Arl8b through its N-terminal acetylation, the mCherry protein was located at the C-terminus of Arl8b.

4.2.3.2.1 Amplification of insert DNA from pGEX4T3-hArl8b

DNA encoding for human Arl8b was amplified from pGEX4T3-hArl8b vector [100] using primers as specified in Chapter 4.1.5.3. The primers were designed to add restriction sites for SacII and XhoI, for easy cloning of the construct. Polymerase chain reaction (PCR) was carried out in a standard reaction volume of 25 µL as shown in Table 4.1. The PCR program used is displayed in Table 4.2. The yielded PCR-products were further analysed on agarose gels.

Table 4.1: Standard PCR reaction mix.

Components	Volume [µL]
5 x FIREPol® Master Mix	5
Primer_fwd (10 pM)	0.625
Primer_rev (10 pM)	0.625
Template (62.5 ng)	0.375
ddH_2O	18.375

Table 4.2: PCR program for amplification of hArl8b.

Temperature [°C]	Time	
95	3 min	
95	30 sec	30 x
63	30 sec	
72	2 min	
72	10 min	
4	∞	

4.2.3.2.2 Colony polymerase chain reaction (PCR)

To analyse transformants yielded from transforming ligation product in *E. coli* DH5α (see Chapter 4.2.4.1) single colonies were picked from agar plates and resuspended in 20 µL sterile water. 10 µL of bacteria suspension were used to inoculate a 4 mL culture in lysogeny broth (2 % (w:v) LB (Lennox)) with either 100 µg/mL ampicillin or kanamycin. The cultures were grown at 37 °C, 200 rpm, overnight. Standard PCRs were carried out as specified in Chapter 4.2.3.2.1 and the PCR product separated by agarose gel electrophoresis. If bands were present

at the appropriate molecular weight, DNA was purified from the respective bacteria cultures and the validity of the sequence confirmed by Sanger-sequencing (Eurofins).

4.2.3.2.3 Agarose gel electrophoresis

To analyse PCR products, the amplificants were separated through agarose gel electrophoresis. The gels were prepared with 1 % (w:v) agarose in Tris-acetate-EDTA (TAE) buffer (40 mM Tris, 20 mM acetic acid, 1 mM EDTA) and stained with Midori green. The gels were run at 100 V for 30 min. As size standard either 100 bp DNA ladder, or 1 kb DNA ladder (Chapter 4.1.1.2) was used. To visualize the amplificants, the gel was placed on an UV-table. Bands with the correct molecular weight were harvested using a scalpel and the DNA was subsequentially extracted with Nucleospin®Gel and PCR Clean-up kit (Macherey-Nagel).

4.2.3.2.4 Digestion and ligation of pmCherry-N1 and hArl8b PCR amplicon

For molecular cloning of the hArl8b-pmCherry-N1 construct, 5 µg of pmCherry-N1 plasmid DNA, as well as the hArl8b PCR amplicon were digested with XhoI and SacII. The digestion was carried out in a water bath at 37 °C, overnight. After digestion, the DNA fragments were cleaned using the Nucleospin®Gel and PCR Clean-up kit according to the manufacturer's directions. For ligation, plasmid backbone and insert DNA were combined in a molecular ratio of 1:5 (see Table 4.3).

Table 4.3 Composition of ligation mixture for molecular cloning of hArl8b-pmCherry-N1.

Component	Amount
pmCherry-N1	100 ng
hArl8b	59.4 ng
T4-ligase buffer	2 µL
1 U T4-ligase	0.2 µL
ddH_2O	Adjust to 20 µL

The ligation was carried out in a water bath at 37 °C, for 20 min. After ligation, 5 µL of ligation product were used for heat shock transformation (Chapter 4.2.4.1). The bacteria were plated on agar plates (2 % (w:v) LB (Lennox), 1.5 % (w:v) agar-agar) containing either 100 µg/mL ampicillin or kanamycin. Transformants were checked for insert DNA by colony PCR (Chapter 4.2.3.2.2).

4.2.4 Molecular biological methods

4.2.4.1 Heat shock transformation of *E. coli*

Heat shock competent *E. coli* were placed on ice and thawed for approximately 30 min, and mixed with 1 µg of plasmid DNA. The bacteria were incubated with the plasmid DNA for another 30 min and placed in a water bath (42 °C, 42 sec) for heat shock. Bacteria were placed on ice for another 5 min, resuspended in 1 mL of LB medium and incubated for 1 h, 37 °C on a rocker. Transformants were selected by plating the bacteria on LB/agar plates with either 100 µg/mL kanamycin or ampicillin and incubating overnight at 37 °C.

4.2.4.2 Cryoconservation of *E. coli*

E. coli containing plasmid DNA of interest, validated by sequencing were kept as glycerol-stocks for long term storage. 4 mL LB, containing 100 µg/mL of either kanamycin or ampicillin were inoculated with a single transformant and cultivated at ~ 200 rpm, 37 °C, overnight. 600 µL of bacteria suspension were transferred to a cryo tube and mixed with 400 µL 50 % glycerol (sterile filtrated). The cryo culture was stored at -80 °C.

4.2.4.3 Heterologous expression of recombinant proteins in *E. coli* BL21 (DE3)

Recombinant proteins used in fusion experiments were expressed in *E. coli* BL21 (DE3). Precultures were prepared in 15 mL LB containing 100 µg/mL of either kanamycin or ampicillin and inoculated with a sterile inoculation loop from glycerol stocks. The precultures were incubated at ~ 200 rpm, 37 °C, ~ 16 h. The resulting culture was used to inoculate the expression culture in a ratio of 1:30. The culture was placed on a rocker at ~ 200 rpm, 37 °C for approximately 3 h before inducing by adding 1 M IPTG/ddH_2O to a final concentration of 1 mM. Expression continued for either ~ 16 h at ~ 200 rpm, 16 °C or 5 h at ~ 200 rpm, 37 °C.

4.2.4.4 Purification of GST-or His_6-tagged proteins

After heterologous expression of recombinant proteins, the bacteria were harvested at 6,000 rcf, 10 min, 4 °C. Supernatant was discarded and the cell pellets either used directly or stored at -20 °C until purification.

4.2.4.4.1 Purification of GST-tagged recombinant proteins

Cells were resuspended in 30 mL PBS, containing 1 mM PMSF (100 mM/2-propanol) and lysed by sonication at 4 °C. Cell homogenates were centrifuged in 2 mL reaction tubes at 17,000 rcf, 4 °C for 30 min. The supernatant was collected in a 50 mL centrifugation tube.

1 mL of glutathione-sepharose was washed with PBS thrice and added to the supernatant. The centrifugation tube was placed on a mixing rotor for 1 h at 4 °C. The glutathione-sepharose was sedimented (1780 rcf, 4 °C, 2 min), using a swing-out rotor and the supernatant was discarded. This step was repeated twice. For elution, glutathione-sepharose was resuspended in 10 mL PBS and loaded onto a disposable polypropylene column. The column was placed on 1.5 mL reaction tubes and the protein of interest eluted in 6 x 500 µL elution buffer (20 mM Tris (pH 8.0), 10 mM glutathione (freshly added)). Protein concentrations of the respective elution fractions were determined (Chapter 4.2.6.2). Relevant fractions were pooled and dialyzed against an excess of homogenization buffer (HB (8.6 %) (250 mM sucrose, 20 mM HEPES (pH 7.2)) for approximately 16 h at 4 °C. The protein solution was aliquoted as needed, snap frozen in liquid nitrogen, and stored at -80 °C.

4.2.4.4.2 Purification of His_6-tagged recombinant proteins

The cell pellet was resuspended in 30 mL IMAC-lysis buffer (50 mM $NaH_2PO_4xH_2O$, 300 mM NaCl (pH 8.0)), containing 1 mM PMSF (100 mM/2-propanol) and homogenized by sonication at 4 °C. Cell lysates were centrifuged at 17,000 rcf, 4 °C for 30 min. 1 mL of Ni-NTA agarose was washed thrice with IMAC-lysis buffer and added to the supernatant, which was incubated on a mixing rotor for 1 h at 4 °C. The Ni-NTA agarose matrix was sedimented (1780 rcf, 4 °C, 2 min), using a swing-out rotor. The supernatant was discarded and the Ni-NTA agarose washed twice with washing buffer (50 mM $NaH_2PO_4xH_2O$, 300 mM NaCl, 20 mM imidazole (pH 8.0)). For elution, the Ni-NTA agarose was resuspended in 10 mL washing buffer and loaded onto a disposable polypropylene column. The column was placed on 1.5 mL reaction tubes and the bound proteins were eluted in 6 fractions of 500 µL each (50 mM $NaH_2PO_4xH_2O$, 300 mM NaCl, 250 mM imidazole (pH 8.0)). The protein concentrations of the respective fractions were determined (Chapter 4.2.6.2) and viable fractions pooled and dialyzed against HB (8.6 %) overnight at 4 °C. After dialysis, the protein solutions were aliquoted, snap frozen in liquid nitrogen, and stored at -80 °C. soluble SNARE domains were dialysed against HB/1xSalt (300 mM NaCl, 250 mM sucrose, 20 mM HEPES (pH 7.2), 1.5 mM $MgCl_2$) to ensure solubility of the proteins.

4.2.4.5 Selection of CRISPR/Cas9-manipulated HeLa knockout mutants

To study the effects of a Rab2a knockout, HeLa cells were genetically modified using the CRISPR/Cas9 system. Serial dilutions of the mixed clones were seeded on 96 well plates and cultivated in DMEM/FBS. Wells in which only one distinct colony of HeLa cells was present

were propagated until three confluent cell culture dishes (Ø 10 cm) were obtained. The cells of one confluent dish were harvested and stored as frozen cryo culture (Chapter 4.2.1.4). A second dish served as backup, in case the cryo culture was not viable. To check whether the selected single clones were deficient of the proteins of interest (POI), RIPA-lysates were prepared (Chapter 4.2.6.1) and analysed via SDS-PAGE and immunoblotting (Chapters 4.2.6.3 & 4.2.6.5).

4.2.4.6 Transfection of HeLa cells with PEI Max®

For ectopic expression of proteins in HeLa cells, PEI Max® was used. The reagent was prepared as aqueous 1 mg/mL solution and the pH adjusted to 7.0, with 0.1 M NaOH. The transfection reagent was stored at 4 °C for up to one month. The cells were passaged the day prior to transfection to achieve optimal confluence of the cells (40 – 60 %). A PEI-DNA mixture was prepared in DMEM/FBS at a 1:3 (w:v) DNA to PEI ratio, using 5 µg of plasmid DNA per cell culture dish. The total volume of PEI-DNA mixture was 120 µL per transfected dish (Ø 10 cm). The mixture was incubated for 20 min at AT to allow for complexation of PEI with plasmid DNA. The transfection mixture was added to the cells and incubated overnight at 37 °C, 5 % CO_2. The old cell culture medium was discarded and fresh DMEM/FBS added to the cells. Incubation continued for another 24 h, at 37 °C, 5 % CO_2 before experiments were conducted.

4.2.4.7 Labelling of endocytic compartments with ferrofluid in HeLa cells

To be able to purify endocytic compartments of different maturation stages or LYS from HeLa cells, compartments were labelled with paramagnetic 10 nm ferrofluid particles (FF). Thereto, 10 µL of FF per cell culture dish were diluted in an appropriate amount of DMEM (1 % (v:v) stable glutamine, 1 % (v:v) Pen Strep, 1 % (v:v) sodium pyruvate) and sonicated for approximately 30 sec. The FF suspension was sterile filtrated, using a Ø 0.2 µm syringe filter and diluted to a final volume of 2.5 mL DMEM/FF (pulse medium) per cell culture dish. The pulse medium, along with 3 mL DMEM/FBS (chase medium) per cell culture dish, was preheated to 37 °C in a water bath before use. Cells were washed once with 3 mL PBS (see Chapter 4.2.1.2) per dish, before 2.5 mL of pulse medium per dish were applied and incubated for 30 min at 37 °C (pulse). The medium was discarded, and cells were washed twice with 3 mL PBS. 3 mL of DMEM/FBS were added to the cells and incubated for 120 min, at 37 °C. The cells were harvested in 2 mL cold PBS, using a rubber policeman, and collected in 50 mL centrifugation tubes (on ice). Cells were washed sequentially in PBS, PBS/5 mM EDTA, and HB (8,6 %)/EGTA (250 mM sucrose, 20 mM HEPES (pH 7.2), 0.5 mM EGTA (pH 8.0),

pH 7.2), for 5 min, 1780 rcf and 4 °C. The cells were resuspended in 2 mL HB (8,6 %)/EGTA, with 40 µL of cOmplete, before they were homogenized with 20 strokes in a Dounce homogenizer. The lysate was collected in 15 mL centrifugation tubes (on ice) and spun down for 5 min, 600 rcf, at 4 °C. The resulting post nuclear supernatant (PNS) was collected, 100 µL PNS per sample were kept for later analysis and the rest was transferred to 1.5 mL reaction tubes mounted on a magnetic rack. Supernatants were incubated on a rocker at 4 °C for 30 min. FF-containing endocytic compartments were harvested and the supernatants discarded. To analyse PNS and endocytic fractions for POI, the protein concentrations were determined (Bradford Assay, Chapter 4.2.6.2) and samples for SDS-PAGE were prepared (Chapters 4.2.6.3). The POI were detected, as specified in Chapter 4.2.6.5.

4.2.4.8 Labelling of endocytic compartments with paramagnetic ferrofluid particles and CTMR-BSA in J774E macrophages

To analyse the extent of fusion events between phagosomes and lysosomes in an *in vitro* experimental setup, lysosomes were labelled with CTMR-BSA (see Chapter 4.2.2.2) and FF, allowing for purification and subsequent detection with a fluorescence microscope. This procedure was done, as previously described in Jeschke et al., 2015. Cells were preloaded with 100 mg/mL CTMR-BSA in DMEM/FBS the day before the experiment and incubated overnight at 37 °C, 5 % CO_2. In parallel, an FF suspension (10 µL per dish) was prepared in 10 mg/mL BSA/PBS and incubated on a rocker at 4 °C overnight. Cells were treated, as specified in Chapter 4.2.4.7, until the cells were harvested. Dissident from Chapter 4.2.4.7, the cells were sequentially washed twice with PBS and twice with HB (8.6 %) (Chapter 4.2.4.7), resuspended in 2 mL HB (8.6 %), and supplemented with 40 µL of 50 x protease inhibitor cocktail (PIC) (1 µM leupeptin, 0.75 mM 1,10-phenantroline, 1 µM pepstatin A, 1 mM pefabloc). The cells were homogenized with 20 strokes in a Dounce homogenizer. The volume of the homogenate was adjusted to 10 mL with HB (8.6 %) and centrifuged for 5 min at 800 rcf and 4 °C. The supernatant was transferred to 1.5 mL reaction tubes mounted on a magnetic rack. Lysosomes were harvested as described in Chapter 4.2.4.7. For the fusion experiment, the concentration of LYS was adjusted to 3 µg/µL. The compartments were stored on ice until used.

4.2.4.9 Preparation of latex bead phagosomes (LBP) from J774E macrophages

To distinguish lysosomes from phagosomes, J774E macrophage cells were preloaded with 1 µm BSA-coated latex beads [8] (Chapter 4.2.2.1). 320 µL of BSA-coated latex bead suspension was washed thrice in PBS (17,000 rcf, 1 min, AT) and diluted in 25 mL DMEM without additives. The medium was preheated to 37 °C in a water bath. Cells from ten confluent cell

culture dishes (Ø 10 cm) were washed once with 5 mL PBS/dish, before adding 2.5 mL of latex bead suspension to each dish. The cells were incubated for 30 min (pulse period), at 37 °C, 5 % CO_2, in parallel to the cells in Chapter 4.2.4.8. Cells were washed thrice with 5 mL PBS/dish and 3 mL of preheated DMEM/FBS were added to each cell culture dish. The cells were incubated for 1 h, 37 °C (chase period), harvested in 2 mL of cold PBS, and stored on ice. Cells were washed as described in Chapter 4.2.4.8. For homogenisation, the cells were resuspended in 2 mL of HB (8.6 %)/1 x PIC and homogenised with 15 strokes in a Dounce homogenizer. PNS was prepared and mixed with 2 mL of HB (62 %) (1.75 M sucrose, 20 mM HEPES (pH 7.2)). The mixture was overlayed with 5 mL HB (25 %) (730 mM sucrose, 20 mM HEPES (pH 7.2)) and 3 mL HB (8.6 %) and centrifuged in a SW40 Ti rotor for 1 h at 42,000 rcf, 4°C. LBPs were harvested from the interphase of the 25 % and 8.6 % HB solutions.

4.2.4.9.1 Preparation of cytosolic proteins from J774E macrophages

For standard fusion (StaFu) experiments, the presence of soluble cytosolic proteins (Cyt) is required (cf. Jeschke et al., 2015). To prepare Cyt, cells from 100 confluent cell culture dishes (Ø 10 cm) were harvested in 2 mL of cold PBS (see Chapter 4.2.1.2) per dish. The cells were sedimented and the supernatant discarded. After that, the cells were sequentially washed with PBS, PBS/5 mM EDTA, and twice with HB (8.6 %) (see Chapter 4.2.4.7) for 5 min at 440 rcf, 4 °C. The cell pellet was resuspended in a total volume of 4 mL HB (8.6 %) and 50 x PIC was added in a 1:49 ratio. The cells were homogenised with 20 strokes, using a Dounce homogenizer and the homogenate centrifuged for 1 h at 150,000 rcf, 4 °C. The supernatant was transferred to a new 1.5 mL reaction tube, a 1:9 dilution prepared. The protein concentration was determined as described in Chapter 4.2.6.2. The concentration was adjusted to 18 or 15 µg/µL (depending on protein concentration of supernatant), aliquoted, and snap frozen in liquid nitrogen. Cytosol was stored at -80 °C.

4.2.4.10 *In vitro* fusion of endocytic compartments with LBP

Cell free fusion experiments were performed as in [2,8]. 12 µg of CTMR-BSA and FF labelled LYS and LBPs were incubated in a fusion-promoting reaction mixture. Fusion of LBP with LYS resulted in colocalization of red fluorescence signal with a latex bead. The composition of a regular Ca^{2+}-dependent (CaFu) and standard fusion (StaFu) reaction mixture is shown in Table 4.4. If possible, all solutions and buffers were prepared in HB. Additionally, CaFu reaction mixes must not contain chelators as EDTA or EGTA, to avoid discrepancies in free [Ca^{2+}]. To allow for ATP-dependent processes to happen, an ATP regenerating system was

added to StaFu reactions (and some CaFu controls). For the ATP regenerating system, a 12 mM ATP solution was prepared in 1 mL HB (8.6 %) and the pH adjusted to 7.0, with KOH. After that, 26 mg creatine phosphate (12 mM end concentration), 10 µL of a 1 M $MgCl_2$ (10 mM), and 1 mg creatine kinase (~ 800 U at 37 °C) from rabbit muscle (Chapter 4.1.1.3) were added. To assess and compare differing characteristics of CaFu and StaFu, both reactions were carried out in parallel. Samples were treated with different pharmacological drugs or recombinant protein(fragments), as specified in the respective results Chapters. Aberrantly to the standard CaFu fusion mixes, experiments carried out with ions other than Ca^{2+} (i.e. Sr^{2+}) or with a range of different Ca^{2+} concentrations were prepared without ADA.

Table 4.4 Composition of standard Ca^{2+} fusion and standard fusion reaction mixtures.

Components	**Standard fusion [µL]**	**Calcium fusion [µL]**
Endocytic compartments 3 µg/µL	4	4
LBP	4.7	4.7
10 x Salt (15 mM $MgCl_2$, 1 M KCl)	3	3
100 nM DTT	0.3	0.3
10 x ATP regenerating system	3	3
15 µg/µL cytosol	4	-
1.8 mM $CaCl_2$	-	2
50 mM EGTA	0.3	-
10 mM ADA	-	3
HB (8.6 %)	ad. to 30	ad. to 30

Fusion reactions were carried out at 37 °C in a water bath for either 10 min (CaFu) or 60 min (StaFu). After incubation, the samples were cooled on ice for approximately 5 min. Samples were treated with 0.3 µL of a 20 µg/µL proteinase K solution and incubated on ice for 15 min. The digestion was stopped by adding 1.5 µL of a 100 mM PMSF/2-propanol solution. 180 µL HB (8.6 %) were added and mixed thoroughly. 200 µL of the reaction mix were placed on a sucrose cushion (HB (25 %)) and centrifuged for 30 min at 1780 rcf and 4 °C. 200 µL of latex beads/fusion product were collected from the interphase and added to a well (24 well plate), equipped with a coverslip and preloaded with 350 µL of a 5 µg/µL BSA solution in HB (8.6 %). The fusion product was centrifuged onto the coverslips (30 min, 1780 rcf, 4 °C). The supernatant was discarded, and the samples fixated overnight in a 4 % para-formaldehyde solution (4 % PFA/HB (8.6 %)). The coverslips were carefully removed from the wells and mounted on microscope slides with 2 µL Mowiol mounting liquid. The extent of fusion between LYS and LBPs was quantified by determining colocalization of red fluorescence signal with LBP for at least 300 latex beads per sample. Only fusion reactions with more than 3 % of

absolute fusion frequency in positive control samples were considered for analysis. Absolute fusion frequencies in positive controls (pos.ctrl.) typically ranged between 8-12 %. Colocalization frequencies are shown relative to their respective pos. ctrl. (**StaFu**: +ATP/+Cyt; **CaFu**: −ATP/−Cyt).

4.2.4.11 Attachment Assay

To assess whether a certain treatment affected the ability of endocytic compartments to bind to each other in a CaFu type reaction, an altered attachment assay protocol was used [9]. The endocytic compartments were prepared as described in Chapters 4.2.4.8 & 4.2.4.9. The reaction mixtures were mostly prepared as indicated in Chapter 4.2.4.10, with the exception that 100 µM of 1-lauroyl-2-hydroxy-sn-glycero-3-phosphocholine (LPC12) were added to each mix. LPC-12 is a cone-shaped glycerophospholipid that favours outward curvature of membranes. Therefore, it impedes the formation of a fusion stalk, SNARE complex assembly [307] and arrests two opposing membranes in a docked state. CaFu-attachment reactions were incubated for 10 min in a water bath. The samples were cooled on ice for 5 min. 30 µL of the samples were mixed with 30 µL of HB (62 %) and overlayed with 1 mL HB (25 %) and 200 µL HB (8.6 %). The small gradients were centrifuged for 30 min at 1780 rcf, 4 °C. 200 µL of LBP suspension were removed from the interface of the 25 % and 8.6 % HB and transferred. The samples were further processed as described in Chapter 4.2.4.10.To compare the extent of compartment fusion and attachment, an *in vitro* fusion assay with identical samples was carried out in parallel. At least 300 LBPs per sample were assessed for attachment of LYS.

4.2.4.12 Preparation of cytosolic and membrane fractions from whole cell lysates

To determine whether the POI's subcellular localization is cytosolic or membrane-bound, a subcellular fractionation of whole cell lysates was carried out. Three confluent cell culture dishes (Ø 10 cm) of HeLa cells were harvested in 2 mL (per dish) cold PBS and stored on ice in a 15 mL centrifugation tube. Cells were sequentially washed with 1 mL PBS/EDTA and HB (8.6 %)/EGTA (440 rcf, 5 min, 4 °C) and resuspended in 750 µL HB (8.6 %)/EGTA, supplemented with 1 x cOmplete. To prepare a PNS, the cells were homogenized with 20 strokes in a Dounce homogenizer, and the homogenates spun down at 800 rcf, 5 min, 4 °C. The protein concentration was determined (see Chapter 4.2.6.2), 60 µg of PNS were mixed with 5 x Laemmli buffer (60 mM Tris/HCl (pH 6.8), 25 % (v:v) glycerol, 5 % (v:v) 2-mercaptoethanol, 2 % (w:v) SDS, 0.1 % (w:v) bromophenol blue) and the sample boiled at 95 °C for 3 min. For the subcellular fractionation, 120 µg of protein were diluted to a final

volume of 750 µL HB (8.6 %)/EGTA and centrifuged in a TLA-55 rotor (186,000 rcf, 30 min, 4°C). Pellets (membrane fractions) were resuspended in 20 µL of 2 x Laemmli buffer (2:5 dilution of 5 x Laemmli buffer) and heated to 95 °C for 3 min. Supernatants (cytosolic fraction) were transferred to a fresh 1.5 mL reaction tube, adjusted to 12 % (v:v) trichloroacetic acid and mixed thoroughly. The proteins were precipitated overnight at 4 °C. Precipitated proteins were sedimented (16,100 rcf, 30 min, 4 °C) and the pellets resuspended in a small volume 2 x Laemmli buffer and neutralized by adding 1 M Tris base (pH 9.0). Samples were boiled at 95 °C for 3 min. The samples were analysed for their protein contents, using SDS-PAGE and immunoblotting.

4.2.5 Fluorometric and Microscopic assays

4.2.5.1 Staining of HeLa cells with Hoechst 33342 and LysoTracker™ Red/Magic Red®

HeLa cells (1.25×10^5) were seeded on an ibidi µ-slide 8 well cover slip and grown overnight (37 °C, 5 % CO_2). Cells were washed once with PBS and 200 µL DMEM/FBS/100 nM Lysotracker™ or Magic Red® were added per well. After incubation (37 °C, 5 % CO_2, 30 min), the cells were washed thrice with PBS. A 1 µg/mL solution of Hoechst 33342 in DMEM/FBS was prepared and 200 µL were added to each well. The cells were incubated for 10 min (37 °C, 5 % CO_2). They were washed once with PBS and 200 µL of DMEM/FBS were added per well. Cells were imaged with the Zeiss Axio Observer.Z1 epifluorescence microscope, equipped with a 100 x oil immersion objective and an HXP lamp.

4.2.5.2 Spectrofluorometric determination of LysoTracker™ Red and Magic Red® fluorescence intensities

1×10^4 HeLa cells per well were seeded in a 96 well plate and cultivated for ~16 h (37 °C, 5 % CO_2). Cells were washed once with PBS and 100 µL of DMEM/FBS/1 µM SYTO13™ or DMEM/FBS/1 µM SYTO13™, supplemented with either 100 nM of Lysotracker™ or Magic Red® was added to the well (37 °C, 30 min, 5 % CO_2). Cells were washed with PBS thrice, DMEM/FBS was added to the wells. SYTO13™ and LT or MR intensities were measured in a Biotek FLx800 fluorescence microplate reader, as indicated in Table 4.5.

Table 4.5: Excitation and emission wavelengths of SYTO13, Lysotracker and Magic Red.

Fluorescent dye	Excitation wavelength [nm]	Emission wavelength [nm]
SYTO13™	488	506
Lysotracker™	577	590
Magic Red®	592	628

To normalize the LT/MR fluorescence intensities to the number of cells analysed per well, the ratio between LT/MR fluorescence and SYTO13 fluorescence signals was determined.

4.2.5.3 Microscopic analysis of ATTO 488-dextran delivery to LysoTracker™ Red stained compartments

1 x 10^5 HeLa cells were seeded onto glass coverslips (Ø 12 mm) in a 24 well plate and cultivated overnight (37 °C, 5 % CO_2). Cells were washed once with PBS and incubated with 1,200 µg/mL ATTO488-dextran in DMEM/FBS for 210 min (pulse) at growing conditions. The medium was discarded, and cells were washed thrice with PBS. DMEM/FBS was added to the wells for 90 min (chase). To visualise acidic compartments, the medium was replaced with DMEM/FBS, containing 100 nM LT, and incubated for 30 min (37 °C, 5 % CO_2). Cells were washed thrice with PBS and treated with 10 µM nocodazole in DMEM/FBS for 20 min (37 °C, 5 % CO_2). Nocodazole is a drug that disrupts microtubules and causes redistribution of compartments that would otherwise be attached to microtubules. This treatment allows for more accurate analysis of colocalization between acidic and dextran-containing compartments. Coverslips were mounted in 0.5 % (w:v) low melting agarose in PBS and analysed by epifluorescence microscopy, using a Zeiss Axio Observer.Z1 epifluorescence microscope, equipped with a 100x oil immersion objective and a HXP lamp. For quantification of colocalization, micrographs were taken and analysed according to Chapter 4.2.7.4.

4.2.5.4 Content mixing assay

1 x 10^5 HeLa cells were seeded onto glass coverslips (Ø 12 mm) in a 24 well plate and cultivated overnight (37 °C, 5 % CO_2). Cells were carefully rinsed with PBS, before adding 300 µL 600 µg/mL ATTO488-dextran in DMEM/FBS and incubated for 8 h at 37 °C, 5 % CO_2 (pulse). The medium was discarded, and cells washed thrice with PBS. 500 µL DMEM/FBS were added to the cells overnight (37 °C, 5 % CO_2). Cells were washed with PBS and incubated with 300 µL of 1200 µg/mL TAMRA-dextran for 180 min (second pulse; 37 °C, 5 % CO_2). Excess dye was removed by washing the cell 3 x with PBS and DMEM/FBS added for another 210 min. Cells were incubated with 10 µM nocodazole in DMEM/FBS for 20 min (37 °C, 5 %

CO_2) and washed once before fixating in 4 % PFA/PBS for 30 min at AT in the dark. Coverslips were mounted in 2 µL Mowiol mounting liquid and analysed by epifluorescence microscopy, using a Zeiss Axio Observer.Z1 epifluorescence microscope, equipped with a 100x oil immersion objective and a HXP lamp. For quantification of colocalization, micrographs were taken and analysed according to Chapter 4.2.7.4.

4.2.6 Biochemical methods

4.2.6.1 Preparation of total cell lysates from HeLa cells (RIPA-lysates)

To analyse single HeLa cell clones for their protein contents (see Chapter 5.7), whole cell lysates from a single confluent cell culture dish (Ø 10 cm) were prepared and analysed for the presence of POI by immunoblotting. The cells were harvested in 2 mL HB (8,6 %)/EGTA, using a rubber policeman. The cells were washed in PBS and HB (8.6 %)/EGTA (440 rcf, 5 min, 4 °C), resuspended in 500 µL RIPA buffer (150 mM NaCl, 25 mM Tris (pH 8.0), 2 mM EDTA (pH 8.0), 10 % (v:v) glycerol, 1 % (v:v) NP-40, 0.5 % (w:v) sodium deoxycholate), and supplemented with 1 x cOmplete. The cells were homogenized by sonication and incubated on ice for 30 min. The lysate was centrifuged for 30 min at 17,000 x g and 4 °C, the supernatant was transferred to a fresh 1.5 mL reaction tube. Protein concentrations were determined (see Chapter 4.2.6.2). 20 µg of protein per sample were diluted in HB/EGTA and 5 x Laemmli buffer to a final concentration of 2 µg/mL. The samples were stored at -20 °C until use.

4.2.6.2 Determination of protein concentration (Bradford Assay)

The determination of the protein concentration was performed directly after purification of relevant subcellular fractions or after lysates were obtained. 2 µL of sample were diluted in 798 µL of the respective buffer, 200 µL Protein Assay Dye Reagent Concentrate (Bio-Rad) added and mixed thoroughly. The absorbance was measured at 595 nm (d = 10 mm) in a Genesis 10 UV photometer (Thermo Electron Corporation). The concentration of protein corresponded to the tenfold of measured absorbance.

4.2.6.3 SDS (sodium dodecyl sulfate) – polyacrylamide gel electrophoresis (SDS-PAGE)

For separation of proteins by their molecular weight, denaturing SDS-PAGE, according to Laemmli (1970), was performed. Total protein extracts were diluted with HB (8,6 %)/EGTA and 5 x Laemmli buffer (see Chapter 4.2.6.1) and incubated at 95 °C for 5 min. A total amount of 15, 20 or 50 µg of protein was loaded onto the polyacrylamide gel. For most PAGEs

resolving gels with 12 % acrylamide were used, for large proteins the percentage was decreased to 7 % acrylamide (see Table 4.6).

Table 4.6 Composition of 12 %/7 % resolving and 4 % stacking polyacrylamide gel.

Components	**4 % stacking gel [mL]**	**12 % resolving gel [mL]**	**7 % resolving gel [mL]**
ddH_2O	3.6	5.5	7
ROTIPHORESE®Gel 40 (37.5:1)	0.63	3.7	2.2
Tris/HCl 1.5 M (pH 6.8)	0.63	-	-
Tris/HCl 1.5 M (pH 8.8)	-	3.1	3.1
10 % SDS (w:v)	0.05	0.125	0.125
10 % APS (w:v)	0.05	0.125	0.125
TEMED	0.005	0.015	0.015

The gels were run at an average voltage of 100 V with 1 x SDS electrophoresis buffer (192 mM glycine, 25 mM Tris, 0.1 % (w/v) SDS). The PageRuler™ Prestained Protein Ladder (Thermo Scientific) was used as size standard.

4.2.6.4 Coomassie staining of SDS-polyacrylamide gels

To monitor the efficiency of purification from heterologous protein expression in *E. coli* BL21, samples were taken at various steps of the purification process (Chapter 4.2.4.4) and prepared for SDS-gel electrophoresis, as described in Chapter 4.2.6.3. The resolving gel was stained with Coomassie staining solution (50 % /w:v) methanol, 10 % (w:v) acetic acid (glacial), 1.5 mM Coomassie brilliant blue) for approximately 1 h on a rocker at AT. For destaining of the gel, Coomassie destaining solution was used (50 % /(w:v) methanol, 10 % (w:v) acetic acid (glacial)). The solution was changed two to three times as needed. The gel was stored in demineralised water.

4.2.6.5 Western blot and detection of proteins of interest (immunoblotting)

The proteins separated by SDS-gel electrophoresis (see Chapter 4.2.6.3) were immobilized on a nitrocellulose (NC) membrane to further analyse the abundance of specific proteins by immunoblotting. For transfer of protein from gel to NC-membrane, a tank blotting method was employed. The gel was stacked between three layers of filter paper on both sides, the nitrocellulose membrane facing the anode and the polyacrylamide gel facing the cathode. The blot sandwich was placed in a blotting tank, filled with transfer buffer (192 mM glycine; 25 mM Tris; 20 % (w:v) methanol). Blotting was carried out for 1 h 30 min at AT and 300 mA

amperage (const.). The membranes were checked for blank areas from air bubbles and evenness of loading by staining with PonceauS solution (5 % (w:v) acetic acid (glacial), 1.3 mM PonceauS). The membrane was treated with blocking solution (see Chapter 4.1.4 for composition), before applying primary antibody. All antibodies used are listed in Chapter 4.1.4. The blot was incubated with primary antibody overnight at 4 °C on a rocker. The primary antibody was removed, and the blot washed thrice with PBS-T (10 min, AT). Depending on the host species of the primary antibody, the blot was incubated with the appropriate secondary antibody (see Chapter 4.1.4.2) for 30 min on a rocker at AT. The NC membrane was washed thrice with PBS-T.

For detection of the POI, ECL-reagent (99 mM Tris-HCl pH 8.8; 0.2 mM coumaric acid; 1.25 mM luminol; 0.003 % H2O2 (freshly added)) was added to the membrane. The chemiluminescence signal was detected on X-ray films (FUJIFILM) and developed, using the CURIX 60 (AGFA).

4.2.6.6 Acid β-galactosidase assay

A photometric assay was performed to determine the activity of acid ß-galactosidase in PNS or endocytic/lysosomal fractions (LYS). The activity of ß-galactosidase was determined by measuring the absorbance of the chromogenic compound *p*-nitrophenol, generated by conversion of *p*-nitrophenol ß-D-galactopyranoside [308]. 60 µL a of either PNS or LYS (1 µg/µL) (see Chapter 4.2.4.8) were used for the assay, mixed with 300 µL ß-galactosidase reaction solution (66 mM citric acid, 7.5 mM *p*-nitrophenol ß-D-galactopyranoside, 1.5 mM sodium citrate dihydrate, 0.7 % (v:v) TX-iodide), and adjusted to a total volume of 450 µL by adding 90 µL demineralised H_2O. The samples were incubated for 30 min at 37 °C. The reaction was stopped by adding 0.5 M Na_2CO_3 and the samples spun down for 5 min at 17,000 rcf, 4 °C. 900 µL of solution were transferred to semi-micro cuvettes (d = 10 mm) and absorbance was measured at 405 nm.

4.2.7 Image and immunoblot analysis

4.2.7.1 Analysis of immunoblots

Immunoblot signal intensities relative to a standard or control sample were quantified using FIJI ('FIJI Is Just ImageJ'; [291,292]). Films were scanned with a resolution of 600 dpi, saved as TIFF, and converted to an 8-bit image. To select a region of interest (ROI), a frame was drawn around the most prominent protein band of interest, using the 'rectangle' tool. The frame should encompass the smallest region to contain the whole band. The rectangle was dragged over the

first lane and selected, using 'Analyse→Gels→Select First Lane'. To select all following lanes, the frame was dragged over each band and set by using 'Analyse→Gels→Select Next Lane'. After all relevant bands were selected, a profile plot of each lane was generated with the command 'Analyse→Gels→Plot Lanes'. To account for background noise, the peak was closed off manually from the baseline for measurement, with the 'straight line' tool. Peaks were selected, using the 'wand' tool. The surface area of the peaks was measured with 'Analyse→Gels→Label Peaks', which labels each peak as a percentage of the total size of all peaks [309]. Relative values were normalized to a control sample that was set to 100 %.

4.2.7.2 Curve fitting for kinetic assessment of protein acquisition

To determine at which time point the tested proteins accumulated on FF endosomes with half-maximal abundance, immunoblots were quantified as described above (Chapter 4.2.7.1). The amount of protein steadily increased until the last time point tested, which was hence defined as 100 %. The data were best described by the logistic function $g(x, a)$.

$$g(x, a) = \frac{a_0}{1+a_1 \cdot e^{-a_2 \cdot x}} + a_3 \qquad (1)$$

a_1, a_2 and a_3 were determined, using the least squares method by vector analysis, including a Nabla-operator and the Levenberg-Marquardt algorithm (PTC, Mathcad 14). The curve fitting was kindly performed by Dr. G. Jeschke [10].

4.2.7.3 Curve fitting for determination of Ca^{2+} dependency of CaFu reaction and attachment

For curve fitting of Ca^{2+}-dependency of fusion and attachment respectively, fusion frequencies of at least 300 beads per sample were determined from three independent experiments. Absolute fusion frequencies were normalized to the 120 µM Ca^{2+} (37 °C) sample and set as 100 % (see Chapter 4.2.4.10). Attachment was determined by assaying at least 300 LBPs for attached LYS (see Chapter 4.2.4.11). Attachment frequencies were subsequentially normalized to the corresponding 120 µM (37 °C) sample. For curve fitting the non-linear fitting tool of Origin Pro 8G was used. Relative fusion frequencies were described using a logistic function (2):

$$y = A2 + \frac{A1-A2}{1+\left(\frac{x}{x_0}\right)^p} \qquad (2)$$

With A1 and A2 being initial and final values of the fitted curve, respectively. x is the [Ca^{2+}] at which each fusion frequency was determined, whereas x_0 is the centre of the curve, representing the [Ca^{2+}] of estimated half-maximal fusion. p represents the power.

Relative attachment frequencies were described using logistic function (3):

$$y = \frac{a}{1+e^{-k(x-x_c)}} \quad (3)$$

a represents the highest y value/ amplitude of the fitted curve. x_c is the centre of the curve and represents $\frac{a}{2}$. k is the coefficient.

4.2.7.4 Analysis of micrographs with FIJI (ImageJ)

The quantification of colocalization between ATTO488-dextran- and LT-containing compartments was performed using FIJI. Mander's correlation coefficients (MCC; M1 and M2) were chosen for quantification, as they are independent from signal intensity. This circumstance necessitates the transformation of micrographs to a binary image [310].

Micrographs of the green (ATTO488-dextran) and the red (LT) channels were exported as TIFF. The micrographs were transformed to an 8-bit rendering, and signal maxima were detected for each channel, respectively, using the 'Find Maxima' command (noise: 10, output: single points). This generated a binary image with points, corresponding to the fluorescence maxima. The points were dilated thrice to better correspond to the size of compartments (Process→Binary→Dilate). The JACoP-Plugin [293] was used to determine MCCs. To assess the amount of random overlap, MCCs were determined with one image rotated by 180° [310]. However, random overlap was negligible (data not shown). This method allows for a distinction between an overlap of compartments, and ATTO488- and LT-positive compartments being attached or in close proximity (cf. [10]). MCCs range between values of 0 and 1, allowing for a depiction of colocalization in percent.

4.2.8 Statistics

For statistical analysis standard deviations (SD) of at least three independent experiments were determined, using MS Office Excel. Individual data points and standard deviation are shown in bar graphs.

5 Results

5.1 Validation of 30'/120' (pulse/chase) protocol to purify FFEs containing lysosomal markers from HeLa cells

To test whether Arl8a and b, Rab7a, HOPS and BORC impact endosome maturation and/or LE with LYS fusion, a suitable assay that allows the purification of late endocytic compartments is needed. Becken and colleagues introduced a cell-free *in vitro* fusion assay for studying maturation stage-specific fusion events in the endosomal pathway of J774E macrophages [238]. In this assay, endocytic compartments are labelled with paramagnetic FF particles [311] in a pulse/chase setup and subsequently purified from cell lysates using a magnet. A. Jeschke introduced a similar experimental approach to purify late endocytic compartments from HeLa cells. The assay's suitability to purify LE/LYS is demonstrated to validate this experimental approach.

Wild type (WT) HeLa cells were pulsed with DMEM/FF for 30 min and washed twice to remove excess FF. After a 120 min chase period, the cells were harvested, washed, and homogenised. The homogenate was spun down at low force to remove cell debris, and a sample of PNS was set aside on ice. FF-containing compartments were purified using a magnetic rack. PNS and FF-endosome (FFE) samples were analysed by SDS-PAGE and subsequent immunoblot analysis (Figure 4 A). During the pulse period, HeLa cells take up FF through endocytosis. After the removal of excess FF, the newly formed FF-containing endosome sequentially passes through various maturation steps from EEs to LEs until an FF-containing LE finally fuses with a LYS, forming a degradative active ELYS [89] (Figure 4 B).

To determine whether the experimental setup is suited to purify LYS, the proteins LAMP1 and Arl8a/b were chosen as marker proteins. Both proteins are mainly located on late endocytic and lysosomal compartments [5,100,312] and are therefore suitable as a measure for the enrichment of LE/LYS contents in FFE fractions compared to PNS. Arl8 and LAMP1 were strongly enriched in FFE fractions, compared to the PNS after a 120 min chase period (Figure 4 C). The purified FFEs in HeLa WT cells equal endocytic compartments of late maturation stages (i.e. LEs/ELYS/LYS). The assay is therefore suited to analyse the delivery of cargo to (E)LYS.

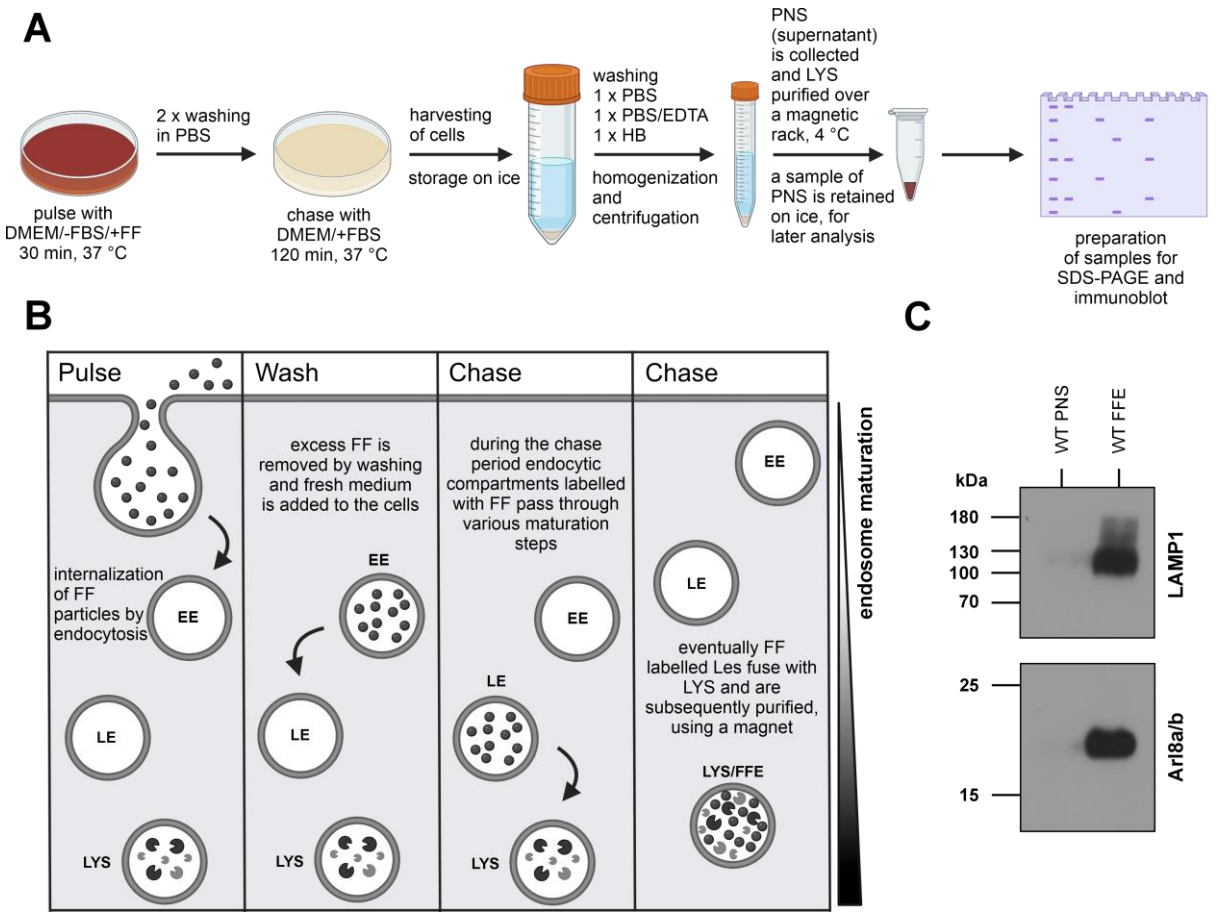

Figure 4: Experimental approach for biochemical purification of LE/LYS from HeLa cells. (**A**) Schematic representation of a lysosome purification protocol. First, HeLa cells are incubated in DMEM, containing ferrofluid (FF) for 30 min (pulse). Afterwards, cells are washed twice, and DMEM/FBS is added for 120 min (chase). After the chase period, the cells are harvested and washed thrice (see figure for details) before homogenisation. To obtain a PNS, the homogenate is centrifuged at low g forces, and the supernatant was transferred to reaction tubes mounted on a magnetic rack. The magnetic rack is incubated at 4 °C for 30 min before discarding the supernatant and harvesting the endocytic ferrofluid-containing compartments. Samples for SDS-PAGE and immunoblot analysis are prepared and analysed (created with BioRender.com). (**B**) Depiction of endocytic internalisation of FF nanoparticles in HeLa cells. First, FF is internalised in an inward budding vesicle. The newly formed FF-laden compartments undergo sequential maturation steps from EEs to LEs until they eventually fuse with acidic, protease-containing LYS (cf. [10], created with BioRender.com). (**C**) Immunoblot for LAMP1 and Arl8a and b in PNS (left) and late endosomal/lysosomal (FFE, right) fractions of WT HeLa cells. 20 µg of either PNS or LYS were loaded on a 12 % denaturing SDS-polyacrylamide gel. One representative blot is shown.

5.2 FF is not transported to LAMP1-containing compartments in KO-cells

To test whether Rab7a, Arl8a/b, HOPS, or BORC are involved in delivering endocytosed material to LYS, LAMP1 levels in PNS and FFE fractions from the respective cell lines were determined. The experiment shown in Figure 5 was repeated in this study to verify data first presented in [10] by A. Jeschke.

PNS fractions were prepared and purified, as shown in Figure 5 A, and subsequently analysed via immunoblotting. Since the Rab7a KO-cells originated from a different parental cell line, compartments from Rab7a KO were compared to their corresponding WT.

LAMP1 levels were strongly reduced (65-75 %) in FFEs (grey bars) purified from Arl8a/b Vps41, myrlysin, diaskedin (Figure 5 A, B), and Rab7a KO cells (Figure 5 C, D), compared to their respective WTs. FFEs from Arl8a/b, diaskedin and Rab7a KOs had the lowest abundance of LAMP1 (Figure 5 B, D). Overall LAMP1 levels (PNS, white bars) across all cell lines were similar or higher than in WT PNS. Reduced LAMP1 levels on FFEs were therefore not due to depletion of LAMP1 in KO cells (Figure 5 B, D). Unexpectedly, LAMP1 levels in Arl8b KO were not reduced (Figure 5 B). Reduction in LAMP1 levels on FFE of Rab7a, Arl8a/b, Vps41, myrlysin, and diaskedin KO cells suggests that delivery of endocytosed FF is inhibited in the absence of these proteins and the complexes they comprise.

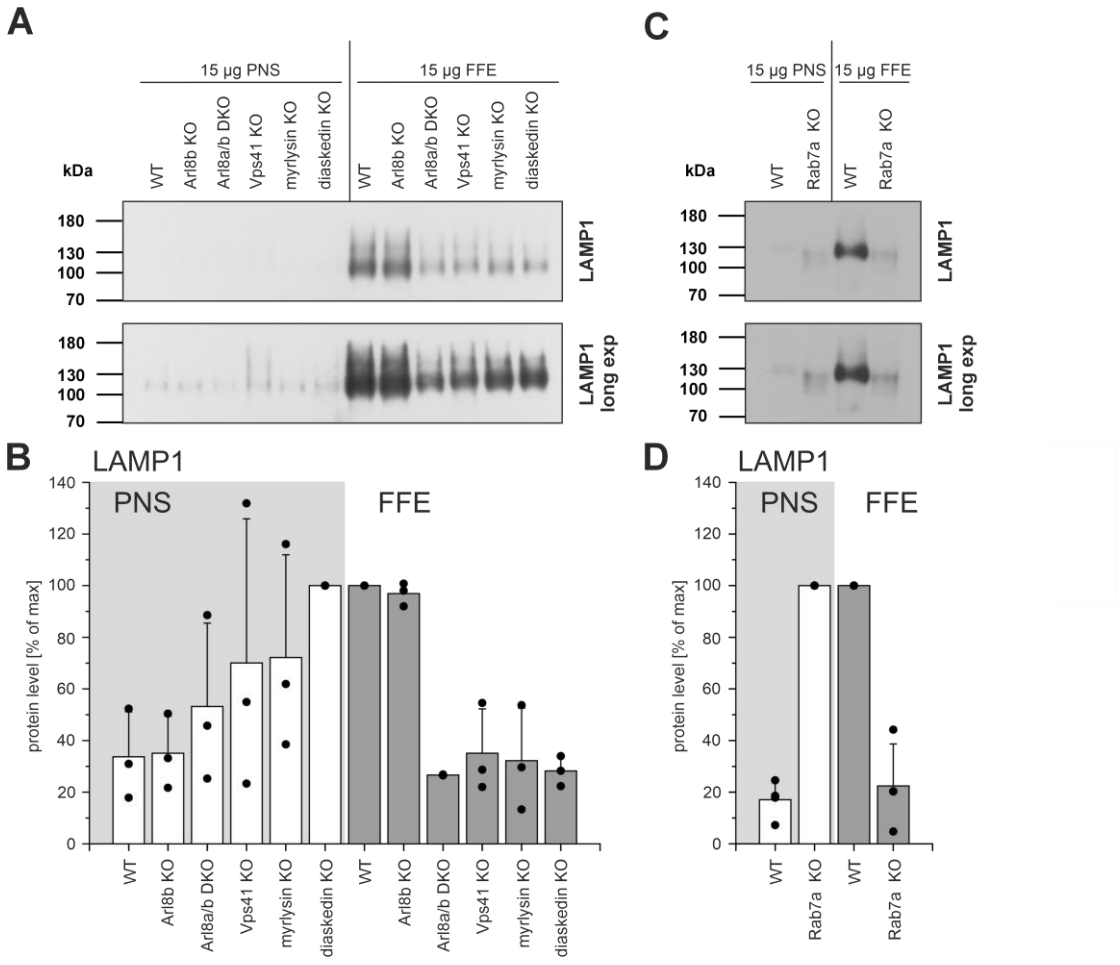

Figure 5: LAMP1 levels in FFEs from Rab7a, Arl8a/b, Vps41, myrlysin, and diaskedin KO cells are reduced compared to WT FFEs. WT and Rab7a, Arl8b, Arl8a/b, Vps41, myrlysin, and diaskedin KO HeLa cells were treated as depicted in Figure 4 A. 15 µg of the harvested PNS and FFE fractions were separated by SDS-PAGE and LAMP1 detected via immunoblotting. (**A, C**) Representative immunoblots, showing LAMP1 abundance of (**A**) Arl8b, Arl8a/b, Vps41, myrlysin, diaskedin KOs, and (**B**) Rab7a KO with their respective WTs. (**B, D**) Signals detected by immunoblotting for LAMP1 were quantified using FIJI [291] and normalised to the highest value of PNS and FFE respectively. Quantitative data is presented as means + SD. Black dots represent single data points (**B**: n=3; **D**: n=4) (cf. [10]).

5.3 FFEs from Rab7a, Arl8a/b, Vps41, myrlysin, and diaskedin KO-cells accumulate less endolysosomal markers

(E)LYS are distinct entities within the endocytic continuum and can be identified by the presence and proteolytic activity of certain proteins and a low pH [312]. Two major classes of proteins are essential for the proper functioning of LYS – integral lysosomal membrane proteins, such as LAMPs (LAMP1 & 2) or CD63 and soluble luminal hydrolases. Approximately 50 different acid hydrolases are present in LYS, each of which has different substrate specificities [313]. Together, these proteins ensure the degradative capacity of LYS and other lysosomal and cellular functions [5].

5.3.1 Acid ß-galactosidase activity is reduced in Rab7a, Arl8b, Arl8a/b, Vps41, myrlysin, and diaskedin KO FFEs

Acid ß-galactosidase activity was quantified in PNS and FFEs of WT and KO cells to further test the hypothesis that cargo delivery to LYS is impaired in cells deficient for Rab7a, Arl8, HOPS, and BORC. It is noteworthy, that in cells lacking either Vps41, myrlysin, or diaskedin the amounts of several other subunits comprising HOPS or BORC respectively are severely depleted [10,314,315]. Therefore, Vps41, myrlysin, and diaskedin KOs are considered to be deficient for the respective complexes. PNS and FFEs were purified from WT, Arl8b, Arl8a/b, Vps41, myrlysin, diaskedin and Rab7a KO-cells as shown in Figure 4 A and used to determine acid ß-galactosidase activity. Enzyme activity was measured by quantifying the absorbance of the chromogenic compound *p*-nitrophenol that originates from the enzymatic conversion of the acid ß-galactosidase pseudo-substrate *p*-nitrophenol ß-D-galactopyranoside [308]. Based on the reduced LAMP1 levels in Rab7a, Arl8a/b, Vps41, myrlysin and diaskedin KOs, acid ß-galactosidase activity was expected to be reduced as well in KO FFEs, while overall activity remained comparable to the WT.

In general, ß-galactosidase activity was significantly higher in FFE fractions than in PNS fractions (Figure 6 A, B). Enzymatic activity was reduced by 30 to 40 % in FFEs from Arl8b, Arl8a/b, Vps41, myrlysin, and diaskedin KOs, compared to the WT. In contrast to LAMP1 FFE levels, acid ß-galactosidase activity was reduced in Arl8b FFEs (Figure 6 A). Acid ß-galactosidase activity in FFEs from Rab7a KO cells was reduced by approximately 50 % compared to the WT (Figure 6 B). The ß-galactosidase activity in PNS fractions ranged around the detection minimum for all cell lines, including the WT. Hence, it could not be determined whether reduction in activity was due to overall reduced activity of acid ß-galactosidase or

reduced amount of viable enzyme in KO cells (Figure 6 A & B). To determine acid ß-galactosidase activity in PNS fractions, 180 µg of PNS from WT cells Arl8b, Arl8a/b, Vps41, myrlysin, and diaskedin KOs were used to conduct the assay. The measured absorbance was still close to the detection minimum, preventing reliable measurement of acid ß-galactosidase activity in PNS fractions (Figure 6 C).

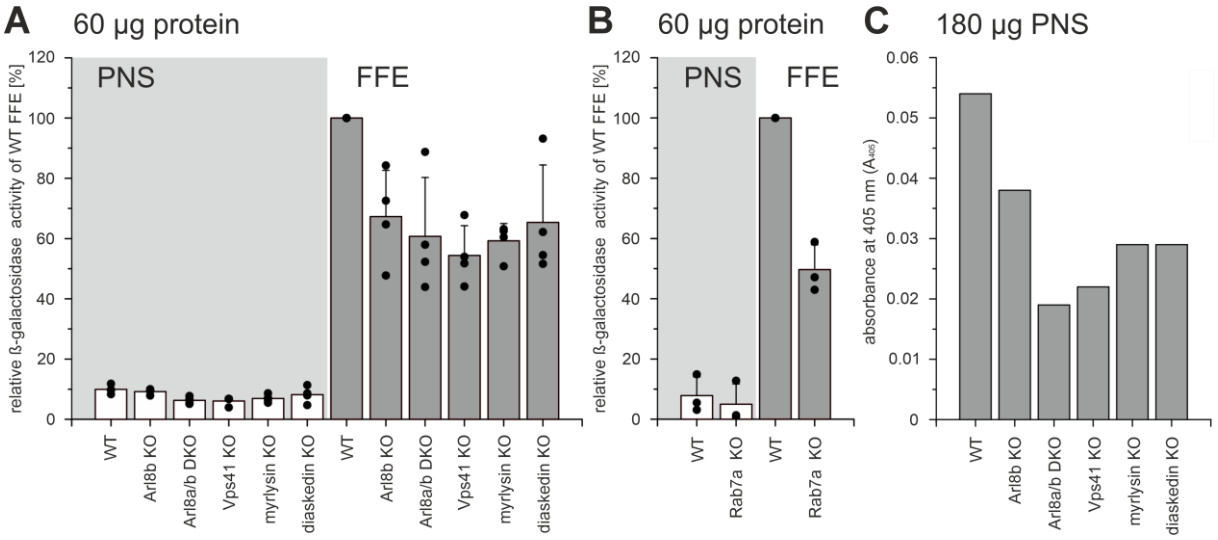

Figure 6: Acid ß-galactosidase activity is reduced in FFEs purified from Rab7a, Arl8b, Arl8a/b, Vps41, myrlysin, and diaskedin KOs. (**A, B**) 60 µg of protein from either PNS or FFE fractions harvested from Rab7a (**B**), Arl8b, Arl8a/b, Vps41, myrlysin and diaskedin KO cells (**A**) and their respective WT were used in an acid ß-galactosidase assay. The absorbance of the chromogenic compound *p*-nitrophenol was measured at 405 nm and normalised to the absorbance measured for the respective WT FFE fraction. Quantitative data is normalised to WT samples and shown as means + SD, single data points are displayed as black dots (**A**: n=4; **B**: n=3). (**C**) 180 µg of PNS was used to determine the basal level of acid ß-galactosidase activity in Arl8b, Arl8a/b, Vps41, myrlysin and diaskedin KO cells relative to the corresponding WT. Data is presented as absorbance at 405 nm (n=1).

5.3.2 Cathepsin B & D levels are reduced in Rab7a, Arl8b, Arl8a/b, Vps41, myrlysin, and diaskedin KO FFEs

The levels of mature cathepsin B and D (mCath B/ mCath D) in FFEs of WT and KO cells were determined to further test the hypothesis that Rab7a, Arl8a/b, HOPS and BORC are involved in delivering cargo to LYS. Mature forms of cathepsin B and D are mostly localised to LYS, making them suitable markers for cargo delivery to LYS [5]. This is also shown by mCath B and D being detected on FFEs even later than LAMP1 and Arl8 (Supp. Figure 2). PNS and FFE fractions were prepared from WT, Rab7a, Arl8b, Arl8a/b, Vps41, myrlysin, and diaskedin KO cells and analysed for mCath B (not for Rab7a KO) and D by immunoblotting. Additionally, 100 µg of PNS obtained by homogenising WT and Arl8b, Arl8a/b, Vps41, myrlysin, and diaskedin KO cells without prior treatment of the cells were analysed for mCath D to assess its overall abundance.

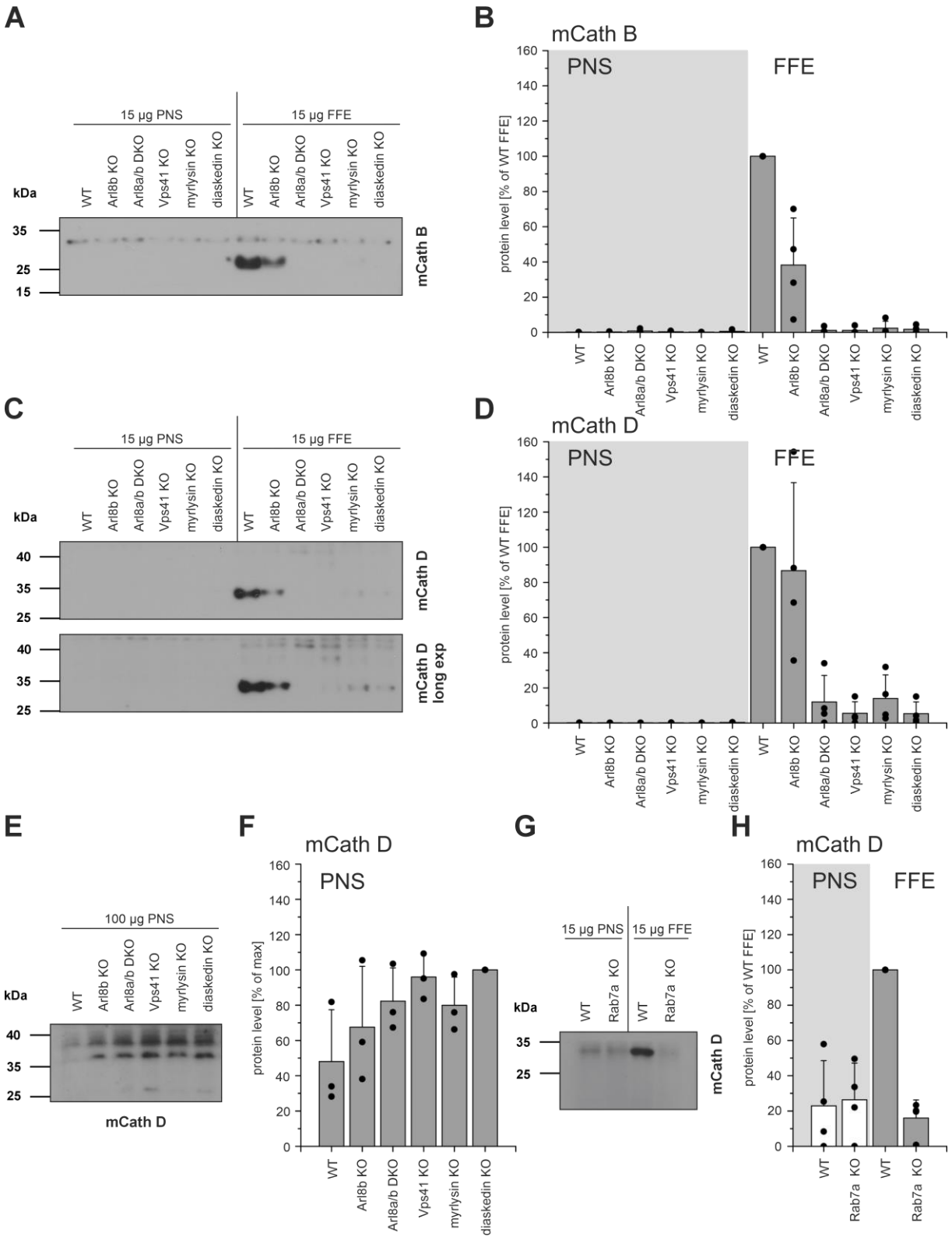

Figure 7: Delivery of FF to mCath B and D containing compartments is impaired in KO cells. See next page for legend.

mCath B was not detected in FFEs from Arl8a/b, Vps41, myrlysin and diaskedin KO cells, while the protein was abundant in FFEs from WT cells. mCath B levels were reduced by approximately 60 % in Arl8b KO, compared to the WT control (Figure 7 A, B).

(**A-D; G+H**) FFEs and PNSs from WT, Rab7a, Arl8b, Arl8a/b, Vps41, myrlysin and diaskedin KO cells were prepared as shown in Figure 4 A. 15 µg of either PNS or FFEs were separated by molecular weight via SDS-PAGE and analysed for (**A, B**) mCath B and (**C+D, G+H**) mCath D by immunoblotting [10]. Representative immunoblots of mCath B (**A**) and mCath D abundance [10] (**C**) are shown for Arl8b, Arl8a/b, Vps41, myrlysin and diaskedin KO cells, as well as mCath D abundance [10] for (**G**) Rab7a KO and their respective WTs [10]. Quantitative data is presented as means + SD (n=4). Values are normalized to the WT FFE sample, individual data points are shown as black dots. **(E**) Representative immunoblot of 100 µg PNS, analysed for mCath D abundance and (**F**) quantification for WT, Arl8b, Arl8a/b, Vps41, myrlysin, diaskedin KO cells (normalized to highest value). Quantitative data is shown as means + SD, black dots indicate single data points (n=3).

The abundance of mCath D in FFEs was similar to mCath B. mCath D levels were reduced by 90 to 95 % in Arl8a/b, Vps41, myrlysin, and diaskedin KOs. In contrast, mCath D levels in Arl8b KO FFEs were comparable to mCath D levels in WT FFEs [10] (Figure 7 C, D). These observations align with reduced LAMP1 levels in KOs, except Arl8b KO (Figure 5). mCath B (Figure 7 A, B) and mCath D (Figure 7 C, D) levels in PNS fractions [10] (15 µg) were below the detection minimum.

Analysis of 100 µg PNS revealed that Arl8b, Arl8a/b, Vps41, myrlysin, and diaskedin KO possess similar amounts of mCath D as the WT, suggesting impaired delivery of FF to mCath D-containing compartments (Figure 7 E, F). The same experimental setup remained inconclusive for mCath B (not shown). mCath D levels in Rab7a KO FFEs were reduced by approximately 85 % compared to the WT. PNS levels on the other hand were comparable to the WT (Figure 7 G, H). Unfortunately, the antibody used for detecting mCath B was discontinued, preventing analysis of Cath B levels in Rab7a KO.

5.3.3 Rab7a, Arl8b, Arl8a/b, Vps41, myrlysin, and diaskedin KO cells have acidic compartments and active cathepsin B

Another hallmark of (E)LYS is the presence of active Cath B and an acidic environment[89]. To test whether KOs possess those hallmarks of (E)LYS, cells were stained with the fluorescent probes LysoTracker Red (LT) and MagicRed (MR). LT is an acidotropic probe that acts as a weak base. It is mostly unprotonated at neutral pH values, allowing the probe to permeate cell membranes freely. In acidic environments, LT is protonated and no longer membrane permeable, thus accumulating in and labelling acidic compartments (Thermo Fischer Scientific). MR on the other hand, is a peptide-conjugated cresyl-violet (Z-Arg-Arg-MR-Arg-Arg). It releases a fluorescent, non-membrane-permeable dye upon enzymatic cleavage to indicate the presence of active Cath B [316].

The ability of KO cells to accumulate LT [10] or MR was assessed in two different ways – a qualitative approach (Figure 8, Figure 9 A-H) and a quantitative measurement of fluorescence intensities (Figure 9 J-M). For the qualitative assessment, WT and KO cells were stained with

either MR (Figure 8) or LT (Figure 9 A-H). Nuclei were stained with Hoechst 33342. All KO cell lines and the respective parental WTs contained active Cath B (Figure 8 A-H) and acidic compartments (Figure 9 A-H). Interestingly, LT- and MR-positive compartments in Arl8b, Arl8a/b, myrlysin, and diaskedin KOs (Figure 8 and Figure 9 B, C, E, F) were mostly located in dense clusters in the perinuclear region. In Vps41 KOs, the distribution of MR-and LT-positive compartments was similar to the WT (Figure 8 & Figure 9 A, D). In contrast, LT- and MR-positive compartments were widely spread across the cell in Rab7a KO cells (Figure 9 & 10 G, H).

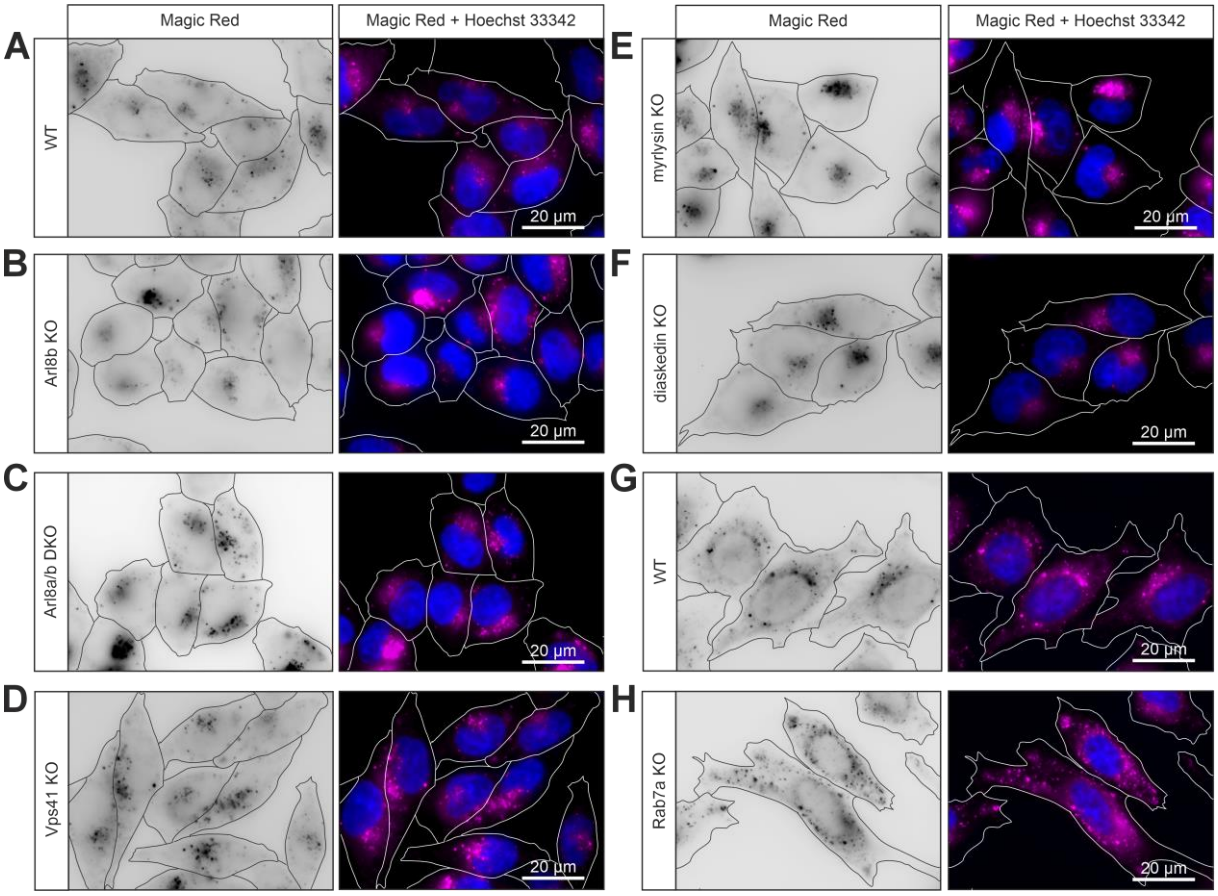

Figure 8: Rab7a, Arl8b, Arl8a/b, Vps41, myrlysin, and diaskedin KO cells have active cathepsin B. (**A-H**) Representative micrographs of MR/ Hoechst 33342 staining of Arl8b, Arl8a/b, Vps41, myrlysin, diaskedin KO cells (**B-F**) or Rab7a KOs [10] (**H**), with their respective WT controls (**A, G**). Cells were incubated with 100 nM LT for 30 min in ibidi 8-well microscopic life cell imaging slides. LT was removed by gentle washing, and nuclei were subsequentially stained with 1 µg/µL Hoechst 33342 for 10 min before imaging. Compartments with Cath B activity are magenta, nuclei appear blue.

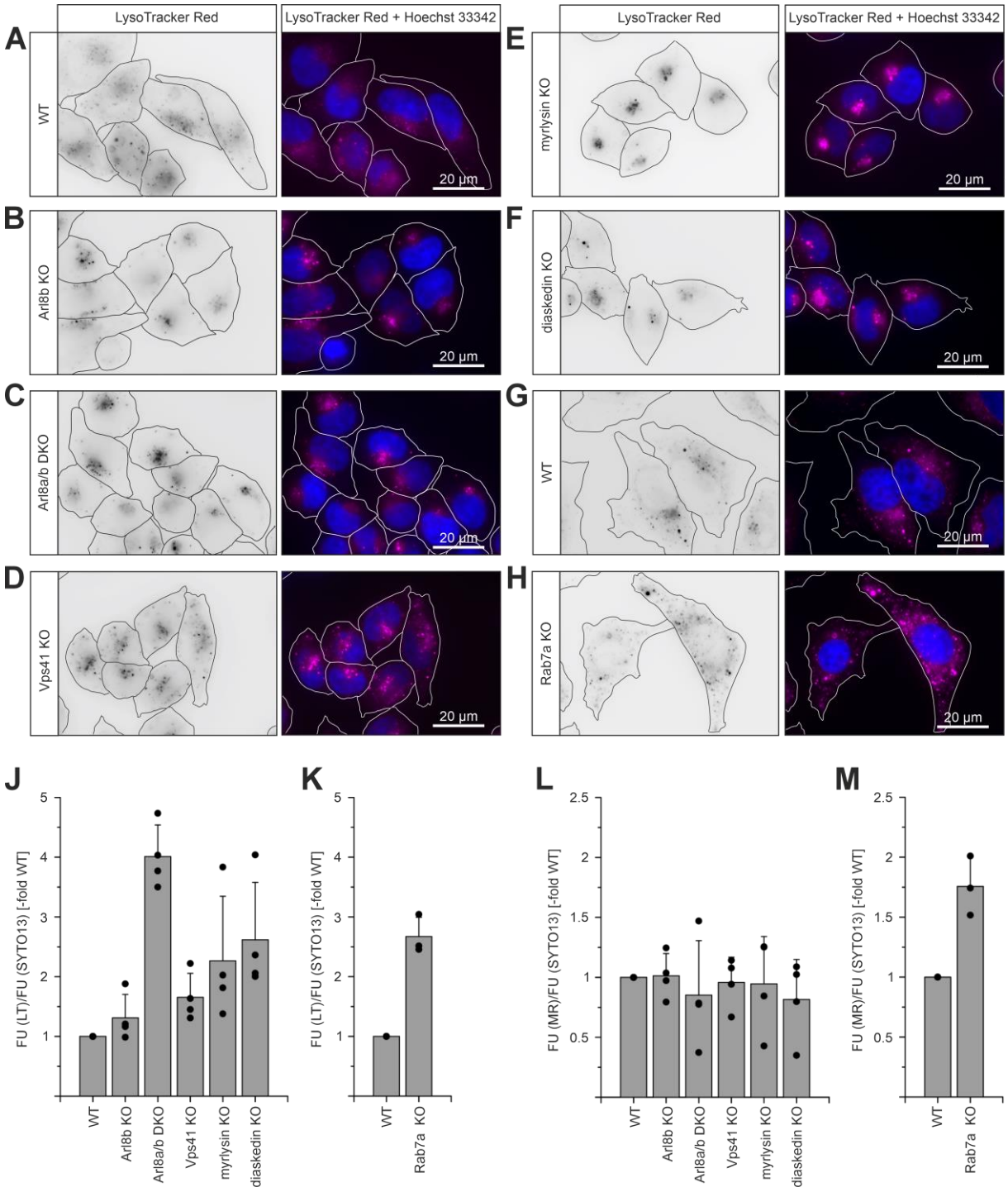

Figure 9: Rab7a, Arl8b, Arl8a/b, Vps41, myrlysin, and diaskedin KO cells possess acidic and hydrolase-active compartments. See next page for legend.

For quantification of fluorescence signal intensities relative to the WT, cells were stained with either LT [10] (Figure 9 J, K) or MR (Figure 9 L, M). Afterwards, nuclei were stained with SYTO13, to normalise to the number of cells per well. Relative LT signal intensities of Arl8b and Vps41 KOs were similar to the WT (Figure 9 J).

(**A-H**) Representative micrographs of LT / Hoechst 33342 staining of Arl8b, Arl8a/b, Vps41, myrlysin, diaskedin KO cells (**B-F**) or Rab7a KOs (**H**), with their respective WT controls (**A, G**). Cells were incubated with 100 nM LT for 30 min in ibidi 8-well microscopic life cell imaging slides. LT Red was removed by gentle washing, and nuclei were subsequentially stained with 1 µg/µL Hoechst 33342 for 10 min before imaging. Acidic compartments are depicted in magenta, nuclei appear blue [10]. (**J-M**) Measurements of fluorescence signal intensities for LT (**J, K**) [10] and MR (**L, M**) staining of Rab7a, Arl8b, Arl8a/b, Vps41, myrlysin and diaskedin KO cells and their respective WTs. Cells were stained with 100 nM of either LT or MR, and signal intensities were determined. Cells were additionally stained with SYTO13. To account for variances in cell number between different wells, signal intensities from LT or MR were normalised to the respective SYTO13 signal. Quantitative data is presented as means + SD single data points are displayed as black dots (n=4). Data is normalised to the respective WT sample [10].

Signal intensities in Arl8a/b, myrlysin, diaskedin (Figure 9 J), and Rab7a (Figure 9 K) KO cells were higher than in the respective WTs. Notably, the LT signal in Arl8a/b DKO cells was increased almost fourfold, whereas it was increased two- to threefold in myrlysin, diaskedin and Rab7a KO (Figure 9 J, K) [10]. Relative MR fluorescence intensities on the other hand were similar across cell lines, except for Rab7a KOs (Figure 9 L, M).

5.4 Colocalization of fluid phase tracers with LT is reduced in Rab7a, Arl8, HOPS, and BORC deficient cells

Delivery of endocytosed FF to LAMP1- or mCath D-containing compartments in Rab7a, Arl8a/b, Vps41, myrlysin, and diaskedin KOs was hampered. To study whether cargo delivery to acidic compartments (i.e. ELYS) [89] was also impaired, colocalization of LT with ATTO488-dextran was analysed microscopically. WT and KO cells were pulsed with ATTO488-dextran for 4 h. ATTO488-dextran containing endosomes were allowed to mature within a 90 min chase period. Acidic compartments were labelled with LT before imaging. Cells were also incubated with nocodazole to reduce perinuclear clustering.

Colocalization between ATTO488-dextran laden and LT-positive compartments was visibly reduced in Arl8a/b, Vps41, myrlysin, diaskedin and Rab7a KO cells compared to the WT, as indicated by less overlap between ATTO488-dextran (green) and LT fluorescence signal (magenta) (Figure 10 A, C-H). This observation was corroborated by the MCCs [317]. Colocalization was reduced by roughly 55 % in Arl8a/b, myrlysin, diaskedin, and Rab7a KOs. Colocalization in Vps41 KO was reduced by approximately 40 %. (Figure 10 K-L). Colocalization between ATTO488-dextran and LT was not reduced in Arl8b KOs (Figure 10 J, K). This was consistent with Arl8b having only moderate or no phenotype distinct from the WT in previous experiments [10]. Hence, cargo trafficking to acidic compartments and consequently (E)LYS is reduced in cells deficient for Rab7a, Arl8a/b, HOPS or BORC [10].

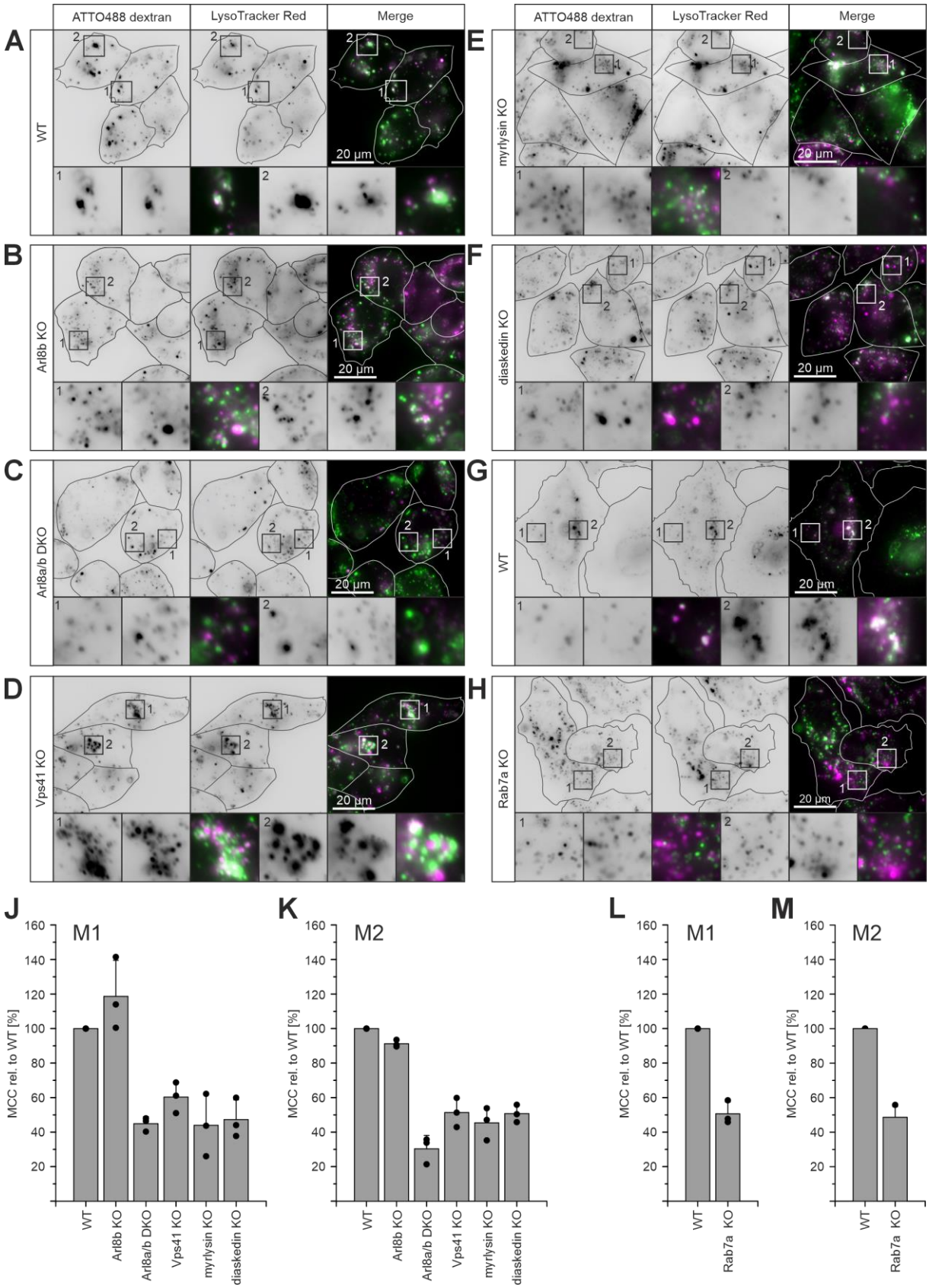

Figure 10: Fluid phase delivery to acidic compartments is reduced in Rab7a, Arl8a/b, Vps41, myrlysin, and diaskedin KO cells. See next page for legend.

Cells were pulsed for 4 h with DMEM/FBS, containing 1200 µg/mL ATOO488-dextran**.** Excess ATTO488-dextran was removed, and fluorescently labelled endocytic compartments were allowed to mature within a 90 min chase period. Acidic compartments were stained with 100 nM LT for 30 min. Before imaging, cells were incubated with 10 µM nocodazole for 20 min. (**A**-**H**) Representative micrographs of fluorescent ATTO488-dextran laden endocytic compartments (green) and LT-stained compartments (magenta) in Arl8b, Arl8a/b, Vps41, myrlysin, diaskedin KO cells (**B-F**) or Rab7a KOs (**H**), with their respective WT controls (**A, G**). Images of either the green or red channels are shown as 8-bit renderings; only the merged images are shown in colour. The boxed areas are shown in the panels below in a 3.75-fold magnification. (**J+K, L+M**) MCCs were determined from three images per cell line and experiment with 5-9 cells per image. M1 determines the fraction of the green signal (ATTO488-dextran compartments) overlapping with the red signal (LT-positive compartments), whereas M2 indicates the overlap of LT-positive compartments with the green signal. Data is presented as means + SD (n=3). Single data points (means of three images) are shown as black dots. MCC values are normalised to the respective WT control [10].

5.4.1 Longer chase periods lead to increased accumulation of endocytosed cargo in compartments of later maturation stages

Delivery of endocytosed dextran to acidic compartments was impaired in cells deficient for Rab7a, Arl8, HOPS, or BORC. However, it is unknown whether cargo delivery to (E)LYS is completely abolished in such cells or merely delayed. To clarify this, colocalization between two fluorescently labelled fluid phase tracers with different pulse/chase periods was determined (not for Rab7a KO). A second approach tested whether FFEs from KO cells accumulate more mCath D after an extended chase period than after the standard chase period.

Endocytic compartments in WT, Arl8b, Arl8a/b, Vps41, myrlysin, and diaskedin KO HeLa cells were labelled with ATTO488-dextran in an 8 h/16 h pulse/chase period to ensure ample time for compartment maturation and cargo transport. A second 2 h/1 h pulse/chase period with TAMRA-dextran as fluid phase marker followed. Cells were incubated with nocodazole to prevent perinuclear clustering of endosomal compartments from hampering colocalization analysis. If endosome maturation was completely interrupted at one point, ATTO488- and TAMRA-dextran would likely end up in the same population of endocytic compartments. This would be reflected by extensive colocalization. If transport were still possible to some extent, it would be expected that ATTO488-dextran would reach compartments of later maturation stages after a prolonged chase period. Therefore, less TAMRA-dextran would reach ATTO488-dextran-containing compartments.

Substantial overlap of ATTO488- and TAMRA-dextran fluorescence signal was observed in WT and Arl8b KO cells, as indicated by white-appearing areas in the magnified panels (Figure 11 A, B). Overlap appeared less extensive in Arl8a/b, Vps41, myrlysin and diaskedin KOs (Figure 11 C-F). The same trends were observed in the MCCs (Figure 11 G, H). M2 describes the portion of TAMRA-dextran fluorescence signal detected in places with ATTO488-dextran signal.

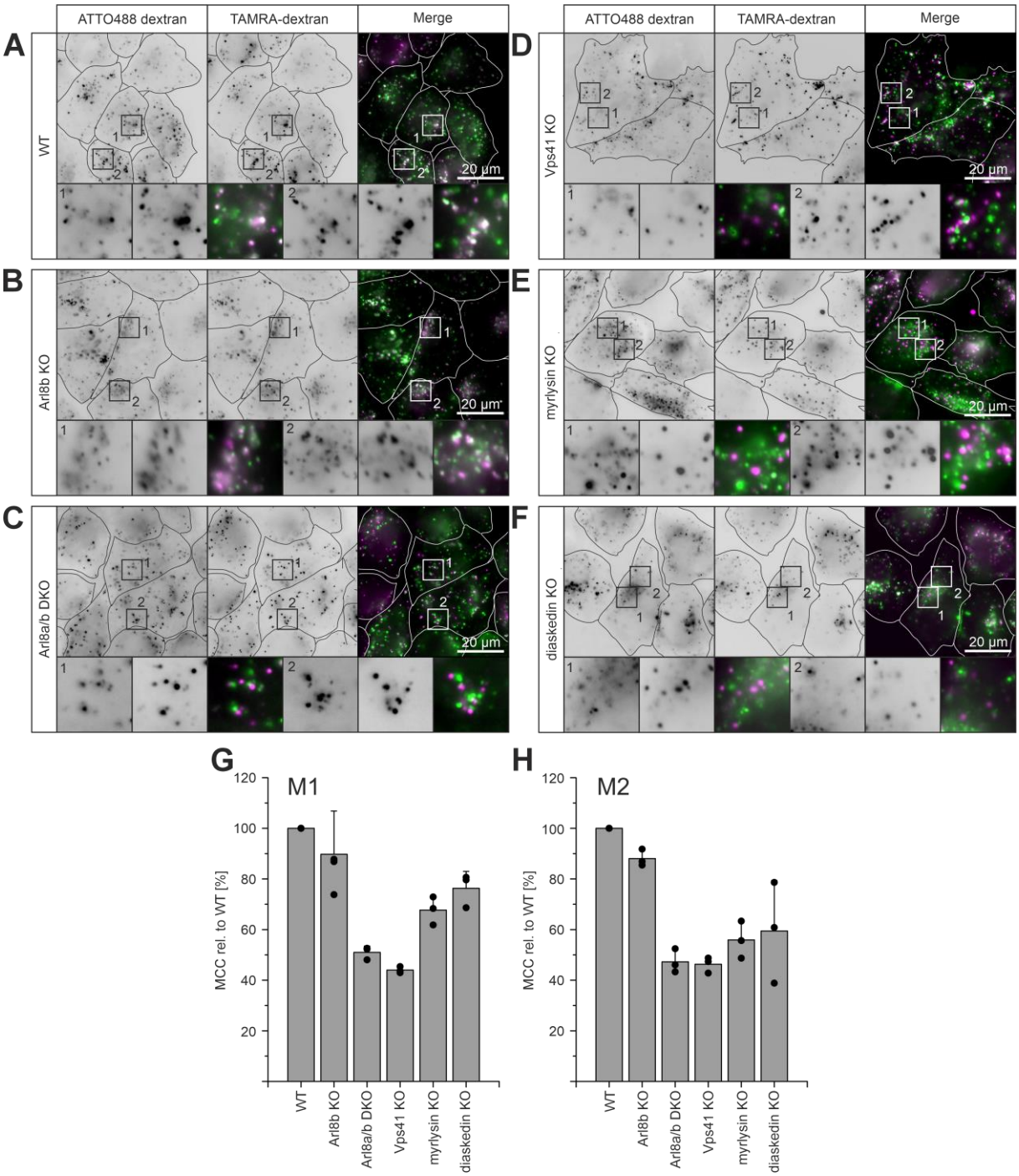

Figure 11: Fluid phase delivery to LYS is not abolished in Arl8b, Arl8a/b, Vps41, myrlysin and diaskedin KOs. Endocytic compartments were labelled with 600 µg/mL ATTO488-dextran (green) for 8 h (pulse). Endocytic compartments were allowed to mature for 16 h (chase). 1200 µg/mL TAMRA-dextran (magenta) were added to the cells and allowed to mature in a second 2 h pulse period. After a 60 min chase period, cells were incubated with 10 µM nocodazole to disrupt microtubules and afterwards fixed in 4 % PFA. Coverslips were mounted in Mowiol, and cells imaged at 488 and 555 nm excitation wavelength. (**A-F**) Representative micrographs of Arl8b, Arl8a/b, Vps41, myrlysin, and diaskedin KO cells (**B-F**) and their corresponding WT (**A**). Images of either the green or red channels are shown as 8-bit renderings. Merged images are shown in colour. Boxed areas are shown in the panels below in a 3.75-fold magnification. (**G, H**) The extent of colocalization between ATTO488- and TAMRA-dextran signals (MCCs) was determined using the JACoP plugin in FIJI [291,293,317]. MCCs were determined from three images per cell line and experiment with 5-9 cells per image. M1 determines the fraction of ATTO488-dextran, overlapping with TAMRA-dextran, whereas M2 indicates the overlap of TAMRA-dextran compartments with a green signal. Data is presented as means + SD (n=3), values were normalised to the WT sample. Single data points are means of three images analysed and shown as black dots.

Since the aim was to determine whether ATTO488-dextran is transported to compartments of later maturation stages than TAMRA-dextran after an extended chase, it is better to focus on the M2 value here (Figure 11 H). In Arl8b-KO, TAMRA-dextran colocalized with ATTO488-dextran to a similar extent as in the WT. Colocalization in Arl8a/b, Vps41, myrlysin, and diaskedin KOs was reduced by approximately 40-50 %, indicating that transport of endocytosed cargo may be delayed rather than abolished (Figure 11 H). Unfortunately, determination of colocalization was not possible for Rab7a KO due to technical issues. Therefore, it is unknown whether transport of endocytosed material to LYS is still possible in Rab7a KO cells. To test this and to validate the conclusions drawn for Arl8b, Arl8a/b, Vps41, myrlysin, and diaskedin KO, the standard protocol for harvesting FFEs was altered to find out whether mCath D was more abundant in FFEs after a longer chase period.

One set of Rab7a, Arl8b, Arl8a/b, Vps41, myrlysin, and diaskedin KOs were subjected to a 30 min/24 h pulse/chase protocol with FF. 150 min before the end of the 24 h chase period, a second set of cells was used to perform a standard FF-assay (Figure 4 A). FFEs were harvested as described previously (Figure 4 A), and FFE samples prepared for SDS-PAGE and immunoblotting. Considering the results of the previous experiment, it was suspected that FFEs in KO cells accumulate more mCath D after a 24 h chase period than after a 2 h chase.

The amounts of mCath D detected after 24 and after 2 h in WT FFEs were similar for both parental WTs. On the other hand, more mCath D was detected in 24 h FFEs than in 2 h FFEs of KO cells (Figure 12). As seen previously (Chapter 5.3.2), mCath D levels in 2 h FFEs from Arl8a/b, Vps41, myrlysin, diaskedin (Figure 12 A, B), and Rab7a KO (Figure 12 C, D) were very low, or not detectable. Notably, mCath D levels in 2 h Arl8b KO FFEs were also reduced by approximately 65 % compared to the 2 h WT FFEs. This observation differed from previously obtained results, where mCath D levels in Arl8b FFEs were similar to WT levels. As expected, based on the preceding experiment (Figure 11), mCath D levels in all KO-FFEs were not only higher after 24 h than they were after 2 h of chase but also similar to WT levels (Figure 12 B, D) [10].

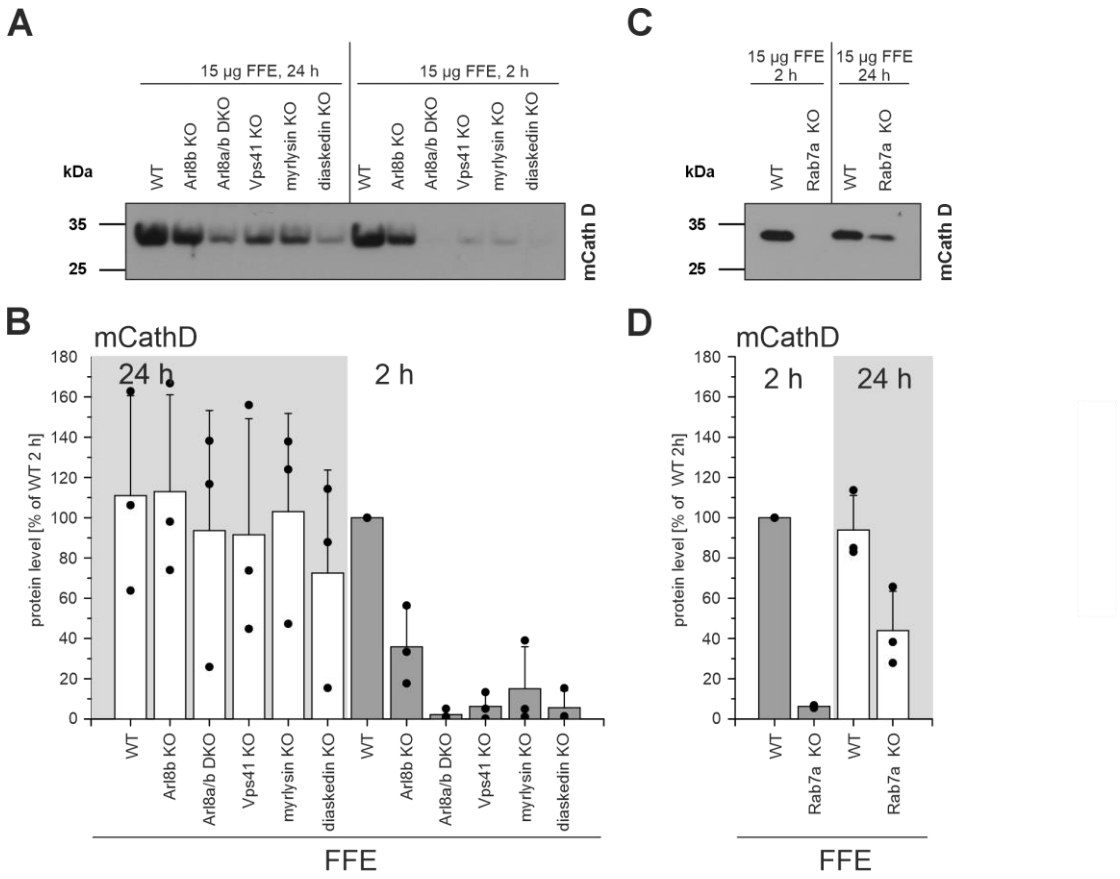

Figure 12: FF delivery to LE/LYS is significantly delayed in Arl8, Vps41, myrlysin, diaskedin, and Rab7a KO-cells. (**A, C**) Representative immunoblots of 15 µg FFEs, purified after either 2 h or 24 h chase from (**A**) Arl8b, Arl8a/b, Vps41, myrlysin, diaskedin, (**C**) Rab7a KO and their respective WT controls. Samples were harvested as shown in Figure 4 A, separated by weight via SDS-PAGE, and analysed for mCath D with immunoblotting. (**B, D**) Immunoblots from three independent experiments were analysed for the abundance of mCath D on FFEs using FIJI [291]. Quantitative data is normalised to the 2 h WT sample and presented as means + SD (n=3). Single data points are shown as black dots [10].

5.5 Analysis of chronological sequence of protein acquisition

Previous experiments have shown that Arl8a and b, Vps41 (HOPS), BORC subunits myrlysin and diaskedin, and Rab7a are needed to transport endocytosed cargo to (E)LYS. It is also well known that all the above proteins hold functions in compartment trafficking and the organisation of fusion between LEs and LYS [105,170,188]. The order in which some of the proteins are recruited to maturing endosomes, particularly in relation to each other, remains elusive in large parts. Although Rab7a, HOPS, Arl8, and BORC interact with each other in a multitude of ways, their functional interdependence is not conclusively described.

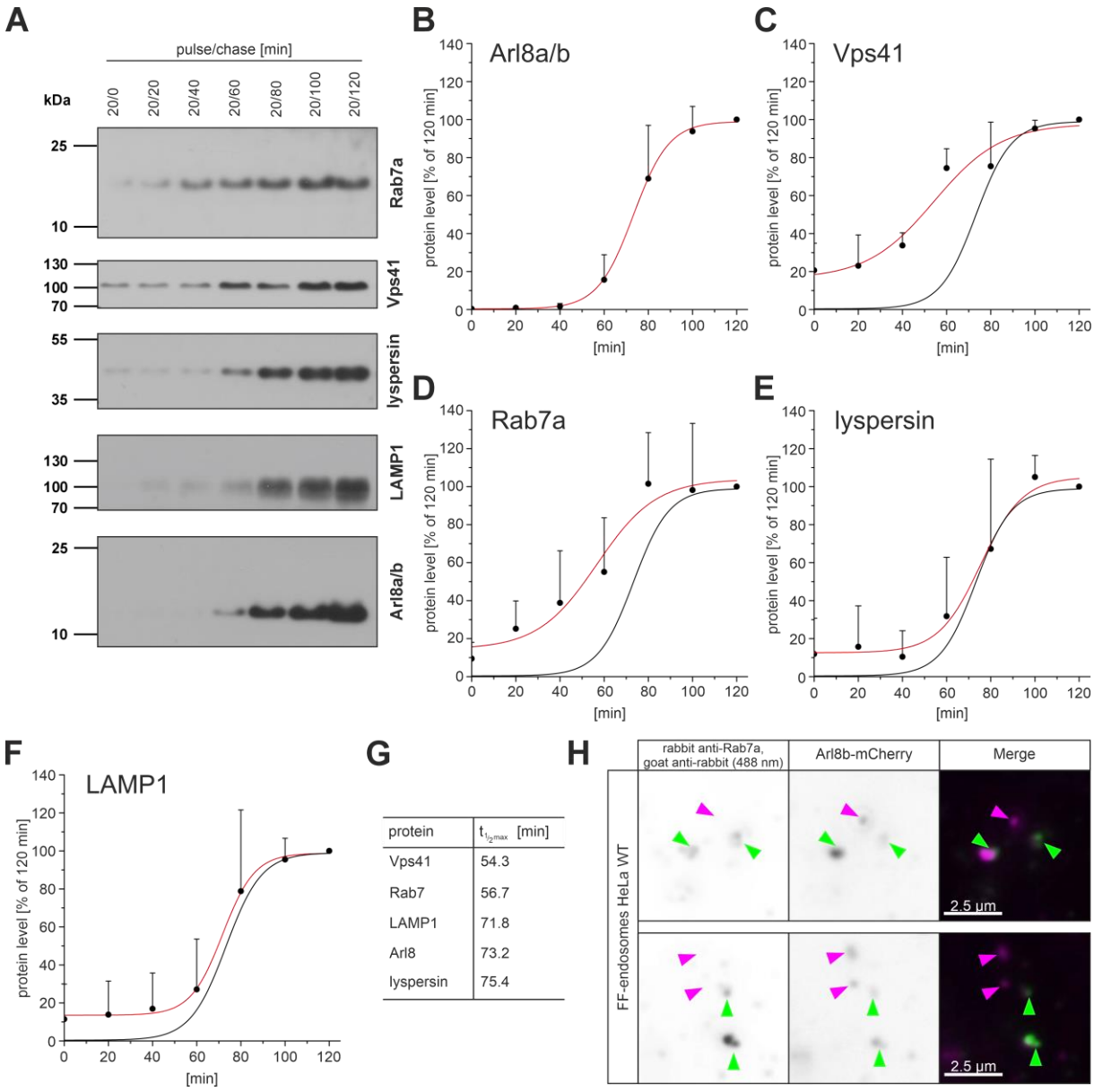

Figure 13: Rab7a and Vps41 are recruited to FFEs before Arl8a/b, lyspersin, and LAMP1. (**A**) Representative immunoblots of FFEs purified from WT HeLa cells after 20'/ (0, 20, 40, 60, 80, 100, 120)' min pulse/chase protocol. Purification of FFEs was carried out as shown in Figure 4 A. Blots were analysed for presence of Rab7a, Vps41, lyspersin, Arl8a/b and LAMP1 [10]. (**B-F**) Blots were quantified with FIJI [291]. Quantitative data from three independent experiments was used to extrapolate a logistic curve fitting for each POI (Dr. G. Jeschke, Mathcad 14, PTC). Curves are shown in red, with means as single black points + SD (n=3). The fitted curve of Arl8a/b (**B**) was added to each diagram for reference. (**G**) Time points of half-maximal protein abundance on FFEs were calculated for each POI [10]. (**H**) Representative micrographs of FFEs purified from WT HeLa cells expressing Arl8b-mCherry. FFEs were additionally stained with rabbit anti-Rab7a antibody and ALEXA488-goat-anti-rabbit antibody to assess distribution of Rab7a (green) and Arl8b-mCherry (magenta) on FFEs. Compartments were imaged with 630 x magnification with 488 and 555 nm excitation wavelength [10].

To determine the consecutive order in which Arl8, HOPS, BORC, and Rab7a are recruited to endosomal membranes, the standard protocol for FFE purification (Figure 4 A) was modified. WT HeLa cells were pulsed with FF for 20 min, and FFEs were harvested after 0, 20, 40, 60, 80, 100, and 120 min of chase. The purified compartments were analysed for Arl8a/b, Vps41, BORC subunit lyspersin, Rab7a, and LAMP1 by SDS-PAGE and immunoblotting.

Immunoblots were used to determine the times at which the respective proteins were detected with half-maximal abundance ($t_{1/2\ max}$).

Rab7a is a well-established marker for LEs [154], whereas Arl8 is suspected to be primarily localised to LYS [100]. Therefore, Rab7a is likely recruited to maturing FFEs before Arl8 is. LAMP1 is most abundant on LYS [65] and is likely recruited late in FFE maturation. The same is assumed for BORC subunit lyspersin [169]. Multiple factors are suspected to anchor or recruit HOPS to endosomal membranes. For example, HOPS binds to Rab7a effector RILP, the dual Rab7a/Arl8 effector PLEKHM1 and is also bound by Arl8 and its effector SKIP [182,183,318]. This circumstance makes it difficult to assume when HOPS is recruited to maturing FFEs.

Substantial amounts of Arl8 were detected late in FFE maturation (Figure 13 A, B) with its $t_{1/2\ max}$ at approximately 70 min of chase (Figure 13 G). Rab7a and HOPS subunit Vps41 were detected well before Arl8 (Figure 13 A, C, D) with $t_{1/2\ max}$ of ~ 55 min (Figure 13 G). Notably, almost no Arl8 was detected on FFEs when Vps41 was already present with half-maximal abundance (Figure 13 C, G). LAMP1 and lyspersin were detected at similar times as Arl8 (Figure 13 A, E-G) [10]. Taken together, the investigated proteins were recruited in two distinct waves. Rab7a and Vps41 were detected comparably early on FFEs, while Arl8, lyspersin, and LAMP1 were recruited late.

Jongsma and colleagues postulated a Rab7a-to-Arl8 switch on LYS, reminiscent of the Rab5-to-Rab7a switch on EEs [99]. Initially, a Rab7a/Arl8 hybrid compartment is formed. The Arl8 effector SKIP acts as a negative effector of Rab7a, leading to its inactivation [99]. If this reasoning is sound, this postulated Rab7a/Arl8 hybrid compartment should be detectable [10]. To verify the existence of a Rab7a/Arl8 hybrid compartment, FFEs from hArl8b-mCherry transfected HeLa cells were stained for endogenous Rab7a and analysed microscopically. Indeed, compartments positive for Rab7a and Arl8b-mCherry (Figure 13 H, green arrow-heads) were present, as well as FFEs only positive for Arl8b-mCherry (Figure 13 H, magenta arrowheads).

During the kinetic assessment of protein acquisition, Rab7a and Arl8 were both present in large quantities on FFEs (Figure 13 D). However, microscopic analysis revealed the existence of an Arl8-only compartment (Figure 13 H). This may be caused by technical limitations of the assay. To assess whether the modified FF-assay is suited to investigate loss or exchange of proteins on FFEs, a pulse/chase protocol with long chase periods was performed. FFEs were harvested after 2, 4, 6, and 24 h of chase and analysed for multiple markers of early and late endosomes using SDS-PAGE and immunoblotting (Figure 14).

Early endocytic marker proteins like EEA1 and TfR [149,319] were still detected after 6 h and only lost after 24 h of chase (Figure 14). Late marker proteins like Vps39, Vps41, lyspersin, mCath D, and LAMP1 on the other hand continued to accumulate on FF-endosomes until 24 h chase. The same tendency was observed for Rab7a and Arl8 (Figure 14).

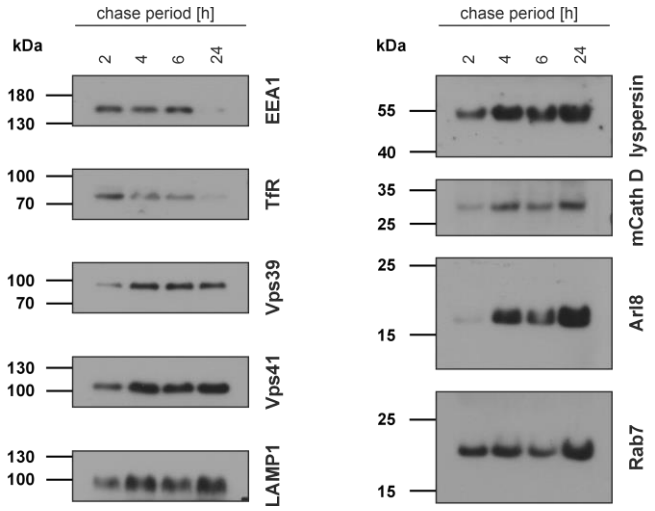

Figure 14: Early endocytic marker proteins are present on FF-endosomes for long periods of time. WT HeLa cells were pulsed with DMEM/FF for 30 min. Excess FF was removed by washing the cells with PBS twice. Endocytic compartments were allowed to mature within 2, 4, 6 or 24 h of chase period before FFEs were harvested as depicted in Figure 4 A. FFEs were analysed for EEA1, TfR, HOPS subunits Vps39 and 41, LAMP1, lyspersin (BORC), mCath D, Arl8a/b and Rab7a [10].

5.5.1 Loss of Rab7a or Vps41 leads to lower levels of Arl8 and BORC on FFEs

The order in which certain proteins are detected on FF-endosomes is a first hint at how the respective proteins interrelate with each other. It is well known that the surveyed proteins interact with each other in multiple ways (see introduction for more detail). However, their functional hierarchy remains elusive [10]. It was tested whether absence of Rab7a, Arl8b, Arl8a/b, Vps41 (HOPS), or myrlysin, and diaskedin (BORC) interferes with recruitment of any of the other proteins. The aim was to better understand the sequence of action regarding Rab7a, HOPS, BORC, and Arl8 and to validate data first collected by A. Jeschke [10]. As done previously, PNS and FFEs were harvested after a 30'/120' pulse/chase protocol and analysed for Rab7a, Arl8a/b, and BORC subunits lyspersin and myrlysin via immunoblotting (Figure 4 A).

Arl8 levels were strongly reduced in PNS and FFEs of Arl8b single KOs compared to the WT and not detectable in Arl8a/b DKO cells (Figure 15 A). Arl8 levels were also strongly reduced in PNS and FFEs of myrlysin and diaskedin KO cells. In Vps41 and Rab7a KO-FFEs, Arl8 levels were moderately reduced (approx. 55 %), whereas PNS levels were comparable to the

WT (Figure 15 A). Rab7a FFE protein levels on the other hand were not significantly reduced in any of the KO cell lines (Figure 15 B). Notably, Rab7a PNS levels were almost thrice as high in Arl8a/b, Vps41, myrlysin, and diaskedin KOs as in Arl8b KO or WT cells. As expected, no Rab7a was detected in Rab7a KO cells (Figure 12 B).

Lyspersin levels were reduced by 90-95 % in FFEs of myrlysin and diaskedin KOs, while lyspersin PNS levels were comparable to the WT in both cell lines (Figure 15 C). Abundance of lyspersin on FFEs of Arl8a/b, Vps41, and Rab7a KOs was also strongly reduced. Overall, lyspersin levels (PNS) were nearly doubled in Arl8a/b and Vps41 KOs compared to the WT. The increase was even more pronounced in PNS fractions of Rab7a KO (Figure 15 C).

Myrlysin levels displayed similar tendencies as lyspersin levels (Figure 15 C, D). As expected, no myrlysin was present in myrlysin KOs. Notably, almost no myrlysin was present in FFE or PNS fractions of diaskedin KO cells. As seen for lyspersin, reduction in myrlysin levels on FFEs was not as pronounced in Arl8a/b, Vps41, and Rab7a KO (50-60 %) as it was for diaskedin KO. Myrlysin PNS levels in Arl8a/b and Vps41 KOs were slightly higher than in the WT. In PNS from Rab7a KOs, myrlysin abundance was more than twice as high as the respective WT control (Figure 15 D). In FFEs of Arl8b KO, lyspersin and myrlysin levels were similar to those of the WT. Only in PNS fractions myrlysin and lyspersin levels were moderately increased (Figure 15 C, D).

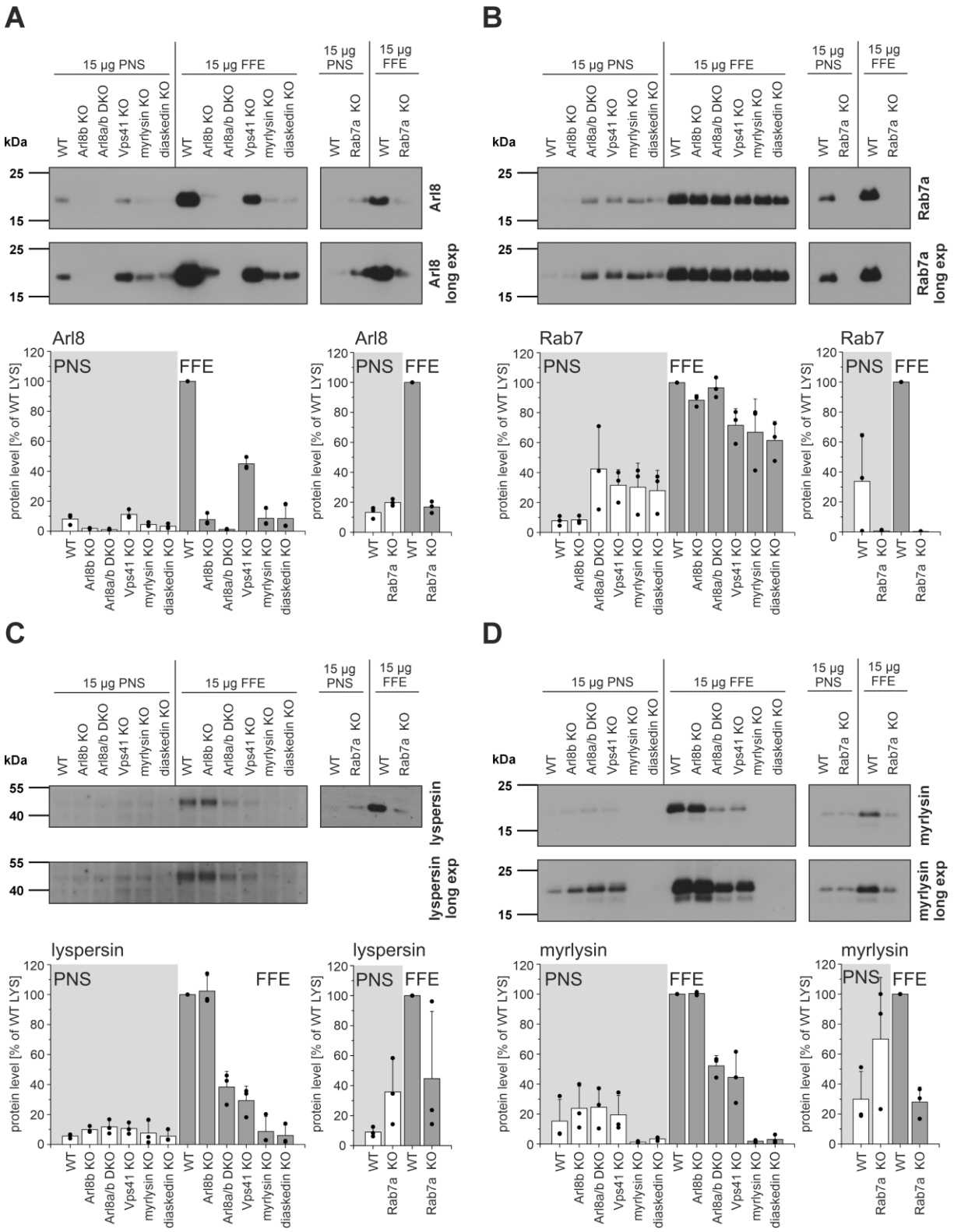

Figure 15: Vps41 and Rab7a are needed for acquisition of Arl8. (**A-D**) PNS and FFEs from Rab7a, Arl8b, Arl8a/b, Vps41, myrlysin, and diaskedin KOs, together with their respective WT controls, were collected after a standard 30'/120' pulse/ chase protocol (Figure 4 A). Samples of both fractions were prepared for SDS-PAGE and subsequent immunoblotting. 15 µg of protein per sample were analysed for (**A**) Arl8a/b, (**B**) Rab7a, (**C**) lyspersin and (**D**) myrlysin. Immunoblots from three independent experiments were quantified using FIJI [291]. Quantitative data is presented as means + SD (n=3) and normalised to the respective WT FFE sample. Individual data points are shown as black dots (c.f. [10]).

5.5.2 Arl8 is not displaced from membranes in absence of Rab7a or Vps41

Immunoblot analysis revealed that FFEs purified from Vps41 and Rab7a KO cells failed to accumulate Arl8 to the same extent as FFEs from WT cells. To explain this, two scenarios are conceivable. 1) As suggested previously (this study, [10]), reduced Arl8 levels on FFEs in Vps41 and Rab7a KO cells could be caused by impaired fusion of Rab7a-containing LEs with Arl8-containing LYS. 2) Less Arl8 could be present on membranes in Vps41 and Rab7a KO cells. To assess which was the case WT, Vps41 and Rab7a KO cells were separated in cytosolic and membrane fractions and analysed for the distribution of Arl8 [10].

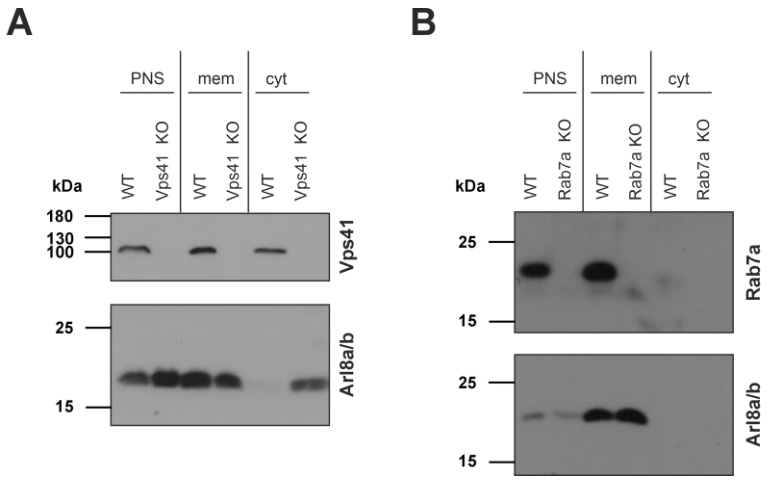

Figure 16: Arl8 is not displaced from FFE membranes in Rab7a or Vps41 KO cells. Representative immunoblots from PNS, intracellular membrane (mem) and cytosolic (cyt) fraction derived from (**A**) Vps41 or (**B**) Rab7a KO cells and their respective parental WT cell lines. 120 µg of PNS fractions for each detected POI were separated into cytosolic and membrane fractions by ultracentrifugation (186,000°rcf, 60 min, 4 °C). Membrane fractions were dissolved in 2 x Laemmli-buffer and stored at -20 °C until use. Cytosolic proteins were precipitated from the supernatant with TCA at 4 °C overnight. The precipitated proteins were sedimented, neutralised with Tris-base, and prepared for SDS-PAGE. 60 µg of PNS and 120 µg of mem and cyt samples (pro rata) were used. The samples were analysed for (**A**) Vps41 (n=3), (**B**) Rab7a (n=2) and Arl8 via immunoblotting. The yielded blots were not quantified [10].

Intracellular membranes (mem) were sedimented by ultracentrifugation of 120 µg of PNS from either WT cells, Vps41 or Rab7a KO cells. Cytosolic proteins (cyt) were precipitated from the supernatant overnight at 4 °C, using TCA. After proteins were sedimented, the remaining supernatant was discarded. SDS-PAGE and immunoblotting were used to analyse 60 µg of PNSs, cytosolic and membrane fractions. If Arl8 were displaced from membranes or recruited less cytosolic levels of Arl8 would be increased while abundance on membranes would be reduced, compared to the WT. In case Arl8 was reduced on FFEs because of impaired LE with LYS fusion, amounts of Arl8 in cytosolic and membrane fractions should be equal among KOs and WT.

Neither Vps41 (Figure 16 A) nor Rab7a (Figure 16 B) were detected in samples of the respective KO cells but in WT controls. Arl8 levels were slightly increased in PNS of Vps41 KO, compared to the WT, while Arl8 levels in membrane fractions were equal for WT and Vps41 KO. Cytosolic Arl8 levels were elevated in Vps41 KO cells (Figure 16 A). Elevated Arl8 levels in Vps41 cytosolic fractions can likely be attributed to overall increased Arl8 levels in Vps41 KOs. No Arl8 was detected in cytosolic fractions of the parental WT of Rab7a KO cells. In Rab7a KO cells overall Arl8 levels (PNS) and Arl8 abundance on membranes were the same as in WT cells (PNS, Figure 16 B). No Arl8 was detected in cytosolic fractions of either the WT or Rab7a KO cells line (Figure 16 B).

5.6 Rab7a and HOPS have different roles in endosome maturation

Apparently, Rab7a and Vps41 (HOPS) play a role in FFEs acquiring Arl8, possibly by acting together and driving the fusion of Rab7 and HOPS-equipped FFEs with Arl8-containing LYS. If this hypothesis is applicable, FFEs in Rab7a and Vps41 KO cells would contain low levels of Arl8, even after long chase periods. Furthermore, if both proteins were involved in the same processes, the experiment's results should be similar for both cell lines [10].

Vps41, Rab7a KOs and their respective WT controls were pulsed with DMEM/FF for 30 min. After removing excess FF by washing, one cell population was allowed to undergo endosome maturation for 24 h, whereas a second population was chased for 2 h (cf. Chapter 5.4.1). FFEs were purified from both cell populations and analysed for Arl8. After 2 h, Arl8 levels on Vps41 KO FFEs (Figure 17 A, B) and Rab7a KO FFEs (Figure 17 C, D) were significantly lower than in the WT control. These results reflected the findings presented in Figure 15 A. Interestingly, the amount of Arl8 detected on Vps41 KO FFEs decreased compared to the amount detected after the 2 h chase period (Figure 17 A, B). On the other hand, Arl8 levels on Rab7a KO FFEs were significantly increased, compared to the 2 h chase period, albeit not as high as in the WT. These findings indicate that Arl8 continues to accumulate on FFEs in Rab7a KOs after prolonged chase periods, whereas it does not in Vps41 KOs [10].

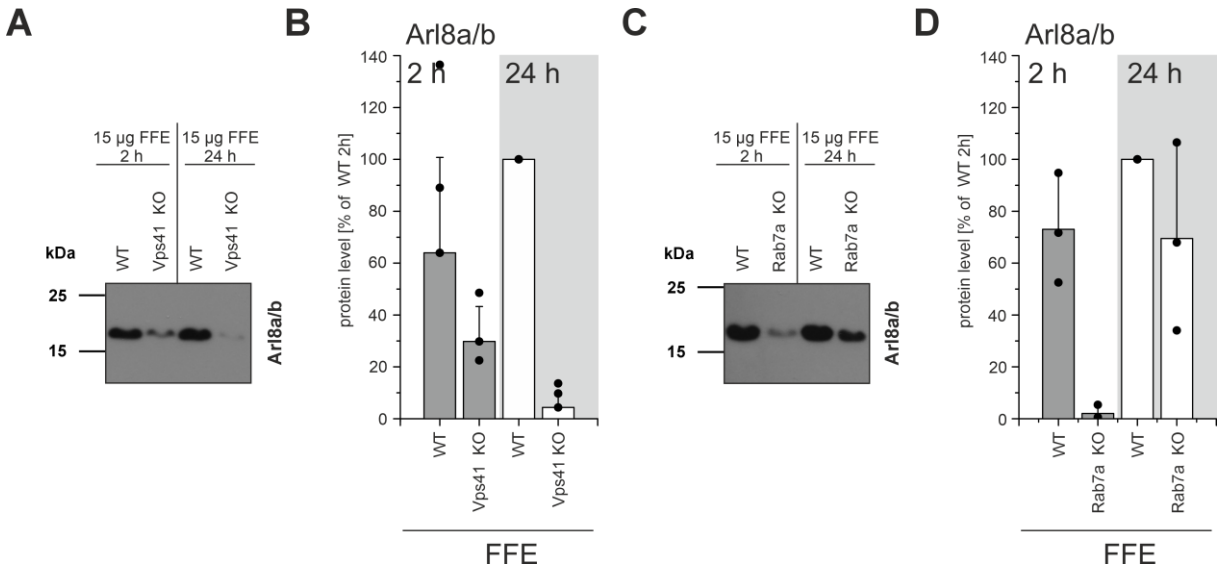

Figure 17: After 24 h of incubation, Arl8 accumulates on FFEs from Rab7a KO cells but not on FFEs from Vps41 KO cells. FFEs were purified after either 2 h or 24 h of chase from (**A, B**) Vps41 or (**C, D**) Rab7a KO cells and their respective parental WT. The samples were prepared for SDS-PAGE and subsequent immunoblotting for Arl8a/b. Representative immunoblots are shown for (**A**) Vps41 and (**B**) Rab7a KO. (**B, D**) Immunoblots from three independent experiments were quantified [291], and the yielded values were normalised to the 24 h WT sample, respectively. Quantitative data is presented as means + SD (n=3), individual data points are shown as black dots [10].

5.6.1 Loss of Rab7a does not alter FFE abundance of HOPS subunits

Previous studies suggested that HOPS is recruited to membranes by its Vps41 subunit interacting with Arl8b in conjunction with the Arl8-effector SKIP [182]. The kinetic assessment revealed that Vps41 and, consequently, HOPS are recruited, before Arl8 is detected on membranes (this study, [10]). Other studies show interaction between HOPS, Rab7a effector RILP, and the dual Arl8/Rab7a effector Plekhm1 [179,183,184]. Given that Rab7a is recruited to membranes of maturing endosomes at the same time as Vps41, this raises the question of whether Rab7a could be indirectly involved in the recruitment of HOPS through its effectors RILP and Plekhm1.

PNS and FFE fractions were prepared from WT and Rab7a KO cells, as depicted in Figure 4 A and subsequently analysed for Vps39 and Vps41 via immunoblotting. Loss of Rab7a had no impact on FFE levels of HOPS subunits Vps39 and Vps41. Moreover, Vps39 and Vps41 abundance in PNS fractions was the same for WT and Rab7a KO cells (Figure 18 A-D). The results align with previously obtained data from A. Jeschke [10]. Compared to the WT situation, Plekhm1 levels were reduced by approximately 40 % on FFEs in Rab7a KO cells. Plekhm1 levels in PNS fractions were twice as high in Rab7a KOs as in WT cells (Figure 18 E, F).

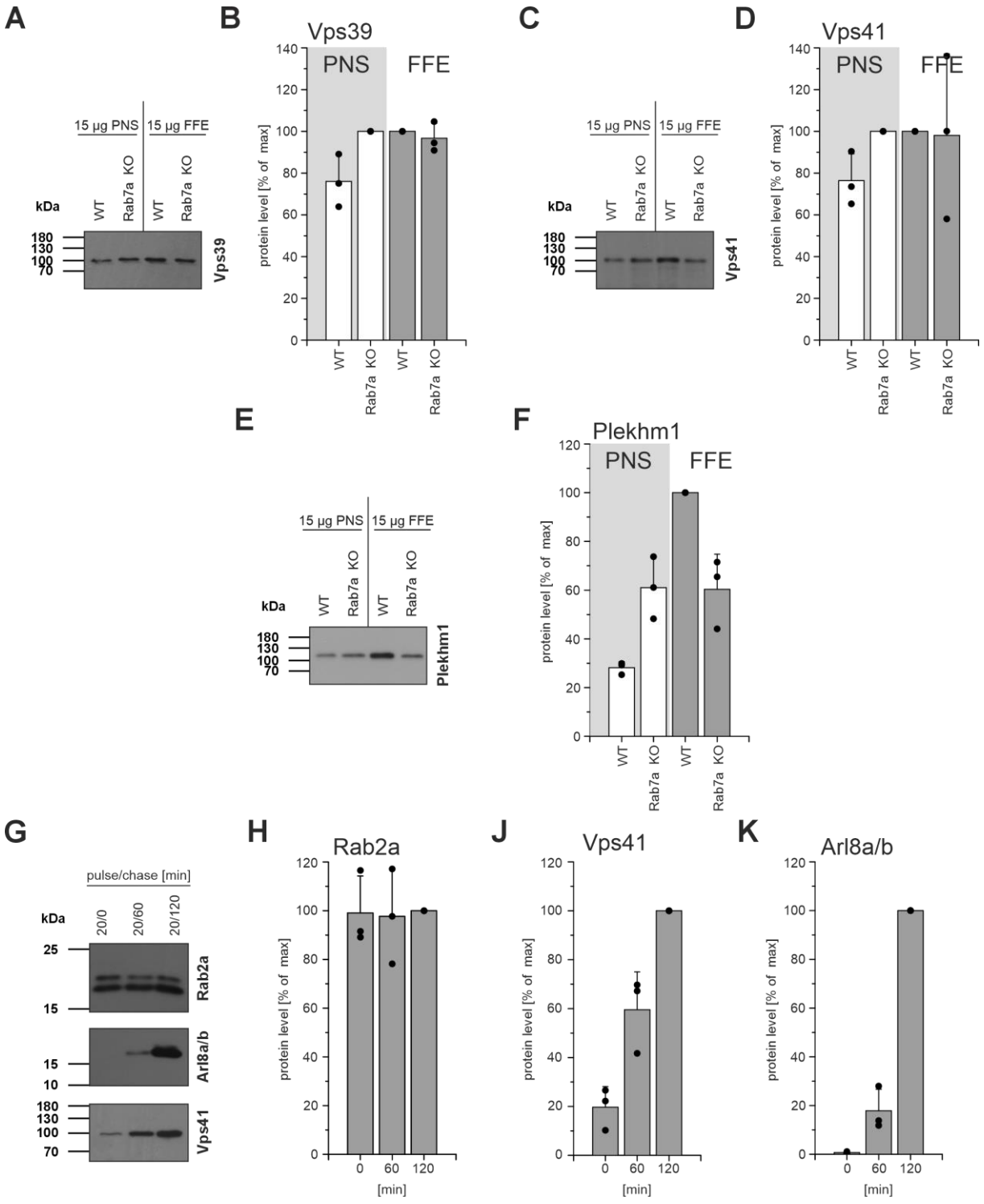

Figure 18: Rab7a is not involved in anchoring of HOPS to FFE membranes, whereas Rab2a is a possible candidate. (**A-D**) PNS fractions and FFEs were purified from WT and Rab7a KO cells. 15 µg of protein per sample were analysed for (**A+B**) Vps39, (**C+D**) Vps41 or (**E+F**) Plekhm1. Immunoblots from three independent experiments were quantified [291], and values were normalised to the highest value of the respective fraction. Quantitative data is presented as means + SD, with individual values shown as black dots (n=3) [10]. (**G-K**) For kinetic assessment if Rab2a was a possible candidate for HOPS recruitment, FFEs from WT HeLa cells were purified after 0, 60 and 120 min of chase after a 20 min pulse period with DMEM/FF. 15µg per sample were analysed for Vps41, Arl8a/b and Rab2a using immunoblotting. (**E**) A representative immunoblot image of the kinetic is shown. Immunoblots from three different experiments were quantified [291], and abundance of (**F**) Rab2a, (**G**) Vps41 and (**H**) Arl8a/b after each respective timepoint were plotted relative to the abundance after 120 min of chase. Data is presented as means + SD, individual values are shown as black dots (n=3) [10].

Lőrincz and colleagues identified Rab2 as an important player in endosome maturation and lysosome-function in *D. melanogaster*, demonstrating that Rab2a binds to HOPS. It was also reported that Rab2a interacts with the Vps39 subunit of HOPS [320,321], making the small GTPase a good candidate for possibly recruiting and anchoring HOPS to endosomal membranes. To test whether Rab2a might be a possible candidate, a similar kinetic approach as in Chapter 5.5 was employed. WT HeLa cells were pulsed with DMEM, containing FF for 20 min. Cells were harvested, and FFEs were purified after 0, 60, and 120 min of chase. FFEs were then analysed for Arl8a/b, Vps41 and Rab2a with immunoblotting (Figure 4 A). If Rab2a were a potential candidate for recruitment of HOPS, it would likely be present at the same time or even before Vps41 on FFEs and before Arl8a/b is detectable. Rab2a was fully present directly after the pulse period (0 min). HOPS could also be detected at 0 min of chase, with 20 % of its maximum abundance and roughly 60 % at 60 min of chase (Figure 18 E, G). Arl8 was not present at 0 min and had only 20 % of its maximum abundance at 60 min (Figure 18 E, H) [10].

5.7 Selection of Rab2a knockout cells

Kinetic assessment (Figure 18 E-H), as well as several studies reporting interaction between Rab2a and subunits of HOPS [1,320,321], identified Rab2a as a possible candidate for the recruitment of the HOPS complex. Furthermore, FFEs purified from Rab2a knockdown cells contained less Vps41 and Arl8 than mock-treated cells, further indicating a role of Rab2a in endosome maturation [10]. Although RNAi has been the gold standard for manipulating gene expression, this technique can be prone to some shortcomings [322], making it necessary to verify the data obtained using RNAi using a CRISPR/Cas9 KO cell line. To date, there is no corresponding KO cell line, which is why a suitable cell line must be created.

The CRISPR/Cas9 treatment of WT HeLa cells was performed by S. Held. For selection, the mixed clones were first assessed for the effectiveness of the treatment. To this end, RIPA-lysates were prepared from either parental WT or CRISPR/Cas9 KO mixed clones and analysed for their Rab2a content via immunoblotting (Figure 19 A). The KO of Rab2a in the CRISPR/Cas9 treated cells was very effective, with only a faint band of Rab2a visible at long exposition.

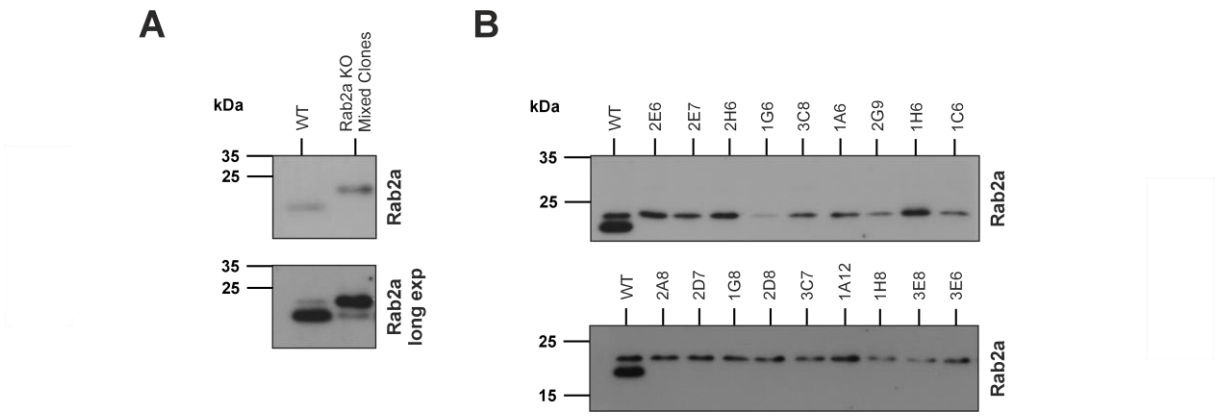

Figure 19: Selection of Rab2a CRISPR/Cas9 KO clones. (**A**) Long and short exposure immunoblots of Rab2a abundance in RIPA-lysates from WT HeLa cells and CRISPR/Cas9 Rab2a KO mixed clones. (**B**) Immunoblots of RIPA-lysates from WT HeLa cells and selected Rab2a KO clones. 5 µg of total lysate were separated on an SDS-PAGE for each sample respectively.

To yield a KO cell line of one defined Rab2a KO clone cells, a serial dilution of cells was prepared in a 96-well plate and scanned for wells containing only one cluster of cells. Cells from such wells were propagated. Once three confluent 10 cm cell culture dishes were obtained, RIPA lysates of all clones were prepared from one confluent cell culture dish and analysed for Rab2a.

All picked clones lacked the lower band, indicative of Rab2a, which was clearly visible in the RIPA lysates of WT cells (Figure 19 B). Interestingly, all selected clones appeared to be deficient for Rab2a, but considering the low overall abundance of Rab2a in the mixed clones (Figure 19 A), this might be due to high knockout efficiency. It was unclear what the upper band visible in the blots represented. One possibility could be that the antibody also recognises the Rab2a paralog Rab2b, but it could also be an unspecific interaction with a different antigen. The 1G9 and 1A12 clones were chosen for further analysis to confirm data from knockdown experiments [10] and to further characterise the phenotype caused by a deficiency for Rab2a.

5.7.1 Loss of Rab2a causes decrease in levels of HOPS subunits and LYS markers

Knockdown of Rab2a caused a significant decrease in Arl8 and Vps41 levels on FFEs, compared to mock-treated cells [10], implying a role for Rab2a in endosome maturation and possibly recruitment of the HOPS complex. To better understand which phenotype is elicited by loss of Rab2a and whether Vps41 and Vps39 levels on FFEs are reduced the newly generated Rab2a KO cell lines were characterised and compared to their parental WT cell line.

WT, as well as 1G9 and 1A12 Rab2a KO cells, were treated according to the standard FF pulse/chase protocol shown in Figure 4 A. Purified PNS and FFE fractions were prepared for

SDS-PAGE and subsequent immunoblotting procedures. The samples were analysed for Rab2a – to confirm the total absence of Rab2a in the KO cell lines – as well as Rab7a, Arl8a/b, lyspersin, mCath D, Vps41, and Vps39. If Rab2a was responsible for recruitment of HOPS, the amount of Vps41 and Vps39 found on FFEs from Rab2a KOs should be decreased compared to the WT control. Similar tendencies were expected for proteins known to appear on FFEs after HOPS (i.e. Arl8a/b, lyspersin, mCath D). Since Rab7a is recruited to FFEs at the same time as HOPS (this study, [10]), loss of Rab2a was expected to have little to no effect on Rab7a levels on FFEs. If Rab2a was merely involved with recruitment and/ or anchoring of HOPS, PNS levels of the POI should be unaffected.

Immunoblot analysis of the abundance of Arl8, Rab7a, mCath D, lyspersin, Vps41, and Vps39 clearly showed that PNS levels were unaffected by KO of Rab2a (Figure 20 A, C-H). Rab2a was not detected in either PNS or on FFEs of both KO cell lines (Figure 20 B). As speculated before, Rab2a KO only had very limited effects on the protein levels of Rab7a on FFEs (Figure 20 D). On the other hand, levels of Arl8, mCath D, lyspersin, Vps39 and Vps41 were reduced compared to WT FFEs. Arl8 and mCath D displayed the strongest reduction with decreases of around 70-85 % (Figure 20 C, E). Reduction in lyspersin, Vps39, and Vps41 levels was less pronounced and ranged around 50-70 % of reduction. Overall, the effects were more pronounced in the 1G9 clone than in the 1A12 clone.

Knockdown experiments performed by L. Pöttgen have shown that reduction of Rab2a levels does not cause redistribution of Vps41 and Arl8 to the cytosol [10]. A fractionation of PNSs in cytosolic and membrane fractions was performed with Rab2a KOs to exclude the possibility that even low levels of Rab2a are sufficient to recruit and anchor HOPS to membranes and to keep the fusion machinery, including Arl8, intact. PNS was prepared from either WT, 1G9 or 1A12 Rab2a KO cells and 120 µg of PNS was separated into cytosolic and intracellular membrane fractions by ultracentrifugation. 60 µg of PNS and all cytosolic and membrane fractions were analysed for Vps41, Rab2a and Arl8a/b via immunoblotting.

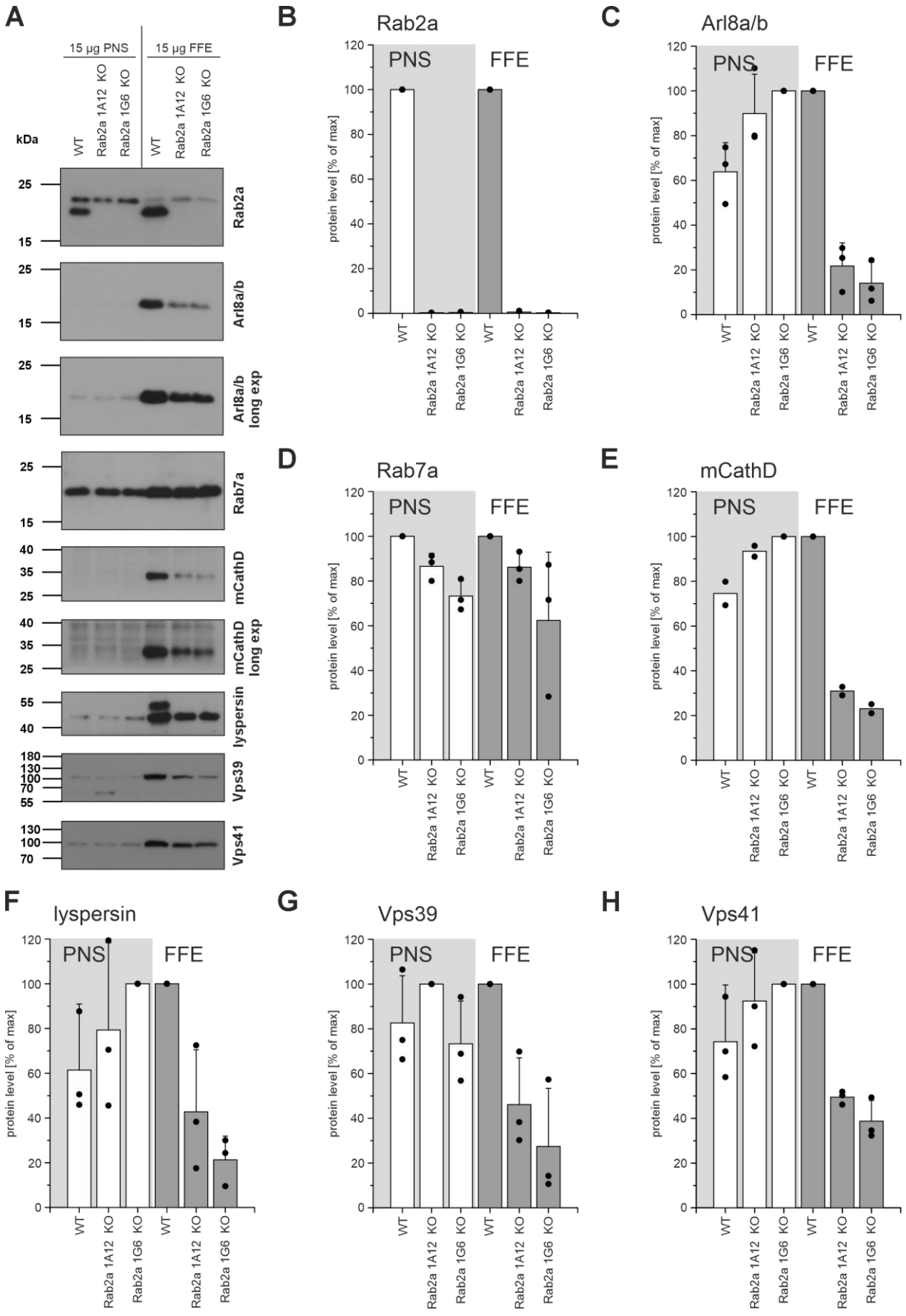

Figure 20: Vps39 and Vps41 levels are reduced on Rab2a KO. See next page for legend.

(**A**) Representative immunoblots from PNSs and FFEs, purified from WT HeLa cells, 1G9 and 1A12 Rab2a KO clones as shown in Figure 4 A. 15 µg of either PNS or FFEs were separated by SDS-PAGE. Subsequently, samples were analysed for Rab2a, Arl8a/b, Rab7a, mCath D, lyspersin, Vps39, and Vps41. (**B**-**H**) Immunoblots from three (two in case of mCath D) independent experiments were quantified. The abundance of (**B**) Rab2a, (**C**) Arl8, (**D**) Rab7a, (**E**) mCath D, (**F**) lyspersin, (**G**) Vps39 and (**H**) Vps41 in PNS and FFE fractions of WT, 1G9 and 1A12 Rab2a KO cells was determined using FIJI [291]. Protein levels were normalised to the highest value of each fraction. Data is presented as means + SD, individual data points are represented by black dots (n=3). For mCath D (**E**), only two blots were quantifiable; therefore, no SD was determined (n=2).

Overall amounts of Arl8 and Vps41 in PNS fractions were the same across all cell lines (Figure 21, PNS). No Rab2a was present in both Rab2a KO cell lines. Protein levels of Rab2a and Arl8 were too low for detection in cytosolic fractions. Only for Vps41 a faint band was visible, with about the same intensity for all three cell lines. Protein levels in membrane fractions of 1G9 and 1A12 were the same as in WT cells for Vps41 and Arl8, proving that there was indeed no displacement of Arl8 or Vps41 to the cytosol.

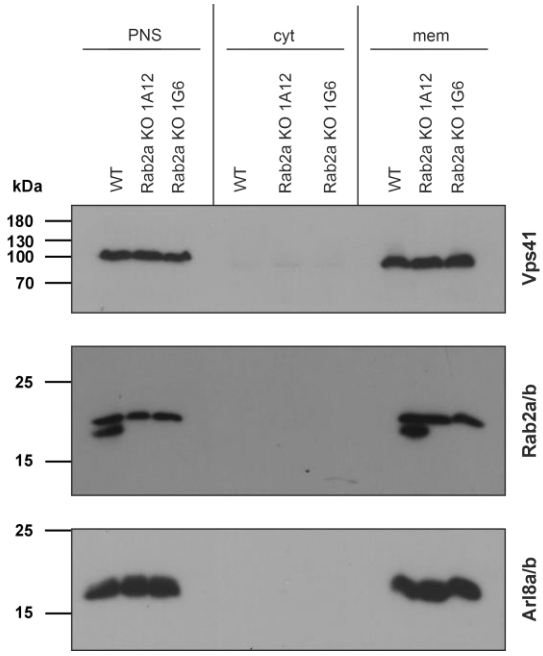

Figure 21: Rab2a KO does not cause HOPS subunit Vps41 to relocate to the cytosol. Representative immunoblot from PNS, intracellular membrane (mem) and cytosolic (cyt) fractions derived from either WT HeLa cells, 1G9 or 1A12 Rab2a KO cell lines. 120 µg of PNS fractions for each detected POI were separated into cytosolic and membrane fractions by ultracentrifugation (186,000°rcf, 60 min, 4 °C). Membrane fractions were dissolved in 2 x Laemmli-buffer and stored at -20 °C until use. Cytosolic proteins were precipitated from the supernatant with TCA at 4 °C overnight. The precipitated proteins were sedimented, neutralized with Tris-base and prepared for SDS-PAGE. 60 µg of PNS and 120 µg of mem and cyt samples (pro rata) were used. The samples were analysed for Vps41, Rab2a and Arl8 via immunoblotting (n=2). The yielded blots were not quantified.

5.8 Micromolar [Ca^{2+}] cause rapid fusion of LBP with LYS *in vitro*

Although there are some differences in endosome and phagosome maturation, it was shown that the same molecular machinery is needed for mediating LE with LYS and phagosome with LYS fusion [9,10]. Both processes are dependent on the sequential actions of small GTPases, tethering factors, SNAREs, their effector proteins and stage-specific sets of PIPs [8–10,47,72]. U. Becken first reported that micromolar [Ca^{2+}] were sufficient to elicit fusion between LBP and LYS *in vitro* [11]. The exact mechanism and the Ca^{2+}-sensing molecules involved in Ca^{2+}-mediated LBP with LYS fusion remain elusive.

Cell-free fusion systems are well suited to investigate fusion-relevant factors in stage-specific setups. Endocytic compartments/ phagosomes are purified after defined time periods. In this case, late phagosomes (LBP) are mixed with FF- and CTMR-BSA-labelled LYS under fusion-promoting conditions (see Chapter 4.2.4.10 for details) in the presence of, for example, pharmacological agents or recombinant proteins. A schematic representation of the workflow can be viewed in Figure 22 A. The relative amount of colocalization between red fluorescence signal (CTMR-BSA) and LBP was determined microscopically to quantify LBP-with-LYS fusion. Figure 22 B illustrates examples of fusion, where LBPs display a ring of red CTMR-fluorescence (Figure 22 B (1)), as well as negative examples of unfused LBP (Figure 22 B (2)). Figure 22 B 3) shows a special case in which a LYS is attached to an LBP but not fused. ATP- and cytosol-dependent StaFu reactions and Ca^{2+}-CaFu reactions were run in parallel to study differences and similarities between both reactions and to identify fusion-relevant factors in CaFu.

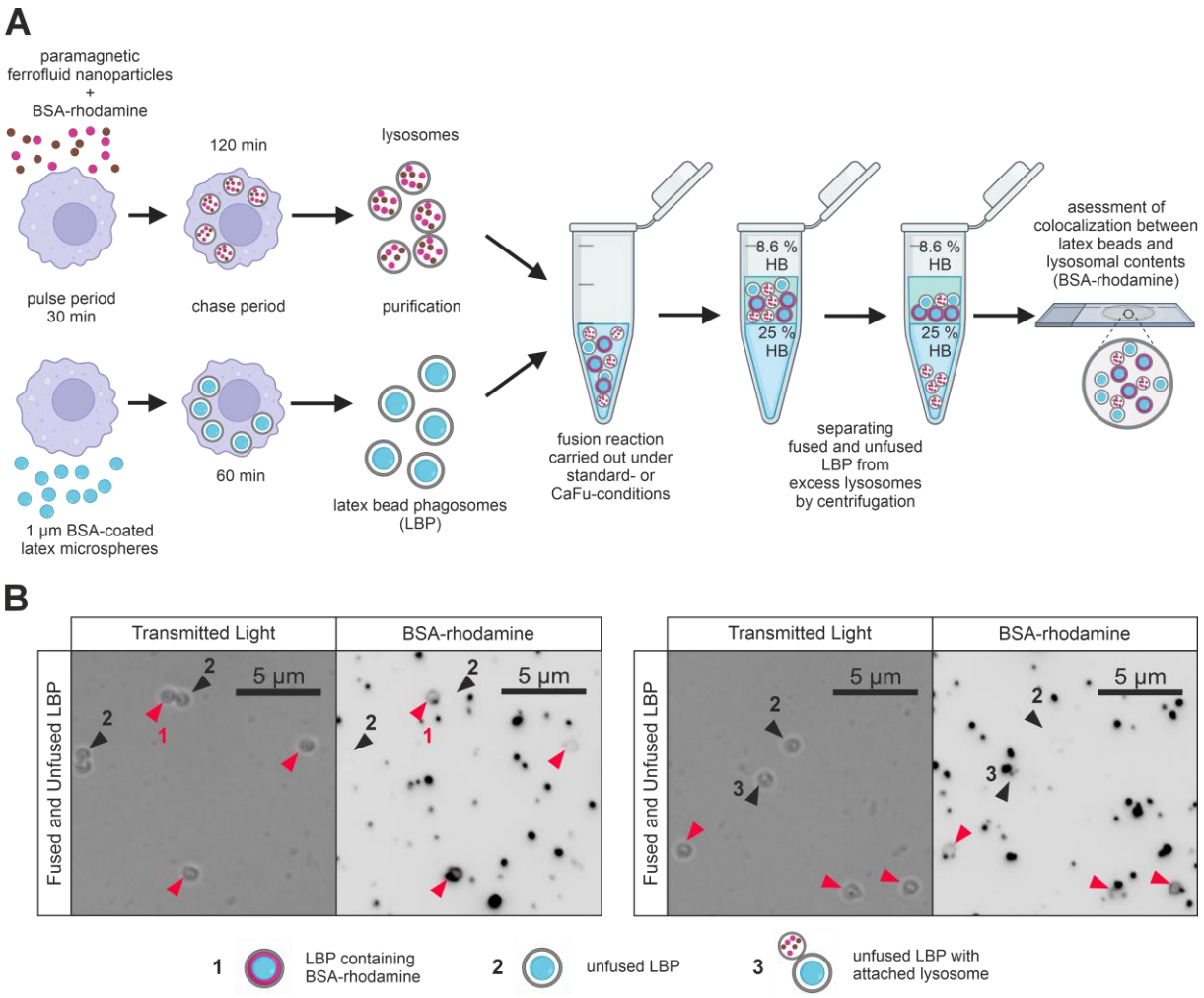

Figure 22: Schematic representation of the *in vitro* fusion assay. (A) J774E macrophages were preloaded with 100 mg/mL CTMR-BSA in DMEM/FBS the night before the experiment. On the day of the experiment, the J774E macrophages labelled with CTMR-BSA were incubated with DMEM/FBS/FF, and a second set of J774E macrophages was pulsed with DMEM containing 1 µm latex beads for 30 min. Non-internalised FF or latex beads were removed by gentle washing of the cells, and endocytic compartments were allowed to mature for either 60 min (LBP) or 120 min (LYS). LBP and LYS were purified as indicated in Chapters 4.2.4.8 and 4.2.4.9. Standard (StaFu) or Ca^{2+}-dependent fusion (CaFu) reaction mixes were prepared according to Chapter 4.2.4.10. For colocalization analysis, the fusion mixes were carefully layered on a 25 % sucrose HB buffer and unfused LYS were sedimented by centrifugation. Fused and unfused LBP, as well as residual unfused LYS, were then sedimented onto a coverslip and fixated with 4 % PFA. The coverslip was mounted on a microscopic slide, and LBP was assessed for their colocalization with a red fluorescence signal (created with BioRender.com). **(B)** Examples of merger events and unfused LBPs. For microscopic assessment of the extent of fusion between fluorescently labelled LYS and LBP, the samples were placed underneath a microscope, and the channels switched between transmission light and red fluorescence signal. 1) Positive merger events are indicated with red arrowheads – a red ring around a 1 µm LBP is visible at 555 nm excitation wavelength. 2) Unfused LBPs are visible under transmission light, but no red fluorescence signal can be detected. 3) Sometimes, an unfused LYS attaches to an LBP and is not removed by centrifugation. In this case, a red dot can be detected at 555 nm right next to an LBP, but no fusion has taken place (created with BioRender.com).

5.8.1 Comparative characterisation of CaFu and StaFu

In her study, U. Becken observed Ca^{2+} mediated fusion – in contrast to fusion under standard conditions – being independent of ATP and cytosol, suggesting that CaFu and StaFu may be fundamentally different [11,13]. U. Becken also observed that 10 µM of RabGDI inhibited StaFu but not CaFu reactions. J. Becker also observed that PI(3)P- and PI(4)P-binding domains had

an inhibitory effect on StaFu but not CaFu [12]. Different reaction conditions and known inhibitors of StaFu were retested in both fusion reactions to highlight differences and similarities of StaFu and CaFu. This ultimately serves to gain a more conclusive understanding of possible mechanisms or proteins involved in CaFu.

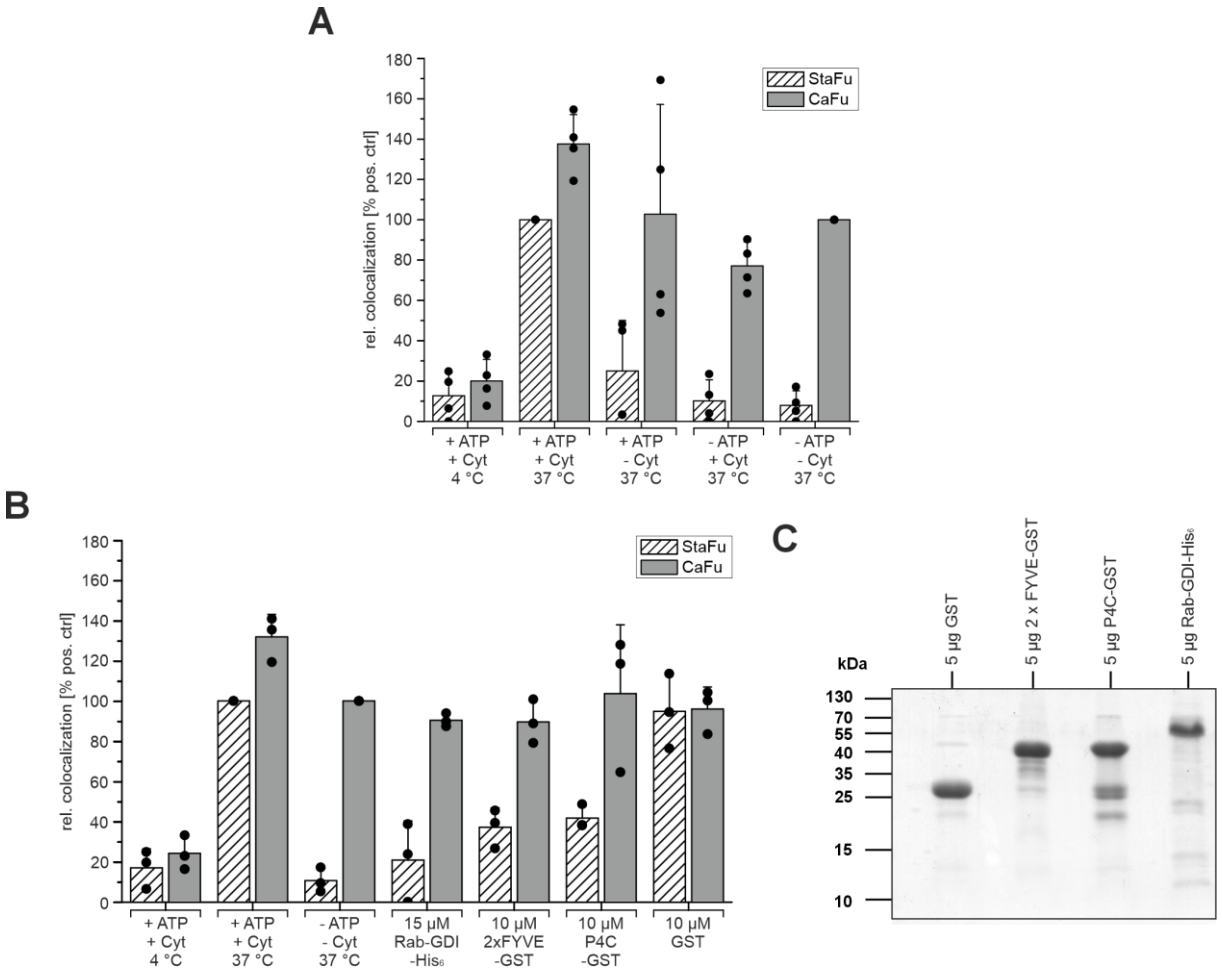

Figure 23: CaFu is independent of ATP, cytosol, Rab GTPases, PI(3)P – and PI(4)P effectors, whereas StaFu is not. J774E macrophages were preloaded with CTMR-BSA overnight before pulsing for 30 min with DMEM/FF. Cells were washed to remove excess FF and subsequentially chased for 120 min. A second set of macrophages was pulsed with 1 µm latex beads in DMEM for 30 min and chased for 60 min after washing. CTMR-BSA labelled LYS were purified from cell homogenates using a magnetic rack, and LBP were purified in a density gradient. CaFu (10 min, 37 °C) and StaFu (60 min, 37 °C) reactions were run in parallel in either (**A**) the presence or absence of ATP, an ATP-regenerating system and 2 mg/mL cytosol (Cyt). CaFu reactions were additionally supplemented with 120 µM of Ca^{2+}. The (+ATP/+Cyt/37 °C) sample served as a positive control for StaFu, and the (−ATP/−Cyt/37 °C) sample served as a positive control for CaFu, absolute fusion frequencies were normalized to their respective control samples. Relative colocalization is presented as means +SD (n=4). Individual data points are shown as black dots. (**B**) CaFu and StaFu reaction mixes containing either 15 µM Rab-GDI, 10 µM 2xFYVE-GST or 10 µM P4C-GST were carried out in parallel. 10 µm GST served as negative control, positive control samples were the same as in (**A**). Data are means of relative colocalization, normalized to the respective positive controls +SD (n=4). Individual data points are shown as black dots [2]. (**C**) His_6 or GST (fusion)proteins were expressed in *E. coli* BL21 DE3 and purified using either Ni-NTA or glutathione-sepharose affinity chromatography. To validate the used proteins, 5 µg of protein were separated by molecular weight on a 12 % SDS-polyacrylamide gel and stained with Coomassie.

To reevaluate the findings of U. Becken under the current experimental standard conditions (i.e. buffering $[Ca^{2+}]_{free}$ with ADA instead of EGTA), StaFu and CaFu reactions with or without ATP and cytosol (Cyt) were run in parallel. No relevant *in vitro* fusion occurred in samples incubated on ice. Unexpectedly, CaFu samples containing ATP and Cyt displayed increased fusion activity compared to the equivalent StaFu sample. In line with previous observations, no significant fusion occurred in StaFu samples without ATP, Cyt, or both. Conversely, fusion was largely unaffected in CaFu samples regardless of presence or absence of Cyt and ATP (Figure 23 A).

StaFu is dependent on the accessibility of PI(3)P and PI(4)P and possibly their effectors during distinct steps in phagosome-lysosome fusion [8,9]. Two powerful tools are available to examine the PIP requirement of fusion. 2 x FYVE consists of two FYVE domains from 'tyrosine kinase substrate Hrs' and is a probe with high affinity for PI(3)P [297]. The 20 kDa C-terminal fragment of the *Legionella pneumophila* protein SidC 'P4C' was reported to bind to PI(4)P [296].

CTMR-BSA and FF labelled LYS and LBP were preincubated with amounts of 2 x FYVE-GST, P4C-GST, RabGDI-His_6 and GST known to inhibit StaFu [9,238]. *In vitro* fusion experiments were carried out under standard conditions (Chapter 4.2.4.10). GST, the purification tag for 2 xFYVE and P4C, did not interfere with *in vitro* fusion. Addition of 10 µM 2 x FYVE-GST and P4C-GST to StaFu reactions decreased colocalization by 60 to 70 % in StaFu-, but not in CaFu-samples (Figure 23 B). 15 µM RabGDI-His_6 reduced StaFu by approximately 80 %. CaFu on the other hand remained largely unaffected by addition of RabGDI (Figure 23 B) [2].

Validation of the used protein fragments is shown in Figure 23 C. Bands of appropriate molecular weights were observed for all recombinant proteins. Although some bands of weak intensity were visible at lower molecular weights, the recombinant proteins are of sufficient purity.

5.9 Analysis of Ca^{2+}-requirements for CaFu-subreactions

In their dissertations, C Hermsen and J. Becker determined the $[Ca^{2+}]$ at which the maximum fusion frequency occurred at 120 µM [12,13]. Intriguingly, $[Ca^{2+}]$ needed for maximum fusion can be lowered to approximately 15 µM when LBP and LYS are brought together by centrifugation [2]. It was hypothesised that CaFu could consist of at least two different Ca^{2+}-sensitive processes. A sensitive fusion-promoting step and a second less sensitive step [2,12].

5.9.1 Analysis of Ca^{2+}-requirement in LBP-LYS attachment and fusion

To verify whether a possible second Ca^{2+}-dependent step in CaFu could be attachment of LBP and LYS an attachment-assay first introduced by A. Jeschke [9] was modified for CaFu.

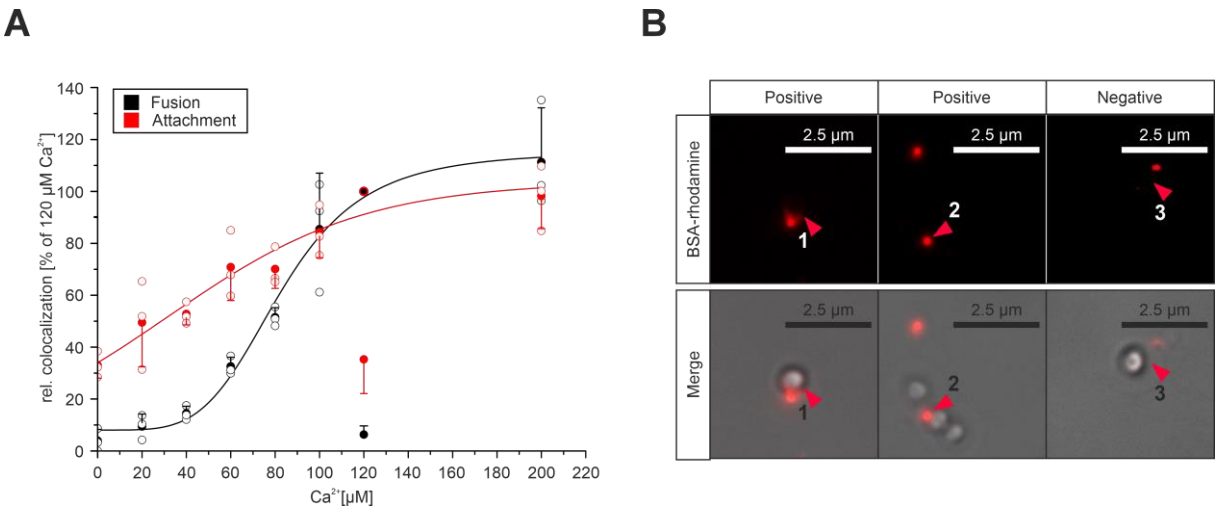

Figure 24: Fusion and attachment are Ca^{2+} dependent. J774E macrophages were preloaded with CTMR-BSA overnight before pulsing for 30 min with DMEM/FF. Cells were washed to remove excess FF and subsequentially chased for 120 min. A second set of macrophages was pulsed with 1 µm latex beads in DMEM for 30 min and chased for 60 min after washing. CTMR-BSA labelled LYS were purified from cell homogenates using a magnetic rack, and LBP were purified in a density gradient. CaFu samples and attachment assay samples were prepared with different [Ca^{2+}] (0, 20, 40, 60, 80, 100, 120, 200 µM). Attachment assay samples were supplemented with 100 µM LPC-12 [9]. Reactions were run for 10 min at 37 °C and afterwards stopped on ice. For the attachment assay samples, the proteinase K digestion was omitted. LBP with at least one LYS attached was considered as positive. (**A**) Colocalization frequencies relative to 120 µM Ca^{2+} (black dot with red outline) were determined, and curve fitting (Origin8Pro) was performed for the mean values from three independent experiments to emphasise the progression of fusion (black curve) or attachment (red curve) in response to increasing [Ca^{2+}]. Mean values are shown as either solid black (+SD) or solid red dots (-SD). Colocalization frequencies of individual experiments are shown as either black (fusion) or red (attachment) circles [2]. (**B**) Exemplary micrographs, showing CTMR-BSA labelled LYS attached to LBP (positive – 1, 2) or a LYS located in proximity, but not attached to an LBP (3). Scale bars are 2.5 µm.

CaFu fusion and attachment assays were carried out in parallel to better compare the two processes and their Ca^{2+} requirements. Regular fusion reaction and attachment reaction mixes were prepared on ice with 0, 20, 40, 60, 80, 100, 120 and 200 µM Ca^{2+}. Attachment assay samples were additionally supplemented with 100 µM LPC-12. Fusion assay samples were processed as usual. Proteinase K treatment was omitted to avoid the risk of separating adherent LYS during the processing of the attachment assay samples.

The curve representing fusion in dependence of [Ca^{2+}] displayed a sigmoidal course, with approximately 10 % of maximum fusion at 0 µM and half-maximal fusion frequency at $[Ca^{2+}]_{50}$ of 80 µM. Fusion frequency between 120 and 200 µM ca^{2+} only increased moderately, indicating that the reaction reached saturation (Figure 24 A, black curve). On the other hand, the attachment curve (red) displayed a soft hyperbolic course. As for the fusion curve, there

was no significant increase in the relative amount of LBP with attached LYS between 120 and 200 µM of Ca^{2+} (Figure 24 A, red curve). Curiously, the relative amount of LBP with attached LYS at 0 µM was already at 35 % of the attachment seen at 120 µM Ca^{2+}, when almost no fusion activity was seen. The same trend was evident for the ice control sample. Usually, the absolute number of LYS attached to LBP was approximately 2 to 2.5 times as high as the absolute number of LBP fused with LYS. LBP-with-LYS fusion, as well as LBP-LYS attachment, are dependent on Ca^{2+} [2]. Figure 24 B shows positive and negative examples for LYS attached to LBP. The CTMR-labelled LYS in the panels on the left were located directly next to the margins of the LBP (1 & 2). In contrast, in the panel on the right, the red arrowhead (3) clearly indicates that the CTMR-labelled LYS was not attached but located in close vicinity to the LBP.

5.9.2 A late endocytic Q-SNARE complex inhibits CaFu

In vitro ATP-and cytosol-dependent phagosome-LYS-fusion (StaFu) is dependent on SNARE proteins and inhibited by the addition of NEM [238]. To examine whether CaFu requires priming activity of NSF and therefore possibly SNARE proteins, the sensitivity of CaFu towards different concentrations of NEM was tested.

CaFu and StaFu reactions were carried out in parallel. HB, LYS, LBP and Cyt were mixed and preincubated with 1, 3 and 5 mM of NEM on ice for 10 min. During the preincubation step, no additional DTT was added. After incubation, NEM was inactivated with equimolar amounts of DTT. Since DTT was also required for the regular fusion mix, the amount of added DTT was adjusted accordingly. A sample of 5 mM NEM was inactivated with equimolar amounts of freshly prepared DTT before adding compartments or Cyt as negative control. In her thesis, U. Becken reported an inhibitory effect of 4 mM NEM on both StaFu and CaFu [11]. If both reactions required priming activity of NSF, it would be expected that both reactions were similarly sensitive to the addition of NEM.

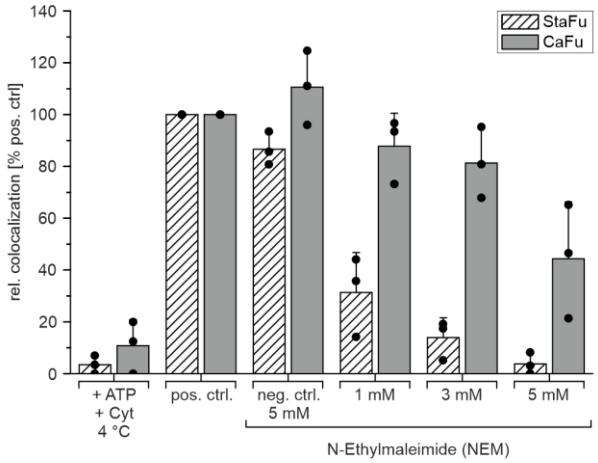

Figure 25: NEM only partially inhibits CaFu at 5 mM. J774E macrophages were preloaded with CTMR-BSA overnight before pulsing for 30 min with DMEM/FF. Cells were washed to remove excess FF and subsequentially chased for 120 min. A second set of macrophages was pulsed with 1 µm latex beads in DMEM for 30 min and chased for 60 min after washing. CTMR-BSA labelled LYS were purified from cell homogenates using a magnetic rack, and LBP were purified in a density gradient. CaFu (10 min, 37 °C) and StaFu (60 min, 37 °C) reactions were run in parallel with either 1, 3 or 5 mM NEM. 5 mM of inactivated NEM were added as negative control. Positive control samples for CaFu and StaFu were prepared as stated before. Data is presented as means of relative colocalization +SD (n=3). Individual data points are shown as black dots [2].

LBP-LYS fusion was not inhibited in StaFu and CaFu samples containing inactivated NEM. Surprisingly, adding as much as 3 mM NEM did not reduce CaFu fusion frequencies, whereas StaFu was reduced by ~ 80%. Furthermore, adding 1 mM NEM to StaFu reactions already decreased colocalization by 75 %. CaFu on the other hand was only decreased by roughly 50 % with 5 mM NEM added. Fusion in the corresponding StaFu sample was similar to the ice control (Figure 25) [2].

To investigate whether CaFu relies on action of SNARE proteins without the participation of NSF, two different approaches were pursued. NSF does not interact directly with *cis*-SNARE complexes but requires action of its cofactors from the SNAP family (α-, β- and γ-SNAP), of which α-SNAP is the most abundant [141]. After α-SNAP binds to *cis*-SNARE complexes, NSF is recruited for ATP-dependent SNARE complex disassembly, rendering the individual SNAREs viable for another round of fusion [302]. α-SNAP is not only needed as cofactor of NSF but also displays regulatory activity in SNARE-mediated fusion independently of NSF [98,323–325]. Recombinant α-SNAP WT and the α-SNAP^{L294A} mutant protein were added to StaFu and Cafu reactions, to further assess whether SNAREs participate in CaFu or not. StaFu and CaFu reaction mixes were prepared in parallel. Fluorescently labelled LYS and LBP were preincubated with different concentrations of α-SNAP-His$_6$ or α-SNAP^{L294A}-His$_6$ (recombinant proteins prepared by D. Schüttenhelm; Figure 26 A & B). The recombinant proteins were purified from *E. coli* BL21, and a Coomassie gel for validation of the proteins is shown in Figure 26 C.

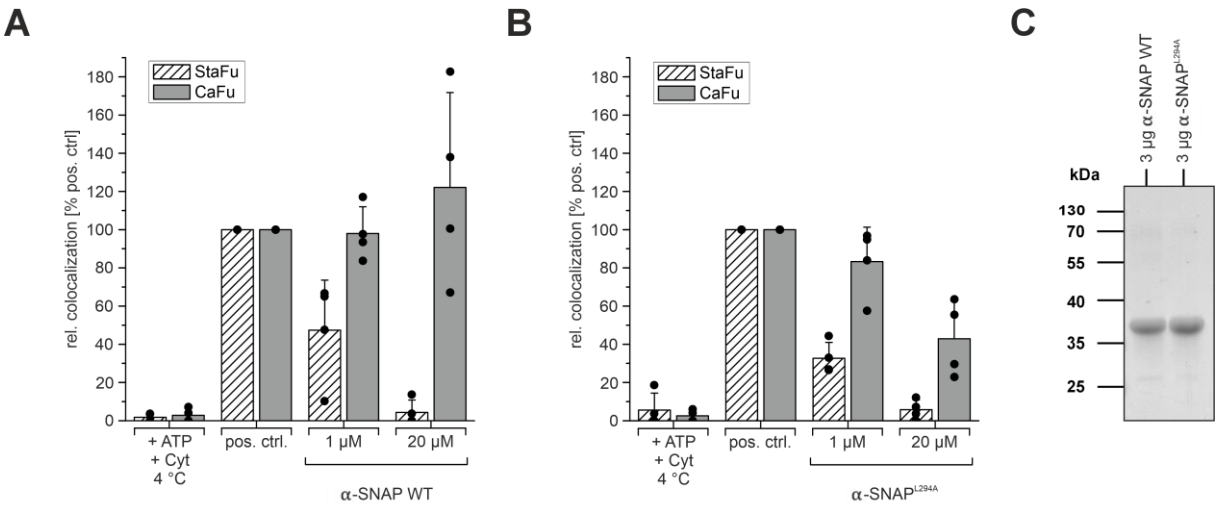

Figure 26: StaFu is inhibited by α-SNAP WT and α-SNAP^{L294A}, whereas Cafu is only partially inhibited by α-SNAP^{L294A}. J774E macrophages were preloaded with CTMR-BSA overnight, before pulsing for 30 min with DMEM/FF. Cells were washed to remove excess FF and subsequentially chased for 120 min. A second set of macrophages was pulsed with 1 µm latex beads in DMEM for 30 min and chased for 60 min after washing. CTMR-BSA labelled LYS were purified from cell homogenates using a magnetic rack, and LBP were purified in a density gradient. CaFu (10 min, 37 °C) and StaFu (60 min, 37 °C) reactions were run in parallel with 1 and 20 µM of (**A**) α-SNAP WT or (**B**) α-SNAP^{L294A} added. Positive control samples for CaFu and StaFu were prepared as stated before. Data are shown as mean of relative colocalization +SD (n=4). Individual data points are shown as black dots [2]. (**C**) His_6 fusion proteins were expressed in *E. coli* BL21 DE3 and purified using Ni-NTA or affinity chromatography. For validation of the used proteins, 3 µg of protein were separated by molecular weight on a 12 % SDS-polyacrylamide gel and stained with Coomassie.

StaFu was inhibited by α-SNAP WT by ~50 % at 1 µM and is fully inhibited by the addition of the comparably low concentration of 20 µM. CaFu on the other hand was not inhibited by adding α-SNAP WT at either concentration. The addition of α-SNAP^{L294A} inhibited StaFu even more effectively than the WT protein. At 1 µM, StaFu was already inhibited by approximately 75 % and was fully inhibited at 20 µM α-SNAP^{L294A}. Adding 1 µM α-SNAP^{L294A} had no effect on CaFu. Moderate reduction in CaFu fusion frequency was only observed at 20 µM α-SNAP^{L294A} (Figure 26 A) [2].

A different approach to investigate SNARE involvement in CaFu was to add recombinant SNARE domains directly to the reaction mixes. This approach has previously been used to investigate SNARE participation in StaFu [238]. The recombinant soluble SNARE domains were expressed in *E.coli* BL21 DE3 and purified using affinity chromatography. Figure 27 B shows a representative coomassie gel of the purified fragments. LBP and fluorophore-labelled LYS were preincubated with 50 µM of either solVti1b-His_6, solStx8-His_6 [299,326], ΔTM-Stx7-GST [122], and VAMP7-longin-His_6 [126] respectively, or 50 µM of a mixture of three SNARE domains consisting of solVti1b/Stx7/Stx8. The 3 Q-SNAREs were preincubated on ice for 90 min, with 16.7 µM of each solSNARE, before adding it to the reaction mix, where they likely formed a preassembled 3-helix bundle [327,328]. CaFu and StaFu reaction mixes were prepared in parallel [2].

If SNAREs were needed for Ca^{2+}-dependent LBP-with-LYS fusion, the added solSNARE domains would likely reduce fusion, as previously reported for StaFu [238].

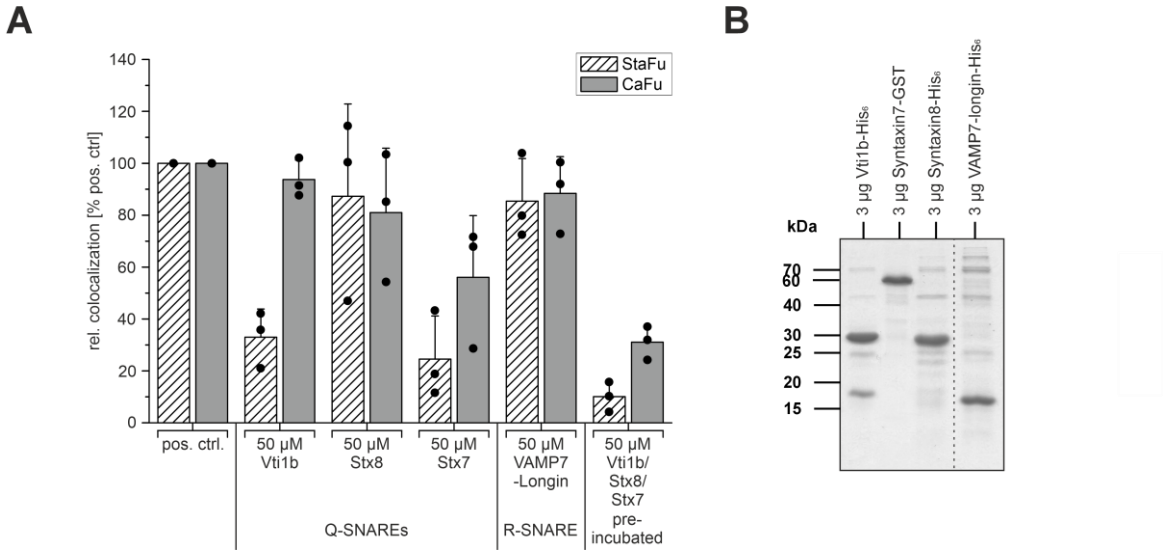

Figure 27: CaFu is likely reliant on a late endosomal Q-SNARE complex. J774E macrophages were preloaded with CTMR-BSA overnight before pulsing for 30 min with DMEM/FF. Cells were washed to remove excess FF and subsequentially chased for 120 min. A second set of macrophages was pulsed with 1 µm latex beads in DMEM for 30 min and chased for 60 min after washing. CTMR-BSA labelled LYS were purified from cell homogenates using a magnetic rack, and LBP were purified in a density gradient. CaFu (10 min, 37 °C) and StaFu (60 min, 37 °C) reactions were run in parallel. (**A**) Either 50 µM of Vti1b-His_6, Stx8-His_6, Stx7-His_6, VAMP7-longin-His_6 or preincubated (90 min, on ice) Vti1b/Stx8/Stx7 (16.7 µM each) were added to the reaction mixes. Positive control samples were prepared as previously stated. Data is shown as means of relative colocalization +SD (n=3). Individual data points are shown as black dots [2]. (**B**) His_6 or GST fusion proteins were expressed in *E. coli* BL21 DE3 and purified using either Ni-NTA or glutathione-sepharose affinity chromatography. For validation of the used proteins, 3 µg of protein were separated by molecular weight on a 12 % SDS-polyacrylamide gel and stained with Coomassie.

solVti1b and ΔTM-Stx7 reduced LBP-with-LYS fusion in StaFu samples considerably by ~70-75 % but had no effect on fusion frequencies in CaFu reactions. The addition of solStx8 and VAMP7-longin had no effect on either reaction Figure 27 A. The mixture of the three soluble Q-SNAREs Vti1b/Stx8/Stx7 strongly inhibited CaFu and StaFu by approximately 70 and 85 % respectively.

5.10 Search for a possible Ca^{2+}-sensor protein and physiological role

5.10.1 High concentrations of Sr^{2+} stimulate LBP with LYS fusion

Some proteins can be activated by various metal ions to different degrees depending on the affinity for the respective ion and its radius [329,330]. Creating a comprehensive ion profile could lead to the identification of a POI that may mediate the CaFu reaction and acts as Ca^{2+} sensor. To expand the ion profile [2] of the CaFu reaction generated by J. Becker, different concentrations of Sr^{2+} were tested for their ability to elicit fusion in a CaFu-type setting.

LBP and LYS were incubated with either 100 µM Ca^{2+} or various concentrations of Sr^{2+} (10, 100, 1000 µM). To match the experimental conditions that J. Becker chose and to avoid deviations from the intended [Sr^{2+}] due to possibly different affinity of Sr^{2+} to ADA, the reaction mixes were prepared without DTT and ADA [2].

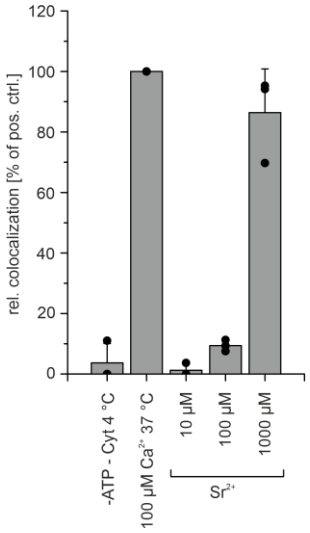

Figure 28: 1 mM of Sr^{2+} stimulates fusion to the same extent as 100 µM Ca^{2+}. J774E macrophages were preloaded with CTMR-BSA overnight before pulsing for 30 min with DMEM/FF. Cells were washed to remove excess FF and subsequentially chased for 120 min. A second set of macrophages was pulsed with 1 µm latex beads in DMEM for 30 min and chased for 60 min after washing. CTMR-BSA labelled LYS were purified from cell homogenates using a magnetic rack, and LBP were purified in a density gradient. CaFu-style reaction mixes, without ADA and DTT, were prepared containing either 100 µM Ca^{2+} or 10, 100 and 100 µM Sr^{2+}. Samples were incubated for 10 min at 37 °C before the reaction was stopped on ice. Absolute colocalization frequencies were normalised to 100 µM Ca^{2+}. Data is presented as means +SD (n=3). Individual data points are presented as black dots [2].

The addition of 10 or 100 µM Sr^{2+} to the reaction did not result in any significant fusion beyond that of the negative control. However, when adding 1000 µM Sr^{2+} to the fusion reaction, fusion was observed to a similar extent as for 100 µM of Ca^{2+} [2] (Figure 28). These results allow expanding the already-known ion spectrum of CaFu (Mn^{2+}, Ba^{2+}, Ca^{2+}) by Sr^{2+}.

5.10.2 CaFu is not inhibited by $cPLA_2$ inhibitor $AACOCF_3$

A CaFu-style reaction can also be elicited by high concentrations of Ba^{2+}, Sr^{2+} and Mn^{2+}. Reynolds et al. postulated that $cPLA_2$ was activated not only by Ca^{2+} but also by Ba^{2+}, Sr^{2+} and Mn^{2+} to about the same extent as with Ca^{2+} [331]. PLA_2 activity has also been described in the context of endosome fusion and G-protein-mediated secretory vesicle fusion [278,332,333], rendering it an interesting candidate for investigation as possible Ca^{2+}-sensor in CaFu.

Arachinodyl trifluoromethyl ketone ($AACOCF_3$) is a tight binding inhibitor of the 85 kDa $cPLA_2$, which inhibits its enzymatic activity [334,335] and has been used to investigate the

participation of $cPLA_2$ in various physiological processes [333,336]. StaFu and CaFu reactions were prepared with LBP and CTMR-BSA labelled LYS from J774E macrophages, preincubated with either 1, 5, 10 or 20 µM of $AACOCF_3$. A sample to which the same volume of EtOH was added as the sample with the highest inhibitor concentration served as a solvent control. If $cPLA_2$ served as the link between Ca^{2+} signal and membrane fusion, a reduction of fusion frequencies would be expected upon adding $AACOCF_3$. Neither addition of $AACOCF_3$ nor EtOH had negative effects on CaFu or StaFu fusion frequencies. The relative extent of fusion was similar to the respective positive control samples for both reactions.

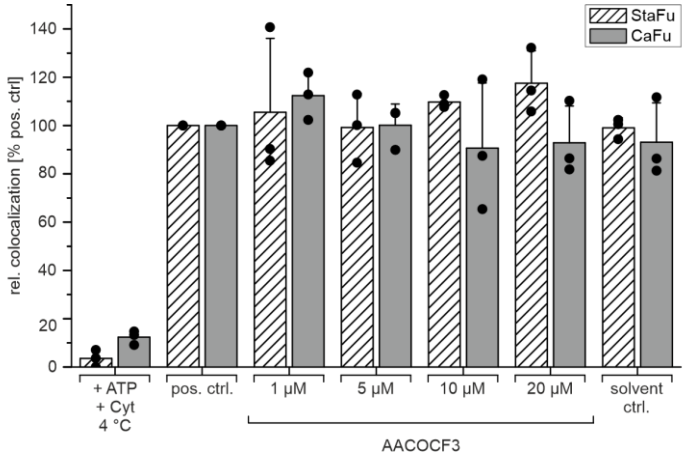

Figure 29: $AACOCF_3$ inhibitor of cytosolic phospholipase A2 has no effect on fusion reactions. J774E macrophages were preloaded with CTMR-BSA overnight before pulsing for 30 min with DMEM/FF. Cells were washed to remove excess FF and subsequentially chased for 120 min. A second set of macrophages was pulsed with 1 µm latex beads in DMEM for 30 min and chased for 60 min after washing. CTMR-BSA labelled LYS were purified from cell homogenates using a magnetic rack, and LBP were purified in a density gradient. CaFu (10 min, 37 °C) and StaFu (60 min, 37 °C) reactions were run in parallel. 1, 5, 10 or 20 µM $AACOCF_3$ were added in a maximum of 2 µL of EtOH. 2 µL of EtOH served as solvent control. Positive control samples were prepared for CaFu and StaFu respectively, as described before (Chapter 4.2.4.10). Absolute colocalization frequencies were normalised to the respective CaFu or StaFu positive controls. Data is shown as means +SD (n=3). Black dots represent individual data points.

5.10.3 LYS from J774E macrophages do not contain myoferlin or Syt-7

Usually, intracellular Ca^{2+} levels range around 100 nM, much less than extracellular [Ca^{2+}] with 2-3 mM. It is only increased moderately (1-10 µM) in many signalling processes [201,337,338]. Membrane rupture on the other hand causes rapid and uncontrolled influx of Ca^{2+} in the cell. Injury repair relies on proteins that act as Ca^{2+}-sensors to detect injury-related Ca^{2+} influx and mediate repair responses. Proteins such as Syts are prime candidates for acting as such sensors. [201,250,339]. Syt-7 is of special interest in this regard since it can be activated by Sr^{2+} and Ba^{2+} as well as Ca^{2+} and has also been implicated in regulating (and limiting) lysosomal exocytosis [268,340,341]. Another promising candidate as Ca^{2+}-sensor in Ca^{2+} dependent fusion of LBP with LYS is the protein myoferlin. It is a type II membrane protein of the ferlin family located on

lysosomes and possesses seven Ca^{2+}-sensitive C2 domains. It has been implicated in myoblast fusion, lysosomal exocytosis in phagocytes, and it is also thought to mediate membrane repair in response to Ca^{2+} influx [274,277,342,343].

To test possible involvement of Syt-7 or myoferlin in CaFu, it was first assessed whether both proteins were present on lysosomal membranes of J774E macrophages. 20 and 50 µg of PNS and purified LYS were analysed for their Syt-7 and myoferlin contents, using SDS-PAGE and subsequent immunoblot analysis.

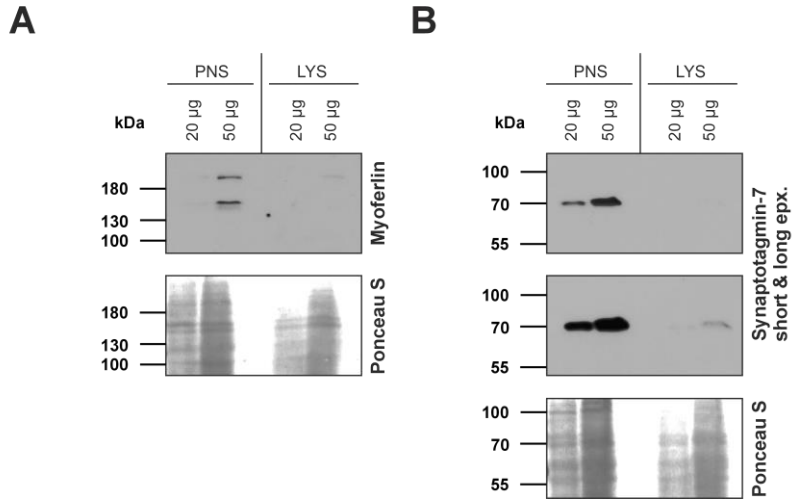

Figure 30: Neither Syt-7 nor myoferlin are present on J774E LYS. J774E macrophages were pulsed with DMEM/FF for 30 min. Excess FF was removed by washing, and endocytic compartments were allowed to mature within a 120 min chase period. LYS were purified from cell homogenates with a magnetic rack and processed for SDS-PAGE. A sample of PNS was set aside on ice beforehand. 20 or 50 µg of PNS or LYS preparations were separated via SDS-PAGE and analysed for (**A**) myoferlin and (**B**) Syt-7 with immunoblotting. A representative blot is shown. Ponceau S staining of nitrocellulose-membrane was performed to assess quality of sample-loading (n=2) [2].

Myoferlin levels in PNS fractions of J774E cells were very low and myoferlin was not enriched on LYS. Almost no myoferlin was detected in the 50 µg LYS sample (Figure 30 A). Syt-7 on the other hand was abundant in PNS samples, but even after long exposure times very little Syt-7 was detected in LYS samples containing 50 µg of protein (Figure 30 B) [2].

5.10.4 GTPγS inhibits StaFu, but not CaFu

Annexins are a family of Ca^{2+}- and lipid-binding proteins, involved in membrane repair mechanisms and exocytic fusion [344–347]. The non-hydrolysable GTP analogue guanosine 5´-[-γ-thio]triphosphate (GTPγS) is known to promote Ca^{2+}-dependent secretion in various cell types [348–350]. Caohuy and colleagues showed that adding 200 µM of GTPγS increased annexin A7 (AnxA7)-driven baseline fusion of PS-liposomes by ~50-60 %, but the activating effect dissipated upon the addition of ~ 500 µM GTPγS [344].

To assess possible participation of AnxA7 in Ca^{2+}-dependent LBP-LYS fusion, CaFu and StaFu reactions were supplemented with various amounts of GTPγS. LBP and CTMR-BSA labelled LYS from J774E macrophages were preincubated with either 20, 100, 500 and 1000 µM GTPγS. Subsequently, fusion reactions were carried out under standard StaFu or CaFu conditions. In the case of AnxA7 involvement in the CaFu reaction, an increase in fusion frequency, similar to the observations of Caohuy and colleagues would be expected. Adding 20 µM of GTPγS led to an insignificant increase in CaFu fusion frequencies. All other concentrations had no effect on CaFu. StaFu was progressively more inhibited when higher [GTPγS] were added. The addition of 20 µM of GTPγS led to partial inhibition of StaFu. Almost full inhibition was achieved with 100 µM of GTPγS [2] (Figure 31).

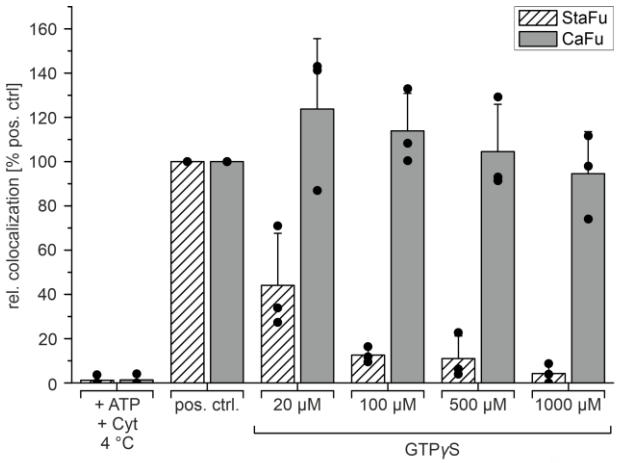

Figure 31: GTPγS has no effect on CaFu, but fully inhibits StaFu at 100 µM. J774E macrophages were preloaded with CTMR-BSA overnight, before pulsing for 30 min with DMEM/FF. Cells were washed to remove excess FF and subsequentially chased for 120 min. A second set of macrophages was pulsed with 1 µm latex beads in DMEM for 30 min and chased for 60 min after washing. CTMR-BSA labelled LYS were purified from cell homogenates using a magnetic rack and LBP were purified in a density gradient. 20, 100, 500 or 1000 µM GTPγS were added to the CaFu and StaFu reaction mixes and preincubated on ice for 10 min. CaFu (10 min, 37 °C) and StaFu (60 min, 37 °C) reactions were run in parallel. Positive control samples for CaFu and StaFu respectively were prepared as stated before (Chapter 4.2.4.10). Absolute colocalization was normalised to the respective positive control samples. Data is presented as means + SD (n=3). Black dots show colocalization from individual experiments [2].

6 Discussion

6.1 Arl8, Rab7a, HOPS, and BORC control acquisition of lysosomal markers on maturing endosomes

Endocytosed cargo marked for degradation is trafficked along the endocytic pathway, subsequently passing through EEs and LEs until it is eventually degraded in ELYS [47]. ELYS are the primary compartments for degradation and are formed by 'kiss and run' or full fusion events of LEs and (storage) LYS [88,89]. The investigated factors Arl8, Rab7a, HOPS and BORC participate in organelle positioning, regulation of LYS acidification, LYS-function, and -biogenesis (see introduction for details). Their involvement in the LE-LYS fusion needs to be assessed in more detail. Many excellent studies investigated the functions of and interactions between Arl8, Rab7a, HOPS, and BORC and their various effectors, primarily focusing on colocalization of certain marker proteins in microscopic assays and pull-down experiments [181–183,351]. However, it has yet to be uncovered in which order Arl8, Rab7a, HOPS and BORC are recruited to endocytic compartments and execute their functions. It also remains elusive how HOPS is recruited and anchored to late endocytic membranes. To better understand the influence of Arl8, Rab7a, HOPS and BORC on cargo transport in the endocytic continuum and how their absence affects the maturation of endocytic compartments, FFEs from different KO cell lines were purified and biochemically analysed for their content of different LYS marker proteins and hydrolase activity. Considering the postulated roles of the investigated proteins and complexes in endosomal and lysosomal biogenesis [105,351,352], it is also important to establish whether all cell lines used possess bona fide LYS or if loss of some of the proteins lead to impaired LYS biogenesis.

6.1.1 Cargo transport to LYS is impaired in cells deficient for Rab7a, Arl8, HOPS, and BORC

For initial assessment, FFEs and PNS fractions from WT, Rab7a, Arl8b, Arl8a/b, Vps41 (HOPS), myrlysin, and diaskedin (BORC) KO Hela cells were purified and analysed for their LAMP1 contents. LAMP1 levels were reduced in FFEs from all KO cell lines, except Arl8b KO (c.f. [10]). LAMP1 levels in PNS were similar to the respective WT control (Arl8b KO) or higher. The data for LAMP1 levels in WT Hela cell PNS and FFE presented here were mostly in line with the data previously presented by A. Jeschke in [10], validating these observations. Only for Arl8b FFEs, a minor reduction in LAMP1 levels on FFEs was observed [10], which

could not be seen here. Another deviation concerns the LAMP1 levels in PNS fractions of Arl8a/b, Vps41, myrlysin, and diaskedin KOs. PNS LAMP1 levels were similar across all cell lines in [10], whereas here, they were elevated in Arl8a/b, Vps41, myrlysin, and diaskedin KOs. Signals measured in PNSs were generally small, which makes them susceptible to increased volatility. Therefore, LAMP1 levels in Arl8a/b, Vps41, myrlysin and diaskedin KO PNS are more likely to be similar to the WT rather than higher. Both data sets reproduced an increase in LAMP1 in PNS fractions of Rab7a KO relative to its respective WT.

Arl8b KO did not display any reduction in FFE LAMP1 levels, which was unexpected. Various studies regarding the functions of Arl8 were conducted using Arl8b KO, KD or Arl8b fusion proteins, as it is the more abundant of the two paralogs [170,181–183]. For example, in lysates from Arl8b-KOs, binding of HOPS subunits Vps18 and Vps41 to PLEKHM1-GST was reduced. The effect was rescued when recombinant Arl8b-HA was added [183]. Garg and colleagues observed a marked reduction in LAMP1-staining fluorescence intensity on maturing IgG-labelled LBP in Arl8b KD RAW cells as opposed to untreated cells [181]. Here, a similar effect was only observed in FFEs when both Arl8 paralogs were knocked out. The same Arl8b KO clone [189] used here only yielded an intermediate phenotype in the 2021 study of Keren-Kaplan and Bonifacino. This circumstance prompted the generation of the Arl8a/b DKO cell line, also used in both studies (this study, [10,163]). KO of Arl8b, therefore seems to be suited to investigate binding of Arl8b to other proteins in pulldown assays [183]. However, this does not appear to be the case for experiments performed in live cells. Arl8a and b are partially redundant (this study, [163]). Arl8a alone seems sufficient to carry out the functions of Arl8 to the extent that no or only a moderate phenotype is elicited. Fittingly, in the GST-pulldown assay, it is also evident that Plekhm1-GST still binds minor amounts of Vps18 and Vps41 in the absence of Arl8b [183]. It can only be speculated if the action of Arl8a also caused this residual binding.

Reduction in LAMP1-levels on FFEs in Rab7a, Arl8a/b, Vps41, myrlysin, and diaskedin KOs (c.f. [10]) suggest that fusion between FF-containing compartments and LAMP1-positive organelles may be impaired. So far, two scenarios could explain the failure of endocytosed cargo to reach LYS: 1) Transport of compartments towards each other is obstructed in KOs and prevents FFEs and LYS from encountering. 2) The missing proteins are directly or indirectly involved in the fusion of LEs with LYS. Loss of either protein could hamper the establishment of the proper fusion machinery [10]. Depletion of LAMP1 in KO cells can also be eliminated, as LAMP1 PNS levels were similar across all cell lines.

These observations raise the question of the maturation status of the FFEs purified from KO cells. It is not possible to answer this question conclusively by solely determining LAMP1 levels on FFEs [312]. For example, Bright et al. postulated the existence of two different lysosomal compartments – ELYS and terminal storage LYS. ELYS are acidic and originate from LEs fusing with LYS. Terminal storage LYS, on the other hand, are thought to be non-acidic storage compartments for mature lysosomal hydrolases with no degradative activity. All three types of compartments exist in a dynamic equilibrium and are positive for LAMP1 [5,88,89]. Furthermore, a significant portion of LAMP1 localizes to non-degradative compartments, devoid of acid hydrolases as cathepsin B or D, or on LAMP1-carriers [353–355]. However, previous studies have assigned Rab7a, HOPS, BORC, and Arl8 to late stages in the endocytic pathway [99,100,105,183].

Previous studies suggest some of the proteins investigated may be involved in lysosome biogenesis [159,351]. Therefore, it must also be clarified what consequences deficiency for Rab7a, Arl8, Vps41, myrlysin, and diaskedin has for the ability of KO cells to degrade endocytosed material. Further experiments must focus on characterising FFEs purified from the KO cell lines and the overall presence and activity of acid hydrolases.

6.1.2 Degradative capacity is limited in FFEs from KO cells

Acid ß-galactosidase activity was measured to analyse the degradative capacities of FFEs from Rab7a, Arl8b, Arl8a/b, Vps41, myrlysin, and diaskedin KOs. Acid ß-galactosidase is a lysosomal hydrolase. It cleaves galactose residues from GM1-gangliosides, galactose-containing oligosaccharides and keratan sulphate (reviewed in [356]). Like Cath D, acid ß-galactosidase is transported to LYS in an M6P-dependent manner, requiring proteolytic processing and acidic pH to be active [357,358]. It is targeted to (endo)lysosomal compartments and hence has its pH optimum at pH 4.5-5.5 [359]. According to Bright and colleagues, degradative activity is mostly limited to ELYS [89], making determining enzymatic activity a well-suited measure for LE/FFE with LYS fusion.

Acid ß-galactosidase activity in FFEs from Arl8b, Arl8a/b, Vps41, myrlysin, and diaskedin KO was reduced by 30 to 40 % and in Rab7a KO by approximately 50 % compared to WT FFEs. Unfortunately, acid ß-galactosidase activity in PNS fractions was near the detection minimum and could not be measured. This was surprising and probably not caused by pH-dependent inactivation of the enzyme. The reaction buffer contains citric acid to accommodate the pH optimum of acid ß-galactosidase (see Chapter 4.2.6.6). It is likely that acid ß-galactosidase is either inhibited, inactivated or broken down in the presence of cytosolic proteins or inhibitors

[360], which would be the case in PNS samples. Acid ß-galactosidase activity is nearly not detectable in WT PNS samples, favouring the hypothesis of inactivation since in WT FFEs, robust acid ß-galactosidase activity can be measured. To test this hypothesis, another acid ß-galactosidase assay could be performed in which WT FFE and another sample in which WT FFE are mixed with an equivalent amount of PNS. If enzyme activity is reduced by such treatment, acid ß-galactosidase activity is most likely impaired in the presence of some cytosolic proteins. The observed reduction in enzyme activity was not as pronounced as the reduction in LAMP1 protein levels. Nonetheless, acid ß-galactosidase activity was reduced in KOs FFEs. Differences in the amount of active acid ß-galactosidase could be attenuated by enzymatic amplification of substrate conversion, leading to an overall less drastic phenotype. A relatively small amount of active enzyme could still yield a relatively high amount of fluorogenic substrate [361].

As overall activity levels in PNS fractions cannot be measured, the reason for reduced activity in FFE fractions of the KO cell lines is difficult to determine. There are two possibilities: 1) FFEs cannot fuse with LYS, which harbour the bulk of active acid ß-galactosidase. Acid ß-galactosidase enters the endocytic pathway in an M6P-dependent fashion. Therefore, a portion of active enzyme is probably already present in LEs [358,362], hence the relatively high remaining enzymatic activity. Such a scenario does not allow for a clear determination of FFE maturation status, but given the remaining ß-galactosidase activity, FFEs possess at least some late endosomal characteristics. 2) Due to the lack of enzyme activity in PNS, it is not possible to determine whether overall cellular acid ß-galactosidase activity in KO cells is the same as for WT cells or if deficiency for some of the proteins investigated causes defects in LYS biogenesis. The latter case would most likely reduce overall levels of active acid ß-galactosidase in KOs. Regardless of what causes low enzymatic activity in PNSs, the assay is not suited to distinguish between these two possible scenarios. Furthermore, a reduction of *in vivo* enzymatic activity, as reported for dominant negative Rab7a variants [351], would be masked by the reaction conditions used in the assay since pH-dependent inactivation of acid ß-galactosidase is reversible [363].

Additionally, PNS fractions and FFEs from WT and KO cells were analysed for their mCath B (not Rab7a KO) and D levels (this study, [10]). mCath D and B are mostly localised in LYS [5] and are commonly used as lysosomal markers [312]. The two acid hydrolases are synthesised as inactive zymogens. They are trafficked through the secretory route and eventually end up in LYS in their active, mature forms. Cath B is a cysteine-protease with endo- and exo-peptidase

activity [364]. It consists of a heavy chain of approximately 25 kDa and a light chain of 5 kDa, linked by a disulfide bond [365]. Cath B is autocatalytically activated at low pH values [67]. Cath D is an asparagine-(endo)protease. Its mature form consists of a 34 kDa heavy chain and a 14 kDa light chain linked through non-covalent interactions. It is presumably activated by cysteine-proteases from its inactive 47 kDa propeptide [66,366–368] but is also thought to activate itself autocatalytically [369,370].

mCath B was not detectable in any of the PNS fractions nor in FFEs from Arl8a/b, Vps41, myrlysin, and diaskedin KOs. In Arl8b KO FFEs, mCath B levels were steeply reduced compared to the WT. Unfortunately, the antibody used for detection of mCath B was discontinued. Protein levels in Rab7a KOs could not be determined as a result. mCath D levels in WT, Arl8b, Arl8a/b, Vps41, myrlysin, and diaskedin KOs behaved similarly to mCath B. The only exception being mCath D levels not being reduced in Arl8b KO compared to WT mCath D levels [10]. Immunoblot analysis of 100 µg PNS revealed that mCath D levels were similar across WT, Arl8b, Arl8a/b, Vps41, myrlysin, and diaskedin KOs. The analysis of 100 µg PNS was inconclusive for mCath B (not shown). In Rab7a KO, mCath D levels were reduced by 85 %, while mCath D levels in Rab7a KO and the WT were similar [10]. Analysis of membrane fractions of WT and KO cells [10] corroborates the observation made here that PNS mCath D levels are similar across all cell lines.

Overall, cellular levels of mCath D (PNS) remain similar across WT and KO cell lines, indicating the existence of functional (E)LYS in KO cells. However, reduced levels of lysosomal hydrolases in FFEs of Rab7a, Arl8a/b, Vps41, myrlysin, and diaskedin KOs hint at hindered trafficking of endocytosed cargo to compartments containing the bulk of active mCath D. Similar observations were made in Arl8b-silenced RAW cells. Transport of endocytosed dextran was delayed, but steady-state distribution of lysosomal markers, such as Cath D, was unchanged [181]. Therefore, Arl8b-silenced cells likely possess bona fide (E)LYS, which cannot be reached by endocytic cargo. In the case of Vps41 KO, this assumption is corroborated by observations from van der Beek and colleagues. Inactive proforms of Cath D and endocytic cargo accumulated in hybrid compartments termed ‘HOPS bodies’. These are positive for early (Rab5, EEA1) and late endocytic (Rab7, LAMP1) markers but lack active Cath D. Although HOPS bodies lack active Cath D and acidification [314], an earlier study reported unaltered lysosomal pH and Cath B activity in Vps41-depleted cells [371]. These findings corroborate the conclusion that HOPS-depleted cells also possess normal (E)LYS.

The findings of Van der Beek et al. also raise the question of whether compartments similar to HOPS bodies are present in Rab7a, Arl8, or BORC-deficient cells and if FFEs from KO cells potentially resemble such compartments. For example, cargo trafficking in Arl8b-silenced cells was delayed [181]. Depletion of Arl8b did not alter the overall colocalization of LAMP1 with Cath D [181]. However, the experimental setup in the study by Garg and colleagues does not allow for the distinction between active and inactive Cath D. HOPS bodies in Vps41 KOs have been shown to contain inactive Cath D and LAMP1 [314]. Therefore, delayed cargo trafficking in Arl8b-depleted cells [181] could potentially be associated with cargo being 'trapped' in compartments resembling 'HOPS bodies'. Considering the interactions of Vps41 (HOPS) with Arl8 [182], it seems likely that depletion of either protein would lead to similar phenotypic characteristics. Moreover, BORC is well-established as recruiter of Arl8. In the absence of several BORC subunits, Arl8 is virtually absent from membranes, which likely results in a similar outcome as Arl8 depletion [169,305].

6.1.3 ELYS are present in Rab7a, Arl8, HOPS, and BORC-deficient cells

Another hallmark of endosome maturation is acidification. The luminal pH of maturing endosomes gradually becomes more acidic, which is important for properly releasing ligands bound to their endocytic receptors and acid hydrolase function [47]. To understand whether deficiency for Rab7a, Arl8, HOPS, or BORC results in defective acidification, cells were stained with LT. Additionally, this should provide insights as to whether functional (E)LYS are present in KO cells.

All cell lines contained LT-positive compartments. Measurement of fluorescence intensities normalised to the absolute number of cells revealed accumulation of similar amounts of LT as in WT cells (Arl8b KO) or more (Rab7a, Arl8a/b, Vps41, myrlysin, diaskedin KO) (this study, [10]). All cell lines being positive for LT indicates the presence of acidic organelles (i.e. (E)LYS, LEs) in KO cells and WT cells alike. This conclusion is mostly congruent with observations made in previous studies using other systems. In Vps41 KD HeLa cells, no significant alterations in lysosome acidification were evident. Numerous LT fluorescence spots were observed, largely disappearing after incubation with vATPase inhibitor Bafilomycin [371]. Moreover, no defects in acidification were reported in Arl8 KO tissues of *Drosophila melanogaster* [372]. Deviating from the observations made here and in [10], in HeLa cells expressing dominant negative Rab7a variants, decreased lysosomal acidification was reported [351]. In the study by Bucci and colleagues, the LT fluorescence signal was decreased compared to control cells. This led to the conclusion that acidity of (E)LYS in cells with dominant negative Rab7a

was reduced. However, LT fluorescence is largely independent of pH and is therefore only suited to qualitatively assess whether acidic compartments (i.e. LEs, (E)LYS) are present. LT fluorescence intensity is dependent on size, number and contents of acidic organelles rather than the pH [312,373]. In line with this, Rosa-Ferreira and colleagues reported increased LT fluorescence in Arl8 deficient *D. melanogaster* tissues and increased compartment size [372], whereas Bucci et al. reported decreased compartment size [351]. It is of note that here and in [10], increased LT fluorescence intensities were reported in Arl8a/b DKO, but not for Rab7a KO. This discrepancy may be caused by the different experimental approaches used here and the study by Bucci and colleagues. Fittingly, normal acidification of LYS was observed in Rab7a KO fibroblasts. The authors proposed LYS generation via a novel non-canonical pathway in these KO cells [374]. Reduced LT-compartment size in cells transiently expressing dominant negative Rab7a [351] might reflect a short-term effect of depletion of functional Rab7a, whereas in Rab7a KO cells, the generation of LYS from REs [374] might reflect a long-term adaptation.

As LT cannot be used to accurately report on the pH of LT-positive compartments, small defects in acidification may not be detectable [312,371]. However, all KO cell lines contain LT-positive compartments. It can be stated that loss of none of the investigated proteins leads to a significant defect in compartment acidification. However, small deviations in compartment acidification cannot be ruled out as organelle positioning is a determinant of luminal pH in LYS [375]. This relies in part on the interplay between Rab7a and Arl8. Generally, LYS localized in the perinuclear region are more acidic than peripheral LYS. These usually contain less Rab7a, leading to reduced levels of the Rab7a effector RILP [375]. RILP helps to recruit the V1G1 subunit of lysosomal v-ATPase, responsible for acidification [376]. Peripheral LYS also show an increased permeability for protons [375].

Representative micrographs showed extensive perinuclear clustering of LT-positive compartments in Arl8a/b, myrlysin, and diaskedin KOs. Clustering was less pronounced in Arl8b KO. LT-positive compartment distribution resembled the WT situation in Vps41 KO. In Rab7a KO, on the other hand, LT-positive compartments were evenly distributed across the whole cell in contrast to the distribution seen in WT cells. These alterations in LT-compartment distribution are likely due to defective compartment positioning as Arl8 and Rab7a are regulators of LE/LYS positioning [78,377]. Numerous studies also reported altered distribution of LYS in cells deficient for Arl8, functional Rab7a, Vps41, myrlysin, and diaskedin. In Arl8b KD RAW cells, LAMP1-positive compartments showed perinuclear clustering [181]. In line with the more pronounced clustering in Arl8a/b DKO cells, compared to only Arl8b KO (this study),

the same Arl8b KO cell line used here still showed some peripheral localization of LYS [163]. No LYS localized to the cell periphery in Arl8a/b DKO cells, which were also used here [163]. These observations also fit well with the known function of Arl8 to mediate anterograde transport of LYS to the cell periphery [377]. In accordance with the study by Johnson and colleagues, these (E)LYS might be more acidic than in WT cells. Inactivation of Rab7a by the Arl8 effector SKIP [99] is likely impaired in cells lacking Arl8, possibly leading to continued perinuclear localization and vATPase recruitment. Conversely, loss of Rab7a might cause reduced acidity. As observed for Rab7a KO in this study, LT-positive compartments were distributed evenly across the cytoplasm, lacking the typical distribution seen in WT cells, in Rab7a KD fibroblasts [351]. However, whether loss of either Arl8, or Rab7a results in altered LYS-acidification cannot be determined using LT. Clustering in BORC-deficient cells might be caused by reduced amounts of Arl8 on LYS membranes [169]. LYS in BORC-deficient cells are localized in dense perinuclear clusters [169]. The perinuclear clustering of LT-positive compartments in myrlysin and diaskedin KOs is in accordance with previous observations in myrlysin and diaskedin KO cells. Loss of BORC subunit myrlysin has been postulated to lead to perinuclear clustering of compartments positive for lysosomal proteins LAMP1, CD63 and Lamtor4 [169]. The same clustering of Lamtor4-positive compartments was reported for diaskedin KO [189]. These observations fit well with BORC and Arl8 functions. BORC is an upstream effector of Arl8 and responsible for Arl8 recruitment and membrane association [169,305]. Loss of myrlysin results in a phenotype similar to Arl8a/b DKO since without BORC as membrane anchor, Arl8 is diffusely distributed and not localized to LYS [305]. HOPS is not implicated in mediating LE/LYS transport despite being linked to Arl8 and BORC functionally [305] and interacting with RILP and SKIP [99,179]. It is therefore not surprising that acidic compartments are distributed in a similar pattern as in WT cells. Van der Beek and colleagues observed some perinuclear clustering of endocytosed cargo in ‘HOPS bodies’, which also contain LE/LYS markers such as Rab7a or LAMP1. However, these compartments were not acidified. It is of note, that these assumptions need to be confirmed by accurately determining the lysosomal pH in these KO cell lines. A suitable probe might be LysoSensor, which exhibits a pH-dependent increase in fluorescence intensity [373].

Another question regards whether Rab7a, Arl8, Vps41, myrlysin, and diaskedin KO cells generally possess (E)LYS with functional hydrolases. An acidified environment is crucial for hydrolase function. Therefore, it seems likely that all KO cells also possess active hydrolases. However, the inability to determine PNS mCath B levels and overall acid ß-galactosidase activity necessitates verifying hydrolase activity by other means. As with LT, cells were stained with the Cath B substrate MR, and fluorescence intensities normalized to the number of cells.

All cell lines contained compartments positive for MR, and MR fluorescence intensities were similar across all cell lines. The distribution pattern observed for LT-positive compartments (this study, [10]) was also prevalent for MR-positive compartments (this study). Likely, the compartment populations stained by LT and MR have substantial overlap. This is also suggested by observations made by Bright and colleagues. MR-positive compartments also extensively accumulated LysoTracker Green, an acidotropic probe similar to LT. The compartments containing active hydrolases were termed ELYS and are postulated to be the primary sites of degradation [89]. The presence of active Cath B suggests that the loss of none of the proteins leads to the loss of functional (E)LYS. This conclusion is in line with results from previous studies. For example, Arl8 deficient tissues in *D. melanogaster* still stained positive with MR. Furthermore, active hydrolases accumulated in acidified compartments [372]. Similar observations were made for Vps41 KD HeLa cells, where the number of MR-positive ELYS was unaltered, compared to control cells [371]. Furthermore, Wang and colleagues report the presence of active Cath D in Rab7a KO fibroblasts [374].

Taken together, the data suggests that Rab7a, Arl8b, Arl8a/b, Vps41, myrlysin, and diaskedin KO cells possess bona fide (E)LYS since overall cellular levels of LAMP1 and mCath D are unchanged in KO cells. Fluorometric assessment also proves the existence of acidic and active Cath B-containing compartments in all KO cell lines. Furthermore, absence of mature cathepsins (except mCath B in Rab7a KO) and reduction in acid ß-galactosidase activity in compartments containing endocytosed FF indicates that Rab7a, Arl8, HOPS, and BORC are needed for delivery of endocytosed cargoes to (E)LYS. This raises the question of whether endocytosed cargo can reach degradative compartments and if fusion of FFE-containing compartments/vesicles with LYS is delayed or completely abrogated in KOs.

6.2 Endocytic traffic is delayed in Arl8a/b, Vps41, myrlysin, diaskedin, and Rab7a KOs

Previous experiments revealed the existence of bona fide (E)LYS with similar amounts of LAMP1 and mCath D in Rab7a, Arl8b, Arl8a/b, Vps41, myrlysin, and diaskedin KO cells [10]. (E)LYS in KOs are also comparable to WT (E)LYS in terms of acidity (LT) and hydrolase activity (MR) (this study, [10]). However, it was shown that lysosomal markers mCath D and LAMP1 are less abundant in FFEs from Arl8a/b, Rab7a, Vps41, myrlysin, and diaskedin KOs than in WT FFEs.

A microscopic approach was chosen to assess whether delivery of endocytosed cargo to acidic compartments (i.e. LE/ ELYS) was hampered in KOs. Bright and colleagues postulated that most degradation occurs in such acidic (LT-positive) compartments [89]. Cells were fed with ATTO488-dextran, and compartments were allowed to mature. Before imaging, acidic compartments were stained with LT, and perinuclear clusters of acidic compartments were dissolved by treatment with nocodazole. MCCs were determined [291,293] to quantify the portion of endocytosed ATTO488-dextran colocalising with acidic LT-positive compartments [10]. In line with previous observations (LAMP1 and mCath D levels in FFE), colocalization in Arl8b KO was not reduced. Colocalization of ATTO488-dextran was markedly reduced in Rab7a, Arl8a/b, Vps41, myrlysin, and diaskedin KOs, compared to the WT control. This is consistent with reduced mCath D and B levels in FFEs from the same KO cell lines [10]. Reduced colocalization of endocytosed dextran with LT suggests reduced fusion of compartments containing endocytosed material with acidic compartments in cells deficient for Arl8a/b, Rab7a, Vps41, myrlysin, and diaskedin. As activation of cathepsins is dependent on acidic pH [378], it is likely that a substantial portion of endocytosed material in KOs does not reach active (E)LYS. This assumption is substantiated by observations made in HOPS-deficient cells. Compartments accumulating endocytosed dextran contained less active Cath D than WT cells and were less acidic [314]. Also in line with this conclusion, fluorescent dextran was transported less to compartments containing active Cath B (MR-positive) in Vps41 and Vps39 KD cells [371].

Apparently, although Rab7a, Arl8a/b, Vps41, myrlysin, and diaskedin KO cells contain enzymatically active (E)LYS, endocytosed material does not reach these compartments. This raised the question of whether cargo transport to LYS was completely abrogated in these KOs or merely delayed. To provide more clarity, ATTO488-dextran labelled compartments were left to mature significantly longer than before (24 h incubation total). This treatment was meant to label compartments at the endpoint of the endocytic pathway (LYS/ storage LYS). Afterwards, cells were fed with TAMRA-dextran in a second pulse/chase. Endocytosed compartments were allowed to mature for a similar time as in the previous experiment. MCCs were calculated to determine the fraction of TAMRA-dextran accumulating in ATTO488-dextran-compartments (content mixing). The experiment could not be performed with Rab7a KOs due to technical issues. In WT cells and Arl8b KO, extensive overlap between green and red fluorescence signals was observed. In this experimental setup, Arl8b showing a similar extent of colocalization between green and red fluorescence signals could have two reasons. Either the transport of cargo is abolished at some point, or endocytic compartments in Arl8b KOs are of the same maturation stage as the WT. Considering the gathered experimental evidence, the

latter is more likely the case. For Arl8a/b, Vps41, myrlysin, and diaskedin, colocalization of TAMRA-dextran with upstream ATTO488-dextran was reduced compared to the WT. This not only suggests that endocytosed cargo can reach compartments as LYS in KOs but also that after the previously used chase periods, the endpoint in cargo trafficking has not yet been reached in KOs. Furthermore, this indicates that transport in Arl8a/b, Vps41, myrlysin, and diaskedin KOs is severely delayed rather than completely abolished.

Similar observations were made for Arl8a/b DKO in a study by Garg and colleagues. Content mixing of two successively internalised fluorescently labelled dextrans was delayed in Arl8b KD cells. The delivery of cargo taken up by receptor-mediated endocytosis (Dil-LDL, antibody-bound CD1d) to dextran-labelled LYS was also delayed [181]. Curiously, the effects described for Arl8b KD [181] cells were only seen for the Arl8a/b DKO cell line but not for the Arl8b single KO cell line (this study). This could be either due to differences between cell lines or represent a long-term adaptation of Arl8b KO cells as a response to Arl8b deficiency. Increased Arl8a expression could potentially be the result of Arl8b depletion. However, this assumption cannot be verified using immunoblotting due to the overall low abundance of Arl8a. Previous studies also acknowledged a moderate phenotype in Arl8b KOs compared to Arl8a/b DKO, which was attributed to at least partial redundance of Arl8a and b [163,189,305].

FFEs that were purified after 24 and 2 h of chase were analysed for their mCath D levels to confirm that transport of endocytosed cargo is delayed in Arl8a/b, Vps41, myrlysin, and diaskedin KOs and to determine whether this is also the case for Rab7a KOs [10]. mCath D was chosen as a marker for multiple reasons. It is already known from previous experiments that overall cellular levels of mCath D are similar across all cell lines used (this study, [10]). mCath D is detected on FFEs late in FFE maturation, comparable to proteins like LAMP1 or Arl8 (Supp. Figure 2). Furthermore, Bright and colleagues describe (E)LYS as hybrid compartment originating from fusion events between LEs and catalytically inactive storage LYS [89]. This suggests that the bulk of mature acid hydrolases (i.e. mCath D) are present in either ELYS or storage LYS. Generally, mCath D levels were higher after 24 h of chase than they were after 2 h of chase in KO cells. Only in the WT FFEs did not show a significant difference in mCath D levels, regardless of the duration of the chase period. After 24 h, mCath D levels in Arl8b, Arl8a/b, Vps41, myrlysin, and diaskedin KOs were almost as high as in WT FFEs. In Rab7a KO, however, mCath D levels increased after 24 h, but not as much as seen with the other KO cell lines (this study, [10]).

These results further substantiate the conclusion that delivery of endocytosed cargo is delayed rather than abrogated in Arl8a/b, Rab7a, Vps41, myrlysin, and diaskedin KOs. Garg and colleagues attributed similar observations as made here [10] to reduced fusion of endocytic compartments with LYS. In their study, Arl8b-silencing led to delayed appearance of LAMP1 on IgG-coated LBP, compared to control cells [181]. This is also congruent with reduced LAMP1 levels on FFEs of KO cells after 2 h of chase (this study; [10]). Effects of Arl8a/b depletion are most likely not caused by decreased dextran uptake. Assessment of TfR-uptake and recycling indicated that endosome maturation is unaffected up to this point, and defects occur downstream of TfR-positive compartments [181].

Delayed trafficking of cargo to LYS in myrlysin and diaskedin KOs can potentially be attributed to reduced levels of Arl8 on LYS in myrlysin and diaskedin KOs [315]. Therefore, it is unsurprising that myrlysin and diaskedin KO phenotypes resemble the Arl8a/b DKO phenotype. Although BORC subunit lyspersin (and not myrlysin or diaskedin) has been reported to be essential for the association of Arl8 with BORC [188], KO of either myrlysin or diaskedin resulted in reduced levels of lyspersin on LYS [315]. Consequently, only little Arl8 is present on LYS in these KO cell lines [315]. Myrlysin is the proposed membrane anchor of BORC and associates with LYS membranes through a myristoylation in its N-terminal sequence [169]. BORC subunits diaskedin and lyspersin were reported to localize less to lysosomal membranes in myrlysin KO cells. Diaskedin KO cells were reported to have the same phenotype as myrlysin KOs [315]. In addition to these results, KD of myrlysin led to significant membrane dissociation of Arl8 and perinuclear redistribution of LYS [169], further substantiating this conclusion.

Transport of endocytosed material to LYS is delayed in Vps41 KOs but not abolished (this study, [10]). In their recent study, Van der Beek and colleagues observed an accumulation of endocytosed cargo in compartments with early and late endocytic markers and inactive cathepsins (HOPS bodies) [314]. As mCath B and D amounts were also reduced in FFEs of Vps41 KOs here [10], FFEs purified after 2 h of chase likely correspond to these ‘HOPS bodies’. After long chase periods, FFEs purified from Vps41 KOs contained similar amounts of mCath D as the WT [10], suggesting that fusion with compartments containing mature hydrolases was still possible. It was reported that ‘HOPS bodies’ also contained autophagy proteins (LC3, p62), which led to the proposition that an alternative, HOPS-independent pathway for the fusion of endosomes with autophagic compartments exists [314]. This possibility should be explored further. Additionally, as Arl8-, myrlysin-, and diaskedin-deficient cells display similar phenotypes, these cell lines should also be included.

In contrast to all other cell lines, FFEs from Rab7a KOs catch up the least amount of mCath D after 24 h of chase, which was a curious observation [10]. Wang and colleagues proposed a non-canonical LYS-biogenesis pathway from Rab4-positive REs in absence of Rab7a [374]. Considering this, it would have been expected that trafficking of endocytosed cargo to these alternative LYS was possible on a larger scale. However, this does not seem to be the case. It is conceivable that, similar to Vps41 KO cells, endosomes first fuse with autophagic compartments and later reach Rab4-LYS. This would generally be possible, as autophagosome-LYS fusion was reportedly unaltered in Rab7a KOs. Another indication that endocytic compartments do not directly fuse with LYS is the observation that Rab5-positive endosomes do not receive LE- and LYS-specific proteins in Rab7a KOs, as would have been the case in WT cells [374]. Future experiments should further investigate how endocytosed material is trafficked to LYS in Rab7a KOs.

In summary, the collected data suggests that the fusion of FFEs with LYS is reduced in Rab7a, Arl8a/b, Vps41, myrlysin, and diaskedin KO cells. As a result, cargo trafficking is significantly slowed down. The determination of the maturation status of FFEs is difficult. Van der Beek and colleagues reported a mixed morphology for HOPS bodies, with characteristic protein markers for both early and late endosomes. Furthermore, accumulation of inactive Cath D proforms in HOPS bodies was observed [314]. Since Arl8, HOPS and BORC functions in LE-LYS fusion are intertwined, one possible explanation could be that in cells deficient for either protein(complex), no bona fide LEs are present, but instead compartments similar to the reported ‘HOPS bodies’. On the other hand, EEA1-positive compartment distribution is unaltered in myrlysin KO cells [379]. Moreover, defects in Arl8b-silenced cells occur downstream of TfR-trafficking, and Rab7a recruitment is unchanged [181]. Diminished fusion of LEs with LYS would likely also lead to increased amounts of pro-cathepsin D in LEs. Thus, it is possible that while early to late endosome conversion is delayed or abrogated in Vps41 KO, bona fide LEs, which are impaired in their ability to fuse with LYS to form ELYS, are present in cells lacking Arl8 and BORC (i.e. myrlysin, diaskedin). In Rab7a, KO LYS are likely generated via an alternative pathway, which is independent of the canonical Rab5 to Rab7 conversion. If similar alternative pathways exist in other KO cells, this further complicates the question of the nature of FFEs from such cells. Unfortunately, the assay used here is not suited to address such questions, as early markers are present for a long time even in FFEs from WT cells. The observed defects were attributed to reduced fusion of FFEs with LYS. With the methods used here, it is not possible to distinguish the cause for delayed cargo delivery to LYS. Delayed delivery could be due to impaired transport of FFEs towards LYS (or vice versa). If one of the

knocked-out proteins was directly required for the fusion of FFEs with LYS, its absence could lead to reduced fusion with LYS [10].

6.3 Rab7a and Vps41 are recruited to endosomes before Arl8 and BORC

6.3.1 Rab7a positive compartments are of an earlier maturation stage than Arl8 positive compartments

The distinction of LEs, ELYS and LYS remains a difficult subject because despite all three compartments being distinct entities, they share multiple marker proteins and exist in dynamic equilibrium with each other [89,312]. Rab7a is essential for the transformation from EEs to LEs [101,153] and the trafficking of endocytosed material from LEs to LYS, as well as LYS positioning [154,380]. Various reports also link Rab7a to LYS, as it is involved in lysosomal biogenesis and LYS-tubulation [351,381]. Moreover, Rab7a- and LAMP1-positive compartments were postulated as terminal compartments for the transport of fluorophore-labelled dextran in HeLa cells [160]. Arl8 is implicated in LYS-tubulation and positioning of LYS as well [170,377,381] and similarly to Rab7a in cargo delivery to LYS [10,165,183,352]. Recently, Rab7a has been proposed to mark endocytic compartments of earlier maturation stages than Arl8 [10,168]. Yet the order in which several proteins appear on maturing endosomes remains elusive.

The consecutive order in which Rab7a, Arl8, Vps41 (HOPS), BORC subunit lyspersin, and LAMP1 can be detected on maturing FFEs was determined. FFEs were purified from WT cells 0, 20, 40, 60, 80, 100, and 120 min after the pulse period and analysed via immunoblotting. The measured abundance was fitted (kindly performed by Dr. G. Jeschke) to determine the time of half-maximal protein abundance on FFEs. Rab7a and Vps41 appeared at roughly the same time during the chase period and significantly earlier than Arl8, lyspersin and LAMP1. These findings suggest that Rab7a is recruited to maturing FFEs substantially earlier than Arl8 is. This indicates that Rab7a can be assigned to endosomes at earlier maturation stages than Arl8. Rab7a being recruited before Arl8 is also consistent with Rab7a levels on FFEs not being affected by deficiency of either Vps41 (HOPS), Arl8, or myrlysin and diaskedin (BORC) (this study, [10]). If either of these proteins were necessary for acquiring Rab7a, they would act upstream of Rab7a and therefore cause reduced amounts of Rab7a on FFEs.

Jongsma and colleagues postulate the existence of a switch between Rab7a and Arl8, reminiscent of the Rab5 to Rab7a switch in the transition from EEs to LEs. In this model, Arl8 effector SKIP acts as a negative regulator of Rab7a by recruiting the putative Rab7a GAP TBC1D15, eventually leading to the inactivation of Rab7a [99]. Such mechanism would

inevitably lead to the formation of an Arl8-only compartment. However, the assay used to determine the order in which late endosomal proteins appear on maturing endosomes was unsuitable for detecting the presumed exchange of Rab7a to Arl8. Immunoblot analysis of FFEs purified after prolonged chase periods revealed that in HeLa cells, early markers such as Rab5 and TfR are only lost after 24 h of chase, and levels of late endocytic markers continued to increase even after 24 h of chase (e.g. Rab7a, Arl8). This caveat prevented evaluating the loss of earlier-stage protein markers and possible exchanges but still allowed evaluation of protein acquisition (this study, [10]). Hence, this method is unsuited to assess whether Rab7a can be attributed to earlier maturation stages than Arl8.

To detect the putative Arl8-only compartment, FFEs purified from HeLa WT cells expressing C-terminally-tagged hArl8b-mCherry were stained with an antibody against Rab7a. Evaluation of the FFEs revealed the presence of Arl8 and Rab7a-positive compartments and the presence of compartments positive only for Arl8. These observations aligned with the proposed Rab7a to Arl8 switch [99], as it was established here that Arl8 resides on more matured endolysosomal compartments than Rab7a [10]. Immunoblot analyses of FFEs purified from J774E macrophage-like cells by L. Pöttgen [10] further support this assumption. In J774E macrophage-like cells, early endosome markers are lost after a comparably short period of time, and late endocytic markers are picked up after early markers are lost [238]. Analysis of the kinetics of acquisition and loss of proteins revealed that after 240 min of chase, Rab7a was slowly lost on maturing FFEs, while Arl8 and Vps41 continued to accumulate. This data validates the conclusion that Rab7a belongs to compartments of earlier maturation stages than Arl8 [10].

In this setting, it seems convincing that LEs, equipped with Rab7a, fuse with Arl8-positive LYS and give rise to a Rab7a-Arl8 hybrid ELYS [10]. Bright and colleagues hypothesised that ELYS are formed upon fusion of LEs with LYS. These ELYS are thought to be acidic, harbour the bulk of active hydrolases, and to be the main degradative compartments [89]. During LYS-reformation, LEs and LYS are reformed from these hybrid organelles [382]. Considering the data gathered by Jongsma and colleagues, Schleinitz et al., 2023, and this study, it seems likely that Rab7a-positive LEs and Arl8-positive LYS are regenerated from ELYS. This could render Arl8 and BORC subunits suitable protein markers for bona fide LYS [10]. Arl8-only organelles could represent a LYS population of terminal storage LYS. Further work has to be dedicated to better characterise Arl8-positive and Rab7a-negative LYS [10]. In line with this, Arl8 has been shown to have limited overlap with LE marker cation-dependent M6PR [166]. Alternative ways to generate Rab7a-Arl8 hybrid organelles, such as recruiting Rab7a to Arl8-positive organelles or

vice versa, are unlikely. Rab7a cannot be recruited to Arl8-decorated LYS as the Rab7a GEF Mon1a/Ccz1 is not present [383]. Furthermore, the presence of Arl8 eventually leads to the inactivation of Rab7a [99]. Association of Arl8 with Rab7a-positive LEs is also unlikely, as the Arl8 membrane anchor BORC is not present on LEs and appears on FFEs at the same time as Arl8 (this study; [10]).

6.3.2 Rab7a- and HOPS-positive FFEs acquire Arl8 and BORC through fusion with LYS

Vps41 (HOPS) being recruited at the same time as Rab7a but earlier than Arl8a/b and BORC subunit lyspersin [10] is a first hint at the functional interplay between Rab7a, HOPS, BORC, and Arl8 in LE-LYS fusion. Moreover, immunoblot analysis in Vps41 and Rab7a KO HeLa cells revealed reduced FFE levels of Arl8, myrlysin, and lyspersin (BORC) in the absence of Vps41 (HOPS) and Rab7a. The abundance of (E)LYS markers, such as LAMP1, mCath B or D, were also reduced on FFEs from Vps41 and Rab7a KOs, as was the colocalization of endocytosed dextran with acidic compartments. At the same time, the existence of functional (E)LYS in Vps41 and Rab7a KOs was verified (this study; [10]). Therefore, it was hypothesised that in Rab7a and Vps41 KO cells, the fusion competence between late endocytic compartments (FFEs) and LYS was severely impaired due to the absence of the respective proteins. It seems plausible to assume that FFEs positive for Rab7a and Vps41 acquire Arl8 and BORC through fusion in light of Arl8/BORC being established as LYS markers and Rab7a and HOPS being present on FFEs earlier.

To exclude the possibility that loss of Rab7a or Vps41 merely lowers the amount of membrane-associated Arl8, it was tested whether cytosolic levels of Arl8 were increased while membrane pools were depleted in the respective KO cell lines. PNS fractions were separated into cytosolic and membrane-containing fractions and analysed for their Arl8 contents. Loss of neither protein led to Arl8 being displaced from membranes or recruited less from cytosolic pools. An increase in cytosolic Vps41 levels was rather due to Arl8 levels being elevated generally in response to the loss of Vps41, as Arl8 membrane levels were unchanged compared to the WT [10]. Apparently, Vps41 (HOPS) and Rab7a are required for acquisition of Arl8 on FFEs, and lower Arl8 levels are not caused by displacement of the protein. Rab7a- and Vps41-positive compartments are presumably equivalent to LEs, while Arl8/BORC-positive compartments are LYS [10].

Khatter and colleagues postulated a role for Arl8b in the recruitment and assembly of the HOPS-complex on LYS. At first glance, the bulk of HOPS being present before Arl8 is recruited in substantial amounts conflicts with these observations [182]. A possible explanation could be that recruitment of HOPS to LEs fulfils different functions in endosome maturation than recruitment of HOPS to LYS by Arl8. The binding of LYS-localised Arl8 to LE-bound HOPS could tether LEs to LYS, promote subsequent fusion, and would likely still take place via interactions of Vps41 with Arl8 [182]. Fittingly, A. Jeschke showed that consecutively active Arl8 Q75L localizes to Vps39- and Vps33a-positive (HOPS-subunits) sites on phagosomes from J774E cells, mimicking LE to LYS tethering. Furthermore, it was shown that phagosomes preincubated with Arl8 Q75L do not fuse with LYS *in vitro* [10]. HOPS present on LEs is therefore needed to tether LEs to LYS. It is unknown if Rab7a and HOPS (indirectly) act together to mediate Arl8 acquisition.

6.3.3 Neither Arl8 nor Rab7a are involved with recruitment of HOPS to LEs

As mentioned before, Vps41 being quantitatively detectable on FFEs earlier than Arl8 conflicts with Arl8 being the recruiter of HOPS [182] in this setting. It was also established, that Arl8b is absent from LEs [10]. Arl8 levels being reduced on FFEs from Vps41 KO cells (this study, [10]) further suggest, that Arl8 is acquired by maturing endosomes through fusion with Arl8-positive LYS. While it is possible that Arl8 recruits HOPS to LYS, the recruitment of HOPS to LEs is most likely mediated by a different protein. Moreover, the recruitment of HOPS to LYS probably fulfils different functions in the endolysosomal pathway than the recruitment to LEs.

Involvement of Rab7a in recruitment of HOPS was excluded as well. Although mammalian Rab7a does not directly interact with HOPS, Rab7a effector Plekhm1 has been shown to also interact with and possibly recruit HOPS to LEs [1,186]. If Rab7a were to be indirectly (via its effectors) responsible for HOPS recruitment to LEs it would be expected that levels of HOPS specific subunits on FFEs were reduced upon loss of Rab7a. This is not the case for either Vps39 or Vps41 (c.f. [10]). Moreover, abundance of Rab7a effector Plekhm1 is reduced, compared to the WT. If Plekhm1 as an effector protein of Rab7a were involved in recruitment of HOPS it would be likely that its reduced abundance would also ultimately result in decreased abundance of Vps39 or Vps41 on FFEs. Consistent with Rab7a not being involved with recruitment of HOPS, FFEs from Rab7a KO cells acquired more Arl8 after 24 h of chase than after 2 h, whereas FFEs from Vps41 KOs did not [10]. This indicates that HOPS is indispensable for cargo delivery to LYS, whereas Rab7a is expendable [10]. Thus, Vps41 (HOPS) and Rab7a do not take part in the same process leading to fusion and consequently Arl8 acquisition. Rab7a

may primarily be involved in microtubule-dependent transport of FFEs towards LYS with its effector RILP and fulfil a function in organizing the machinery necessary for tethering and fusion, in concert with Plekhm1 [10,158,167,183]. The Rab7a effectors may bind to HOPS during this process and possibly stabilize HOPS mediated tethering of LEs to LYS, but do not seem to be essential for HOPS membrane association and tethering/fusion.

The bulk of HOPS is present on LEs without help of Arl8 for recruitment (this study, [10]). This indicates, Arl8 being necessary for tethering by binding to the Vps41 subunit of an LE-localized HOPS complex, rather than recruiting the HOPS complex to LYS for LE-LYS fusion. This assumption is also corroborated by data presented in Schleinitz et al., 2023. Consecutively active Arl8b localizes to sites where HOPS subunits are present. Moreover, preincubation of phagosomes with Arl8b Q75L inhibits fusion of LBPs with LYS, whereas the dominant negative T34N variant, which does not bind to Vps41 does not [10,182]. This also suggests, that ELYS may be formed by fusion of Rab7a- and HOPS-positive LEs with Arl8-positive LYS [10].

Recruitment of HOPS by Arl8b to LYS may serve different functions in endosome maturation. For example, HOPS in concert with SKIP and Arl8b is needed for recruitment of the Rab7a GAP TBC1D15 [99]. On ELYS both, Arl8b and Rab7a are present on the same membrane instead of opposed membranes (this study, [10]). The proposed fusion of Rab7a-harbouring LEs with Arl8-positive LYS would lead to the generation of Rab7a-Arl8 hybrid ELYS [10]. It is conceivable, that for LYS reformation, Rab7a must be removed from ELYS membranes for formation of Arl8-only domains to occur, which then bud off to form terminal storage LYS. In support of this hypothesis A. Jeschke showed spatial separation of membrane domains containing Rab7a or Arl8b on the same phagosome [10]. The same was shown for Rab7a and Arl8 on LEs/LYS by stimulated emission depletion (STED) microscopy [183]. Recruitment of HOPS to Arl8b-SKIP on LYS may therefore be vital for LYS-reformation, after LE with LYS fusion. To prove this further research must be conducted.

Furthermore, ‘proofreading’ capabilities of HOPS for forming SNARE complexes have been described in yeast [192]. Considering the amounts of HOPS that was needed to stimulate fusion versus chaperoning SNARE complex assembly, it was concluded that more than one HOPS complex per SNARE complex was needed for proofreading, whereas one complex was sufficient to mediate fusion [191]. If this applies to mammalian HOPS as well, Arl8 recruiting additional HOPS to sites of LE-LYS fusion for proofreading of *trans*-SNARE complexes could also be conceivable.

6.4 Rab2a is involved in recruitment of HOPS to LEs

Although Arl8 directly and Rab7a indirectly, via its effectors, bind to and interact with HOPS, neither of the two GTPases is responsible for recruiting HOPS to LEs. Alternatively, HOPS may be trafficked to compartments like endosomes or autophagosomes via a Golgi-derived vesicle, where HOPS is bound to the Ras-like GTPase Rab2a [1]. In support of this, Rab2a was shown to bind to the Vps39 subunit of HOPS in pulldown assays [321]. For an initial assessment of whether Rab2a could be a suitable candidate for delivery of HOPS to LEs, a kinetic with only three time points was used here. Rab2a was already fully present on FFEs directly after pulsing WT HeLa cells with FF. Low amounts of Vps41 were also detected right after the pulse period. 50 % of the maximally detected Vps41 was present after 1 h of chase, which fits well with the previously determined timepoint of half-maximal Vps41 abundance. In contrast, Arl8 was not detected on FFEs right after the pulse period. After 60 min, only about 20 % of maximum Arl8 levels were measured on FFEs [10]. Since Rab2a was already present on FFEs before the bulk of Vps41, Rab2a could be involved in recruiting or delivering HOPS to maturing endosomes [10]. Indeed, Rab2a KD experiments performed by L. Pöttgen revealed lowered Arl8 and Vps41 abundance on FFEs of siRNA-treated HeLa WT cells, suggesting that Rab2a might play a role in its recruitment or delivery to FFEs [10].

To further characterise the impact of Rab2a on endosome maturation, protein acquisition, and possible recruitment of HOPS, Rab2a KO cell lines were generated. The original knockout was performed by S. Held. Two clones were selected for further analysis, and KO of Rab2a was confirmed by immunoblot analysis. As determined for Rab2a KD [10], the Rab2a KOs displayed a reduction in FFE abundance of Arl8 and HOPS-specific subunits Vps39 and Vps41 on FFEs (this study). Furthermore, a reduction in abundance of late endocytic/ endolysosomal proteins mCath D and lyspersin (BORC) was observed for FFEs purified from Rab2a KOs. On the other hand, Rab7a FFE levels were not reduced compared to the WT, except for one data point of the 1G6 clone. Therefore, Rab2a KO elicits a similar phenotype as Vps41 or myrlysin/diaskedin KO. These observations agree with data describing perturbed lysosomal trafficking in Rab2a deficient *Drosophila melanogaster* larvae [384]. Rab2a deficiency having the same characteristics as Vps41 KO could indicate participation of Rab2a in recruitment of HOPS. Experiments in HeLa WT and Rab2a KO cells, in which cells were fractioned in cytosolic and membranous fractions, revealed that Arl8 was not displaced from membranes. Cytosolic levels of Arl8 were not detectable. These results consolidate a possible role of Rab2a in recruitment/delivery of HOPS to LE membranes.

Rab2 is mainly located at the Golgi apparatus and traffics on carriers from Golgi to endosomal structures, to which it likely associates only transiently [1,10,320]. Consecutively active Rab2a has accumulated at Rab7a-positive vacuoles in cultured *Drosophila melanogaster* cells [320]. Lőrincz and colleagues postulated a model in which HOPS is transported to Rab7a-positive LEs via Golgi-derived CVs. In this model, Rab2a binds to the Vps39 subunit of HOPS and is proposed to hand the HOPS complex over to an effector of Rab7a [1]. Brefeldin A (BFA) is a drug that abrogates transport along the biosynthetic route. Treating HeLa cells with BFA reduced the acquisition of Rab2a, Vps41, and Arl8 on FFEs (experiment performed by A. Jeschke), which aligns with the model [10]. This finding corroborates a TGN origin of HOPS-carrying vesicles. Rab2a KD resulted in the formation of LAMP1- and LC3-positive structures, which likely represent amphisomes [1]. The same phenotype was observed in Vps41 KO [314], further suggesting a link between HOPS function for LE-LYS fusion and Rab2a. In line with this, sites of Arl8 Q75L-binding to LBP have been shown to contain Rab2a and HOPS [10].

6.4.1 Anchoring of HOPS likely depends on multiple factors

Although Rab2a has been shown to fulfil a role in recruiting/delivering the HOPS complex to LEs, it remains unclear how exactly HOPS is anchored to late endosomal/lysosomal membranes and how LE-LYS tethering is stabilised. Membrane fractionation experiments with Rab2a KD (L. Pöttgen) [10] and KO cells (this study) did not show displacement of Vps41 subunits from membranes. Moreover, even in Arl8a/b DKO cells with additional Rab2a KD, Vps41 levels on intracellular membranes were unaltered [10]. Therefore, neither Rab2a nor Arl8 are major membrane anchors for HOPS. A role for Rab7a or its effectors in HOPS recruitment was also dismissed. KO of Rab7a did reduce FFE levels of Plekhm1 but not Vps39 or Vps41, which would be expected if Plekhm1 was a main anchor point for HOPS. Lőrincz and colleagues speculated that HOPS may bind to Rab7a effectors like Plekhm1 (or another Rab7a effector), as it was reported that Plekhm1 binds to and recruits HOPS subunits Vps39 and Vps41 [1,184]. However, the binding of Plekhm1 to Vps41 was challenged by findings that interactions of Plekhm1 were sufficient to recruit Vps39, but not Vps41. [183,186].

Lőrincz and colleagues hypothesised that HOPS as a whole may be bound to Rab2a at its Vps39 subunit and accepted on the late endosomal site by an effector of Rab7a. Since Plekhm1 is likely not a suitable acceptor, this role could alternatively be fulfilled by RILP, which has been shown to bind to the Vps41 subunit and has been discussed to recruit HOPS [179,385]. HOPS is also conceivable to be anchored to Rab2a and bound by Plekhm1 at its Vps39 subunit, stabilising LE-LYS tethering and HOPS membrane association. It is unclear whether this

scenario is likely regarding HOPS anchoring in LE-LYS fusion, because LBP-tethering sites were shown to be devoid of Rab7a, but positive for HOPS and [10]. Thus, it is uncertain whether a Rab7a effector would anchor HOPS in the absence of Rab7a.

Moreover, HOPS membrane association could be reinforced by binding to PI(4)P. Preincubation of (phago)lysosomal membranes with PI(4)P binding protein fragment P4C decreased Vps41 levels [9]. Therefore, HOPS anchoring to LE membranes may be the product of multiple factors stabilising the membrane association rather than the action of one major anchoring factor. The matter of HOPS membrane anchoring is further complicated because, as speculated above, HOPS may also fulfil functions on LYS independently of tethering [99]. HOPS could be anchored to LYS by different interaction partners than required for anchoring to LE membranes. Further work has to be dedicated to identifying how the HOPS complex is anchored to LE and/or LYS membranes.

6.5 Significance and limitations of the FF-assay

The newly developed FF-assay has been extensively used in this study to monitor the maturation of endocytic FF-laden compartments, which are allowed to mature *in vivo* and under physiological conditions. It is well suited to directly and thoroughly evaluate phenotypes elicited by KO of certain POI. Differences in protein composition of maturing FFEs to the WT can be easily determined. Combined analysis of the distribution of POI between PNS and FFEs, as well as supplementary analysis of the distribution of POI between cytosolic and membranous fractions, allows initial conclusions to be drawn about the cause of the expression of different phenotypes. For example, lowered FFE levels of a POI, while overall (PNS) levels remain similar to the WT, may indicate reduced recruitment or displacement of the POI from endocytic membranes. It is also possible that the bulk of protein is present on or within endocytic compartments but is not reached by the cargo used to purify compartments. Additional analysis of cytosolic and membrane fractions may reveal whether the POI is recruited less/displaced or if cargo did not arrive in compartments containing the POI. However, the assay is not suited to determine whether the exchange of markers, e.g. Rab5 to Rab7a switch or loss of EEA1, is hindered in KO cells due to slow FF-trafficking in HeLa cells. For example, the postulated impairment of Rab5 to Rab7a conversion in Vps41 KO [314] cannot be seen using the FF-assay. Moreover, if a knocked-out protein is important for multiple steps during endosome maturation and possibly at an earlier stage than the one investigated, it is not possible to study this particular protein function properly [386]. On the other hand, this has no impact on determining the order in

which certain proteins are acquired by maturing FFE. Hence, the classical FF-assay, in combination with modified versions (i.e. kinetic assessment), allows for the indirect study of interactions and relationships between multiple proteins *in vivo*. In addition, microscopic or *in vitro* fusion-assays should be used to analyse the collected data obtained using the different variants of the FF-assay. This could, for example, shed more light on how HOPS is anchored to LE and/or LYS membranes. It could further determine whether cargo is delivered to acidic compartments with active acid hydrolases after prolonged chase periods in KO cells. An *in vitro* fusion-assay using only cytosol and compartments purified from HeLa cells is yet to be established.

6.6 Working Model of endosome maturation

Using the FF-assay, cargo trafficking in WT, Rab7a, Arl8b, Arl8a/b, Vps41, myrlysin, and diaskedin KO cells has been extensively surveyed. Transport of endocytosed material is impaired in KO cells compared to the WT. Figure 32 aims to depict the differences in cargo trafficking between WT and KO HeLa cells. Considering some newly published data, some questions remain to be addressed going forward.

In WT HeLa cells (Figure 32; left panel), cargo first reaches EEs, from which it is then trafficked along the endo-lysosomal pathway. Maturing endocytic compartments receive newly synthesised acid hydrolases, which are not yet fully processed via CVs, originating from the TGN. Endosomes also become gradually more acidified, which helps to process the proforms of hydrolases into their active forms. Upon fusion of LEs with LYS, a hybrid-compartment, the ELYS, is formed, where most degradation takes place. (storage) LYS are thought to primarily act as non-acidic storage compartments for mature acid hydrolases [89]. FFEs purified at this stage contain an abundance of lysosomal markers such as LAMP1, mCath B or D (this study, [10]). LEs and LYS are reformed from ELYS eventually.

In KO-cells, however (Figure 32; right panel), cargo accumulates in non-acidic compartments which only contain reduced amounts of hydrolytic enzymes such as mCath D/mCath B or lysosomal marker LAMP1 (this study; [10]). Upon longer chase periods, cargo is transported to compartments of later maturation stages, which contain similar amounts of mCath D as the corresponding WT FFEs [10]. However, these compartments were not characterised further. Complementing the data presented here and in Schleinitz et al., 2023, Van der Beek and colleagues showed that in Vps41 KO cells, cargo accumulates in hybrid-compartments with early and late markers. The so-called ‘HOPS-bodies’ were identified as amphisomes and

contained no active Cath D but increased levels of inactive pro-Cath D, although active Cath D was present in general. Additionally, release of pro Cath D from CI-M6PR and its recycling to the TGN was impaired in Vps41 KO [314]. It needs to be investigated whether this is also the case for the other KO cell lines. Considering these findings, the question remains of whether cargo is delivered to (E)LYS. This is corroborated by the observation that Vps41 KO FFEs do not accumulate similar amounts of Arl8 after 24 h of chase – which has been shown to primarily locate to LYS – as the WT. Another question that arises concerns the nature of the later mCath D-containing compartments in Arl8a/b, myrlysin and diaskedin KO cells. Since both Vps41 and Arl8 are essential for LE-LYS tethering [10,182], it is questionable whether fusion of FFE with LYS is possible in Arl8a/b and BORC deficient cells via the canonical route.

Bearing this in mind, assessing the acidity and digestive capacity of the late mCath D-containing compartments in all KO cell lines is necessary. In case of Rab7a KO it is likely that LYS are formed via an alternative pathway independent of the classical endolysosomal route [374]. Furthermore, Rab7a KO cells acquired Arl8 only after prolonged chase periods, which indicated that Rab7a can be substituted for [10]. As LYS in Rab7a KO are generated from Rab4-positive REs the question arises of how endocytic cargo ends up in these alternative LYS [374].

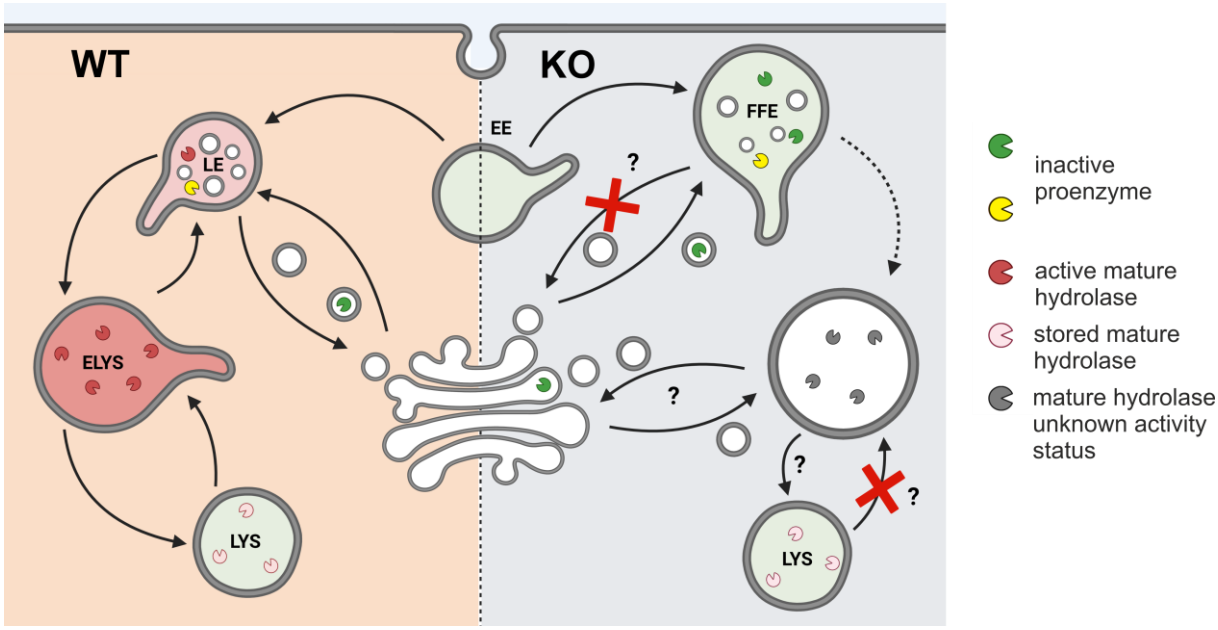

Figure 32: Schematic representation of cargo trafficking in WT and KO HeLa cells. See text for details. Small 'packman'-icons are used to indicate the activity and maturation status of acid hydrolases. Green and orange icons represent inactive proenzyme forms of acid hydrolases. Red icons are mature and active acid hydrolases, while colourless icons with red outlines represent mature but inactive (stored) acid hydrolases. Grey icons represent mature hydrolases of unknown activity status. This illustration was created using BioRender.com.

Rab7a is acquired by FFEs at the same time as Vps41 and substantially earlier than Arl8, lyspersin or LAMP1 [10]. Additionally, immunoblotting of FFEs from the different KO cell lines

revealed that Rab7a levels are not affected by KO of Arl8, Vps41, or BORC subunits myrlysin and diaskedin (this study, [10]). Therefore, Rab7a membrane association and its functions appear to be largely independent of Arl8, HOPS and BORC. Arl8 acquisition, on the other hand, depends on HOPS (Vps41). Considering the data presented here, it seems more likely that HOPS is present on LEs and that lysosomal Arl8 binds it via the Vps41 subunit, tethering LEs and LYS together [10]. Recruitment of Vps41 and HOPS to LYS via Arl8 could still be necessary to carry out other functions, such as reforming Arl8-only compartments from Rab7a-Arl8 hybrid compartments [99] or proofreading of forming SNARE complexes [191,192].

As Arl8 does not recruit Vps41 (HOPS) to LEs, the question of how HOPS is recruited for LE-LYS tethering remains. Indirect participation of Rab7a via its effectors was ruled out, as Rab7a KO does not cause reduced Vps39 or Vps41 levels on FFEs [10], although Plekhm1 levels are reduced, for example. Additionally, Vps41 is crucial for Arl8 acquisition on FFEs, whereas Rab7a was not, indicating that both proteins may participate in different processes [10]. Lőrincz et al. postulated Rab2a as a possible recruiter of Arl8, possibly delivering HOPS to LEs [1]. Indeed, substantial amounts of Rab2a were present on LEs even before Vps41 [10]. KO of Rab2a (this study) yielded a similar phenotype as Vps41 KD [10] and FFEs failed to accumulate (endo)lysosomal proteins such as LAMP1, Arl8, lyspersin, and mCath D as well as HOPS subunits Vps41 and Vps39 to the same extent as the parental WT. Therefore, it is highly likely that Rab2a is involved in recruiting HOPS [10].

Although Rab2a is most likely involved in recruiting HOPS, it is not the main membrane anchor of HOPS. Further work must identify how HOPS is anchored to membranes and how exactly LE-LYS tethering is stabilised. Figure 33 aims to provide a schematic overview of the interplay between Rab2a, Rab7a, Arl8, HOPS, and some of their effectors.

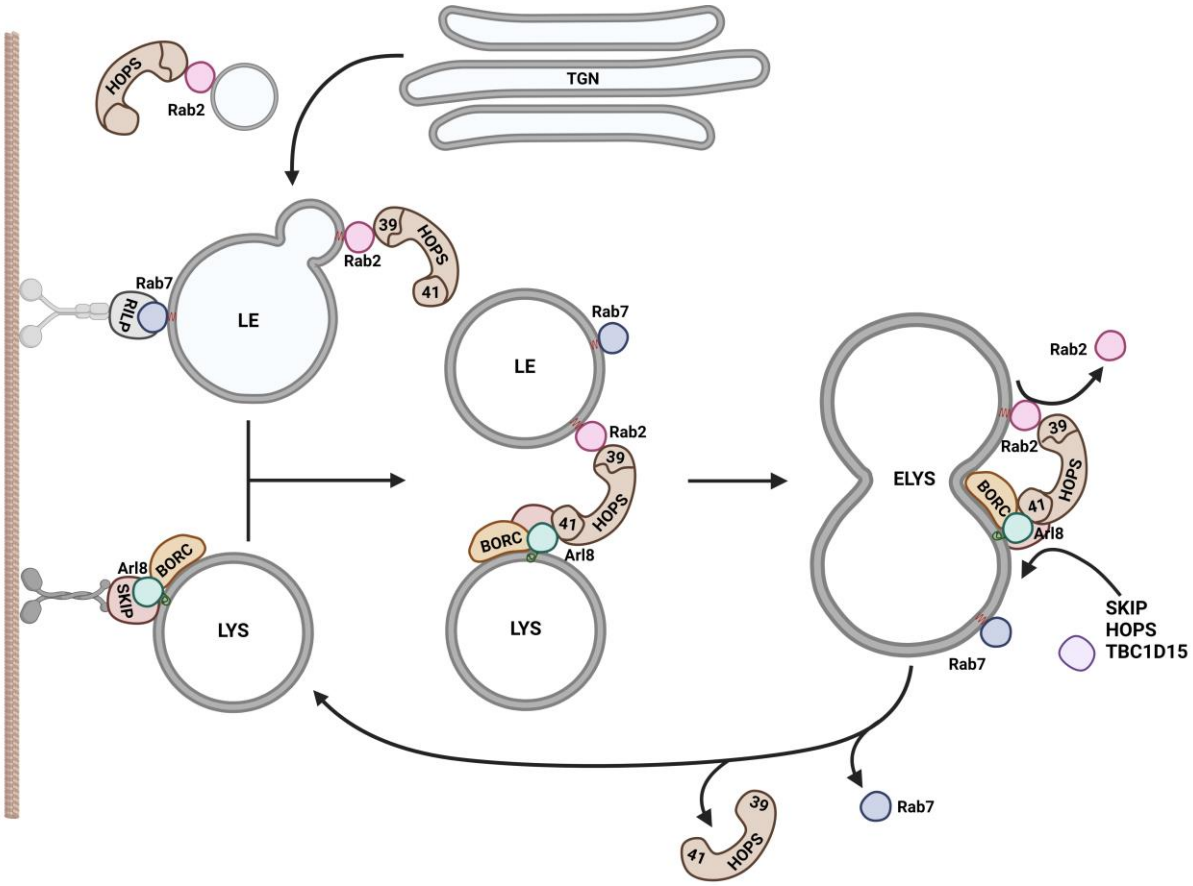

Figure 33: Working model of LE with LYS fusion. LEs are transported towards the MT minus-end via dynein-dynactin, bound to Rab7a-RILP. LYS are transported towards the plus-end via SKIP bound to kinesin-1. SKIP is bound to the small GTPase Arl8, which is in turn associated to lysosomal membranes by BORC. The HOPS complex is presumed to be trafficked on TGN-derived CVs, bound by Rab2a at its Vps39 subunit. LEs and LYS are tethered together by HOPS, bound to Arl8 on LYS and to Rab2a on LEs. Rab7a has been shown to not localize to sites of presumed LE-LYS tethering. Upon fusion of LEs with LYS, a hybrid-compartment is generated, from which Rab2a and Rab7a are displaced and Arl8-positive LYS reformed [10]. This illustration was created using BioRender.com.

6.7 Ca^{2+}-triggered LBP with LYS fusion

Phagosome with LYS fusion and subsequent killing and destruction of particles or pathogens ingested by cells of the innate immune system is the ultimate goal of phagocytosis. The Haas-group has developed an elaborate *in vitro* fusion assay to better understand and dissect this process. This assay allows the dissection of specific subreactions and fusion events in phagosome maturation, circumventing many caveats in classical *in vivo* assays [8,238]. Although much work has been dedicated to shed light on the requirement of a Ca^{2+}-signal in phagosome with LYS fusion, this subject is still somewhat debated (reviewed in [203]). In a previous study, Ulrike Becken and colleagues showed that fusion of *E. coli*-containing phagolysosomes with LYS was partially inhibited by adding the Ca^{2+} chelator BAPTA, pointing to a requirement of Ca^{2+} in phagosome with LYS fusion [238]. Curiously, U. Becken also observed an *in vitro* fusion reaction later termed CaFu, which was triggered by adding micromolar [Ca^{2+}] and was

independent of ATP and cytosol [11]. Proteins involved in this CaFu reaction are yet to be identified.

6.8 CaFu is independent of cytosolic factors, Rab GTPases and PI(3)P- and PI(4)P-binding proteins

Fusion reactions between organelles or vesicles in the endocytic/ phagocytic pathway are typically dependent on an array of proteins (i.e. Ras-like GTPases, tethering factors, regulatory proteins) recruited from the cytosol when appropriate [47]. Another prerequisite for SNARE-mediated fusion events in the endocytic pathway is the requirement for ATP, which is necessary in a priming step, where *cis*-SNARE complexes are separated by the concerted action of NSF and its cofactor α-SNAP [387].

The requirement of both fusion reactions for ATP and Cyt was retested here to gain a more conclusive understanding of how CaFu and StaFu differ and how CaFu may be mediated. As expected, StaFu did not occur significantly in samples lacking ATP, Cyt, or both. However, in samples solely lacking Cyt, fusion was observed to some minor extent, possibly reflecting a residual pool of fusion-relevant proteins still active and membrane bound on the purified organelles themselves [238]. In contrast, CaFu was unaffected by any of the experimental conditions. Unexpectedly, the extent of fusion in +ATP + Cyt 37 °C CaFu samples exceeded the fusion frequency of equivalent StaFu (pos. ctrl.) samples. This differed from observations made by U. Becken, who reported similar fusion extents for both reactions under these conditions [11]. Previous experiments showed that depending on the cytosol preparation, StaFu fusion frequencies could exceed those of CaFu or yield a similar fusion extent [2]. Therefore, it might be possible that the cytosol preparation used in this study generally yields lower fusion activity in StaFu samples than in CaFu samples.

To exclude the possibility that residual ATP contaminating the organelle preparations obscures the ATP requirement of CaFu, J. Becker performed CaFu experiments with apyrase and a hexokinase/glucose ATP-depleting system [388]. CaFu did occur regardless of the treatment, whereas StaFu was inhibited by both apyrase and the ATP-depleting system [2]. Effects of residual cytosol in organelle preparations were negligible as well [12]. An inhibitory effect of ATP [11] could not be reproduced here. CaFu is thus independent of ATP and cytosol (i.e. cytosolic proteins), which is fundamentally different from StaFu. This observation could point to the reaction mechanism of CaFu being independent of cytosolic factors, including Rab GTPases, tethering proteins, and NSF. Independence of CaFu from ATP also pulls participation

of SNARE proteins into question, which require ATP-driven NSF activity for priming [113]. Ca^{2+}-triggered exocytosis of cortical vesicles in sea urchin eggs is also elicited in the absence of ATP but becomes increasingly less sensitive to Ca^{2+} as time progresses [255]. The final process of membrane merger in cortical vesicles in sea urchin eggs is suspected to be independent of the action of SNARE proteins. SNAREs may rather have an important modulatory role in this process, affecting fusion efficiency [389]. A second possible interpretation could be that cytosolic and ATP-dependent factors already performed their function. The machinery needed for fusion might already be primed and ready to go. The machinery is triggered once sufficient [Ca^{2+}] is present, possibly by removing a fusion-inhibiting protein. This would require fusion-competent machinery on LBP and/or LYS membranes, arrested by a Ca^{2+}-sensitive 'clamp', before purification of the organelles from whole cells. Such a scenario would be reminiscent of neurotransmitter release at the presynapse, where already docked and primed vesicles only need the influx of extracellular Ca^{2+} for fusion with the presynaptic PM [202,390]. A caveat with the here investigated system would be, that the fusion partners do not initially exist in a pre-docked state, but rather have to 'find' a suitable fusion partner in the reaction buffer volume, before Ca^{2+} is added, to successfully fuse. Furthermore, the machinery would have to stay active during the purification process. This seems possible, considering the above-mentioned observations by U. Becken [238]. It remains to be investigated whether such a scenario would encompass SNAREs and components of the classical fusion machinery or is mediated by an alternative fusion apparatus and how Ca^{2+} is sensed.

Phosphatidylinositol (PI) is a glycerophospholipid that can be mono-, bis- or tris-phosphorylated at the inositol headgroup, forming PIPs. PIPs are present in distinct pools on many intracellular membranes and have regulatory capabilities in many processes, such as membrane trafficking [391,392]. The distribution of PIPs on specific organelles is tightly regulated through the distribution of compartment-specific PI kinases and phosphatases [393]. PIPs contribute to regulating membrane docking and fusion processes by aiding in the recruitment of effector proteins, enabling binding of specific effector proteins, such as Ras-like GTPases, tethering proteins and SNAREs via PIP-interacting domains [98,193,391]. PIPs not only participate in recruiting effectors and creating protein domains on organelles, but they also modulate the activity level of their binding partners, actively participating in regulating docking and fusion [394]. In addition, changes in the phosphorylation status of PIPs or PIP-composition of membranes further alter protein function by modulating the physical properties of lipid bilayers [395]. PIP-binding domains are a suitable tool for evaluating the possible participation of PIP effector proteins in fusion reactions. In sufficient abundance, these protein domains compete with

endogenous PIP-binding partners and thus inhibit PIP-dependent cellular processes [386]. The PI(4)P-binding P4C protein fragment from the *Legionella pneumophila* protein SidC and the PI(3)P-binding 2xFYVE-domain [296,297] were previously used to decipher the PIP requirement for specific subreactions in conventional phagosome-LYS fusion (StaFu) [8,9]. Adding both probes prevented content mixing of phagosomes and lysosomes (StaFu) *in vitro*, and P4C also reduced binding but to a smaller extent [8].

Small GTPases of the Rab family are another important group of proteins directly involved in organizing and recruiting the protein apparatus needed for fusion [69,94]. Rab proteins are subjected to an activation-inactivation cycle determined by the phosphorylation state of the bound guanosine nucleotide [102]. Rab-GDI was first described by Ullrich et al. as a protein that removes Rab(GDP) proteins from membranes [90]. In StaFu reactions, Rab-GDI blocks content mixing but does not interfere with phagosome-lysosome binding [8].

To further elucidate the requirements of CaFu for proteins and lipids essential for StaFu, the sensitivity of both reactions to PI(3)P- and PI(4)P-binding domains and Rab-GDI were tested in parallel. Fusion in samples containing the PI(4)P-binding domain P4C, PI(3)P-binding domain 2xFYVE, or Rab-GDI was reduced for StaFu, as reported previously [8,9,238], but had no effect on CaFu fusion frequencies. Adding GST to fusion samples had no effect on either reaction, suggesting that the reduction in fusion for StaFu depended on the masking of PI(3)P and PI(4)P and was not caused by the GST purification tag [2]. The results align with observations of U. Becken, who did report no inhibitory effect of 10 µM Rab-GDI on CaFu in an EGTA buffered system [11] and of J. Becker, who observed no inhibition of CaFu in the presence of P4C or 2xFYVE [12]. However, no increased fusion activity (CaFu) for 2xFYVE was evident in this study. The heterologously expressed protein fragments are of sufficient purity. Although some bands of weak intensity are visible at lower molecular weights, possibly indicating truncation of the GST-tag (P4C and 2 x FYVE) and proteolytic cleavage to a small extent.

The observations of PIP-binding domains and Rab-GDI not influencing CaFu fusion frequency fit well with the previous results of CaFu being independent of Cyt and, therefore, of cytosolic proteins. Many proteins participating in fusion events were shown to be recruited to membrane domains enriched in certain PIPs from the cytosol. Important regulators of phagosome with LYS fusion, such as Arl8, HOPS, and BORC, are suspected to bind to PIPs or to depend on the accessibility of PIPs for membrane association [8,9,148,193]. Additionally, it was shown that lack of ATP in *in vitro* fusion reactions decreased membrane contents in PIPs considerably, leading to fewer putative docking points for PIP-dependent proteins [8]. Therefore, it is unlikely that CaFu

needs proteins that rely on certain PIPs to perform their function in LBP-LYS fusion. Furthermore, Rab-GDI would extract Rab GTPases, which may still be present on LBP or LYS membranes after purification of the organelles. This effect has been reported to inhibit StaFu, suggesting Rab dependence of the process [238,298]. CaFu, on the other hand, was not sensitive to Rab-GDI, indicating that Rab-GTPases are expendable to initiate membrane merger in the presence of Ca^{2+}.

Taken together, these findings suggest that CaFu and StaFu are very different in their requirements for ATP, cytosolic proteins, PI(3)P and PI(4)P and their effectors, as well as Rab GTPases. This could either hint at two distinct reaction modes or suggest that CaFu might correspond to a step late in phagosome-LYS fusion and may not require any of the aforementioned factors anymore [2].

6.9 Attachment and Fusion are both Ca^{2+}-dependent

Many membrane fusion reactions like exocytosis of synaptic vesicles [202,240], PM repair [246,249], and exocytosis of secretory granules in sea urchin eggs are triggered by Ca^{2+}-fluxes. Ca^{2+}-sensing proteins involved in fusion processes display Ca^{2+}-sensitivities over a broad range of concentrations [268]. Different Ca^{2+} concentrations can elicit a graded response, where only subsets of available vesicles undergo fusion [241]. Maximum fusion efficiency of the *in vitro* CaFu reaction was observed at 120 µM Ca^{2+}. Fusion frequencies gradually increased in correspondence to rising $[Ca^{2+}]_{free}$ [2,11–13].

Indeed, fusion frequency plotted against $[Ca^{2+}]$ showed a sigmoidal curve progression, with $[Ca^{2+}]_{50}$ at 80 µM and maximum fusion around 120 µM Ca^{2+2}. Unexpectedly, fusion frequency does not increase suddenly and sharply as $[Ca^{2+}]$ rises when a putative Ca^{2+} fusion promoter is activated. This observation could indicate a heterogenous vesicle population, with vesicles of different sensitivities towards Ca^{2+}. Such gradual increase in fusion frequency depending on $[Ca^{2+}]$ was observed in sea urchin egg secretory vesicles [241]. Possibly, a fusion promoting protein with dynamic Ca^{2+} sensitivity could be involved [396], or multiple Ca^{2+}-dependent proteins on multiple vesicles. Experiments performed by J. Becker favour a hypothesis that at least two Ca^{2+}-sensitive steps are necessary for Ca^{2+}-dependent LBP-LYS fusion to happen [2].

If there really are multiple distinct Ca^{2+}-sensitive steps in CaFu, it would likely be attachment of LBP and LYS and their subsequent fusion reaction. J. Becker already observed that maximum fusion yield can be increased when LBP and LYS are brought closely together by

gentle centrifugation, possibly omitting the need for prior tethering of organelles. Such treatment lowered the [Ca^{2+}] needed for maximum fusion efficiency to ~ 15 µM [2]. Yet, under standard CaFu conditions, maximum fusion frequency is observed at [Ca^{2+}] ten times higher. This suggests that a second Ca^{2+}-requiring step occurs before the actual fusion. To test if this second step was indeed an attachment of LBP and LYS, an attachment assay [9] was performed here at various [Ca^{2+}]. Under normal conditions, maximum fusion occurs at approximately 120 µM Ca^{2+}, but the centrifugation experiment shows that fusion needs low [Ca^{2+}]. Therefore, attachment should be maximal at concentrations that support maximum fusion. This was the case, verifying that fusion and attachment are Ca^{2+}-dependent processes with different Ca^{2+}-sensitivities [2]. In the assay, extensive binding of LYS to LBP was observed even when no or little Ca^{2+} was present and little to no fusion was observed. This attachment seems to be non-productive and of no physiological value, as the corresponding ice control samples (negative controls) display similar amounts of attachment. Attachment requiring high [Ca^{2+}] also explains the absence of a steep increase in fusion frequencies at rising [Ca^{2+}], possibly making attachment the limiting step for CaFu.

Whether the observed attachment represents tethering in the classical sense remains to be investigated since CaFu does not require some factors involved in classical phagosome-lysosome fusion. Usually, Rab GTPases would recruit their effectors, i.e. tethering proteins from the cytosol and building fusion-promoting microdomains containing fusion-regulating proteins [47]. Many of such proteins also require PIPs as binding sites, which in turn need ATP to be generated (see Introduction and Chapter 6.10). None of the above-mentioned factors is essential to CaFu, and until now, no proteins involved in CaFu have been identified. This raises the question of how Ca^{2+}-dependent attachment of LBP and LYS is mediated before fusion. Unfortunately, direct involvement of proteins in the attachment process could not be tested here due to technical caveats (not shown). Trypsin treatment of LBP and LYS illustrated that proteins are required for CaFu in general [2]. However, it is unclear if proteins are required for attachment and fusion or only one of the subreactions. This poses questions regarding CaFu protein requirements that should be addressed in the future: 1) Does CaFu require the action of only one protein during attachment and fusion or more? 2) Is attachment or fusion mediated by a Ca^{2+}-dependent mechanism that does not rely on activating a specific Ca^{2+}-sensitive protein?

Mechanisms that would not necessarily involve action of specific Ca^{2+}-binding proteins could involve electrostatic interactions between Ca^{2+}, phospholipids, and proteins present on membranes. Ca^{2+}-dependent clustering of proteins was observed, independent of the presence

of Ca^{2+}-binding sites, domain structure and membrane anchoring mechanism [397]. One mechanism by which Ca^{2+} enables clustering is the compensation for negative charges in protein clusters and from negatively charged lipid head groups [397,398]. Computer modelling also revealed that Ca^{2+} facilitates fusion of phospholipid micelles by creating a hydrophobic surface at the fusion site, binding two micelles together and promoting a pre-stalk state in conjunction with water expulsion from the inter-micellar space [399]. Generation of protein domains in the presence of Ca^{2+} could facilitate attachment by bringing together proteins capable of initiating contact between LBP and LYS and subsequent fusion. Furthermore, Ca^{2+} could facilitate the attachment of approaching vesicles by lowering the energy barrier between membranes in aqueous solutions.

In summary, CaFu consists of two calcium-dependent steps with distinct Ca^{2+} requirements: attachment and fusion [2]. Maximum attachment needs higher [Ca^{2+}] than fusion, explaining why CaFu under standard reaction conditions needs similar [Ca^{2+}]. Relevant protein(s) involved in CaFu are yet to be identified [2].

6.10 CaFu does not need priming activity from NSF but requires SNARE proteins

A fundamental question regarding CaFu is whether membrane merger is mediated by SNARE proteins. NSF associates with membrane-bound SNAREs in an ATP- and SNAP-dependent fashion and recycles *cis*-SNARE complexes for subsequent rounds of fusion. This process is called priming [113,302]. The cysteine alkylating agent NEM inhibits NSF at concentrations as low as 1 mM [400]. Inhibitory effects of NEM may therefore indicate a requirement for NSF and a role for SNARE proteins. This is the case for ATP- and Cyt-dependent LBP-LYS fusion (StaFu), which is sensitive to NEM treatment and inhibited by cytosolic SNARE-domains [238]. The Ca^{2+}-dependent *in vitro* fusion reactions investigated here contain neither ATP nor Cyt. Residual membrane-bound NSF and α-SNAP are likely not active under CaFu reaction conditions. Therefore, NSF participation in CaFu is unlikely. To further exclude a role for NSF in CaFu, the sensitivity of this reaction to NEM in comparison to StaFu was tested in this study.

As previously reported, StaFu was sensitive to NEM and fusion was almost fully inhibited after the addition of 1 mM NEM. CaFu showed partial inhibition at 5 mM NEM, whereas DTT-inactivated NEM did not inhibit (this study, [2]). Such partial inhibition of CaFu at high NEM concentrations does not necessarily reflect inhibition of NSF. Other proteins, such as Anx A2, also have been reported to be inhibited by NEM [220,401]. NEM is an alkylation agent that

predominantly alkylates cysteine residues, which are among the rarest amino acids in eukaryotic proteins [402,403]. High concentrations of NEM likely lead to alkylation of cysteine residues of various other proteins present on LBP or LYS membranes, eventually leading to decreased fusion efficiency. The results indicate that NSF really is dispensable for the *in vitro* CaFu reaction. If SNARE proteins are required, they do not rely on priming by NSF, at least at that point. Membrane fusion in the absence of NSF has also been witnessed in sea urchin egg secretory granules [257]. CVs are recruited and become attached to the PM during egg maturation. At this point, all components needed for CV-PM fusion and Ca^{2+}-sensing are already present and 'ready to go'. Synchronous exocytosis is triggered by a rise in intracellular [Ca^{2+}] once a sperm enters the cell to prevent polyspermy. In this exocytic reaction, the relevant proteins have already undergone priming and docking, leaving only a rise in [Ca^{2+}] as a requirement to elicit fusion [255,404]. In the setup used, it cannot be excluded that NSF may be needed at an earlier stage before purification of the organelles. It is generally conceivable that unbound SNAREs are already present on LBPs and LYS membranes at the time of purification from whole cells. This scenario would require one or more Ca^{2+}-sensitive SNARE-binding protein(s) arresting these SNAREs in a metastable fusion-ready state, similar to Syt I and complexin at synaptic vesicles [253].

Although α-SNAP as cofactor of NSF is indispensable for the reuse of SNARE proteins, it was shown that binding of α-SNAP to SNAREs like syntaxin 1 (Stx1) inhibits certain fusion events independent of NSF [405,406]. Furthermore, Park and colleagues showed that α-SNAP WT also binds to some partially zippered *trans*-SNARE complexes, arresting the zippering reaction and preventing membrane fusion [407]. More recently, Schwartz and colleagues also uncovered the ability of Sec17 to differentially either promote or inhibit SNARE-dependent fusion, depending on the presence or absence of the SM-subunit Vps33 of HOPS [112]. A mutant variant of α-SNAP in which leucine 294 is changed to an alanine residue (α-SNAP^{L294A}) is unable to stimulate the ATPase activity of NSF but retains its ability to bind to NSF [387]. Several studies reported that adding α-SNAP^{L294A} effectively inhibits SNARE-mediated fusion events [98,323–325] and generally seems to be a more potent fusion inhibitor than α-SNAP WT.

Here, both α-SNAP variants were used to investigate a possible SNARE involvement in CaFu. If SNAREs are involved in the CaFu reaction, CaFu should be inhibited by the α-SNAP^{L294A} variant and possibly by α-SNAP WT. StaFu was already partially inhibited by adding 1 µM of either α-SNAP WT or α-SNAP^{L294A} and fully inhibited by adding 20 µM of both recombinant proteins. Adding 20 µM α-SNAP^{L294A} partially inhibited CaFu [2]. This suggests that although

CaFu is much less sensitive to α-SNAP^{L294A} than StaFu, partial inhibition can possibly be attributed to SNAREs being involved in the CaFu reaction. CaFu's sensitivity to high concentrations of α-SNAP^{L294A} is most likely not a reflection of a need for NSF after all. If that were the case, it would be expected that both StaFu and CaFu would be similarly sensitive to α-SNAP^{L294A} treatment, due to the inability of the mutant variant to stimulate ATPase activity. Furthermore, there is no ATP present in the CaFu reaction mix, making NSF activity unlikely, regardless [2].

To consolidate the suspicion that membrane merger in CaFu is mediated by SNAREs, it was tested here whether recombinant cytosolic domains of certain SNAREs had an inhibitory effect on CaFu. If SNAREs were involved in the CaFu reaction, solSNAREs could compete with endogenous membrane-anchored SNAREs for incorporation in a *trans*-SNARE complex. Incorporation of anchorless solSNAREs would yield a non-productive SNARE complex, unable to drive fusion between LBP and LYS [238,239,408–411]. Similarly, if the cognate R-SNARE needed for CaFu was VAMP7, excess of the longin domain could impair the ability of endogenous VAMP7 to bind to the corresponding Q-SNAREs, preventing fusion [2,238,410]. For ATP- and Cyt-dependent fusion, U. Becken showed that the recombinant cytosolic Vti1b-His$_6$ domain (solVti1b) reduced *in vitro* fusion when preincubated (90 min) with LYS and *E. coli*-containing phagosomes (ECP) and a mixture consisting of three preincubated solQ-SNAREs Vti1b, Stx7, and Stx8 [238]. This particular Q-SNARE complex was shown to mediate heterotypic fusion of LEs with LYS in concert with its corresponding R-SNARE, VAMP7 [410,412].

Here, the singular soluble SNARE domains ΔTM-Stx7 and solVti1b decreased StaFu fusion frequency [2]. This was surprising because, earlier, fusion inhibition by solVti1b was observed only after 90 min of preincubation with ECP and LYS and not when the SNARE-fragment was directly added to the reaction mix. Furthermore, solStx7-His$_6$ had no inhibitory effect [11,238]. These differences are likely due to small deviances in the execution of the here presented experiment and the experiment by U. Becken. U. Becken hypothesised that incorporation of soluble SNARE domains could take longer than for full-length SNAREs due to the SNARE domains not being in a sterically favourable orientation. Hence, no decrease in fusion efficiency was observed when solVti1b was added directly before the fusion reaction was started [11]. In this study, SNAREs were preincubated with LBP and LYS for 10 min, possibly allowing for the incorporation of some soluble SNARE domains during that time. The reason for soluble Stx7 inhibiting in this study, but not in the study by U. Becken, could also lie in the different

purification tags used. Here, ΔTM-Stx7 was expressed as GST fusion protein. The larger purification tag could impair the formation of a four α-helix bundle [413].

Here, CaFu was inhibited by none of the single solSNARE domains [2]. An explanation for the differential sensitivity of StaFu and CaFu to single sol SNARE domains could be that endogenous fusion-promoting Q-SNARE subcomplexes may already be present on membranes under CaFu conditions [327,328]. The existence of a loosely assembled Q-SNARE complex could exclude single SNARE domains from incorporation into a forming *trans*-SNARE complex between LBP and LYS. StaFu, on the other hand, likely passes through the classical steps of priming, tethering, docking and fusion during incubation, making StaFu susceptible to inhibitors of these reactions (this study, [8,9,238]). An active priming reaction would allow for the incorporation of solSNAREs into a *trans*-SNARE complex. Such a SNARE complex could, as a result of one of the SNAREs lacking a TMD, fail to exert sufficient force to allow membrane merger [121,124]. Furthermore, it has been discussed whether tilting of SNARE-TMDs is an important step in facilitating fusion pore formation [138]. This process could also be impaired by adding anchorless SNARE domains.

Both reactions were effectively inhibited by adding a preincubated mixture of solVti1b/Stx7/Stx8 in this study. During preincubation, the three SNARE domains lacking their TMDs likely formed a Q-SNARE subcomplex, as hypothesised previously [327,328]. Such a Q-SNARE subcomplex would be able to engage its cognate R-SNARE. Still, it would fail to catalyse fusion and also compete with endogenous Q-SNARE subcomplexes present on the membranes of purified LBP or LYS, effectively preventing fusion [238,239,408–411]. Indeed, experiments showed that both VAMP7 and VAMP8 formed SDS-resistant complexes with solVti1b/Stx7/Stx8 and that preincubation of the three Q-SNAREs with either R-SNARE successfully competed fusion inhibition [238].

VAMP7/TI-VAMP possesses a folded N-terminal longin domain consisting of ~120 amino acids, which is able to interact with its respective core domain, thereby restricting pairing of VAMP7 with other SNAREs and regulating *trans*-SNARE complex-formation [126,414,415]. However, in this study, VAMP7 longin-domain did not decrease fusion frequency in either StaFu or CaFu. U. Becken previously established a likely role for VAMP7 as R-SNARE involved in ECP-LYS fusion and also reported a decrease in fusion when ECPs and LYS were preincubated with VAMP7 AA1-188 [11,238]. Therefore, VAMP7 longin failing to inhibit StaFu is most likely not a reflection of VAMP7 not being involved, but rather of the longin domain not being sufficient to inhibit fusion. Considering that VAMP7 longin preferentially adopts a

closed conformation to modulate SNARE-complex formation, it seems plausible that the endogenous longin-domain may only release the core domain of VAMP7 just in time for complex formation [126]. Such a mechanism would make it difficult for recombinant longin to bind to and prevent SNARE interaction before a *trans*-SNARE complex has formed. On the other hand, it was reported that VAMP7 could form complexes with SNAP25 and Syntaxin 1A *in vitro*, even in its closed conformation [126].

Taken together, SNARE participation in driving membrane fusion in CaFu is very likely. The most plausible scenario, in this case, is that the SNAREs required for CaFu already went through a priming reaction before organelles were purified, explaining the overall low sensitivity of CaFu to established inhibitors of StaFu. Three Q-SNAREs are likely already present in a Q_{abc}-subcomplex held in a metastable activated state by an accessory protein, preventing premature *trans*-SNARE complex formation. The protein(s) involved in this arrest would liberate the subcomplex in the presence of Ca^{2+}. Such a mechanism could also explain the consumption of Ca^{2+}-sensitive fusion activity when organelles are exposed to low [Ca^{2+}], insufficient to support efficient attachment [2]. Fusion itself only needs around 15 µM of Ca^{2+} to activate the fusion machinery, which would lead to the formation of non-productive SNARE complexes without proper fusion partners [2]. Members of the Munc and Syt protein families are known to bind to SNAREs and guide SNARE-complex assembly when appropriate [416,417]. In addition to a scenario where a Q_{abc}-SNARE subcomplex is bound by an inhibitory protein, it would also be possible that only one or two of the involved SNAREs are directly restricted from forming complexes while still being able to interact with other SNAREs [416–418]. An example for such a regulation is Stx1, which is bound by Munc18-1, stabilising a closed non-activating conformation, with its α-helical H3-domain folded onto the SNARE motif [417]. Stx1 is reported to form clusters (also in correspondence to elevated [Ca^{2+}]) [419] and to interact with SNAREs [417]. When appropriate, Munc18-1, in concert with Munc13-1, induces a conformational change in Stx1, converting it into its active form, allowing for guided interaction with SNAP-25 [416,418]. Ca^{2+}-bound Syt I competes with complexin for SNARE complex binding, ultimately dislodging complexin and unlocking the complex for fusion [253,390]. The LE/LYS SNARE Stx7 and Vti1b also possess N-terminal α-helical domains. The N-terminal domain of Stx7 preferentially assumes a closed conformation like Stx1, whereas the N-terminal domain of Vti1b adopts an open conformation. Both SNAREs likely contribute to CaFu, as preincubated solVti1b/Stx7/Stx8 were able to inhibit the R-SNARE present on LBP and LYS. Although it has to be considered that SNARE-pairing can be promiscuous [408]. Munc13 has also been reported to contribute to tethering and liposome clustering in a Ca^{2+}-dependent fashion, interact

with the LE/LYS SNARE proteins Stx7 and VAMP8, and contribute to LE maturation [420,420–422]. These examples make Munc proteins, and Munc13-4 in particular, interesting candidates as Ca^{2+}-sensors in CaFu. Parallels between sea urchin CV fusion and CaFu are extensive. However, the involvement of SNAREs as mediators of the final fusion event and the participation of a 'SNARE-arresting' protein factor are a major difference between both processes, as SNAREs are reported not to be essential for CV fusion [260,404]. Vti1b/Stx7/Stx8 are already well-established as late endosomal SNAREs, which, in concert with VAMP7, mediate LE-LYS fusion [238,410], making these prime candidates for the SNAREs participating in CaFu. Other possible candidates could be a Q-SNARE complex comprising Vti1b/Stx13/Stx8 and VAMP8 as alternative SNAREs [238]. Furthermore, Stx11 and Stx3 have also been reported to be present on late endocytic or phagocytic compartments, although Stx11 may have a fusion-inhibiting function on LYS [423]. Future experiments should further investigate the participation of particular SNARE proteins and a possible Ca^{2+}-dependent SNARE complex disruption, as reported by Tahara et al.

6.11 Ion profile may aid in the search for Ca^{2+}-sensing protein

There is strong evidence suggesting involvement of SNARE proteins in CaFu. The working hypothesis is that a fusion-ready complex consisting of three Q-SNAREs is held from forming complexes via a protein, which is displaced in a Ca^{2+}-dependent manner. Such a protein must either be capable of sensing an increase in [Ca^{2+}] itself or rely on the action of another Ca^{2+}-activatable protein for displacement. One example of such a protein pair is Syt I and complexin at synaptic vesicles [253]. Another great unknown is the protein requirement of LBP-LYS attachment. Regardless of the exact mechanism or protein requirements of CaFu subreactions, there must be a Ca^{2+}-sensing protein which acts as a bridge between elevated [Ca^{2+}] and fusion of LBP and LYS. Many Ca^{2+}-sensing proteins are known to be also activated by metal ions other than Ca^{2+}. In some cases, exocytosis, for example, can also be triggered by Sr^{2+} and Ba^{2+} [424–426]. CaFu occurs not only in the presence of 120 µM Ca^{2+} but also in the presence of 1 mM Ba^{2+} and Mn^{2+} [2]. Ion sensitivities have been investigated for many proteins. An ion spectrum that is as comprehensive as possible may help identify proteins putatively involved in CaFu.

Additional analysis in this study revealed that 1 mM Sr^{2+} supports fusion of LBP and LYS in the absence of ATP and Cyt to its full extent as well [2]. Homotypic fusion of cortical vesicles from sea urchin eggs can also be triggered by Sr^{2+} and Ba^{2+}, albeit at higher concentrations than with Ca^{2+}. This is similar to the observations made here and by J. Becker [2]. Sensitivity to Mn^{2+}

has not been tested in the study by Coorssen and colleagues. It is of note that CV were brought in contact with each other by centrifugation to mimic exocytosis of CV at the PM [260]. Furthermore, it is questionable if Sr^{2+} and Ba^{2+} sensitivity of CV fusion is based on the same mechanism as CaFu, as Coorssen and colleagues excluded the participation of SNAREs in membrane merger [260], for which there is strong evidence in CaFu. Based on the generated ion spectrum of CaFu, Syt-7 and $cPLA_2$ were tested for their involvement in CaFu.

It is worth noting that the determination of ion spectra should not be considered absolute. For many Ca^{2+}-sensitive proteins, the full ion sensitivities to divalent cations may not be known. Protein activation in response to cations may also differ due to detection methods, buffer composition, and protein production methods. Omitting candidate proteins from investigation due to ill-fitting ion sensitivities may be detrimental in the search for the Ca^{2+}-sensing protein in CaFu.

6.11.1 $cPLA_2$ does not mediate CaFu

Human cytosolic phospholipase A_2 is another prime candidate for a Ca^{2+} sensor in CaFu. It is activated not only by Ca^{2+}, but also by Mn^{2+}, Ba^{2+}, and Sr^{2+} [331] and thus perfectly fits in the ion spectrum determined for CaFu. PLA_2 enzymes are involved in mediating fusion events in endosome fusion and G-protein-mediated secretory vesicle fusion [278,332,333]. The function of PLA_2 enzymes in fusion is not well understood. $cPLA_2$ belongs to a group of enzymes that are well-known for their role in inflammation and immune function by generating arachidonic acid (AA). AA is subsequentially metabolised to eicosanoids (like prostaglandins), which serve as second messengers [278]. Free fatty acids, such as arachidonic acid (AA), have been associated with increased secretion, possibly increasing membrane fluidity, favouring non-bilayer configurations, introducing fusion-promoting membrane curvature, or creating lipid domains for certain fusion-promoting proteins [278].

$AACOCF_3$ is a well-established inhibitor of $cPLA_2$ and has been used to investigate $cPLA_2$ participation in CaFu. It is an analogue of AA, in which the carboxyl group is replaced by a trifluoromethyl ketone moiety. It binds tightly to $cPLA_2$ and effectively inhibits enzyme activity [334]. NMR studies revealed that $AACOCF_3$ is bound in the enzyme's active site without irreversibly modifying the enzyme. Molar excess of $AACOCF_3$ unspecifically associates with hydrophobic regions of $cPLA_2$ [335].

Here, neither $AACOCF_3$ nor the EtOH solvent control had an inhibitory effect on CaFu. Therefore, $cPLA_2$ is likely not involved in CaFu and does not act as a Ca^{2+}-sensor. Another caveat that makes $cPLA_2$ unsuitable as a candidate is that $cPLA_2$ associates with membranes in response to elevated $[Ca^{2+}]$. Not only is CaFu independent of Cyt, but it was shown that after trypsin treatment, fusion competence cannot be restored when adding Cyt. The sought-after protein is therefore not recruited from the cytosol.

6.12 CaFu does not mimic PM repair

A physiological function is yet to be determined for CaFu. It has been shown that CaFu has extensive parallels with exocytic mechanisms, such as exocytosis of secretory granules in sea urchin eggs or the release of neurotransmitters at the presynapse [253,255,257]. These parallels could indicate a mechanistic overlap and a possible physiological function of this purely Ca^{2+}-dependent fusion mechanism. In PM membrane repair mechanisms, fusion of numerous LYS with the PM to reseal the damaged area has been well characterised [201,246]. Given CaFu's parallels with exocytic events, it is imperative to investigate whether Ca^{2+}-dependent LBP-LYS fusion mimics PM repair.

Syts are good candidates to act as Ca^{2+} sensors in CaFu [267,339]. Syt-7 has been reported to localize to dense-core vesicles, LYS, and the PM in various cell types and to mediate exocytic processes in the context of PM repair, phagocytic cup formation, and exocytosis of dense-core vesicles [214,246,340,341,427,428]. Syt-7 was reported to be half-maximally activated by $[Sr^{2+}]_{1/2}$ of 260 µM and $[Ba^{2+}]_{1/2}$ of 563 µM [268]. However, Syt-7 has been reported to be activated with $[Ca^{2+}]_{1/2}$ of 0.3 µM, which is likely too sensitive for CaFu. However, Ca^{2+} sensitivity can be modulated to some degree, depending on the lipid composition of membranes [268]. Syt I is a less likely candidate to function in CaFu, as it is solely activated by Ca^{2+}. Similarly, Syt IX is activated by Sr^{2+} but not by Ba^{2+}. Syt-7 has been extensively studied in the context of exocytosis and PM repair [250,341,427–429].

Here, in a western-blot analysis, a 70 kDa band was detected in J774E PNS but not in LYS [2], which likely represents Syt-7. Most commonly, a 45 kDa form of Syt-7 is detected. Sugita et al. uncovered that in rat brain tissues, multiple Syt-7 proteins with molecular weights ranging from 45 to 90 kDa are present [430]. However, the major Syt-7 isoform present in mouse brain has been reported to have a molecular weight of ~ 65 kDa [431]. The 70 kDa form therefore likely represents a Syt-7 protein generated by alternative splicing. Absence of Syt-7 from LYS, derived from J774E macrophages under the same experimental conditions as LYS used for *in*

vitro fusion assays, excludes Syt-7 as Ca^{2+}-sensor in CaFu. Furthermore, CaFu is unlikely to mimic Syt-7-mediated lysosomal exocytosis in membrane repair. This conclusion is consolidated by data from PM-resealing experiments with SLO-induced damage, which has a different ion sensitivity than the CaFu reaction [2].

Proteins of the ferlin family contain C2 domains, much like proteins of the Syt-family. The C2A domain binds to negatively charged phospholipid membranes in the presence of Ca^{2+}, whereas none of the other C2 domains display lipid binding properties [342,343]. As a potential Ca^{2+}-sensor protein in CaFu, myoferlin is of special interest. It has roles in multiple membrane trafficking and fusion events, such as myoblast fusion, repair mechanisms after muscle injury, and lysosomal exocytosis in mouse macrophages [274,275,277]. Myoferlin mostly localizes the PM but is also found at the nucleus (function not known) and on LYS [277,342]. It was concluded from previous experiments that proteins involved in CaFu must be tightly associated with their membranes [2]. This circumstance renders myoferlin particularly interesting in this context, as it is anchored to membranes via a TMD, with its C2 domains (7 in total) protruding into the cytosol [271,272]. Although no direct interaction for myoferlin with SNARE-proteins is known, a fusion-promoting role for otoferlin via interactions of its C2F domains with SNARE-proteins has been described [432,433]. If myoferlin were to also interact with SNAREs, this would fit well with the current hypothesis.

Even though myoferlin seems to be a promising candidate as a Ca^{2+}-sensor, only very little myoferlin was detected in J774E PNS fractions (this study), as a ~ 200 kDa band in immunoblot analysis and none was detected in LYS fractions. Similar to Syt-7, absence of myoferlin on LYS excludes a myoferlin-driven mechanism for CaFu. Additional data shows that myoferlin C2A half-maximally binds to PS-containing membranes at 1 µM Ca^{2+} [342]. Even though Ca^{2+}-dependent binding may be modulated by lipid composition, membrane binding of myoferlin is likely too sensitive for CaFu since attachment in CaFu requires around 100-120 µM Ca^{2+}. Myoferlin was also not detected in proteomics analyses in purified LYS [2], further corroborating the conclusion that myoferlin is not the searched-for Ca^{2+}-sensor in CaFu.

Similar to ferlins, annexins are a family of Ca^{2+}-regulated phospholipid-binding proteins. As Syts, annexins are differentially capable of sensing [Ca^{2+}] and translocate from the cytosol to acidic phospholipid-containing membranes upon binding of Ca^{2+} [284,286]. Annexins have been ascribed roles in membrane fusion events, such as exocytosis and membrane repair [201,289,344,346,434]. Their molecular properties make annexins interesting candidates for linking membranes together and function in generating membrane contact sites, thereby exerting

crucial functions in membrane trafficking and regulating signalling pathways in concert with numerous other Ca^{2+}-sensitive proteins [286,435]. Anx A7 specifically is known for its roles in Ca^{2+}- and GTP-driven exocytosis [344], exocytosis of lamellar bodies in lung alveolar cells [436], and participating in ESCRT-dependent and -independent membrane repair mechanisms [437,438]. In PM repair, Anx A7 forms a complex with apoptosis-linked gene-2 (ALG-2) to enable binding of ALG-2 and ALG-2-interacting protein X (ALIX). Subsequently, the ESCRT III complex is assembled, and the injured membrane portion of the PM is excised and shed [438]. Contrary to the ESCRT-dependent PM repair mechanism, Anx A7 was recently found to also participate in an ESCRT-independent repair mechanism at lysosomal membranes. Ebstrup and colleagues speculated that Anx A7 may be directly recruited to ruptured lysosomal membranes, where it promotes repair through its membrane curvature-inducing and cross-linking properties [437]. Due to the already described functions of Anx A7, it becomes necessary to investigate the possible participation of Anx A7 in CaFu. Fitting with the hypothesis that membrane merger in CaFu is driven by SNAREs, Ca^{2+}-regulated binding of Anx A7 to SNAP23 was observed and may facilitate membrane fusion in surfactant secretion [436]. Even though Anx A7 can link membranes together and facilitate exocytosis, they are difficult candidates concerning mediating membrane attachment and fusion. As discussed before, CaFu likely relies on membrane-bound proteins, which are not easily removed. However, Anx A7 (and all annexins, for that matter) only transiently associates with membranes in the presence of Ca^{2+} and would probably be lost during purification of LBP and LYS. Another caveat making Anx A7 involvement in CaFu unlikely is the fact that Anx A7 GTPase activity, which enhances PS liposome fusion, is stimulated by Ca^{2+} and Mg^{2+} but not by adding Sr^{2+} or Ba^{2+} [344]. This ion spectrum does not fit with the spectrum determined for CaFu. To experimentally exclude Anx A7 participation in CaFu, the fusion-enhancing effect of GTPγS in Anx A7-mediated fusion was assessed in CaFu reactions (this study). Caohuy and colleagues observed a ~ 150-fold increase in baseline PS-liposome fusion when adding 200 µM GTPγS. The effect was lost at higher concentrations [344]. No such effect was observed in CaFu or StaFu reactions, excluding participation of Anx A7 in either Ca^{2+}-dependent LBP-LYS fusion or ATP/Cyt-dependent fusion [2].

None of the investigated proteins implicated in membrane repair were identified to participate in CaFu. This strongly indicates that CaFu is not a surrogate reaction for lysosomal exocytosis in PM repair. This conclusion is supported by the ion specificity observed for streptolysin O (SLO)-induced damage repair deviating from the ion specificity of CaFu [2]. Furthermore, the possibility of participation of Anx A2 was excluded as well [12,13], which also pulls a possible involvement of dysferlin into question, which is associated with membrane repair in muscle

cells [439]. Although CaFu is not involved in PM repair mechanisms, the reaction still has extensive parallels with other secretory events, as mentioned before. These parallels should not be dismissed in the ongoing search for proteins involved in CaFu. Relevant protein(s) may be found in other exocytic events.

6.13 Working model for CaFu reaction

Standard *in vitro* fusion of LBP with LYS (StaFu) is carried out in a buffer system reconstituting the physiological conditions inside the cell, including cytosolic proteins and an ATP-regenerating system. This experimental system has been proven to be invaluable in mechanistically dissecting different steps in phagosome maturation, and the factors involved [238]. In a similar experimental setup, Ca^{2+}-dependent fusion of LBP with LYS that was independent of ATP or Cyt has been discovered by U. Becken [11]. Although extensively investigated, the exact mechanism, the proteins involved, and a physiological function remained elusive in large parts (this study, [2,11–13]). The previously presented results are summarised, and a preliminary working model of the CaFu reaction compared to StaFu is created using these and findings from previous work.

CaFu, in contrast to StaFu, was shown not to be reliant on the presence of ATP, cytosolic proteins, PI(3)P- and PI(4)P-binding proteins, and Rab GTPases in this and previous studies (this study,[2,12,13,238]). Furthermore, CaFu does not need priming activity from NSF (this study), therefore deviating from the established requirements of StaFu (this study,[2,8,9,11]). SNARE-involvement in CaFu was proven with high probability using solSNARE domains (this study; [2]). The same solSNARE-domains were also shown to have an inhibitory effect on the StaFu reaction [238]. It was concluded that since classical priming and Rab-mediated tethering essential to StaFu were neither needed nor feasible in CaFu, SNAREs most likely already proceeded through priming before LBP or LYS were purified and arrested in a metastable fusion-competent Q_{abc} SNARE subcomplex. If such a protein exists, it either releases the SNARE-complex once a sufficient [Ca^{2+}] is present or is displaced by another protein in response to elevated [Ca^{2+}]. The hypothesis of a SNARE-arresting protein also fits well with the observation of J. Becker that fusion competence is consumed when [Ca^{2+}] that support sub-maximal fusion are added [2]. The fusion-inhibiting protein is likely to bind to the Q_{abc}-SNARE complex. If it were to bind to the cognate R-SNARE, the preincubated Q_a-, Q_b-, and Q_c-SNAREs would not be able to bind to the R-SNARE *in vitro* and prevent fusion.

Further experiments revealed that fusion and attachment before fusion depend on Ca^{2+} in CaFu (this study; [2]). Maximum attachment is yielded at a similar [Ca^{2+}] as maximum fusion under standard CaFu conditions. Fusion has been shown to occur at much lower [Ca^{2+}] when LBP and LYS were brought closely together by gentle centrifugation by J. Becker. This illustrates a differential Ca^{2+} requirement for attachment and fusion [2]. Furthermore, the conclusion suggests itself that either one protein with differential Ca^{2+}-sensitivity for different functions, or multiple Ca^{2+}-sensitive proteins are needed for CaFu. Although it is known that proteins are involved in CaFu [2], it is necessary to determine whether specific proteins are involved in attachment and fusion or are only needed for the fusion reaction. Electrostatic interactions between membrane-bound proteins (which would not necessarily need to be Ca^{2+}-sensitive), Ca^{2+}, and anionic lipids could potentially contribute to organelle attachment. Purely electrostatic interactions between Ca^{2+} and anionic lipids of the organelle membranes are also possible. Preliminary experiments addressing this question were unfortunately unsuccessful due to technical difficulties (not shown). On the other hand, the possibility of the existence of differentially Ca^{2+}-sensitive organelle populations seems less likely, since fusion yield cannot be increased by adding more Ca^{2+} after organelles have already been exposed to low [Ca^{2+}], a feature that has been observed for CV in sea urchin eggs [2,257].

Regardless of the exact mechanism, CaFu needs a Ca^{2+}-sensing protein factor. Since other divalent metal ions are also capable of stimulating activity in Ca^{2+}-sensitive proteins, the previously determined ion spectrum, including Ca^{2+}, Ba^{2+}, and Mn^{2+} determined by J. Becker, was expanded by Sr^{2+} (this study; [2]). This yielded $cPLA_2$ [331] and Syt-7 [268] as possible Ca^{2+} sensor proteins. Because of the extensive similarities with exocytic processes, PM repair was hypothesised to be a putative physiological function for CaFu. Syt-7 already fit well with this. Additionally, participation of myoferlin and Anx A7 in CaFu was tested. None of the tested proteins are likely to contribute to CaFu. Syt-7 and myoferlin are largely absent from LYS and therefore unable to mediate CaFu (this study). Here, a well-established inhibitor [334,336] of $cPLA_2$ had no inhibitory effect on CaFu, ruling out participation of $cPLA_2$. Also, no stimulation of baseline fusion frequency, as previously reported for Anx A7-mediated fusion upon the addition of GTPγS by Caohuy et al., was observed here [344]. With the observation of J. Becker in mind, which postulates a different ion spectrum for membrane repair than for CaFu, the possibility of CaFu being a mimic of membrane repair was rejected.

Taking together the previously presented data, the preliminary working model for CaFu compared to StaFu is as follows: 1) SNAREs are primed in an NSF, α-SNAP and ATP-

dependent fashion before purification of LBP or LYS in J774E macrophages. A Q_a, Q_b, and Q_c-SNARE are aggregated into a 'prefusion complex' and arrested by an inhibitory protein, preventing premature unproductive assembly of ternary SNARE complexes. This fusion-inhibiting protein is yet to be identified. It is of note that in a StaFu-type setting, *cis*-SNARE complexes can be disassembled by NSF and α-SNAP *in vitro*.

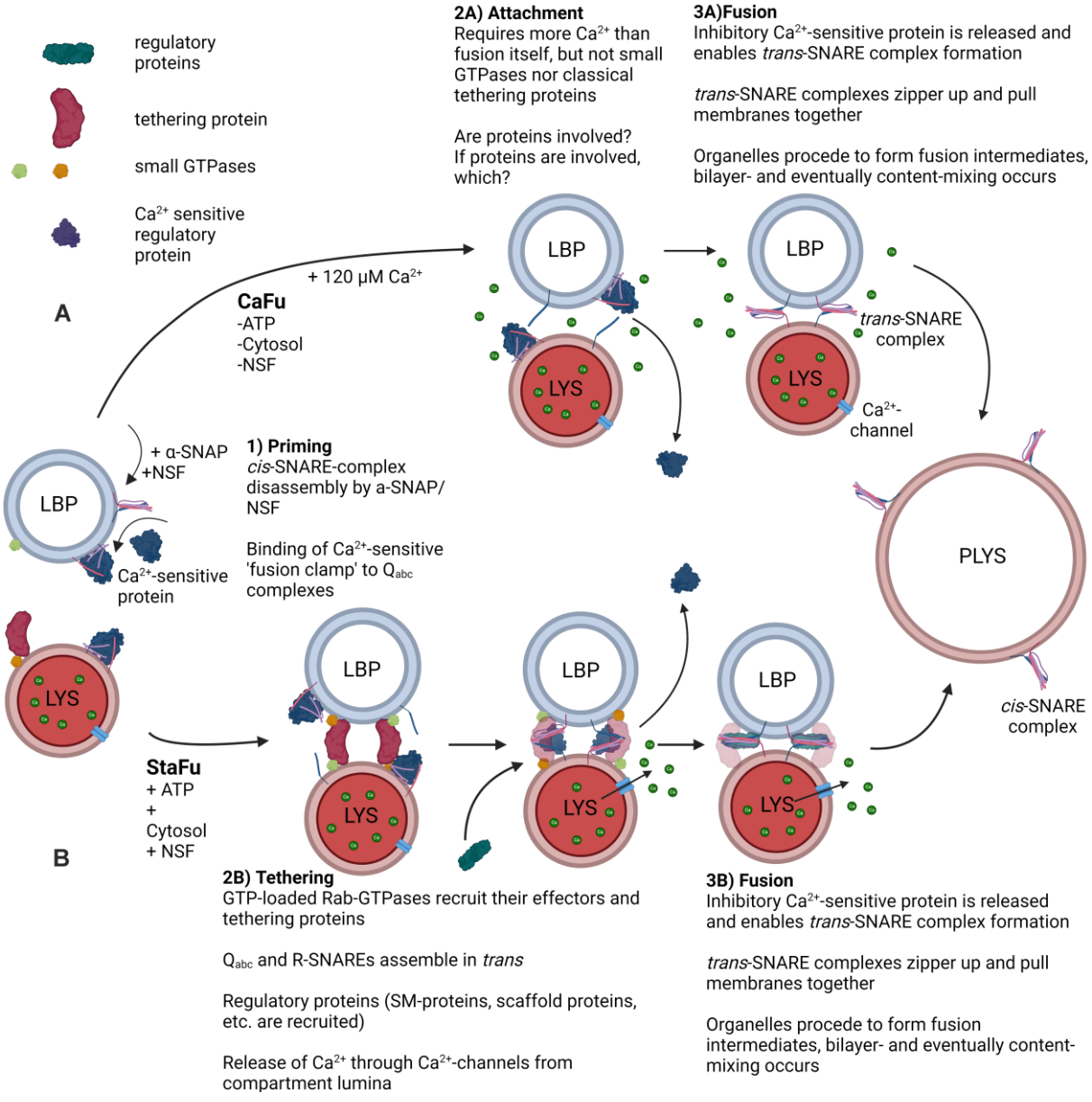

Figure 34: Schematic model of CaFu/StaFu reaction mechanisms. See text for details. Illustration created using BioRender.com.

This is not possible under standard CaFu conditions; hence, fusion competence is consumed once the SNAREs are exposed to Ca^{2+}. This putative fusion regulating protein is likely a membrane protein. However, it could also be a protein soluble in the cytosol (as depicted in Figure 34) if it tightly binds to the Q_{abc}-complex and is not lost during purification. 2B).

Once purified LBP and LYS are exposed to the StaFu reaction conditions, LBP and LYS proceed through the classical small GTPase- and tethering-protein-dependent tethering step. A fusogenic protein domain attaching LBP and LYS is formed, accumulating fusion-promoting lipids and regulatory proteins, such as SM-proteins or Syts. A Ca^{2+} channel located on LYS opens and transiently releases Ca^{2+} (endogenous Ca^{2+}) from the compartment lumen, transiently increasing local [Ca^{2+}] in the reaction buffer. The Ca^{2+}-sensitive 'fusion clamp' is released and allows for the formation of a ternary SNARE-complex in *trans*. 3B) The SNARE-domains 'zipper up', eventually driving membrane merger and content mixing between LBP and LYS. 2A) Under CaFu reaction conditions, no cytosolic proteins are present. Attachment is either mediated by electrostatic interactions (as discussed above) or by a Ca^{2+}-sensitive protein firmly attached to the membrane. Attachment needs higher [Ca^{2+}] than the fusion reaction. 3A) Once exposed to low micromolar [Ca^{2+}] (exogenous Ca^{2+}], the Q_{abc}-SNARE-arresting protein is released, and the Q_{abc}-SNAREs assemble into a ternary complex with their cognate R-SNARE. SNARE-pairing can occur in *cis* or *trans* if unpaired SNAREs come into contact when the 'fusion clamp' is released. *Cis*-pairing would lead to non-productive complex formation.

It was previously shown that phagosome-LYS fusion in J774E [2] and the *in vitro* StaFu reaction depend on Ca^{2+}. CaFu likely represents a 'shortcut' to one of the last steps in regular phagosome with LYS fusion. Still, given its extensive parallels to exocytic events, a CaFu-type reaction might also be relevant for other physiological functions (c.f. [2]). If CaFu is a subreaction of regular phagosome-LYS fusion, the release of endogenous Ca^{2+} from the LYS lumen is likely to occur to trigger the final step of fusion in StaFu, as well as *in vivo*. Identification of a Ca^{2+} channel involved in *in vitro* and *in vivo* phagosome-LYS fusion would be needed to corroborate this hypothesis. Previous attempts at identifying a Ca^{2+} channel involved in StaFu yielded negative or inconclusive results [12,13]. Future work must also focus on the identification of Ca^{2+}-sensitive protein(s) in CaFu and must determine whether attachment is brought about by proteins or electrostatic effects.

7 Outlook

7.1 Further assessment of cargo delivery to digestive compartments

Here, FFEs contained similar amounts of mCath D as the WT after letting FFEs mature for a significantly longer time period (this study; [10]). However, it is unknown if this Cath D is also active and if endocytosed material can be degraded in these compartments. This should be assayed in different ways. First, it should be tested whether endocytosed ATTO488-dextran colocalises with acidic compartments (LT) to a similar extent as in WT cells after 24 hours of chase. Next, dextran delivery to compartments containing active Cath D should be tested. SiRlysosome could be used as a tool for this, as it labels active Cath D. As for the LT colocalization assay, a short and a long chase period should be used to assess whether endocytosed cargo is delivered to digestive compartments. If possible, distribution/ colocalization of acidic compartments and active Cath D should be investigated, using LT and SiRlysosome as well. Van der Beek and colleagues also determined and compared the distribution of all Cath D (including pro Cath D forms) vs. active Cath D in HOPS-depleted cells, using antibodies against active and inactive Cath D forms and SiRlysosome to label active Cath D [314]. Such an approach could also benefit the KOs used here, as cargo in Rab7a, Arl8a/b, myrlysin, and diaskedin KOs displays similar behaviour as in Vps41 KOs. Endocytosed material could potentially be accumulated in similar hybrid compartments as reported for Vps41 KO cells [314]. The digestive capacity in the investigated KOs, compared to WT cells, could further be assayed using DQ-BSA. DQ-BSA is an endocytic probe. In its uncleaved state, the fluorescence of the coupled fluorophore is quenched. Dequenching happens once BSA is proteolytically cleaved upon enzymatic digestion [440]. Impaired digestion would therefore result in lower fluorescence intensities than in cells with functional digestive compartments.

'HOPS bodies' found in HOPS deficient cells were positive for autophagic markers such as LC3 for example [314]. Together with the observations made in this study, that endocytosed cargo can reach compartments containing mCath D it seems likely, that cargo transport to LYS is mediated via an HOPS-independent autophagic pathway [10,314]. To test if endocytosed material might be trafficked to KO LYS via autophagic compartments colocalization between endocytosed fluorescent dextran and autophagic proteins could be tracked after various chase periods in a microscopic assay.

7.2 pH measurement of endocytic compartments

Labelling of acidic compartments with LT showed that all KO cells possessed sufficiently acidic compartments to accumulate the acidic probe (this study; [10]). Moreover, staining with MR also revealed that Rab7a, Arl8a/b, Vps41, myrlysin, and diaskedin cells also had active Cath B. However, staining with LT is insufficient to determine small differences in LYS acidification. An earlier report by Pols and colleagues did not find severe defects in acidification after KD of HOPS subunits Vps39 or Vps41, using LT as acidotropic probe [371]. However, a recent study uncovered that endocytic compartments were less acidic in Vps39 KO cells than in control cells [314]. As the proteins investigated contribute to LYS positioning, a determinant for LYS acidification (reviewed in [312]) or are linked to endosome acidification via their effectors [376], this should be investigated in more detail. LysoSensor is a probe similar to LT, which can be used as a pH indicator and could be used to determine if acidity is altered in KOs in general [373]. To monitor the pH of maturing endocytic compartments in WT and KO cells, fluorescein-dextran could be used to measure intraluminal pH [314], as fluorescein fluorescence is pH-dependent. These experiments should allow determining the effect of Rab7a, Arl8a/b, Vps41, myrlysin, and diaskedin KO on endosome/LYS acidification more conclusively.

7.3 Anchoring of HOPS

HOPS is most likely delivered to maturing LEs on TGN-derived CVs bound to Rab2a [1]. However, Rab2a cannot be the main membrane anchor of the HOPS complex on LEs (this study, [1,10]). Further experiments are required to shed more light on how HOPS might be anchored on LEs and LYS. It appears that multiple proteins might be involved in HOPS anchoring, as KD of Rab2a in Arl8a/b DKO HeLa cells did not displace HOPS from membranes. However, Arl8 is thought to bind to HOPS on LYS [10]. To shed more light on HOPS anchoring on LEs, a Rab2a/Rab7a DKO HeLa cell line could be used to assess whether HOPS-specific subunits are displaced from membranes in a cellular fractionation experiment. Although direct Rab7a participation in anchoring of HOPS was ruled out and participation of Rab7a effector Plekhm1 does not seem likely at this point (this study, [10]), the possibility of RILP or Plekhm1 participation in HOPS anchoring should be carefully assessed. To this end, KD of either protein in the Rab2a/Rab7a DKO cell line could be a useful tool, provided that such a treatment yields viable cells. Moreover, there is evidence that HOPS anchoring requires PI(4)P [9]. Furthermore, HOPS bound to Arl8/BORC and/or SKIP on LYS could also make contact with Rab2a on LEs [10].

7.4 Requirements for LBP-LYS attachment in CaFu

Here, attachment of LBP and LYS was shown to be dependent on [Ca^{2+}], which support maximum fusion [2]. However, it is unknown whether attachment is mediated by a Ca^{2+}-sensitive protein or if it is based on electrostatic interactions between Ca^{2+} ions and negatively charged lipids and possibly proteins on the cytosolic side of compartment membranes [397,398]. Preliminary experiments addressing this question were unsuccessful due to technical difficulties. Trypsin treatment of LBP and LYS, which were previously treated with LPC-12 (for the attachment assay), led to lysis of these compartments. Optimization of the protocol used could potentially circumvent these issues. If attachment of LBP and LYS is indeed dependent on proteins it must be clarified whether a specific Ca^{2+}-binding protein mediates attachment, or if unspecific Ca^{2+}-induced clustering of proteins and membranes results in attachment. Additionally, it could be tested, if the [Ca^{2+}] used in CaFu assays is sufficient to bring about clustering and attachment of artificial liposomes, via electrostatic interactions.

7.5 Putative candidate proteins to act as Ca^{2+}-sensors in CaFu

An interesting candidate for participating in membrane attachment and possibly also in mediating SNARE-dependent fusion of LBP and LYS is Munc13-4. Munc13-4 possesses two C2 domains and binds SNAREs in a Ca^{2+}-dependent fashion [441]. Chicka and colleagues showed, that Munc13-4 was able to enhance *in vitro* SNARE-mediated fusion of proteoliposomes in a Ca^{2+} and PS-dependent manner [442]. These circumstances would fit well with the data gathered thus far. Involvement of Munc13-4 could be tested by using Munc-13-4 KD J774E macrophages for *in vitro* fusion experiments. Due to the poor transfection efficiency in macrophages, the use of siRNA in this setup might not be possible. Alternatively, presence of Munc13-4 on LYS could be tested by SDS-PAGE and subsequent immunoblotting or staining of Munc13-4 on LBP and subsequent microscopic assessment. A more generalized approach to investigate involvement of other Munc13 proteins (1-3) would be the use of phorbol esters. Phorbol esters are most commonly described in the context of protein kinase C activation. However, phorbol esters are also capable of binding to C1 domains in Munc13 family members [443]. Since ATP requirement in CaFu was ruled out, an effect of phorbol esters on CaFu would hint to participation of Munc family members rather than an involvement of protein kinase C. To verify the participation of Vti1b, Stx7, and Stx8 antibodies against the respective SNAREs could be utilized in CaFu reactions.

7.6 Identification of Ca^{2+}-channels

Phagosome-with LYS-fusion has been shown to be Ca^{2+}-dependent *in vivo* [2]. If CaFu has a physiological counterpart in living cells, the origin of Ca^{2+}-fluxes that lead to membrane fusion *in vivo* must be determined. It is most likely, that Ca^{2+} is released from LYS themselves, via Ca^{2+}-channels. In her thesis, C. Hermsen evaluated the participation of the lysosomal Ca^{2+}-channel TRPML-1 in phagosome-LYS fusion. The TRMPL-1 inhibitor verapamil [444] inhibited LBP-LYS fusion, but TRPML-1 as source for Ca^{2+} fluxes from the LYS was dismissed as phagosome maturation was unaltered in a stable TRPML-1 KD cell line [13]. However, TRPML-1 remains an interesting candidate a Ca^{2+}-channel in phagosome-LYS fusion. Estradiol methyl ether (EDME) is an inhibitor for TRPML-1. Two aza analogs have been recently described (methoxypyridine and a methoxypyrimidine), of which the methoxypyridine largely retained its inhibitory effect, whereas the methoxypyrimidine does not display significant inhibitory activity towards TRPML-1 [445]. EDME and its analogs could be used to further explore a possible role for TRPML-1 as Ca^{2+}-channel in phagosome-with-LYS fusion. TRPML-1 was also shown to be activated by $PI(3,5)P_2$ and rapamycin [446]. Experiments with inhibitors of TRPML-1 could be supplemented by using rapamycin and possibly a $PI(3,5)P_2$ in fusion reactions. J. Becker investigated P2X4 for involvement with phagosome-LYS fusion by using 5-BDBD as inhibitor. The treatment had no effect and a role for P2X4 in phagosome-LYS fusion was therefore excluded [12]. To verify that P2X4 does not trigger Ca^{2+} signaling for phagosome-LYS fusion, the P2X4 inhibitors BX430 and BAY-1797 could be tested [447]. Possible roles for other Ca^{2+}-channels that have not yet been mentioned in phagosome-LYS fusion should also be considered.

8 Bibliography

1. Lőrincz, P., Tóth, S., Benkő, P., Lakatos, Z., Boda, A., Glatz, G., Zobel, M., Bisi, S., Hegedűs, K., Takáts, S., et al. (2017). Rab2 promotes autophagic and endocytic lysosomal degradation. J. Cell Biol. *216*, 1937–1947. https://doi.org/10.1083/jcb.201611027.
2. Becker, J., Schleinitz, A., Hermsen, C., Rappold, S., Saftig, P., Jeschke, A., and Haas, A. (2023). Rab GTPase regulation of phagosome–lysosome fusion is bypassed in the presence of micromolar Ca2+. J. Cell Sci. *136*, jcs260806. https://doi.org/10.1242/jcs.260806.
3. Desjardins, M., Huber, Lukas A., P., Robert G., and Griffiths, G. (1994). Biogenesis of phagolysosomes proceeds through a sequential series of interactions with the endocytic apparatus. J. Cell Biol. *124*, 677–688.
4. Luzio, J.P., Parkinson, M.D.J., Gray, S.R., and Bright, N.A. (2009). The delivery of endocytosed cargo to lysosomes. Biochem. Soc. Trans. *37*, 1019–1021. https://doi.org/10.1042/BST0371019.
5. Saftig, P., and Klumperman, J. (2009). Lysosome biogenesis and lysosomal membrane proteins: trafficking meets function. Nat. Rev. Mol. Cell Biol. *10*, 623–635. https://doi.org/10.1038/nrm2745.
6. Settembre, C., Fraldi, A., Medina, D.L., and Ballabio, A. (2013). Signals for the lysosome: a control center for cellular clearance and energy metabolism. Nat. Rev. Mol. Cell Biol. *14*, 283–296. https://doi.org/10.1038/nrm3565.
7. Doherty, G.J., and McMahon, H.T. (2009). Mechanisms of Endocytosis. Annu. Rev. Biochem. *78*, 857–902. https://doi.org/10.1146/annurev.biochem.78.081307.110540.
8. Jeschke, A., Zehethofer, N., Lindner, B., Krupp, J., Schwudke, D., Haneburger, I., Jovic, M., Backer, J.M., Balla, T., Hilbi, H., et al. (2015). Phosphatidylinositol 4-phosphate and phosphatidylinositol 3-phosphate regulate phagolysosome biogenesis. Proc. Natl. Acad. Sci. U. S. A. *112*, 4636–4641. https://doi.org/10.1073/pnas.1423456112.
9. Jeschke, A., and Haas, A. (2018). Sequential actions of phosphatidylinositol phosphates regulate phagosome-lysosome fusion. Mol. Biol. Cell *29*, 452–465. https://doi.org/10.1091/mbc.E17-07-0464.
10. Schleinitz, A., Pöttgen, L.-A., Keren-Kaplan, T., Pu, J., Saftig, P., Bonifacino, J.S., Haas, A., and Jeschke, A. (2023). Consecutive functions of small GTPases guide HOPS-mediated tethering of late endosomes and lysosomes. Cell Rep. *42*, 111969. https://doi.org/10.1016/j.celrep.2022.111969.
11. Becken, U. (2011). Zellfreie Rekonstitution der Fusion Bakterien-enthaltender Phagosomen mit endozytischen Kompartimenten.
12. Becker, J. (2020). Charakterisierung unkanonischer calciumvermittelter Fusion von Phagosomen mit Lysosomen.
13. Hermsen, C. (2017). Die v-ATPase und Calcium in der Regulation der Fusion von Phagosomen mit Lysosomen.
14. Bonazzi, M., and Cossart, P. (2006). Bacterial entry into cells: A role for the endocytic machinery. FEBS Lett. *580*, 2962–2967. https://doi.org/10.1016/j.febslet.2006.04.010.
15. Di Fiore, P.P., and von Zastrow, M. (2014). Endocytosis, Signaling, and Beyond. Cold Spring Harb. Perspect. Biol. *6*, a016865. https://doi.org/10.1101/cshperspect.a016865.
16. Hoeller, D., Volarevic, S., and Dikic, I. (2005). Compartmentalization of growth factor receptor signaling. Curr. Opin. Cell Biol. *17*, 107–111. https://doi.org/10.1016/j.ceb.2005.01.001.
17. Marsh, M., and Helenius, A. (2006). Virus Entry: Open Sesame. Cell *124*, 729–740. https://doi.org/10.1016/j.cell.2006.02.007.
18. Sorkin, A., and von Zastrow, M. (2009). Endocytosis and signalling: intertwining molecular networks. Nat. Rev. Mol. Cell Biol. *10*, 609–622. https://doi.org/10.1038/nrm2748.
19. Collawn, J.F., Stangel, M., Kuhn, L.A., Esekogwu, V., Jing, S., Trowbridge, I.S., and Tainer, J.A. (1990). Transferrin Receptor Internalization Sequence YXRF Implicates a Tight Turn As the Structural Recognition Motif for Endocytosis. Cell, 1061–1072.
20. Kaksonen, M., and Roux, A. (2018). Mechanisms of clathrin-mediated endocytosis. Nat. Rev. Mol. Cell Biol. *19*, 313–326. https://doi.org/10.1038/nrm.2017.132.
21. Schmid, E.M., Ford, M.G.J., Burtey, A., Praefcke, G.J.K., Peak-Chew, S.-Y., Mills, I.G., Benmerah, A., and McMahon, H.T. (2006). Role of the AP2 β-Appendage Hub in Recruiting

Partners for Clathrin-Coated Vesicle Assembly. PLoS Biol. *4*, e262. https://doi.org/10.1371/journal.pbio.0040262.
22. Sorkin, A. (2004). Cargo recognition during clathrin-mediated endocytosis: a team effort. Curr. Opin. Cell Biol. *16*, 392–399. https://doi.org/10.1016/j.ceb.2004.06.001.
23. Hinrichsen, L., Meyerholz, A., Groos, S., and Ungewickell, E.J. (2006). Bending a membrane: How clathrin affects budding. Proc. Natl. Acad. Sci. U. S. A. *103*, 8715–8720. https://doi.org/10.1073/pnas.0600312103.
24. Nossal, R. (2001). Energetics of Clathrin Basket Assembly. Traffic *2*, 138–147. https://doi.org/10.1034/j.1600-0854.2001.020208.x.
25. Praefcke, G.J.K., and McMahon, H.T. (2004). The dynamin superfamily: universal membrane tubulation and fission molecules? Nat. Rev. Mol. Cell Biol. *5*, 133–147. https://doi.org/10.1038/nrm1313.
26. Böcking, T., Upadhyayula, S., Rapoport, I., Capraro, B.R., and Kirchhausen, T. (2018). Reconstitution of Clathrin Coat Disassembly for Fluorescence Microscopy and Single-Molecule Analysis. Methods Mol. Biol. Clifton NJ *1847*, 121–146. https://doi.org/10.1007/978-1-4939-8719-1_10.
27. Sousa, R., Liao, H.-S., Cuéllar, J., Jin, S., Valpuesta, J.M., Jin, A.J., and Lafer, E.M. (2016). Clathrin Coat Disassembly Illuminates the Mechanisms of Hsp70 Force Generation. Nat. Struct. Mol. Biol. *23*, 821–829. https://doi.org/10.1038/nsmb.3272.
28. Matthaeus, C., and Taraska, J.W. (2021). Energy and Dynamics of Caveolae Trafficking. Front. Cell Dev. Biol. *8*, 614472. https://doi.org/10.3389/fcell.2020.614472.
29. Rothberg, K.G., Heuser, J.E., Donzell, W.C., Ying, Y.-S., Glenney, J.R., and Anderson, R.G.W. (1992). Caveolin, a protein component of caveolae membrane coats. Cell *68*, 673–682. https://doi.org/10.1016/0092-8674(92)90143-Z.
30. Dietzen, D.J., Hastings, W.R., and Lublin, D.M. (1995). Caveolin Is Palmitoylated on Multiple Cysteine Residues. J. Biol. Chem. *270*, 6838–6842. https://doi.org/10.1074/jbc.270.12.6838.
31. Monier, S., Dietzen, D.J., Hastings, W.R., Lublin, D.M., and Kurzchalia, T.V. (1996). Oligomerization of VIP21-caveolin in vitro is stabilized by long chain fatty acylation or cholesterol. FEBS Lett. *388*, 143–149. https://doi.org/10.1016/0014-5793(96)00519-4.
32. Kiss, A.L., and Botos, E. (2009). Endocytosis via caveolae: alternative pathway with distinct cellular compartments to avoid lysosomal degradation? J. Cell. Mol. Med. *13*, 1228–1237. https://doi.org/10.1111/j.1582-4934.2009.00754.x.
33. Lim, J.P., and Gleeson, P.A. (2011). Macropinocytosis: an endocytic pathway for internalising large gulps. Immunol. Cell Biol. *89*, 836–843. https://doi.org/10.1038/icb.2011.20.
34. Salloum, G., Bresnick, A.R., and Backer, J.M. (2023). Macropinocytosis: mechanisms and regulation. Biochem. J. *480*, 335–362. https://doi.org/10.1042/BCJ20210584.
35. Lin, X.P., Mintern, J.D., and Gleeson, P.A. (2020). Macropinocytosis in Different Cell Types: Similarities and Differences. Membranes *10*, 177. https://doi.org/10.3390/membranes10080177.
36. Rabinovitch, M. (1995). Professional and non-professional phagocytes: an introduction. Trends Cell Biol. *5*, 85–87. https://doi.org/10.1016/S0962-8924(00)88955-2.
37. Mantegazza, A.R., Magalhaes, J.G., Amigorena, S., and Marks, M.S. (2013). Presentation of phagocytosed antigens by MHC class I and II. Traffic Cph. Den. *14*, 135–152. https://doi.org/10.1111/tra.12026.
38. Rosales, C., and Uribe-Querol, E. (2017). Phagocytosis: A Fundamental Process in Immunity. BioMed Res. Int. *2017*. https://doi.org/10.1155/2017/9042851.
39. Brown, E.J. (1991). Complement receptors and phagocytosis. Curr. Opin. Immunol. *3*, 76–82. https://doi.org/10.1016/0952-7915(91)90081-B.
40. Nimmerjahn, F., and Ravetch, J.V. (2010). FcγRs in Health and Disease. In Negative Co-Receptors and Ligands Current Topics in Microbiology and Immunology., R. Ahmed and T. Honjo, eds. (Springer Berlin Heidelberg), pp. 105–125. https://doi.org/10.1007/82_2010_86.
41. Rosales, C., and Uribe-Querol, E. (2013). Fc receptors: Cell activators of antibody functions. Adv. Biosci. Biotechnol. *04*, 21–33. https://doi.org/10.4236/abb.2013.44A004.
42. Bohdanowicz, M., and Grinstein, S. (2013). Role of Phospholipids in Endocytosis, Phagocytosis, and Macropinocytosis. Physiol. Rev. *93*, 69–106. https://doi.org/10.1152/physrev.00002.2012.
43. Freeman, S.A., and Grinstein, S. (2014). Phagocytosis: receptors, signal integration, and the cytoskeleton. Immunol. Rev. *262*, 193–215. https://doi.org/10.1111/imr.12212.

44. Levin, R., Grinstein, S., and Canton, J. (2016). The life cycle of phagosomes: formation, maturation, and resolution. Immunol. Rev. *273*, 156–179. https://doi.org/10.1111/imr.12439.
45. Haas, A. (2007). The Phagosome: Compartment with a License to Kill. Traffic *8*, 311–330. https://doi.org/10.1111/j.1600-0854.2006.00531.x.
46. Alwan, H.A.J., Van Zoelen, E.J.J., and Van Leeuwen, J.E.M. (2003). Ligand-induced Lysosomal Epidermal Growth Factor Receptor (EGFR) Degradation Is Preceded by Proteasome-dependent EGFR De-ubiquitination. J. Biol. Chem. *278*, 35781–35790. https://doi.org/10.1074/jbc.M301326200.
47. Huotari, J., and Helenius, A. (2011). Endosome maturation: Endosome maturation. EMBO J. *30*, 3481–3500. https://doi.org/10.1038/emboj.2011.286.
48. Octave, J.-N., Schneider, Y.-J., Trouet, A., and Crichton, R.R. (1983). Iron uptake and utilization by mammalian cells. I: Cellular uptake of transferrin and iron. Trends Biochem. Sci. *8*, 217–220. https://doi.org/10.1016/0968-0004(83)90217-7.
49. Fairn, G.D., and Grinstein, S. (2012). How nascent phagosomes mature to become phagolysosomes. Trends Immunol. *33*, 397–405. https://doi.org/10.1016/j.it.2012.03.003.
50. Flannagan, R.S., Jaumouillé, V., and Grinstein, S. (2012). The Cell Biology of Phagocytosis. Annu. Rev. Pathol. Mech. Dis. *7*, 61–98. https://doi.org/10.1146/annurev-pathol-011811-132445.
51. Lee, H.-J., Woo, Y., Hahn, T.-W., Jung, Y.M., and Jung, Y.-J. (2020). Formation and Maturation of the Phagosome: A Key Mechanism in Innate Immunity against Intracellular Bacterial Infection. Microorganisms *8*, 1298. https://doi.org/10.3390/microorganisms8091298.
52. Gruenberg, J., Griffiths, G., and Howell, K.E. (1989). Characterization of the early endosome and putative endocytic carrier vesicles in vivo and with an assay of vesicle fusion in vitro. J. Cell Biol. *108*, 1301–1316. https://doi.org/10.1083/jcb.108.4.1301.
53. Helenius, A., Mellmann, I., Wall, D., and Hubbard, A. (1983). Endosomes. Elsevier Sci. Publ. B V.
54. Diaz, R., Mayorga, L., and Stahl, P. (1988). In vitro fusion of endosomes following receptor-mediated endocytosis. J. Biol. Chem. *263*, 6093–6100. https://doi.org/10.1016/S0021-9258(18)68754-X.
55. Naslavsky, N., and Caplan, S. (2018). The enigmatic endosome – sorting the ins and outs of endocytic trafficking. J. Cell Sci. *131*, jcs216499. https://doi.org/10.1242/jcs.216499.
56. Salzman, N.H., and Maxfield, F.R. (1988). Intracellular fusion of sequentially formed endocytic compartments. J. Cell Biol. *106*, 1083–1091.
57. Lafourcade, C., Sobo, K., Kieffer-Jaquinod, S., Garin, J., and Van Der Goot, F.G. (2008). Regulation of the V-ATPase along the Endocytic Pathway Occurs through Reversible Subunit Association and Membrane Localization. PLoS ONE *3*, e2758. https://doi.org/10.1371/journal.pone.0002758.
58. Maxfield, F.R., and Yamashiro, D.J. (1987). Endosome Acidification and the Pathways of Receptor-Mediated Endocytosis. *Advances in Experimental Medicine and Biology*, pp 189-198. https://doi.org/10.1007/978-1-4684-5442-0_16.
59. Mellman, I. (1996). Endocytosis and Molecular Sorting. Annu. Rev. Cell Dev. Biol. *12*, 575–625. https://doi.org/10.1146/annurev.cellbio.12.1.575.
60. Elkin, S.R., Lakoduk, A.M., and Schmid, S.L. (2016). Endocytic Pathways and Endosomal Trafficking: A Primer. Wien. Med. Wochenschr. 1946 *166*, 196–204. https://doi.org/10.1007/s10354-016-0432-7.
61. Grant, B.D., and Donaldson, J.G. (2009). Pathways and mechanisms of endocytic recycling. Nat. Rev. Mol. Cell Biol. *10*, 597–608. https://doi.org/10.1038/nrm2755.
62. Jones, M.C., Caswell, P.T., and Norman, J.C. (2006). Endocytic recycling pathways: emerging regulators of cell migration. Curr. Opin. Cell Biol. *18*, 549–557. https://doi.org/10.1016/j.ceb.2006.08.003.
63. Maxfield, F.R., and McGraw, T.E. (2004). Endocytic recycling. Nat. Rev. Mol. Cell Biol. *5*, 121–132. https://doi.org/10.1038/nrm1315.
64. Choudhury, Q.G., Mckay, D.T., Flower, R.J., and Croxtall, J.D. (2000). Investigation into the involvement of phospholipases A2 and MAP kinases in modulation of AA release and cell growth in A549 cells. Br. J. Pharmacol. *131*, 255–265. https://doi.org/10.1038/sj.bjp.0703573.

65. Cook, N.R., Row, P.E., and Davidson, H.W. (2004). Lysosome Associated Membrane Protein 1 (Lamp1) Traffics Directly from the TGN to Early Endosomes. Traffic *5*, 685–699. https://doi.org/10.1111/j.1600-0854.2004.00212.x.
66. Gieselmann, V., Hasilik, A., and von Figura, K. (1985). Processing of human cathepsin D in lysosomes in vitro. J. Biol. Chem. *260*, 3215–3220. https://doi.org/10.1016/S0021-9258(18)89493-5.
67. Mach, L., Mort, J.S., and Glössl, J. (1994). Maturation of human procathepsin B. Proenzyme activation and proteolytic processing of the precursor to the mature proteinase, in vitro, are primarily unimolecular processes. J. Biol. Chem. *269*, 13030–13035. https://doi.org/10.1016/S0021-9258(18)99979-5.
68. Bonifacino, J.S., and Rojas, R. (2006). Retrograde transport from endosomes to the trans-Golgi network. Nat. Rev. Mol. Cell Biol. *7*, 568–579. https://doi.org/10.1038/nrm1985.
69. Zerial, M., and McBride, H. (2001). Rab proteins as membrane organizers. Nat. Rev. Mol. Cell Biol. *2*, 107–117. https://doi.org/10.1038/35052055.
70. Raiborg, C., Bache, K.G., Gillooly, D.J., Madshus, I.H., Stang, E., and Stenmark, H. (2002). Hrs sorts ubiquitinated proteins into clathrin-coated microdomains of early endosomes. Nat. Cell Biol. *4*, 394–398. https://doi.org/10.1038/ncb791.
71. Sachse, M., Urbé, S., Oorschot, V., Strous, G.J., and Klumperman, J. (2002). Bilayered Clathrin Coats on Endosomal Vacuoles Are Involved in Protein Sorting toward Lysosomes. Mol. Biol. Cell *13*, 1313–1328. https://doi.org/10.1091/mbc.01-10-0525.
72. Scott, C.C., Vacca, F., and Gruenberg, J. (2014). Endosome maturation, transport and functions. Semin. Cell Dev. Biol. *31*, 2–10. https://doi.org/10.1016/j.semcdb.2014.03.034.
73. Mylvaganam, S., Freeman, S.A., and Grinstein, S. (2021). The cytoskeleton in phagocytosis and macropinocytosis. Curr. Biol. *31*, R619–R632. https://doi.org/10.1016/j.cub.2021.01.036.
74. Gruenberg, J., and Stenmark, H. (2004). The biogenesis of multivesicular endosomes. Nat. Rev. Mol. Cell Biol. *5*, 317–323. https://doi.org/10.1038/nrm1360.
75. Gruenberg, J. (2001). The endocytic pathway: a mosaic of domains. Nat. Rev. Mol. Cell Biol. *2*, 721–730. https://doi.org/10.1038/35096054.
76. Cantalupo, G., Alifano, P., Roberti, V., Bruni, C.B., and Bucci, C. (2001). Rab-interacting lysosomal protein (RILP): the Rab7 effector required for transport to lysosomes. EMBO J. *20*, 683–693. https://doi.org/10.1093/emboj/20.4.683.
77. Harada, A., Takei, Y., Kanai, Y., Tanaka, Y., Nonaka, S., and Hirokawa, N. (1998). Golgi Vesiculation and Lysosome Dispersion in Cells Lacking Cytoplasmic Dynein. J. Cell Biol. *141*, 51–59. https://doi.org/10.1083/jcb.141.1.51.
78. Jordens, I., Fernandez-Borja, M., Marsman, M., Dusseljee, S., Janssen, L., Calafat, J., Janssen, H., Wubbolts, R., and Neefjes, J. (2001). The Rab7 effector protein RILP controls lysosomal transport by inducing the recruitment of dynein-dynactin motors. Curr. Biol. *11*, 1680–1685. https://doi.org/10.1016/S0960-9822(01)00531-0.
79. Sanchez, A.D., and Feldman, J.L. (2017). Microtubule-organizing centers: from the centrosome to non-centrosomal sites. Curr. Opin. Cell Biol. *44*, 93–101. https://doi.org/10.1016/j.ceb.2016.09.003.
80. Fukuda, M., Viitala, J., Matteson, J., and Carlsson, S.R. (1988). Cloning of cDNAs encoding human lysosomal membrane glycoproteins, h-lamp-1 and h-lamp-2. Comparison of their deduced amino acid sequences. J. Biol. Chem. *263*, 18920–18928. https://doi.org/10.1016/S0021-9258(18)37370-8.
81. Staudt, C., Puissant, E., and Boonen, M. (2016). Subcellular Trafficking of Mammalian Lysosomal Proteins: An Extended View. Int. J. Mol. Sci. *18*, 47. https://doi.org/10.3390/ijms18010047.
82. Hunziker, W., and Geuze, H.J. (1996). Intracellular trafficking of lysosomal membrane proteins. BioEssays *18*, 379–389. https://doi.org/10.1002/bies.950180508.
83. Kundra, R., and Kornfeld, S. (1999). Asparagine-linked Oligosaccharides Protect Lamp-1 and Lamp-2 from Intracellular Proteolysis. J. Biol. Chem. *274*, 31039–31046. https://doi.org/10.1074/jbc.274.43.31039.
84. Lewis, V., Green, S.A., Marsh, M., Vihko, P., Helenius, Ari, and Mellman, Ira (1985). Glycoproteins of the lysosomal membrane. J. Cell Biol. *100*, 1839–1847.
85. Ishidoh, K., and Kominami, E. (2002). Processing and Activation of Lysosomal Proteinases. Biol. Chem. *383*, 1827–1831. https://doi.org/10.1515/BC.2002.206.

86. Feng, X., Liu, S., and Xu, H. (2023). Not just protons: Chloride also activates lysosomal acidic hydrolases. J. Cell Biol. *222*, e202305007. https://doi.org/10.1083/jcb.202305007.
87. Hirst, J., Futter, C.E., and Hopkins, C.R. (1998). The Kinetics of Mannose 6-Phosphate Receptor Trafficking in the Endocytic Pathway in HEp-2 Cells: The Receptor Enters and Rapidly Leaves Multivesicular Endosomes without Accumulating in a Prelysosomal Compartment. Mol. Biol. Cell *9*, 809–816.
88. Bright, N.A., Gratian, M.J., and Luzio, J.P. (2005). Endocytic Delivery to Lysosomes Mediated by Concurrent Fusion and Kissing Events in Living Cells. Curr. Biol. *15*, 360–365. https://doi.org/10.1016/j.cub.2005.01.049.
89. Bright, N.A., Davis, L.J., and Luzio, J.P. (2016). Endolysosomes Are the Principal Intracellular Sites of Acid Hydrolase Activity. Curr. Biol. *26*, 2233–2245. https://doi.org/10.1016/j.cub.2016.06.046.
90. Mullock, B.M., Bright, N.A., Fearon, C.W., Gray, S.R., and Luzio, J. (1998). Fusion of Lysosomes with Late Endosomes Produces a Hybrid Organelle of Intermediate Density and Is NSF Dependent. J. Cell Biol. *140*, 591–601. https://doi.org/10.1083/jcb.140.3.591.
91. Repnik, U., Česen, M.H., and Turk, B. (2013). The Endolysosomal System in Cell Death and Survival. Cold Spring Harb. Perspect. Biol. *5*, a008755. https://doi.org/10.1101/cshperspect.a008755.
92. Griffiths, G., Matteoni, R., Back, R., and Hoflack, B. (1990). Characterization of the cation-independent mannose 6-phosphate receptor-enriched prelysosomal compartment in NRK cells. J. Cell Sci. *95*, 441–461. https://doi.org/10.1242/jcs.95.3.441.
93. Bissig, C., Hurbain, I., Raposo, G., and van Niel, G. (2017). PIKfyve activity regulates reformation of terminal storage lysosomes from endolysosomes. Traffic *18*, 747–757. https://doi.org/10.1111/tra.12525.
94. Wandinger-Ness, A., and Zerial, M. (2014). Rab Proteins and the Compartmentalization of the Endosomal System. Cold Spring Harb. Perspect. Biol. *6*, a022616. https://doi.org/10.1101/cshperspect.a022616.
95. Colicelli, J. (2004). Human RAS Superfamily Proteins and Related GTPases. Sci. STKE Signal Transduct. Knowl. Environ. *2004*, RE13. https://doi.org/10.1126/stke.2502004re13.
96. Corbeel, L., and Freson, K. (2008). Rab proteins and Rab-associated proteins: major actors in the mechanism of protein-trafficking disorders. Eur. J. Pediatr. *167*, 723–729. https://doi.org/10.1007/s00431-008-0740-z.
97. Diekmann, Y., Seixas, E., Gouw, M., Tavares-Cadete, F., Seabra, M.C., and Pereira-Leal, J.B. (2011). Thousands of Rab GTPases for the Cell Biologist. PLoS Comput. Biol. *7*, e1002217. https://doi.org/10.1371/journal.pcbi.1002217.
98. Christoforidis, S., McBride, H.M., Burgoyne, R.D., and Zerial, M. (1999). The Rab5 effector EEA1 is a core component of endosome docking. Nature *397*, 621–625. https://doi.org/10.1038/17618.
99. Jongsma, M.L., Bakker, J., Cabukusta, B., Liv, N., van Elsland, D., Fermie, J., Akkermans, J.L., Kuijl, C., van der Zanden, S.Y., Janssen, L., et al. (2020). SKIP-HOPS recruits TBC1D15 for a Rab7-to-Arl8b identity switch to control late endosome transport. EMBO J. *39*. https://doi.org/10.15252/embj.2019102301.
100. Khatter, D., Sindhwani, A., and Sharma, M. (2015). Arf-like GTPase Arl8: Moving from the periphery to the center of lysosomal biology. Cell. Logist. *5*. https://doi.org/10.1080/21592799.2015.1086501.
101. Poteryaev, D., Datta, S., Ackema, K., Zerial, M., and Spang, A. (2010). Identification of the Switch in Early-to-Late Endosome Transition. Cell *141*, 497–508. https://doi.org/10.1016/j.cell.2010.03.011.
102. Cherfils, J., and Zeghouf, M. (2013). Regulation of Small GTPases by GEFs, GAPs, and GDIs. Physiol. Rev. *93*, 269–309. https://doi.org/10.1152/physrev.00003.2012.
103. Ungermann, C., and Kümmel, D. (2019). Structure of membrane tethers and their role in fusion. Traffic *20*, 479–490. https://doi.org/10.1111/tra.12655.
104. Baker, R.W., Jeffrey, P.D., Zick, M., Phillips, B.P., Wickner, W.T., and Hughson, F.M. (2015). A direct role for the Sec1-Munc18-family protein Vps33 as a template for SNARE assembly. Science *349*, 1111–1114. https://doi.org/10.1126/science.aac7906.

105. Balderhaar, H.J. k., and Ungermann, C. (2013). CORVET and HOPS tethering complexes - coordinators of endosome and lysosome fusion. J. Cell Sci. *126*, 1307–1316. https://doi.org/10.1242/jcs.107805.
106. Wartosch, L., Günesdogan, U., Graham, S.C., and Luzio, J.P. (2015). Recruitment of VPS33A to HOPS by VPS16 Is Required for Lysosome Fusion with Endosomes and Autophagosomes. Traffic Cph. Den. *16*, 727–742. https://doi.org/10.1111/tra.12283.
107. Weber, T., Zemelman, B.V., McNew, J.A., Westermann, B., Gmachl, M., Parlati, F., Söllner, T.H., and Rothman, J.E. (1998). SNAREpins: Minimal Machinery for Membrane Fusion. Cell *92*, 759–772. https://doi.org/10.1016/S0092-8674(00)81404-X.
108. Wickner, W., and Schekman, R. (2008). Membrane fusion. Nat. Struct. Mol. Biol. *15*, 658–664.
109. Harrison, S.C. (2015). Viral membrane fusion. Virology *0*, 498–507. https://doi.org/10.1016/j.virol.2015.03.043.
110. Moss, T.J., Andreazza, C., Verma, A., Daga, A., and McNew, J.A. (2011). Membrane fusion by the GTPase atlastin requires a conserved C-terminal cytoplasmic tail and dimerization through the middle domain. Proc. Natl. Acad. Sci. *108*, 11133–11138. https://doi.org/10.1073/pnas.1105056108.
111. Gerst, J.E. (2003). SNARE regulators: matchmakers and matchbreakers. Biochim. Biophys. Acta BBA - Mol. Cell Res. *1641*, 99–110. https://doi.org/10.1016/S0167-4889(03)00096-X.
112. Schwartz, M.L., Nickerson, D.P., Lobingier, B.T., Plemel, R.L., Duan, M., Angers, C.G., Zick, M., and Merz, A.J. (2017). Sec17 (α-SNAP) and an SM-tethering complex regulate the outcome of SNARE zippering in vitro and in vivo. eLife *6*, e27396. https://doi.org/10.7554/eLife.27396.
113. Whiteheart, S.W., Rossnagel, K., Buhrow, S.A., Brunner, M., Jaenicke, R., and Rothman, J.E. (1994). N-ethylmaleimide-sensitive fusion protein: a trimeric ATPase whose hydrolysis of ATP is required for membrane fusion. J. Cell Biol. *126*, 945–954. https://doi.org/10.1083/jcb.126.4.945.
114. Zick, M., Orr, A., Schwartz, M.L., Merz, A.J., and Wickner, W.T. (2015). Sec17 can trigger fusion of *trans* -SNARE paired membranes without Sec18. Proc. Natl. Acad. Sci. *112*, E2290–E2297. https://doi.org/10.1073/pnas.1506409112.
115. Fasshauer, D., Sutton, R.B., Brunger, A.T., and Jahn, R. (1998). Conserved structural features of the synaptic fusion complex: SNARE proteins reclassified as Q- and R-SNAREs. Proc. Natl. Acad. Sci. U. S. A. *95*, 15781–15786.
116. Sutton, R.B., Fasshauer, D., Jahn, R., and Brunger, A.T. (1998). Crystal structure of a SNARE complex involved in synaptic exocytosis at 2.4 Å resolution. Nature *395*, 347–353. https://doi.org/10.1038/26412.
117. Hong, W. (2005). SNAREs and traffic. Biochim. Biophys. Acta BBA - Mol. Cell Res. *1744*, 120–144. https://doi.org/10.1016/j.bbamcr.2005.03.014.
118. Parlati, F., McNew, J.A., Fukuda, R., Miller, R., Söllner, T.H., and Rothman, J.E. (2000). Topological restriction of SNARE-dependent membrane fusion. Nature *407*, 194–198. https://doi.org/10.1038/35025076.
119. Südhof, T.C., and Rothman, J.E. (2009). Membrane Fusion: Grappling with SNARE and SM Proteins. Science *323*, 474–477. https://doi.org/10.1126/science.1161748.
120. Cheever, M.L., Sato, T.K., De Beer, T., Kutateladze, T.G., Emr, S.D., and Overduin, M. (2001). Phox domain interaction with PtdIns(3)P targets the Vam7 t-SNARE to vacuole membranes. Nat. Cell Biol. *3*, 613–618. https://doi.org/10.1038/35083000.
121. Han, J., Pluhackova, K., and Böckmann, R.A. (2017). The Multifaceted Role of SNARE Proteins in Membrane Fusion. Front. Physiol. *8*, 5. https://doi.org/10.3389/fphys.2017.00005.
122. Mascia, L., and Langosch, D. (2007). Evidence that late-endosomal SNARE multimerization complex is promoted by transmembrane segments. Biochim. Biophys. Acta BBA - Biomembr. *1768*, 457–466. https://doi.org/10.1016/j.bbamem.2006.12.008.
123. Ungermann, C., and Langosch, D. (2005). Functions of SNAREs in intracellular membrane fusion and lipid bilayer mixing. J. Cell Sci. *118*, 3819–3828. https://doi.org/10.1242/jcs.02561.
124. Wehland, J.-D., Lygina, A.S., Kumar, P., Guha, S., Hubrich, B.E., Jahn, R., and Diederichsen, U. (2016). Role of the transmembrane domain in SNARE protein mediated membrane fusion: peptide nucleic acid/peptide model systems. Mol. Biosyst. *12*, 2770–2776. https://doi.org/10.1039/C6MB00294C.

125. Dietrich, L.E.P., Boeddinghaus, C., LaGrassa, T.J., and Ungermann, C. (2003). Control of eukaryotic membrane fusion by N-terminal domains of SNARE proteins. Biochim. Biophys. Acta BBA - Mol. Cell Res. *1641*, 111–119. https://doi.org/10.1016/S0167-4889(03)00094-6.
126. Vivona, S., Liu, C.W., Strop, P., Rossi, V., Filippini, F., and Brunger, A.T. (2010). The Longin SNARE VAMP7/TI-VAMP Adopts a Closed Conformation. J. Biol. Chem. *285*, 17965–17973. https://doi.org/10.1074/jbc.M110.120972.
127. Baker, R.W., and Hughson, F.M. (2016). Chaperoning SNARE assembly and disassembly. Nat. Rev. Mol. Cell Biol. *17*, 465–479. https://doi.org/10.1038/nrm.2016.65.
128. Mima, J., and Wickner, W. (2009). Complex Lipid Requirements for SNARE- and SNARE Chaperone-dependent Membrane Fusion. J. Biol. Chem. *284*, 27114–27122. https://doi.org/10.1074/jbc.M109.010223.
129. Zick, M., Stroupe, C., Orr, A., Douville, D., and Wickner, W.T. (2014). Membranes linked by trans-SNARE complexes require lipids prone to non-bilayer structure for progression to fusion. eLife *3*, e01879. https://doi.org/10.7554/eLife.01879.
130. Lou, X., and Shin, Y.-K. (2016). SNARE zippering. Biosci. Rep. *36*, e00327. https://doi.org/10.1042/BSR20160004.
131. Deak, F., Shin, O.-H., Kavalali, E.T., and Sudhof, T.C. (2006). Structural Determinants of Synaptobrevin 2 Function in Synaptic Vesicle Fusion. J. Neurosci. *26*, 6668–6676. https://doi.org/10.1523/JNEUROSCI.5272-05.2006.
132. McNew, J.A., Weber, T., Parlati, F., Johnston, R.J., Melia, T.J., Söllner, T.H., and Rothman, J.E. (2000). Close Is Not Enough. J. Cell Biol. *150*, 105–118.
133. Rand, R.P., and Parsegian, V.A. (1984). Physical force considerations in model and biological membranes. Can. J. Biochem. Cell Biol. *62*, 752–759. https://doi.org/10.1139/o84-097.
134. Leikin, S., Parsegian, V.A., Yang, W.-H., and Walrafen, G.E. (1997). Raman spectral evidence for hydration forces between collagen triple helices. Proc. Natl. Acad. Sci. *94*, 11312–11317. https://doi.org/10.1073/pnas.94.21.11312.
135. Risselada, H.J., and Grubmüller, H. (2021). How proteins open fusion pores: insights from molecular simulations. Eur. Biophys. J. *50*, 279–293. https://doi.org/10.1007/s00249-020-01484-3.
136. Cohen, F.S., and Melikyan, G.B. (2004). The Energetics of Membrane Fusion from Binding, through Hemifusion, Pore Formation, and Pore Enlargement. J. Membr. Biol. *199*, 1–14. https://doi.org/10.1007/s00232-004-0669-8.
137. Chernomordik, L.V., Zimmerberg, J., and Kozlov, M.M. (2006). Membranes of the world unite! J. Cell Biol. *175*, 201–207. https://doi.org/10.1083/jcb.200607083.
138. Fang, Q., and Lindau, M. (2014). How Could SNARE Proteins Open a Fusion Pore? Physiology *29*, 278–285. https://doi.org/10.1152/physiol.00026.2013.
139. van den Bogaart, G., Holt, M.G., Bunt, G., Riedel, D., Wouters, F.S., and Jahn, R. (2010). One SNARE complex is sufficient for membrane fusion. Nat. Struct. Mol. Biol. *17*, 358–364. https://doi.org/10.1038/nsmb.1748.
140. Block, M.R., Glick, B.S., Wilcox, C.A., Wieland, F.T., and Rothman, J.E. (1988). Purification of an N-ethylmaleimide-sensitive protein catalyzing vesicular transport. Proc. Natl. Acad. Sci. U. S. A. *85*, 7852–7856.
141. Clary, D.O., Griff, I.C., and Rothman, J.E. (1990). SNAPs, a family of NSF attachment proteins involved in intracellular membrane fusion in animals and yeast. Cell *61*, 709–721. https://doi.org/10.1016/0092-8674(90)90482-T.
142. Kitano, M., Nakaya, M., Nakamura, T., Nagata, S., and Matsuda, M. (2008). Imaging of Rab5 activity identifies essential regulators for phagosome maturation. Nature *453*, 241–245. https://doi.org/10.1038/nature06857.
143. Lippé, R., Miaczynska, M., Rybin, V., Runge, A., and Zerial, M. (2001). Functional Synergy between Rab5 Effector Rabaptin-5 and Exchange Factor Rabex-5 When Physically Associated in a Complex. Mol. Biol. Cell *12*, 2219–2228.
144. Kälin, S., Hirschmann, D.T., Buser, D.P., and Spiess, M. (2015). Rabaptin5 is recruited to endosomes by Rab4 and Rabex5 to regulate endosome maturation. J. Cell Sci., jcs.174664. https://doi.org/10.1242/jcs.174664.

145. Zhu, H., Liang, Z., and Li, G. (2009). Rabex-5 Is a Rab22 Effector and Mediates a Rab22-Rab5 Signaling Cascade in Endocytosis. Mol. Biol. Cell *20*, 4720–4729. https://doi.org/10.1091/mbc.E09-06-0453.
146. Vieira, O.V., Botelho, R.J., Rameh, L., Brachmann, S.M., Matsuo, T., Davidson, H.W., Schreiber, A., Backer, J.M., Cantley, L.C., and Grinstein, S. (2001). Distinct roles of class I and class III phosphatidylinositol 3-kinases in phagosome formation and maturation. J. Cell Biol. *155*, 19–26. https://doi.org/10.1083/jcb.200107069.
147. Callaghan, J., Nixon, S., Bucci, C., Toh, B.-H., and Stenmark, H. (1999). Direct interaction of EEA1 with Rab5b. Eur. J. Biochem. *265*, 361–366. https://doi.org/10.1046/j.1432-1327.1999.00743.x.
148. Simonsen, A., Lippe, R., Christoforidis, S., Gaullier, J.-M., Brech, A., Callaghan, J., Toh, B.-H., Murphy, C., Zerial, M., and Stenmark, H. (1998). EEA1 links PI(3)K function to Rab5 regulation of endosome fusion. Nature *394*, 494–498. https://doi.org/10.1038/28879.
149. Mu, F.-T., Callaghan, J.M., Steele-Mortimer, O., Stenmark, H., Parton, R.G., Campbell, P.L., McCluskey, J., Yeo, J.-P., Tock, E.P.C., and Toh, B.-H. (1995). EEA1, an Early Endosome-Associated Protein. EEA1 IS A CONSERVED α-HELICAL PERIPHERAL MEMBRANE PROTEIN FLANKED BY CYSTEINE "FINGERS" AND CONTAINS A CALMODULIN-BINDING IQ MOTIF. J. Biol. Chem. *270*, 13503–13511. https://doi.org/10.1074/jbc.270.22.13503.
150. Wilson, J.M., de Hoop, M., Zorzi, N., Toh, B.-H., Dotti, C.G., and Parton, R.G. (2000). EEA1, a Tethering Protein of the Early Sorting Endosome, Shows a Polarized Distribution in Hippocampal Neurons, Epithelial Cells, and Fibroblasts. Mol. Biol. Cell *11*, 2657–2671.
151. Solinger, J.A., and Spang, A. (2013). Tethering complexes in the endocytic pathway: CORVET and HOPS. FEBS J. *280*, 2743–2757. https://doi.org/10.1111/febs.12151.
152. van der Beek, J., Jonker, C., van der Welle, R., Liv, N., and Klumperman, J. (2019). CORVET, CHEVI and HOPS – multisubunit tethers of the endo-lysosomal system in health and disease. J. Cell Sci. *132*, jcs189134. https://doi.org/10.1242/jcs.189134.
153. Rink, J., Ghigo, E., Kalaidzidis, Y., and Zerial, M. (2005). Rab Conversion as a Mechanism of Progression from Early to Late Endosomes. Cell *122*, 735–749. https://doi.org/10.1016/j.cell.2005.06.043.
154. Vanlandingham, P.A., and Ceresa, B.P. (2009). Rab7 Regulates Late Endocytic Trafficking Downstream of Multivesicular Body Biogenesis and Cargo Sequestration. J. Biol. Chem. *284*, 12110–12124. https://doi.org/10.1074/jbc.M809277200.
155. Nordmann, M., Cabrera, M., Perz, A., Bröcker, C., Ostrowicz, C., Engelbrecht-Vandré, S., and Ungermann, C. (2010). The Mon1-Ccz1 Complex Is the GEF of the Late Endosomal Rab7 Homolog Ypt7. Curr. Biol. *20*, 1654–1659. https://doi.org/10.1016/j.cub.2010.08.002.
156. Progida, C., Cogli, L., Piro, F., De Luca, A., Bakke, O., and Bucci, C. (2010). Rab7b controls trafficking from endosomes to the TGN. J. Cell Sci. *123*, 1480–1491. https://doi.org/10.1242/jcs.051474.
157. Yang, M., Chen, T., Han, C., Li, N., Wan, T., and Cao, X. (2004). Rab7b, a novel lysosome-associated small GTPase, is involved in monocytic differentiation of human acute promyelocytic leukemia cells. Biochem. Biophys. Res. Commun. *318*, 792–799. https://doi.org/10.1016/j.bbrc.2004.04.115.
158. Johansson, M., Rocha, N., Zwart, W., Jordens, I., Janssen, L., Kuijl, C., Olkkonen, V.M., and Neefjes, J. (2007). Activation of endosomal dynein motors by stepwise assembly of Rab7–RILP–p150Glued, ORP1L, and the receptor βlll spectrin. J. Cell Biol. *176*, 459–471. https://doi.org/10.1083/jcb.200606077.
159. Zhang, M., Chen, L., Wang, S., and Wang, T. (2009). Rab7: roles in membrane trafficking and disease.
160. Humphries, W.H., Szymanski, C.J., and Payne, C.K. (2011). Endo-Lysosomal Vesicles Positive for Rab7 and LAMP1 Are Terminal Vesicles for the Transport of Dextran. PLoS ONE *6*, e26626. https://doi.org/10.1371/journal.pone.0026626.
161. Wang, T., Ming, Z., Xiaochun, W., and Hong, W. (2011). Rab7: Role of its protein interaction cascades in endo-lysosomal traffic. Cell. Signal. *23*, 516–521. https://doi.org/10.1016/j.cellsig.2010.09.012.

162. Kahn, R.A., Cherfils, J., Elias, M., Lovering, R.C., Munro, S., and Schurmann, A. (2006). Nomenclature for the human Arf family of GTP-binding proteins: ARF, ARL, and SAR proteins. J. Cell Biol. *172*, 645–650. https://doi.org/10.1083/jcb.200512057.
163. Keren-Kaplan, T., and Bonifacino, J.S. (2021). ARL8 Relieves SKIP Autoinhibition to Enable Coupling of Lysosomes to Kinesin-1. Curr. Biol. CB *31*, 540-554.e5. https://doi.org/10.1016/j.cub.2020.10.071.
164. Li, Y., Kelly, W.G., Logsdon Jr., J.M., Schurko, A.M., Harfe, B.D., Hill-Harfe, K.L., and Kahn, R.A. (2004). Functional genomic analysis of the ADP-ribosylation factor family of GTPases: phylogeny among diverse eukaryotes and function in C. elegans. FASEB J. *18*, 1834–1850. https://doi.org/10.1096/fj.04-2273com.
165. Nakae, I., Fujino, T., Kobayashi, T., Sasaki, A., Kikko, Y., Fukuyama, M., Gengyo-Ando, K., Mitani, S., Kontani, K., and Katada, T. (2010). The Arf-like GTPase Arl8 Mediates Delivery of Endocytosed Macromolecules to Lysosomes in Caenorhabditis elegans. Mol. Biol. Cell *21*, 2434–2442. https://doi.org/10.1091/mbc.E09-12-1010.
166. Hofmann, I., and Munro, S. (2006). An N-terminally acetylated Arf-like GTPase is localised to lysosomes and affects their motility. J. Cell Sci. *119*, 1494–1503. https://doi.org/10.1242/jcs.02958.
167. Ma, X., Liu, K., Li, J., Li, H., Li, J., Liu, Y., Yang, C., and Liang, H. (2018). A non-canonical GTPase interaction enables ORP1L-Rab7-RILP complex formation and late endosome positioning. J. Biol. Chem. *293*, 14155–14164. https://doi.org/10.1074/jbc.RA118.001854.
168. Jongsma, M.L.M., Berlin, I., Wijdeven, R.H.M., Janssen, L., Janssen, G.M.C., Garstka, M.A., Janssen, H., Mensink, M., van Veelen, P.A., Spaapen, R.M., et al. (2016). An ER-Associated Pathway Defines Endosomal Architecture for Controlled Cargo Transport. Cell *166*, 152–166. https://doi.org/10.1016/j.cell.2016.05.078.
169. Pu, J., Schindler, C., Jia, R., Jarnik, M., Backlund, P., and Bonifacino, J.S. (2015). BORC, a Multisubunit Complex that Regulates Lysosome Positioning. Dev. Cell *33*, 176–188. https://doi.org/10.1016/j.devcel.2015.02.011.
170. Rosa-Ferreira, C., and Munro, S. (2011). Arl8 and SKIP Act Together to Link Lysosomes to Kinesin-1. Dev. Cell *21*, 1171–1178. https://doi.org/10.1016/j.devcel.2011.10.007.
171. Kim, B.Y., Ueda, M., Kominami, E., Akagawa, K., Kohsaka, S., and Akazawa, C. (2003). Identification of mouse Vps16 and biochemical characterization of mammalian Class C Vps complex. Biochem. Biophys. Res. Commun. *311*, 577–582. https://doi.org/10.1016/j.bbrc.2003.10.030.
172. Kim, B.Y., Krämer, H., Yamamoto, A., Kominami, E., Kohsaka, S., and Akazawa, C. (2001). Molecular Characterization of Mammalian Homologues of Class C Vps Proteins That Interact with Syntaxin-7. J. Biol. Chem. *276*, 29393–29402. https://doi.org/10.1074/jbc.M101778200.
173. Pirooz, S.D., He, S., Zhang, T., Zhang, X., Zhao, Z., Oh, S., O'Connell, D., Khalilzadeh, P., Amini-Bavil-Olyaee, S., Farzan, M., et al. (2014). UVRAG is required for virus entry through combinatorial interaction with the class C-Vps complex and SNAREs. Proc. Natl. Acad. Sci. U. S. A. *111*, 2716–2721. https://doi.org/10.1073/pnas.1320629111.
174. Graham, S.C., Wartosch, L., Gray, S.R., Scourfield, E.J., Deane, J.E., Luzio, J.P., and Owen, D.J. (2013). Structural basis of Vps33A recruitment to the human HOPS complex by Vps16. Proc. Natl. Acad. Sci. U. S. A. *110*, 13345–13350. https://doi.org/10.1073/pnas.1307074110.
175. Kuhlee, A., Raunser, S., and Ungermann, C. (2015). Functional homologies in vesicle tethering. FEBS Lett. *589*, 2487–2497. https://doi.org/10.1016/j.febslet.2015.06.001.
176. Brett, C.L., Plemel, R.L., Lobinger, B.T., Vignali, M., Fields, S., and Merz, A.J. (2008). Efficient termination of vacuolar Rab GTPase signaling requires coordinated action by a GAP and a protein kinase. J. Cell Biol. *182*, 1141–1151. https://doi.org/10.1083/jcb.200801001.
177. Ostrowicz, C.W., Bröcker, C., Ahnert, F., Nordmann, M., Lachmann, J., Peplowska, K., Perz, A., Auffarth, K., Engelbrecht-Vandré, S., and Ungermann, C. (2010). Defined Subunit Arrangement and Rab Interactions Are Required for Functionality of the HOPS Tethering Complex. Traffic *11*, 1334–1346. https://doi.org/10.1111/j.1600-0854.2010.01097.x.
178. Wurmser, A.E., Sato, T.K., and Emr, S.D. (2000). New Component of the Vacuolar Class C-Vps Complex Couples Nucleotide Exchange on the Ypt7 Gtpase to Snare-Dependent Docking and Fusion. J. Cell Biol. *151*, 551–562.

179. Lin, X., Yang, T., Wang, S., Wang, Z., Yun, Y., Sun, L., Zhou, Y., Xu, X., Akazawa, C., Hong, W., et al. (2015). RILP interacts with HOPS complex via VPS41 subunit to regulate endocytic trafficking. Sci. Rep. *4*, 7282. https://doi.org/10.1038/srep07282.
180. van der Kant, R., Jonker, C.T.H., Wijdeven, R.H., Bakker, J., Janssen, L., Klumperman, J., and Neefjes, J. (2015). Characterization of the Mammalian CORVET and HOPS Complexes and Their Modular Restructuring for Endosome Specificity. J. Biol. Chem. *290*, 30280–30290. https://doi.org/10.1074/jbc.M115.688440.
181. Garg, S., Sharma, M., Ung, C., Tuli, A., Barral, D.C., Hava, D.L., Veerapen, N., Besra, G.S., Hacohen, N., and Brenner, M.B. (2011). Lysosomal Trafficking, Antigen Presentation, and Microbial Killing Are Controlled by the Arf-like GTPase Arl8b. Immunity *35*, 182–193. https://doi.org/10.1016/j.immuni.2011.06.009.
182. Khatter, D., Raina, V.B., Dwivedi, D., Sindhwani, A., Bahl, S., and Sharma, M. (2015). The small GTPase Arl8b regulates assembly of the mammalian HOPS complex on lysosomes. J. Cell Sci. *128*, 1746–1761. https://doi.org/10.1242/jcs.162651.
183. Marwaha, R., Arya, S.B., Jagga, D., Kaur, H., Tuli, A., and Sharma, M. (2017). The Rab7 effector PLEKHM1 binds Arl8b to promote cargo traffic to lysosomes. J. Cell Biol. *216*, 1051–1070. https://doi.org/10.1083/jcb.201607085.
184. McEwan, D.G., Popovic, D., Gubas, A., Terawaki, S., Suzuki, H., Stadel, D., Coxon, F.P., Miranda de Stegmann, D., Bhogaraju, S., Maddi, K., et al. (2015). PLEKHM1 Regulates Autophagosome-Lysosome Fusion through HOPS Complex and LC3/GABARAP Proteins. Mol. Cell *57*, 39–54. https://doi.org/10.1016/j.molcel.2014.11.006.
185. Rawet-Slobodkin, M., and Elazar, Z. (2015). PLEKHM1: A Multiprotein Adaptor for the Endolysosomal System. Mol. Cell *57*, 1–3. https://doi.org/10.1016/j.molcel.2014.12.022.
186. Wijdeven, R.H., Janssen, H., Nahidiazar, L., Janssen, L., Jalink, K., Berlin, I., and Neefjes, J. (2016). Cholesterol and ORP1L-mediated ER contact sites control autophagosome transport and fusion with the endocytic pathway. Nat. Commun. *7*, 11808. https://doi.org/10.1038/ncomms11808.
187. Jia, R., Guardia, C.M., Pu, J., Chen, Y., and Bonifacino, J.S. (2017). BORC coordinates encounter and fusion of lysosomes with autophagosomes. Autophagy *13*, 1648–1663. https://doi.org/10.1080/15548627.2017.1343768.
188. Filipek, P.A., de Araujo, M.E.G., Vogel, G.F., De Smet, C.H., Eberharter, D., Rebsamen, M., Rudashevskaya, E.L., Kremser, L., Yordanov, T., Tschaikner, P., et al. (2017). LAMTOR/Ragulator is a negative regulator of Arl8b- and BORC-dependent late endosomal positioning. J. Cell Biol. *216*, 4199–4215. https://doi.org/10.1083/jcb.201703061.
189. Guardia, C.M., Farías, G.G., Jia, R., Pu, J., and Bonifacino, J.S. (2016). BORC Functions Upstream of Kinesins 1 and 3 to Coordinate Regional Movement of Lysosomes Along Different Microtubule Tracks. Cell Rep. *17*, 1950–1961. https://doi.org/10.1016/j.celrep.2016.10.062.
190. Collins, K.M., and Wickner, W.T. (2007). trans-SNARE complex assembly and yeast vacuole membrane fusion. Proc. Natl. Acad. Sci. *104*, 8755–8760. https://doi.org/10.1073/pnas.0702290104.
191. Krämer, L., and Ungermann, C. (2011). HOPS drives vacuole fusion by binding the vacuolar SNARE complex and the Vam7 PX domain via two distinct sites. Mol. Biol. Cell *22*, 2601–2611. https://doi.org/10.1091/mbc.e11-02-0104.
192. Starai, V.J., Hickey, C.M., and Wickner, W. (2008). HOPS Proofreads the trans-SNARE Complex for Yeast Vacuole Fusion. Mol. Biol. Cell *19*, 2500–2508. https://doi.org/10.1091/mbc.E08-01-0077.
193. Stroupe, C., Collins, K.M., Fratti, R.A., and Wickner, W. (2006). Purification of active HOPS complex reveals its affinities for phosphoinositides and the SNARE Vam7p. EMBO J. *25*, 1579–1589. https://doi.org/10.1038/sj.emboj.7601051.
194. Fujita, N., Huang, W., Lin, T., Groulx, J.-F., Jean, S., Nguyen, J., Kuchitsu, Y., Koyama-Honda, I., Mizushima, N., Fukuda, M., et al. (2017). Genetic screen in Drosophila muscle identifies autophagy-mediated T-tubule remodeling and a Rab2 role in autophagy. eLife *6*, e23367. https://doi.org/10.7554/eLife.23367.
195. Christensen, K.A., Myers, J.T., and Swanson, J.A. (2002). pH-dependent regulation of lysosomal calcium in macrophages. J. Cell Sci. *115*, 599–607. https://doi.org/10.1242/jcs.115.3.599.

196. Nunes, P., and Demaurex, N. (2010). The role of calcium signaling in phagocytosis. J. Leukoc. Biol. *88*, 57–68. https://doi.org/10.1189/jlb.0110028.
197. Cheng, X., Zhang, X., Yu, L., and Xu, H. (2015). Calcium signaling in membrane repair. Semin. Cell Dev. Biol. *45*, 24–31. https://doi.org/10.1016/j.semcdb.2015.10.031.
198. Endo, M. (2006). Calcium Ion as a Second Messenger With Special Reference to Excitation-Contraction Coupling. J. Pharmacol. Sci. *100*, 519–524. https://doi.org/10.1254/jphs.CPJ06004X.
199. Groenendyk, J., Agellon, L.B., and Michalak, M. (2021). Calcium signaling and endoplasmic reticulum stress. Int. Rev. Cell Mol. Biol. Acad. Press *Volume 363*, pages 1-20. https://doi.org/10.1016/bs.ircmb.2021.03.003.
200. Hay, J.C. (2007). Calcium: a fundamental regulator of intracellular membrane fusion? EMBO Rep. *8*, 236–240. https://doi.org/10.1038/sj.embor.7400921.
201. Li, Z., and Shaw, G.S. (2023). Role of calcium-sensor proteins in cell membrane repair. Biosci. Rep. *43*, BSR20220765. https://doi.org/10.1042/BSR20220765.
202. Südhof, T.C. (2012). Calcium Control of Neurotransmitter Release. Cold Spring Harb. Perspect. Biol. *4*, a011353. https://doi.org/10.1101/cshperspect.a011353.
203. Westman, J., Grinstein, S., and Maxson, M. (2019). Revisiting the role of calcium in phagosome formation and maturation. J. Leukoc. Biol. https://doi.org/10.1002/JLB.MR1118-444R.
204. Bagur, R., and Hajnóczky, G. (2017). Intracellular Ca2+ sensing: role in calcium homeostasis and signaling. Mol. Cell *66*, 780–788. https://doi.org/10.1016/j.molcel.2017.05.028.
205. Parekh, A.B., and Putney, J.W. (2005). Store-Operated Calcium Channels. Physiol. Rev. *85*, 757–810. https://doi.org/10.1152/physrev.00057.2003.
206. Brini, M., and Carafoli, E. (2011). The Plasma Membrane Ca2+ ATPase and the Plasma Membrane Sodium Calcium Exchanger Cooperate in the Regulation of Cell Calcium. Cold Spring Harb. Perspect. Biol. *3*, a004168. https://doi.org/10.1101/cshperspect.a004168.
207. Grimm, C., Hassan, S., Wahl-Schott, C., and Biel, M. (2012). Role of TRPML and Two-Pore Channels in Endolysosomal Cation Homeostasis. J. Pharmacol. Exp. Ther. *342*, 236–244. https://doi.org/10.1124/jpet.112.192880.
208. Morgan, A.J., Davis, L.C., and Galione, A. (2021). Choreographing endo-lysosomal Ca2+ throughout the life of a phagosome. Biochim. Biophys. Acta BBA - Mol. Cell Res. *1868*, 119040. https://doi.org/10.1016/j.bbamcr.2021.119040.
209. Ogunbayo, O.A., Zhu, Y., Shen, B., Agbani, E., Li, J., Ma, J., Zhu, M.X., and Evans, A.M. (2015). Organelle-specific Subunit Interactions of the Vertebrate Two-pore Channel Family. J. Biol. Chem. *290*, 1086–1095. https://doi.org/10.1074/jbc.M114.610493.
210. Grabmayr, H., Romanin, C., and Fahrner, M. (2020). STIM Proteins: An Ever-Expanding Family. Int. J. Mol. Sci. *22*, 378. https://doi.org/10.3390/ijms22010378.
211. Nwokonko, R.M., Cai, X., Loktionova, N.A., Wang, Y., Zhou, Y., and Gill, D.L. (2017). The STIM-Orai Pathway: Conformational Coupling Between STIM and Orai in the Activation of Store-Operated Ca2+ Entry. Adv. Exp. Med. Biol. *993*, 83–98. https://doi.org/10.1007/978-3-319-57732-6_5.
212. Soboloff, J., Rothberg, B.S., Madesh, M., and Gill, D.L. (2012). STIM proteins: dynamic calcium signal transducers. Nat. Rev. Mol. Cell Biol. *13*, 549–565. https://doi.org/10.1038/nrm3414.
213. Patel, S., and Docampo, R. (2010). Acidic calcium stores open for business: expanding the potential for intracellular Ca2+ signaling. Trends Cell Biol. *20*, 277–286. https://doi.org/10.1016/j.tcb.2010.02.003.
214. Becker, S.M., Delamarre, L., Mellman, I., and Andrews, N.W. (2009). Differential role of the Ca2+ sensor synaptotagmin VII in macrophages and dendritic cells. Immunobiology *214*, 495–505. https://doi.org/10.1016/j.imbio.2008.11.006.
215. Lundqvist-Gustafsson, H., Gustafsson, M., and Dahlgren, C. (2000). Dynamic Ca2+changes in neutrophil phagosomes A source for intracellular Ca2+during phagolysosome formation? Cell Calcium *27*, 353–362. https://doi.org/10.1054/ceca.2000.0130.
216. Nunes-Hasler, P., Maschalidi, S., Lippens, C., Castelbou, C., Bouvet, S., Guido, D., Bermont, F., Bassoy, E.Y., Page, N., Merkler, D., et al. (2017). STIM1 promotes migration, phagosomal maturation and antigen cross-presentation in dendritic cells. Nat. Commun. *8*, 1852. https://doi.org/10.1038/s41467-017-01600-6.

217. Sawyer, D.W., Sullivan, J.A., and Mandell, G.L. (1985). Intracellular Free Calcium Localization in Neutrophils During Phagocytosis. Science *230*, 663–666. https://doi.org/10.1126/science.4048951.
218. Gerasimenko, J.V., Tepikin, A.V., Petersen, O.H., and Gerasimenko, O.V. (1998). Calcium uptake via endocytosis with rapid release from acidifying endosomes. Curr. Biol. *8*, 1335–1338. https://doi.org/10.1016/S0960-9822(07)00565-9.
219. Nunes, P., Cornut, D., Bochet, V., Hasler, U., Oh-Hora, M., Waldburger, J.-M., and Demaurex, N. (2012). STIM1 Juxtaposes ER to Phagosomes, Generating Ca2+ Hotspots that Boost Phagocytosis. Curr. Biol. *22*, 1990–1997. https://doi.org/10.1016/j.cub.2012.08.049.
220. Mayorga, L.S., Berón, W., Sarrouf, M.N., Colombo, M.I., Creutz, C., and Stahl, P.D. (1994). Calcium-dependent fusion among endosomes. J. Biol. Chem. *269*, 30927–30934. https://doi.org/10.1016/S0021-9258(18)47370-X.
221. Malik, Z.A., Thompson, C.R., Hashimi, S., Porter, B., Iyer, S.S., and Kusner, D.J. (2003). Cutting Edge: *Mycobacterium tuberculosis* Blocks Ca2+ Signaling and Phagosome Maturation in Human Macrophages Via Specific Inhibition of Sphingosine Kinase. J. Immunol. *170*, 2811–2815. https://doi.org/10.4049/jimmunol.170.6.2811.
222. Malik, Z.A., Denning, G.M., and Kusner, D.J. (2000). Inhibition of Ca2+ Signaling by Mycobacterium tuberculosisIs Associated with Reduced Phagosome–Lysosome Fusion and Increased Survival within Human Macrophages. J. Exp. Med. *191*, 287–302.
223. Vergne, I., Chua, J., and Deretic, V. (2003). Tuberculosis Toxin Blocking Phagosome Maturation Inhibits a Novel Ca2+/Calmodulin-PI3K hVPS34 Cascade. J. Exp. Med. *198*, 653–659. https://doi.org/10.1084/jem.20030527.
224. Dayam, R.M., Saric, A., Shilliday, R.E., and Botelho, R.J. (2015). The Phosphoinositide-Gated Lysosomal Ca2+ Channel, TRPML1, Is Required for Phagosome Maturation. Traffic *16*, 1010–1026. https://doi.org/10.1111/tra.12303.
225. Di, A., Kiya, T., Gong, H., Gao, X., and Malik, A.B. (2017). Role of the phagosomal redox-sensitive TRP channel TRPM2 in regulating bactericidal activity of macrophages. J. Cell Sci. *130*, 735–744. https://doi.org/10.1242/jcs.196014.
226. Lévêque, M., Penna, A., Le Trionnaire, S., Belleguic, C., Desrues, B., Brinchault, G., Jouneau, S., Lagadic-Gossmann, D., and Martin-Chouly, C. (2018). Phagocytosis depends on TRPV2-mediated calcium influx and requires TRPV2 in lipids rafts: alteration in macrophages from patients with cystic fibrosis. Sci. Rep. *8*, 4310. https://doi.org/10.1038/s41598-018-22558-5.
227. Zhang, Z., Cui, P., Zhang, K., Chen, Q., and Fang, X. (2017). Transient Receptor Potential Melastatin 2 Regulates Phagosome Maturation and Is Required for Bacterial Clearance in *Escherichia coli* Sepsis. Anesthesiology *126*, 128–139. https://doi.org/10.1097/ALN.0000000000001430.
228. Tsujikawa, H., Yu, A.S., Xie, J., Yue, Z., Yang, W., He, Y., and Yue, L. (2015). Identification of key amino acid residues responsible for internal and external pH sensitivity of Orai1/STIM1 channels. Sci. Rep. *5*, 16747. https://doi.org/10.1038/srep16747.
229. Cao, Q., Zhong, X.Z., Zou, Y., Murrell-Lagnado, R., Zhu, M.X., and Dong, X.-P. (2015). Calcium release through P2X4 activates calmodulin to promote endolysosomal membrane fusion. J. Cell Biol. *209*, 879–894. https://doi.org/10.1083/jcb.201409071.
230. Huang, P., Zou, Y., Zhong, X.Z., Cao, Q., Zhao, K., Zhu, M.X., Murrell-Lagnado, R., and Dong, X.-P. (2014). P2X4 Forms Functional ATP-activated Cation Channels on Lysosomal Membranes Regulated by Luminal pH. J. Biol. Chem. *289*, 17658–17667. https://doi.org/10.1074/jbc.M114.552158.
231. Kim, H.J., Li, Q., Tjon-Kon-Sang, S., So, I., Kiselyov, K., A Soyombo, A., and Muallem, S. (2008). A novel mode of TRPML3 regulation by extracytosolic pH absent in the varitint-waddler phenotype. EMBO J., 197–1205. https://doi.org/10.1038/emboj.2008.56.
232. Lelouvier, B., and Puertollano, R. (2011). Mucolipin-3 Regulates Luminal Calcium, Acidification, and Membrane Fusion in the Endosomal Pathway. J. Biol. Chem. *286*, 9826–9832. https://doi.org/10.1074/jbc.M110.169185.
233. Jaconi, M.E.E., Lew, D.P., Carpentier, J.-L., Magnusson, K.E., Sjögren, M., and Stendahl, O. (1990). Cytosolic free calcium elevation mediates the phagosome-lysosome fusion during phagocytosis in human neutrophils. J. Cell Biol. *110*, 1555–1564.

234. Myers, J.T., and Swanson, J.A. (2002). Calcium spikes in activated macrophages during Fcγ receptor-mediated phagocytosis. J. Leukoc. Biol. *72*, 677–684. https://doi.org/10.1189/jlb.72.4.677.
235. Dickson, E.J., Duman, J.G., Moody, M.W., Chen, L., and Hille, B. (2012). Orai-STIM–mediated Ca2+ release from secretory granules revealed by a targeted Ca2+ and pH probe. Proc. Natl. Acad. Sci. U. S. A. *109*, E3539–E3548. https://doi.org/10.1073/pnas.1218247109.
236. Mogami, H., Tepikin, A.V., and Petersen, O.H. (1998). Termination of cytosolic Ca2+ signals: Ca2+ reuptake into intracellular stores is regulated by the free Ca2+ concentration in the store lumen. EMBO J. *17*, 435–442. https://doi.org/10.1093/emboj/17.2.435.
237. Zimmerli, S. (1996). Phagosome-lysosome fusion is a calcium-independent event in macrophages. J. Cell Biol. *132*, 49–61.
238. Becken, U., Jeschke, A., Veltman, K., and Haas, A. (2010). Cell-free fusion of bacteria-containing phagosomes with endocytic compartments. Proc. Natl. Acad. Sci. *107*, 20726–20731. https://doi.org/10.1073/pnas.1007295107.
239. Pryor, P.R., Mullock, B.M., Bright, N.A., Gray, S.R., and Luzio, J.P. (2000). The Role of Intraorganellar Ca2+In Late Endosome–Lysosome Heterotypic Fusion and in the Reformation of Lysosomes from Hybrid Organelles. J. Cell Biol. *149*, 1053–1062.
240. Augustine, G.J. (2001). How does calcium trigger neurotransmitter release? Curr. Opin. Neurobiol. *11*, 320–326. https://doi.org/10.1016/S0959-4388(00)00214-2.
241. Blank, P.S., Cho, M.-S., Vogel, S.S., Kaplan, D., Kang, A., Malley, J., and Zimmerberg, J. (1998). Submaximal Responses in Calcium-triggered Exocytosis Are Explained by Differences in the Calcium Sensitivity of Individual Secretory Vesicles. J. Gen. Physiol. *112*, 559–567.
242. Terasaki, M., Miyake, K., and McNeil, P.L. (1997). Large Plasma Membrane Disruptions Are Rapidly Resealed by Ca2+-dependent Vesicle–Vesicle Fusion Events. J. Cell Biol. *139*, 63–74.
243. Idone, V., Tam, C., Goss, J.W., Toomre, D., Pypaert, M., and Andrews, N.W. (2008). Repair of injured plasma membrane by rapid Ca2+-dependent endocytosis. J. Cell Biol. *180*, 905–914. https://doi.org/10.1083/jcb.200708010.
244. Jimenez, A.J., Maiuri, P., Lafaurie-Janvore, J., Divoux, S., Piel, M., and Perez, F. (2014). ESCRT machinery is required for plasma membrane repair. Science, 343(6174):1247136. https://doi.org/doi: 10.1126/science.1247136.
245. Keyel, P.A., Loultcheva, L., Roth, R., Salter, R.D., Watkins, S.C., Yokoyama, W.M., and Heuser, J.E. (2011). Streptolysin O clearance through sequestration into blebs that bud passively from the plasma membrane. J. Cell Sci. *124*, 2414–2423. https://doi.org/10.1242/jcs.076182.
246. Reddy, A., Caler, E.V., and Andrews, N.W. (2001). Plasma Membrane Repair Is Mediated by Ca2+-Regulated Exocytosis of Lysosomes. Cell *106*, 157–169. https://doi.org/10.1016/S0092-8674(01)00421-4.
247. Tam, C., Idone, V., Devlin, C., Fernandes, M.C., Flannery, A., He, X., Schuchman, E., Tabas, I., and Andrews, N.W. (2010). Exocytosis of acid sphingomyelinase by wounded cells promotes endocytosis and plasma membrane repair. J. Cell Biol. *189*, 1027–1038. https://doi.org/10.1083/jcb.201003053.
248. McNeil, P.L., Vogel, S.S., Miyake, K., and Terasaki, M. (2000). Patching plasma membrane disruptions with cytoplasmic membrane. J Cell Sci. https://doi.org/doi: 10.1242/jcs.113.11.1891.
249. Andrews, N.W., de Almeida, P.E., and Corrotte, M. (2014). Damage Control: Cellular Mechanisms of Plasma Membrane Repair. Trends Cell Biol. *24*, 734–742. https://doi.org/10.1016/j.tcb.2014.07.008.
250. Andrews, N.W. (2005). Membrane Resealing: Synaptotagmin VII Keeps Running the Show. Sci. STKE *2005*. https://doi.org/10.1126/stke.2822005pe19.
251. Bansal, D., and Campbell, K.P. (2004). Dysferlin and the plasma membrane repair in muscular dystrophy. Trends Cell Biol. https://doi.org/doi: 10.1016/j.tcb.2004.03.001.
252. Lin, Y.-C., Chipot, C., and Scheuring, S. (2020). Annexin-V stabilizes membrane defects by inducing lipid phase transition. Nat. Commun. *11*, 230. https://doi.org/10.1038/s41467-019-14045-w.
253. Tang, J., Maximov, A., Shin, O.-H., Dai, H., Rizo, J., and Südhof, T.C. (2006). A Complexin/Synaptotagmin 1 Switch Controls Fast Synaptic Vesicle Exocytosis. Cell *126*, 1175–1187. https://doi.org/10.1016/j.cell.2006.08.030.

254. Roggero, C.M., De Blas, G.A., Dai, H., Tomes, C.N., Rizo, J., and Mayorga, L.S. (2007). Complexin/Synaptotagmin Interplay Controls Acrosomal Exocytosis. J. Biol. Chem. *282*, 26335–26343. https://doi.org/10.1074/jbc.M700854200.
255. Baker, P.F., and Whitaker, M.J. (1978). Influence of ATP and calcium on the cortical reaction in sea urchin eggs. Nature *276*, 513–515. https://doi.org/10.1038/276513a0.
256. Vacquier, V.D. (1975). The isolation of intact cortical granules from sea urchin eggs: Calcium ions trigger granule discharge. Dev. Biol. *43*, 62–74. https://doi.org/10.1016/0012-1606(75)90131-1.
257. Whalley, T., Timmers, K., Coorssen, J., Bezrukov, L., Kingsley, D.H., and Zimmerberg, J. (2004). Membrane fusion of secretory vesicles of the sea urchin egg in the absence of NSF. J. Cell Sci. *117*, 2345–2356. https://doi.org/10.1242/jcs.01077.
258. Sasaki, H., and Epel, D. (1983). Cortical vesicle exocytosis in isolated cortices of sea urchin eggs: Description of a turbidometric assay and its utilization in studying effects of different media on discharge. Dev. Biol. *98*, 327–337. https://doi.org/10.1016/0012-1606(83)90363-9.
259. Whitaker, M. (1987). How calcium may cause exocytosis in sea urchin eggs. Biosci Rep, 383–397. https://doi.org/10.1007/BF01362502.
260. Coorssen, J.R., Blank, P.S., Tahara, M., and Zimmerberg, J. (1998). Biochemical and Functional Studies of Cortical Vesicle Fusion: The SNARE Complex and Ca2+ Sensitivity. J. Cell Biol. *143*, 1845–1857.
261. Vogel, S.S., and Zimmerberg, J. (1992). Proteins on exocytic vesicles mediate calcium-triggered fusion. Proc. Natl. Acad. Sci. U. S. A. *89*, 4749–4753.
262. Thomas, N.L., Dart, C., and Helassa, N. (2023). Editorial: The role of calcium and calcium binding proteins in cell physiology and disease. Front. Physiol. *14*, 1228885. https://doi.org/10.3389/fphys.2023.1228885.
263. Lewit-Bentley, A., and Réty, S. (2000). EF-hand calcium-binding proteins. Curr. Opin. Struct. Biol., 637–643.
264. Corbalan-Garcia, S., and Gómez-Fernández, J.C. (2014). Signaling through C2 domains: More than one lipid target. Biochim. Biophys. Acta BBA - Biomembr. *1838*, 1536–1547. https://doi.org/10.1016/j.bbamem.2014.01.008.
265. Nalefski, E.A., and Falke, J.J. (1996). The C2 domain calcium-binding motif: structural and functional diversity. Protein Sci. Publ. Protein Soc. *5*, 2375–2390.
266. Chen, C., and Jonas, P. (2017). Synaptotagmins: That's Why So Many. Neuron *94*, 694–696. https://doi.org/10.1016/j.neuron.2017.05.011.
267. Craxton, M. (2004). Synaptotagmin gene content of the sequenced genomes. BMC Genomics *5*, 43. https://doi.org/10.1186/1471-2164-5-43.
268. Bhalla, A., Tucker, W.C., and Chapman, E.R. (2005). Synaptotagmin Isoforms Couple Distinct Ranges of Ca2+, Ba2+, and Sr2+ Concentration to SNARE-mediated Membrane Fusion. Mol. Biol. Cell *16*, 4755–4764. https://doi.org/10.1091/mbc.e05-04-0277.
269. Hui, E., Bai, J., Wang, P., Sugimori, M., Llinas, R.R., and Chapman, E.R. (2005). Three distinct kinetic groupings of the synaptotagmin family: Candidate sensors for rapid and delayed exocytosis. Proc. Natl. Acad. Sci. *102*, 5210–5214. https://doi.org/10.1073/pnas.0500941102.
270. Martin, T.F.J. (2015). PI(4,5)P2-binding effector proteins for vesicle exocytosis. Biochim. Biophys. Acta *1851*, 785–793. https://doi.org/10.1016/j.bbalip.2014.09.017.
271. Jiménez, J.L., and Bashir, R. (2007). In silico functional and structural characterisation of ferlin proteins by mapping disease-causing mutations and evolutionary information onto three-dimensional models of their C2 domains. J. Neurol. Sci. *260*, 114–123. https://doi.org/10.1016/j.jns.2007.04.016.
272. Perin, M.S., Fried, V.A., Mignery, G.A., Jahn, R., and Südhof, T.C. (1990). Phospholipid binding by a synaptic vesicle protein homologous to the regulatory region of protein kinase C. Nature *345*, 260–263. https://doi.org/10.1038/345260a0.
273. Davis, D.B. (2000). Myoferlin, a candidate gene and potential modifier of muscular dystrophy. Hum. Mol. Genet. *9*, 217–226. https://doi.org/10.1093/hmg/9.2.217.
274. Doherty, K.R., Cave, A., Davis, D.B., Delmonte, A.J., Posey, A., Earley, J.U., Hadhazy, M., and McNally, E.M. (2005). Normal myoblast fusion requires myoferlin. Dev. Camb. Engl. *132*, 5565–5575. https://doi.org/10.1242/dev.02155.

275. Bernatchez, P.N., Sharma, A., Kodaman, P., and Sessa, W.C. (2009). Myoferlin is critical for endocytosis in endothelial cells. Am. J. Physiol.-Cell Physiol. *297*, C484–C492. https://doi.org/10.1152/ajpcell.00498.2008.
276. Gupta, S., Yano, J., Mercier, V., Htwe, H.H., Shin, H.R., Rademaker, G., Cakir, Z., Ituarte, T., Wen, K.W., Kim, G.E., et al. (2021). Lysosomal retargeting of Myoferlin mitigates membrane stress to enable pancreatic cancer growth. Nat. Cell Biol. *23*, 232–242. https://doi.org/10.1038/s41556-021-00644-7.
277. Miyatake, Y., Yamano, T., and Hanayama, R. (2018). Myoferlin-Mediated Lysosomal Exocytosis Regulates Cytotoxicity by Phagocytes. J. Immunol. *201*, 3051–3057. https://doi.org/10.4049/jimmunol.1800268.
278. Brown, W.J., Chambers, K., and Doody, A. (2003). Phospholipase A2 (PLA2) Enzymes in Membrane Trafficking: Mediators of Membrane Shape and Function. Traffic *4*, 214–221. https://doi.org/10.1034/j.1600-0854.2003.00078.x.
279. Dabral, D., and Coorssen, J.R. (2019). Combined Targeted Omic and Functional Assays Identify Phospholipases A2 that Regulate Docking/Priming in Calcium-Triggered Exocytosis. Cells *8*, 303. https://doi.org/10.3390/cells8040303.
280. Perisic, O., Fong, S., Lynch, D.E., Bycroft, M., and Williams, R.L. (1998). Crystal Structure of a Calcium-Phospholipid Binding Domain from Cytosolic Phospholipase A2. J. Biol. Chem. *273*, 1596–1604. https://doi.org/10.1074/jbc.273.3.1596.
281. Mayorga, L.S., Colombo, M.I., Lennartz, M., Brown, E.J., Rahman, K.H., Weiss, R., Lennon, P.J., and Stahl, P.D. (1993). Inhibition of endosome fusion by phospholipase A2 (PLA2) inhibitors points to a role for PLA2 in endocytosis. Proc. Natl. Acad. Sci. U. S. A. *90*, 10255–10259.
282. Ward, K.E., Sengupta, R., Ropa, J.P., Amiar, S., and Stahelin, R.V. (2020). The Cytosolic Phospholipase A2α N-Terminal C2 Domain Binds and Oligomerizes on Membranes with Positive Curvature. Biomolecules *10*, 647. https://doi.org/10.3390/biom10040647.
283. Grewal, T., Rentero, C., Enrich, C., Wahba, M., Raabe, C.A., and Rescher, U. (2021). Annexin Animal Models—From Fundamental Principles to Translational Research. Int. J. Mol. Sci. *22*, 3439. https://doi.org/10.3390/ijms22073439.
284. Monastyrskaya, K., Babiychuk, E.B., Hostettler, A., Rescher, U., and Draeger, A. (2007). Annexins as intracellular calcium sensors. Cell Calcium *41*, 207–219. https://doi.org/10.1016/j.ceca.2006.06.008.
285. Morgan, R.O., Martin-Almedina, S., Iglesias, J.M., Gonzalez-Florez, M.I., and Fernandez, M.P. (2004). Evolutionary perspective on annexin calcium-binding domains. Biochim. Biophys. Acta BBA - Mol. Cell Res. *1742*, 133–140. https://doi.org/10.1016/j.bbamcr.2004.09.010.
286. Gerke, V., Creutz, C.E., and Moss, S.E. (2005). Annexins: linking Ca2+ signalling to membrane dynamics. Nat. Rev. Mol. Cell Biol. *6*, 449–461. https://doi.org/10.1038/nrm1661.
287. Gabel, M., Royer, C., Thahouly, T., Calco, V., Gasman, S., Bader, M.-F., Vitale, N., and Chasserot-Golaz, S. (2020). Annexin A2 Egress during Calcium-Regulated Exocytosis in Neuroendocrine Cells. Cells *9*, 2059. https://doi.org/10.3390/cells9092059.
288. Gabel, M., and Chasserot-Golaz, S. (2016). Annexin A2, an essential partner of the exocytotic process in chromaffin cells. J. Neurochem. *137*, 890–896. https://doi.org/10.1111/jnc.13628.
289. Oshry, L., Meers, P., Mealy, T., and Tauber, A.I. (1991). Annexin-mediated membrane fusion of human neutrophil plasma membranes and phospholipid vesicles. Biochim. Biophys. Acta BBA - Biomembr. *1066*, 239–244. https://doi.org/10.1016/0005-2736(91)90192-B.
290. Zaks, W.J., and Creutz, C.E. (1990). Evaluation of the annexins as potential mediators of membrane fusion in exocytosis. J. Bioenerg. Biomembr. *22*, 97–120. https://doi.org/10.1007/BF00762942.
291. Schindelin, J., Arganda-Carreras, I., Frise, E., Kaynig, V., Longair, M., Pietzsch, T., Preibisch, S., Rueden, C., Saalfeld, S., Schmid, B., et al. (2012). Fiji - an Open Source platform for biological image analysis. Nat. Methods *9*. https://doi.org/10.1038/nmeth.2019.
292. Schneider, C.A., Rasband, W.S., and Eliceiri, K.W. (2012). NIH Image to ImageJ: 25 years of Image Analysis. Nat. Methods *9*, 671–675.
293. Bolte, S., and Cordelières, F.P. (2006). A guided tour into subcellular colocalization analysis in light microscopy. J. Microsc. *224*, 213–232. https://doi.org/10.1111/j.1365-2818.2006.01706.x.

294. Takats, S., Stillman, D., Cheslack-Postava, F., Abaev, B., Bagdonas, M., Jellinek, A., Najdek, T., Petrov, D., Rentka, M., Vasilakis, M., et al. (2024). Zotero. Version Zotero 7.0.5 (Corporation for Digital Scholarship).
295. Bertram, E.M., Hawley, R.G., and Watts, T.H. (2002). Overexpression of rab7 enhances the kinetics of antigen processing and presentation with MHC class II molecules in B cells. Int. Immunol. *14*, 309–318. https://doi.org/10.1093/intimm/14.3.309.
296. Ragaz, C., Pietsch, H., Urwyler, S., Tiaden, A., Weber, S.S., and Hilbi, H. (2008). The Legionella pneumophila phosphatidylinositol-4 phosphate-binding type IV substrate SidC recruits endoplasmic reticulum vesicles to a replication-permissive vacuole. Cell. Microbiol. *10*, 2416–2433. https://doi.org/10.1111/j.1462-5822.2008.01219.x.
297. Gillooly, D.J., Morrow, I.C., Lindsay, M., Gould, R., Bryant, N.J., Gaullier, J.-M., Parton, R.G., and Stenmark, H. (2000). Localization of phosphatidylinositol 3-phosphate in yeast and mammalian cells. EMBO Jounal *Vol.19*, 4577–4588. https://doi.org/10.1093/emboj/19.17.4577.
298. Ullrich, O., Stenmark, H., Alexandrov, K., Huber, L.A., Kaibuchi, K., Sasaki, T., Takai, Y., and Zerial, M. (1993). Rab GDP dissociation inhibitor as a general regulator for the membrane association of rab proteins. J. Biol. Chem. *268*, 18143–18150. https://doi.org/10.1016/S0021-9258(17)46822-0.
299. Antonin, W., Holroyd, C., Fasshauer, D., Pabst, S., Fischer von Mollard, G., and Jahn, R. (2000). A SNARE complex mediating fusion of late endosomes defines conserved properties of SNARE structure and function. EMBO J. *19*, 6453–6464. https://doi.org/10.1093/emboj/19.23.6453.
300. Verderio, C., Cagnoli, C., Bergami, M., Francolini, M., Schenk, U., Colombo, A., Riganti, L., Frassoni, C., Zuccaro, E., Danglot, L., et al. (2012). TI-VAMP/VAMP7 is the SNARE of secretory lysosomes contributing to ATP secretion from astrocytes. Biol. Cell *104*, 213–228. https://doi.org/10.1111/boc.201100070.
301. Marz, K.E., Lauer, Joshua M., and Hanson, Phyllis (2003). Defining the SNARE Complex Binding Surface of Î±-SNAP | Elsevier Enhanced Reader. https://doi.org/10.1074/jbc.M302003200.
302. Barnard, Morgan, A., and Burgoyne, R.D. (1997). Stimulation of NSF ATPase Activity by α-SNAP Is Required for SNARE Complex Disassembly and Exocytosis. J. Cell Biol. *139*, 875–883.
303. Diement, S., Leech, M.S., and Stahl, P.D. (1987). Generation of Macrophage Variants With 5-Azacytidine: Selection for Mannose Receptor Expression. J. Leukoc. Biol. *Volume 42*, Pages 485-490. https://doi.org/10.1002/jlb.42.5.485.
304. Fiani, M.L., Beitz, J., Turvy, D., Blum, J.S., and Stahl, P.D. (1998). Regulation of mannose receptor synthesis and turnover in mouse J774 macrophages. J. Leukoc. Biol. *64*, 85–91. https://doi.org/10.1002/jlb.64.1.85.
305. Anderson, J., Walker, G., and Pu, J. (2022). BORC-ARL8-HOPS ensemble is required for lysosomal cholesterol egress through NPC2. Mol. Biol. Cell *33*, ar81. https://doi.org/10.1091/mbc.E21-11-0595-T.
306. Sydor, T., Von Bargen, K., Becken, U., Spuerck, S., Nicholson, V.M., Prescott, J.F., and Haas, A. (2008). A mycolyl transferase mutant of Rhodococcus equi lacking capsule integrity is fully virulent. Vet. Microbiol. *128*, 327–341. https://doi.org/10.1016/j.vetmic.2007.10.020.
307. Melia, T.J., You, D., Tareste, D.C., and Rothman, J.E. (2006). Lipidic Antagonists to SNARE-mediated Fusion. J. Biol. Chem. *281*, 29597–29605. https://doi.org/10.1074/jbc.M601778200.
308. Miller, J.H. (1972). Experiments in Molecular Genetics (Cold Spring Harbor Laboratory Press).
309. Stael, S., Miller, L.P., Fernández-Fernández, Á.D., and Van Breusegem, F. (2022). Detection of Damage-Activated Metacaspase ActivityActivitiesby Western Blot in Plants. In Plant Proteases and Plant Cell Death: Methods and Protocols Methods in Molecular Biology., M. Klemenčič, S. Stael, and P. F. Huesgen, eds. (Springer US), pp. 127–137. https://doi.org/10.1007/978-1-0716-2079-3_11.
310. Dunn, K.W., Kamocka, M.M., and McDonald, J.H. (2011). A practical guide to evaluating colocalization in biological microscopy. Am. J. Physiol.-Cell Physiol. *300*, C723–C742. https://doi.org/10.1152/ajpcell.00462.2010.
311. Li, H., Stolz, D.B., and Romero, G. (2005). Characterization of Endocytic Vesicles Using Magnetic Microbeads Coated with Signalling Ligands. Traffic *6*, 324–334. https://doi.org/10.1111/j.1600-0854.2005.00274.x.

312. Barral, D.C., Staiano, L., Guimas Almeida, C., Cutler, D.F., Eden, E.R., Futter, C.E., Galione, A., Marques, A.R.A., Medina, D.L., Napolitano, G., et al. (2022). Current methods to analyze lysosome morphology, positioning, motility and function. Traffic *23*, 238–269. https://doi.org/10.1111/tra.12839.
313. Lübke, T., Lobel, P., and Sleat, D.E. (2009). Proteomics of the lysosome. Biochim. Biophys. Acta BBA - Mol. Cell Res. *1793*, 625–635. https://doi.org/10.1016/j.bbamcr.2008.09.018.
314. Van Der Beek, J., De Heus, C., Sanza, P., Liv, N., and Klumperman, J. (2024). Loss of the HOPS complex disrupts early-to-late endosome transition, impairs endosomal recycling and induces accumulation of amphisomes. Mol. Biol. Cell, mbc.E23-08-0328. https://doi.org/10.1091/mbc.E23-08-0328.
315. Yordanov, T.E., Hipolito, V.E.B., Liebscher, G., Vogel, G.F., Stasyk, T., Herrmann, C., Geley, S., Teis, D., Botelho, R.J., Hess, M.W., et al. (2019). Biogenesis of lysosome-related organelles complex-1 (BORC) regulates late endosomal/lysosomal size through PIKfyve-dependent phosphatidylinositol-3,5-bisphosphate. Traffic Cph. Den. *20*, 674–696. https://doi.org/10.1111/tra.12679.
316. Creasy, B.M., Hartmann, C.B., White, F.K.H., and McCoy, K.L. (2007). New assay using fluorogenic substrates and immunofluorescence staining to measure cysteine cathepsin activity in live cell subpopulations. Cytometry A *71A*, 114–123. https://doi.org/10.1002/cyto.a.20365.
317. Manders, E.M.M., Verbeek, F.J., and Aten, J.A. (1992). Measurement of co-localization of objects in dual-colour confocal images. J. Microsc. *169*, 375–382. https://doi.org/10.1111/j.1365-2818.1993.tb03313.x.
318. Lin, X., Yang, T., Wang, S., Wang, Z., Yun, Y., Sun, L., Zhou, Y., Xu, X., Akazawa, C., Hong, W., et al. (2014). RILP interacts with HOPS complex via VPS41 subunit to regulate endocytic trafficking. Sci. Rep. *4*, 7282. https://doi.org/10.1038/srep07282.
319. Mayle, K.M., Le, A.M., and Kamei, D.T. (2012). The Intracellular Trafficking Pathway of Transferrin. Biochim. Biophys. Acta *1820*, 264–281. https://doi.org/10.1016/j.bbagen.2011.09.009.
320. Gillingham, A.K., Sinka, R., Torres, I.L., Lilley, K.S., and Munro, S. (2014). Toward a Comprehensive Map of the Effectors of Rab GTPases. Dev. Cell *31*, 358–373. https://doi.org/10.1016/j.devcel.2014.10.007.
321. Kajiho, H., Kajiho, Y., Frittoli, E., Confalonieri, S., Bertalot, G., Viale, G., Di Fiore, P.P., Oldani, A., Garre, M., Beznoussenko, G.V., et al. (2016). RAB2A controls MT1-MMP endocytic and E-cadherin polarized Golgi trafficking to promote invasive breast cancer programs. EMBO Rep. *17*, 1061–1080. https://doi.org/10.15252/embr.201642032.
322. Goel, K., and Ploski, J.E. (2022). RISC-y Business: Limitations of Short Hairpin RNA-Mediated Gene Silencing in the Brain and a Discussion of CRISPR/Cas-Based Alternatives. Front. Mol. Neurosci. *15*, 914430. https://doi.org/10.3389/fnmol.2022.914430.
323. Baur, T., Ramadan, K., Schlundt, A., Kartenbeck, J., and Meyer, H.H. (2007). NSF- and SNARE-mediated membrane fusion is required for nuclear envelope formation and completion of nuclear pore complex assembly in *Xenopus laevis* egg extracts. J. Cell Sci. *120*, 2895–2903. https://doi.org/10.1242/jcs.010181.
324. De Paola, M., Bello, O.D., and Michaut, M.A. (2015). Cortical Granule Exocytosis Is Mediated by Alpha-SNAP and N-Ethilmaleimide Sensitive Factor in Mouse Oocytes. PLOS ONE *10*, e0135679. https://doi.org/10.1371/journal.pone.0135679.
325. Lippert, U., Ferrari, D.M., and Jahn, R. (2007). Endobrevin/VAMP8 mediates exocytotic release of hexosaminidase from rat basophilic leukaemia cells. FEBS Lett. *581*, 3479–3484. https://doi.org/10.1016/j.febslet.2007.06.057.
326. Antonin, W., Dulubova, I., Araç, D., Pabst, S., Plitzner, J., Rizo, J., and Jahn, R. (2002). The N-terminal Domains of Syntaxin 7 and vti1b Form Three-helix Bundles That Differ in Their Ability to Regulate SNARE Complex Assembly. J. Biol. Chem. *277*, 36449–36456. https://doi.org/10.1074/jbc.M204369200.
327. Alpadi, K., Kulkarni, A., Comte, V., Reinhardt, M., Schmidt, A., Namjoshi, S., Mayer, A., and Peters, C. (2012). Sequential Analysis of Trans-SNARE Formation in Intracellular Membrane Fusion. PLoS Biol. *10*, e1001243. https://doi.org/10.1371/journal.pbio.1001243.

328. Fukuda, R., McNew, J.A., Weber, T., Parlati, F., Engel, T., Nickel, W., Rothman, J.E., and Söllner, T.H. (2000). Functional architecture of an intracellular membrane t-SNARE. Nature *407*, 198–202. https://doi.org/10.1038/35025084.
329. Darnall, D.W., and Birnbaum, E.R. (1970). Rare Earth Metal Ions as Probes of Calcium Ion Binding Sites in Proteins. J. Biol. Chem. *245*, 6484–6486. https://doi.org/10.1016/S0021-9258(18)62634-1.
330. Reynolds, L.J., Hughes, L.L., Louis, A.I., Kramer, R.M., and Dennis, E.A. (1993). Metal ion and salt effects on the phospholipase A2, lysophospholipase, and transacylase activities of human cytosolic phospholipase A2. Biochim. Biophys. Acta BBA - Lipids Lipid Metab. *1167*, 272–280. https://doi.org/10.1016/0005-2760(93)90229-3.
331. Reynolds, L.J., Hughes, L.L., Louis, A.I., Kramer, R.M., and Dennis, E.A. (1993). Metal ion and salt effects on the phospholipase A2, lysophospholipase, and transacylase activities of human cytosolic phospholipase A2. Biochim. Biophys. Acta *1167*, 272–280. https://doi.org/10.1016/0005-2760(93)90229-3.
332. Doody, A.M., Antosh, A.L., and Brown, W.J. (2009). Cytoplasmic Phospholipase A2 Antagonists Inhibit Multiple Endocytic Membrane Trafficking Pathways. Biochem. Biophys. Res. Commun. *388*, 695–699. https://doi.org/10.1016/j.bbrc.2009.08.067.
333. Sattar, A.A., and Haque, R. (2006). Cytosolic PLA2 in Zymogen Granule Fusion and Amylase Release: Inhibition of GTP-induced Fusion by Arachidonyl Trifluoromethyl Ketone Points to cPLA2 in G-Protein-mediated Secretory Vesicle Fusion. J. Biochem. (Tokyo) *141*, 77–84. https://doi.org/10.1093/jb/mvm007.
334. Street, I.P., Lin, H.K., Laliberte, F., Ghomashchi, F., Wang, Z., Perrier, H., Tremblay, N.M., Huang, Z., Weech, P.K., and Gelb, M.H. (1993). Slow- and tight-binding inhibitors of the 85-kDa human phospholipase A2. Biochemistry *32*, 5935–5940. https://doi.org/10.1021/bi00074a003.
335. Trimble, L.A., Street, I.P., Perrier, H., Tremblay, N.M., Weech, P.K., and Bernstein, M.A. (1993). NMR structural studies of the tight complex between a trifluoromethyl ketone inhibitor and the 85-kDa human phospholipase A2. Biochemistry *32*, 12560–12565. https://doi.org/10.1021/bi00210a002.
336. Riendeau, D., Guay, J., Weech, P.K., Laliberté, F., Yergey, J., Li, C., Desmarais, S., Perrier, H., Liu, S., and Nicoll-Griffith, D. (1994). Arachidonyl trifluoromethyl ketone, a potent inhibitor of 85-kDa phospholipase A2, blocks production of arachidonate and 12-hydroxyeicosatetraenoic acid by calcium ionophore-challenged platelets. J. Biol. Chem. *269*, 15619–15624. https://doi.org/10.1016/S0021-9258(17)40726-5.
337. Clapham, D.E. (2007). Calcium Signaling. Cell *131*, 1047–1058. https://doi.org/10.1016/j.cell.2007.11.028.
338. Inesi, G., and Tadini-Buoninsegni, F. (2014). Ca2+/H+ exchange, lumenal Ca2+ release and Ca2+/ATP coupling ratios in the sarcoplasmic reticulum ATPase. J. Cell Commun. Signal. *8*, 5–11. https://doi.org/10.1007/s12079-013-0213-7.
339. Sugita, S., Shin, O.-H., Han, W., Lao, Y., and Südhof, T.C. (2002). Synaptotagmins form a hierarchy of exocytotic Ca2+ sensors with distinct Ca2+ affinities. EMBO J. *21*, 270–280. https://doi.org/10.1093/emboj/21.3.270.
340. Jaiswal, J.K., Chakrabarti, S., Andrews, N.W., and Simon, S.M. (2004). Synaptotagmin VII Restricts Fusion Pore Expansion during Lysosomal Exocytosis. PLoS Biol. *2*, e233. https://doi.org/10.1371/journal.pbio.0020233.
341. Martinez, I., Chakrabarti, S., Hellevik, T., Morehead, J., Fowler, K., and Andrews, N.W. (2000). Synaptotagmin VII Regulates Ca2+-Dependent Exocytosis of Lysosomes in Fibroblasts. J. Cell Biol. *148*, 1141–1150.
342. Davis, D.B., Doherty, K.R., Delmonte, A.J., and McNally, E.M. (2002). Calcium-sensitive Phospholipid Binding Properties of Normal and Mutant Ferlin C2 Domains. J. Biol. Chem. *277*, 22883–22888. https://doi.org/10.1074/jbc.M201858200.
343. Posey, A.D., Demonbreun, A., and McNally, E.M. (2011). Ferlin proteins in myoblast fusion and muscle growth. Curr. Top. Dev. Biol. *96*, 203–230. https://doi.org/10.1016/B978-0-12-385940-2.00008-5.
344. Caohuy, H., Srivastava, M., and Pollard, H.B. (1996). Membrane fusion protein synexin (annexin VII) as a Ca2+/GTP sensor in exocytotic secretion. Proc. Natl. Acad. Sci. U. S. A. *93*, 10797–10802.

345. Gerke, V., and Moss, S.E. (2002). Annexins: From Structure to Function. Physiol. Rev. *82*, 331–371. https://doi.org/10.1152/physrev.00030.2001.
346. Pollard, H.B., Burns, A.L., and Rojas, E. (1990). Synexin (annexin VII): A cytosolic calcium-binding protein which promotes membrane fusion and forms calcium channels in artificial bilayer and natural membranes. J. Membr. Biol. *117*, 101–112. https://doi.org/10.1007/BF01868677.
347. Potez, S., Luginbühl, M., Monastyrskaya, K., Hostettler, A., Draeger, A., and Babiychuk, E.B. (2011). Tailored Protection against Plasmalemmal Injury by Annexins with Different Ca2+ Sensitivities. J. Biol. Chem. *286*, 17982–17991. https://doi.org/10.1074/jbc.M110.187625.
348. Ahnert-Hilger, G., Dayanithi, G., Spicher, K., and Nordmann, J.J. (1992). G-Proteins mediate inhibition and activation of Ca2+-induced exocytosis from SLO-permeabilized peptidergic nerve endings. Biosci. Rep. *12*, 463–469. https://doi.org/10.1007/BF01122034.
349. Monck, J.R., and Fernandez, J.M. (1994). The exocytotic fusion pore and neurotransmitter release. Neuron *12*, 707–716. https://doi.org/10.1016/0896-6273(94)90325-5.
350. Neher, E. (1988). The influence of intracellular calcium concentration on degranulation of dialysed mast cells from rat peritoneum. J. Physiol. *395*, 193–214.
351. Bucci, C., Thomsen, P., Nicoziani, P., McCarthy, J., and van Deurs, B. (2000). Rab7: A Key to Lysosome Biogenesis. Mol. Biol. Cell *11*, 467–480.
352. Boda, A., Lőrincz, P., Takáts, S., Csizmadia, T., Tóth, S., Kovács, A.L., and Juhász, G. (2019). Drosophila Arl8 is a general positive regulator of lysosomal fusion events. Biochim. Biophys. Acta BBA - Mol. Cell Res. *1866*, 533–544. https://doi.org/10.1016/j.bbamcr.2018.12.011.
353. Cheng, X.-T., Xie, Y.-X., Zhou, B., Huang, N., Farfel-Becker, T., and Sheng, Z.-H. (2018). Characterization of LAMP1-labeled nondegradative lysosomal and endocytic compartments in neurons. J. Cell Biol. *217*, 3127–3139. https://doi.org/10.1083/jcb.201711083.
354. Cheng, X.-T., Xie, Y.-X., Zhou, B., Huang, N., Farfel-Becker, T., and Sheng, Z.-H. (2018). Revisiting LAMP1 as a marker for degradative autophagy-lysosomal organelles in the nervous system. Autophagy *14*, 1472–1474. https://doi.org/10.1080/15548627.2018.1482147.
355. Baba, K., Kuwada, S., Nakao, A., Li, X., Okuda, N., Nishida, A., Mitsuda, S., Fukuoka, N., Kakeya, H., and Kataoka, T. (2020). Different localization of lysosomal-associated membrane protein 1 (LAMP1) in mammalian cultured cell lines. Histochem. Cell Biol. *153*, 199–213. https://doi.org/10.1007/s00418-019-01842-z.
356. Pshezhetsky, A.V., and Ashmarina, M. (2001). Lysosomal Multienzyme Complex: Biochemistry, Genetics, and Molecular Pathophysiology. Prog. Nucleic Acid Res. Mol. Biol., 81–114. https://doi.org/10.1016/s0079-6603(01)69045-7.
357. Van Der Spoel, A., Bonten, E., and d'Azzo, A. (2000). Processing of Lysosomal β-Galactosidase. J. Biol. Chem. *275*, 10035–10040. https://doi.org/10.1074/jbc.275.14.10035.
358. Zhang, S., McCarter, J.D., Okamura-Oho, Y., Yaghi, F., Hinek, A., Withers, S.G., and Callahan, J.W. (1994). Kinetic mechanism and characterization of human beta-galactosidase precursor secreted by permanently transfected Chinese hamster ovary cells. Biochem. J. *304*, 281–288.
359. The UniProt Consortium (2019). UniProt: a worldwide hub of protein knowledge. Nucleic Acids Res. *47*, D506–D515. https://doi.org/10.1093/nar/gky1049.
360. Gupta, M., Pandey, H., and Sivakumar, S. (2017). Intracellular Delivery of β-Galactosidase Enzyme Using Arginase-Responsive Dextran Sulfate/Poly-l-arginine Capsule for Lysosomal Storage Disorder. ACS Omega *2*, 9002–9012. https://doi.org/10.1021/acsomega.7b01230.
361. Nobori, T., Kawamura, M., Yoshida, R., Joichi, T., Kamino, K., Kishimura, A., Baba, E., Mori, T., and Katayama, Y. (2020). Fluorescence Signal Amplification by Using β-Galactosidase for Flow Cytometry; Advantages of an Endogenous Activity-Free Enzyme. Anal. Chem. *92*, 3069–3076. https://doi.org/10.1021/acs.analchem.9b04471.
362. Lin, S.X., Mallet, W.G., Huang, A.Y., and Maxfield, F.R. (2004). Endocytosed Cation-Independent Mannose 6-Phosphate Receptor Traffics via the Endocytic Recycling Compartment en Route to the trans-Golgi Network and a Subpopulation of Late Endosomes. Mol. Biol. Cell *15*, 721–733. https://doi.org/10.1091/mbc.E03-07-0497.
363. Hiraiwa, M., Saitoh, M., Arai, N., Shiraishi, T., Odani, S., Uda, Y., Ono, T., and O'Brien, J.S. (1997). Protective protein in the bovine lysosomal b-galactosidase complex. Biochim. Biophys. Acta *1341*, 189–199.
364. Cavallo-Medved, D., Moin, K., and Sloane, B. (2011). Cathepsin B. AFCS-Nat. Mol. Pages *2011*, A000508.

365. Mort, J.S., and Buttle, D.J. (1997). Cathepsin B. Int. J. Biochem. Cell Biol. *29*, 715–720. https://doi.org/10.1016/S1357-2725(96)00152-5.
366. Benes, P., Vetvicka, V., and Fusek, M. (2008). CATHEPSIN D – MANY FUNCTIONS OF ONE ASPARTIC PROTEASE. Crit. Rev. Oncol. Hematol. *68*, 12–28. https://doi.org/10.1016/j.critrevonc.2008.02.008.
367. Erickson, A.H., Conner, G.E., and Blobel, G. (1981). Biosynthesis of a lysosomal enzyme. Partial structure of two transient and functionally distinct NH2-terminal sequences in cathepsin D. J. Biol. Chem. *256*, 11224–11231. https://doi.org/10.1016/S0021-9258(19)68581-9.
368. Laurent-Matha, V., Derocq, D., Prébois, C., Katunuma, N., and Liaudet-Coopman, E. (2006). Processing of human cathepsin D is independent of its catalytic function and auto-activation: involvement of cathepsins L and B. J. Biochem. (Tokyo) *139*, 363–371. https://doi.org/10.1093/jb/mvj037.
369. Heinrich, M., Wickel, M., Schneider-Brachert, W., Sandberg, C., Gahr, J., Schwandner, R., Weber, T., Brunner, J., Krönke, M., and Schütze, S. (2000). Cathepsin D targeted by acid sphingomyelinase-derived ceramide Corrigendum. EMBO J. *19*, 315–315. https://doi.org/10.1038/sj.emboj.7592140.
370. Heinrich, M., Wickel, M., Schneider-Brachert, W., Sandberg, C., Gahr, J., Schwandner, R., Weber, T., Saftig, P., Peters, C., Brunner, J., et al. (1999). Cathepsin D targeted by acid sphingomyelinase-derived ceramide. EMBO J. *18*, 5252–5263. https://doi.org/10.1093/emboj/18.19.5252.
371. Pols, M.S., Ten Brink, C., Gosavi, P., Oorschot, V., and Klumperman, J. (2013). The HOPS Proteins HVPS41 and HVPS39 Are Required for Homotypic and Heterotypic Late Endosome Fusion. Traffic *14*, 219–232. https://doi.org/10.1111/tra.12027.
372. Rosa-Ferreira, C., Sweeney, S.T., and Munro, S. (2018). The small G protein Arl8 contributes to lysosomal function and long-range axonal transport in *Drosophila*. Biol. Open *7*, bio035964. https://doi.org/10.1242/bio.035964.
373. Product Data Sheet (2013). LysoTracker and LysoSensor Probes.
374. Wang, G.M., Xu, P., Yu, K., Guo, S.S., and Faessler, R. (2024). Rab7 deficiency induces lysosome formation from recycling endosomes leading to an increased degradation of cell surface proteins. Preprint, https://doi.org/10.1101/2024.05.13.593900 https://doi.org/10.1101/2024.05.13.593900.
375. Johnson, D.E., Ostrowski, P., Jaumouillé, V., and Grinstein, S. (2016). The position of lysosomes within the cell determines their luminal pH. J. Cell Biol. *212*, 677–692. https://doi.org/10.1083/jcb.201507112.
376. De Luca, M., Cogli, L., Progida, C., Nisi, V., Pascolutti, R., Sigismund, S., Di Fiore, P.P., and Bucci, C. (2015). RILP regulates vacuolar ATPase through interaction with the V1G1 subunit. J. Cell Sci. *128*, 2565–2565. https://doi.org/10.1242/jcs.175323.
377. Bagshaw, R.D., Callahan, J.W., and Mahuran, D.J. (2006). The Arf-family protein, Arl8b, is involved in the spatial distribution of lysosomes. Biochem. Biophys. Res. Commun. *344*, 1186–1191. https://doi.org/10.1016/j.bbrc.2006.03.221.
378. Yadati, T., Houben, T., Bitorina, A., and Shiri-Sverdlov, R. (2020). The Ins and Outs of Cathepsins: Physiological Function and Role in Disease Management. Cells *9*, 1679. https://doi.org/10.3390/cells9071679.
379. Jia, R., and Bonifacino, J.S. (2019). Lysosome Positioning Influences mTORC2 and AKT Signaling. Mol. Cell *75*, 26-38.e3. https://doi.org/10.1016/j.molcel.2019.05.009.
380. Guerra, F., and Bucci, C. (2016). Multiple Roles of the Small GTPase Rab7. Cells *5*. https://doi.org/10.3390/cells5030034.
381. Mrakovic, A., Kay, J.G., Furuya, W., Brumell, J.H., and Botelho, R.J. (2012). Rab7 and Arl8 GTPases are Necessary for Lysosome Tubulation in Macrophages. Traffic *13*, 1667–1679. https://doi.org/10.1111/tra.12003.
382. Luzio, J.P., Pryor, P.R., and Bright, N.A. (2007). Lysosomes: fusion and function. Nat. Rev. Mol. Cell Biol. *8*, 622–632. https://doi.org/10.1038/nrm2217.
383. Yasuda, S., Morishita, S., Fujita, A., Nanao, T., Wada, N., Waguri, S., Schiavo, G., Fukuda, M., and Nakamura, T. (2015). Mon1-Ccz1 activates Rab7 only on late endosome and dissociates from lysosome in mammalian cells. J. Cell Sci., jcs.178095. https://doi.org/10.1242/jcs.178095.

384. Lund, V.K., Madsen, K.L., and Kjaerulff, O. (2018). Drosophila Rab2 controls endosome-lysosome fusion and LAMP delivery to late endosomes. Autophagy *14*, 1520–1542. https://doi.org/10.1080/15548627.2018.1458170.
385. van der Kant, R., Fish, A., Janssen, L., Janssen, H., Krom, S., Ho, N., Brummelkamp, T., Carette, J., Rocha, N., and Neefjes, J. (2013). Late endosomal transport and tethering are coupled processes controlled by RILP and the cholesterol sensor ORP1L. J. Cell Sci. *126*, 3462–3474. https://doi.org/10.1242/jcs.129270.
386. Jeschke, A., and Haas, A. (2016). Deciphering the roles of phosphoinositide lipids in phagolysosome biogenesis. Commun. Integr. Biol. *9*, e1174798. https://doi.org/10.1080/19420889.2016.1174798.
387. Barnard, Morgan, A., and Burgoyne, R.D. (1997). Stimulation of NSF ATPase Activity by ␣-SNAP Is Required for SNARE Complex Disassembly and Exocytosis. J. Cell Biol. *139*, 9.
388. Thorngren, N., Collins, K.M., Fratti, R.A., Wickner, W., and Merz, A.J. (2004). A soluble SNARE drives rapid docking, bypassing ATP and Sec17/18p for vacuole fusion. EMBO J. *23*, 2765–2776. https://doi.org/10.1038/sj.emboj.7600286.
389. Abbineni, P.S., Hibbert, J.E., and Coorssen, J.R. (2013). Critical Role of Cortical Vesicles in Dissecting Regulated Exocytosis: Overview of Insights Into Fundamental Molecular Mechanisms. Biol. Bull. *224*, 200–217. https://doi.org/10.1086/BBLv224n3p200.
390. Zhou, Q., Zhou, P., Wang, A.L., Wu, D., Zhao, M., Südhof, T.C., and Brunger, A.T. (2017). The primed SNARE–complexin–synaptotagmin complex for neuronal exocytosis. Nature *548*, 420–425. https://doi.org/10.1038/nature23484.
391. Kutateladze, T.G. (2010). Translation of the phosphoinositide code by PI effectors. Nat. Chem. Biol. *6*, 507–513. https://doi.org/10.1038/nchembio.390.
392. Rusten, T.E., and Stenmark, H. (2006). Analyzing phosphoinositides and their interacting proteins. Nat. Methods *3*, 251–258. https://doi.org/10.1038/nmeth867.
393. Posor, Y., Jang, W., and Haucke, V. (2022). Phosphoinositides as membrane organizers. Nat. Rev. Mol. Cell Biol. *23*, 797–816. https://doi.org/10.1038/s41580-022-00490-x.
394. Falkenburger, B.H., Jensen, J.B., Dickson, E.J., Suh, B.-C., and Hille, B. (2010). Phosphoinositides: lipid regulators of membrane proteins. J. Physiol. *588*, 3179–3185. https://doi.org/10.1113/jphysiol.2010.192153.
395. Rusinova, R., Hobart, E.A., Koeppe, R.E., and Andersen, O.S. (2013). Phosphoinositides alter lipid bilayer properties. J. Gen. Physiol. *141*, 673–690. https://doi.org/10.1085/jgp.201310960.
396. Singh, P., Mukherji, S., Basak, S., Hoffmann, M., and Das, D.K. (2022). Dynamic Ca2+ sensitivity stimulates the evolved SARS-CoV-2 spike strain-mediated membrane fusion for enhanced entry. Cell Rep. *39*, 110694. https://doi.org/10.1016/j.celrep.2022.110694.
397. Zilly, F.E., Halemani, N.D., Walrafen, D., Spitta, L., Schreiber, A., Jahn, R., and Lang, T. (2011). Ca2+ induces clustering of membrane proteins in the plasma membrane via electrostatic interactions. EMBO J. *30*, 1209–1220. https://doi.org/10.1038/emboj.2011.53.
398. Himschoot, E., Pleskot, R., Van Damme, D., and Vanneste, S. (2017). The ins and outs of Ca2+ in plant endomembrane trafficking. Curr. Opin. Plant Biol. *40*, 131–137. https://doi.org/10.1016/j.pbi.2017.09.003.
399. Tsai, H.-H.G., Juang, W.-F., Chang, C.-M., Hou, T.-Y., and Lee, J.-B. (2013). Molecular mechanism of Ca2+-catalyzed fusion of phospholipid micelles. Biochim. Biophys. Acta BBA - Biomembr. *1828*, 2729–2738. https://doi.org/10.1016/j.bbamem.2013.07.022.
400. Beckers, C.J.M., Block, M.R., Glick, B.S., Rothman, J.E., and Balch, W.E. (1989). Vesicular transport between the endoplasmic reticulum and the Golgi stack requires the NEM-sensitive fusion protein. Nature *339*, 397–398. https://doi.org/10.1038/339397a0.
401. Singh, T.K., and Liu, L. (2000). Modification of Cysteine Residues by N-Ethylmaleimide Inhibits Annexin II Tetramer Mediated Liposome Aggregation. Arch. Biochem. Biophys. *381*, 235–240. https://doi.org/10.1006/abbi.2000.1994.
402. Paulech, J., Solis, N., and Cordwell, S.J. (2013). Characterization of reaction conditions providing rapid and specific cysteine alkylation for peptide-based mass spectrometry. Biochim. Biophys. Acta BBA - Proteins Proteomics *1834*, 372–379. https://doi.org/10.1016/j.bbapap.2012.08.002.
403. Pe'er, I., Felder, C.E., Man, O., Silman, I., Sussman, J.L., and Beckmann, J.S. (2004). Proteomic signatures: Amino acid and oligopeptide compositions differentiate among phyla. Proteins Struct. Funct. Bioinforma. *54*, 20–40. https://doi.org/10.1002/prot.10559.

404. Tahara, M., Coorssen, J.R., Timmers, K., Blank, P.S., Whalley, T., Scheller, R., and Zimmerberg, J. (1998). Calcium Can Disrupt the SNARE Protein Complex on Sea Urchin Egg Secretory Vesicles without Irreversibly Blocking Fusion. J. Biol. Chem. *273*, 33667–33673. https://doi.org/10.1074/jbc.273.50.33667.
405. Barszczewski, M., Chua, J.J., Stein, A., Winter, U., Heintzmann, R., Zilly, F.E., Fasshauer, D., Lang, T., and Jahn, R. (2008). A Novel Site of Action for α-SNAP in the SNARE Conformational Cycle Controlling Membrane Fusion. Mol. Biol. Cell *19*, 776–784. https://doi.org/10.1091/mbc.E07-05-0498.
406. Rodríguez, F., Bustos, M.A., Zanetti, M.N., Ruete, M.C., Mayorga, L.S., and Tomes, C.N. (2011). α-SNAP Prevents Docking of the Acrosome during Sperm Exocytosis because It Sequesters Monomeric Syntaxin. PLoS ONE *6*, e21925. https://doi.org/10.1371/journal.pone.0021925.
407. Park, Y., Vennekate, W., Yavuz, H., Preobraschenski, J., Hernandez, J.M., Riedel, D., Walla, P.J., and Jahn, R. (2014). α-SNAP Interferes with the Zippering of the SNARE Protein Membrane Fusion Machinery. J. Biol. Chem. *289*, 16326–16335. https://doi.org/10.1074/jbc.M114.556803.
408. Brandhorst, D., Zwilling, D., Rizzoli, S.O., Lippert, U., Lang, T., and Jahn, R. (2006). Homotypic fusion of early endosomes: SNAREs do not determine fusion specificity. Proc. Natl. Acad. Sci. *103*, 2701–2706. https://doi.org/10.1073/pnas.0511138103.
409. Hua, Y., and Scheller, R.H. (2001). Three SNARE complexes cooperate to mediate membrane fusion. Proc. Natl. Acad. Sci. U. S. A. *98*, 8065–8070. https://doi.org/10.1073/pnas.131214798.
410. Pryor, P.R., Mullock, B.M., Bright, N.A., Lindsay, M.R., Gray, S.R., Richardson, S.C.W., Stewart, A., James, D.E., Piper, R.C., and Luzio, J.P. (2004). Combinatorial SNARE complexes with VAMP7 or VAMP8 define different late endocytic fusion events. EMBO Rep. *5*, 590–595. https://doi.org/10.1038/sj.embor.7400150.
411. Ward, D.M., Pevsner, J., Scullion, M.A., Vaughn, M., and Kaplan, J. (2000). Syntaxin 7 and VAMP-7 are Soluble N-Ethylmaleimide–sensitive Factor Attachment Protein Receptors Required for Late Endosome–Lysosome and Homotypic Lysosome Fusion in Alveolar Macrophages. Mol. Biol. Cell *11*, 2327–2333.
412. Advani, R.J., Yang, B., Prekeris, R., Lee, K.C., Klumperman, J., and Scheller, R.H. (1999). Vamp-7 Mediates Vesicular Transport from Endosomes to Lysosomes. J. Cell Biol. *146*, 765–776. https://doi.org/10.1083/jcb.146.4.765.
413. Harper, S., and Speicher, D.W. (2008). Expression and Purification of GST Fusion Proteins. Curr. Protoc. Protein Sci. *52*. https://doi.org/10.1002/0471140864.ps0606s52.
414. Martinez-Arca, S., Alberts, P., Zahraoui, A., Louvard, D., and Galli, T. (2000). Role of Tetanus Neurotoxin Insensitive Vesicle-Associated Membrane Protein (Ti-Vamp) in Vesicular Transport Mediating Neurite Outgrowth. J. Cell Biol. *149*, 889–900.
415. Rossi, V., Banfield, D., Vacca, M., Dietrich, L., Ungermann, C., Desposito, M., Galli, T., and Filippini, F. (2004). Longins and their longin domains: regulated SNAREs and multifunctional SNARE regulators. Trends Biochem. Sci. *29*, 682–688. https://doi.org/10.1016/j.tibs.2004.10.002.
416. Ma, C., Su, L., Seven, A.B., Xu, Y., and Rizo, J. (2013). Reconstitution of the Vital Functions of Munc18 and Munc13 in Neurotransmitter Release. Science *339*, 421–425. https://doi.org/10.1126/science.1230473.
417. Yang, X., Tu, W., Gao, X., Zhang, Q., Guan, J., and Zhang, J. (2023). Functional regulation of syntaxin-1: An underlying mechanism mediating exocytosis in neuroendocrine cells. Front. Endocrinol. *14*, 1096365. https://doi.org/10.3389/fendo.2023.1096365.
418. Lee, S., Shin, J., Jung, Y., Son, H., Shin, J., Jeong, C., Kweon, D.-H., and Shin, Y.-K. (2020). Munc18-1 induces conformational changes of syntaxin-1 in multiple intermediates for SNARE assembly. Sci. Rep. *10*, 11623. https://doi.org/10.1038/s41598-020-68476-3.
419. Milovanovic, D., Platen, M., Junius, M., Diederichsen, U., Schaap, I.A.T., Honigmann, A., Jahn, R., and Van Den Bogaart, G. (2016). Calcium Promotes the Formation of Syntaxin 1 Mesoscale Domains through Phosphatidylinositol 4,5-Bisphosphate. J. Biol. Chem. *291*, 7868–7876. https://doi.org/10.1074/jbc.M116.716225.
420. Chicka, M.C., Ren, Q., Richards, D., Hellman, L.M., Zhang, J., Fried, M.G., and Whiteheart, S.W. (2016). Role of Munc13-4 as a Ca2+-dependent tether during platelet secretion. Biochem. J. *473*, 627–639. https://doi.org/10.1042/BJ20151150.
421. He, J., Johnson, J.L., Monfregola, J., Ramadass, M., Pestonjamasp, K., Napolitano, G., Zhang, J., and Catz, S.D. (2016). Munc13-4 interacts with syntaxin 7 and regulates late endosomal

maturation, endosomal signaling, and TLR9-initiated cellular responses. Mol. Biol. Cell *27*, 572–587. https://doi.org/10.1091/mbc.E15-05-0283.

422. Papantoniou, C., Laugks, U., Betzin, J., Capitanio, C., Ferrero, J.J., Sánchez-Prieto, J., Schoch, S., Brose, N., Baumeister, W., Cooper, B.H., et al. (2023). Munc13- and SNAP25-dependent molecular bridges play a key role in synaptic vesicle priming. Sci. Adv. *9*, eadf6222. https://doi.org/10.1126/sciadv.adf6222.
423. Dingjan, I., Linders, P.T.A., Verboogen, D.R.J., Revelo, N.H., Ter Beest, M., and Van Den Bogaart, G. (2018). Endosomal and Phagosomal SNAREs. Physiol. Rev. *98*, 1465–1492. https://doi.org/10.1152/physrev.00037.2017.
424. Neves, G., Neef, A., and Lagnado, L. (2001). The actions of barium and strontium on exocytosis and endocytosis in the synaptic terminal of goldfish bipolar cells. J. Physiol. *535*, 809–824. https://doi.org/10.1111/j.1469-7793.2001.t01-1-00809.x.
425. Searl, T.J., and Silinsky, E.M. (2002). Evidence for two distinct processes in the final stages of neurotransmitter release as detected by binomial analysis in calcium and strontium solutions. J. Physiol. *539*, 693–705. https://doi.org/10.1113/jphysiol.2001.013129.
426. Xu-Friedman, M.A., and Regehr, W.G. (2000). Probing Fundamental Aspects of Synaptic Transmission with Strontium. J. Neurosci. *20*, 4414–4422. https://doi.org/10.1523/JNEUROSCI.20-12-04414.2000.
427. Czibener, C., Sherer, N.M., Becker, S.M., Pypaert, M., Hui, E., Chapman, E.R., Mothes, W., and Andrews, N.W. (2006). Ca2+ and synaptotagmin VII–dependent delivery of lysosomal membrane to nascent phagosomes. J. Cell Biol. *174*, 997–1007. https://doi.org/10.1083/jcb.200605004.
428. MacDougall, D.D., Lin, Z., Chon, N.L., Jackman, S.L., Lin, H., Knight, J.D., and Anantharam, A. (2018). The high-affinity calcium sensor synaptotagmin-7 serves multiple roles in regulated exocytosis. J. Gen. Physiol. *150*, 783–807. https://doi.org/10.1085/jgp.201711944.
429. Bacaj, T., Wu, D., Yang, X., Morishita, W., Zhou, P., Xu, W., Malenka, R.C., and Südhof, T.C. (2013). Synaptotagmin-1 and Synaptotagmin-7 Trigger Synchronous and Asynchronous Phases of Neurotransmitter Release. Neuron *80*, 947–959. https://doi.org/10.1016/j.neuron.2013.10.026.
430. Sugita, S., Han, W., Butz, S., Liu, X., Fernández-Chacón, R., Lao, Y., and Südhof, T.C. (2001). Synaptotagmin VII as a Plasma Membrane Ca2+ Sensor in Exocytosis. Neuron *30*, 459–473. https://doi.org/10.1016/S0896-6273(01)00290-2.
431. Fukuda, M., Ogata, Y., Saegusa, C., Kanno, E., and Mikoshiba, K. (2002). Alternative splicing isoforms of synaptotagmin VII in the mouse, rat and human. Biochem. J. *365*, 173–180. https://doi.org/10.1042/BJ20011877.
432. Ramakrishnan, N.A., Drescher, M.J., Morley, B.J., Kelley, P.M., and Drescher, D.G. (2014). Calcium Regulates Molecular Interactions of Otoferlin with Soluble NSF Attachment Protein Receptor (SNARE) Proteins Required for Hair Cell Exocytosis. J. Biol. Chem. *289*, 8750–8766. https://doi.org/10.1074/jbc.M113.480533.
433. Hams, N., Padmanarayana, M., Qiu, W., and Johnson, C.P. (2017). Otoferlin is a multivalent calcium-sensitive scaffold linking SNAREs and calcium channels. Proc. Natl. Acad. Sci. *114*, 8023–8028. https://doi.org/10.1073/pnas.1703240114.
434. Carroll, A.D., Moyen, C., Kesteren, P.V., Tooke, F., Battey, N.H., and Brownlee, C. Ca2⁺, Annexins, and GTP Modulate Exocytosis from Maize Root Cap Protoplasts.
435. Enrich, C., Lu, A., Tebar, F., Rentero, C., and Grewal, T. (2022). Annexins Bridging the Gap: Novel Roles in Membrane Contact Site Formation. Front. Cell Dev. Biol. *9*, 797949. https://doi.org/10.3389/fcell.2021.797949.
436. Gerelsaikhan, T., Vasa, P.K., and Chander, A. (2012). Annexin A7 and SNAP23 interactions in alveolar type II cells and in vitro: A role for Ca2+ and PKC. Biochim. Biophys. Acta BBA - Mol. Cell Res. *1823*, 1796–1806. https://doi.org/10.1016/j.bbamcr.2012.06.010.
437. Ebstrup, M.L., Sønder, S.L., Fogde, D.L., Heitmann, A.S.B., Dietrich, T.N., Dias, C., Jäättelä, M., Maeda, K., and Nylandsted, J. (2024). Annexin A7 mediates lysosome repair independently of ESCRT-III. Front. Cell Dev. Biol. *11*, 1211498. https://doi.org/10.3389/fcell.2023.1211498.
438. Sønder, S.L., Boye, T.L., Tölle, R., Dengjel, J., Maeda, K., Jäättelä, M., Simonsen, A.C., Jaiswal, J.K., and Nylandsted, J. (2019). Annexin A7 is required for ESCRT III-mediated plasma membrane repair. Sci. Rep. *9*, 6726. https://doi.org/10.1038/s41598-019-43143-4.

439. Bittel, D.C., Chandra, G., Tirunagri, L.M.S., Deora, A.B., Medikayala, S., Scheffer, L., Defour, A., and Jaiswal, J.K. (2020). Annexin A2 Mediates Dysferlin Accumulation and Muscle Cell Membrane Repair. Cells *9*, 1919. https://doi.org/10.3390/cells9091919.
440. Vázquez, C.L., and Colombo, M.I. (2009). Chapter 6 Assays to Assess Autophagy Induction and Fusion of Autophagic Vacuoles with a Degradative Compartment, Using Monodansylcadaverine (MDC) and DQ-BSA. In Methods in Enzymology, p. Pages 85-95.
441. Boswell, K.L., James, D.J., Esquibel, J.M., Bruinsma, S., Shirakawa, R., Horiuchi, H., and Martin, T.F.J. (2012). Munc13-4 reconstitutes calcium-dependent SNARE-mediated membrane fusion. J. Cell Biol. *197*, 301–312. https://doi.org/10.1083/jcb.201109132.
442. Chicka, M.C., Ren, Q., Richards, D., Hellman, L.M., Zhang, J., Fried, M.G., and Whiteheart, S.W. (2016). Role of Munc13-4 as a Ca2+-dependent tether during platelet secretion. Biochem. J. *473*, 627–639. https://doi.org/10.1042/BJ20151150.
443. Silinsky, E.M., and Searl, T.J. (2003). Phorbol esters and neurotransmitter release: more than just protein kinase C? Br. J. Pharmacol. *138*, 1191–1201. https://doi.org/10.1038/sj.bjp.0705213.
444. Li, G., Huang, D., Hong, J., Bhat, O.M., Yuan, X., and Li, P.-L. (2019). Control of lysosomal TRPML1 channel activity and exosome release by acid ceramidase in mouse podocytes. Am. J. Physiol.-Cell Physiol. *317*, C481–C491. https://doi.org/10.1152/ajpcell.00150.2019.
445. Rühl, P., and Bracher, F. (2023). Aza Analogs of the TRPML1 Inhibitor Estradiol Methyl Ether (EDME). Molecules *28*, 7428. https://doi.org/10.3390/molecules28217428.
446. Gan, N., Han, Y., Zeng, W., Wang, Y., Xue, J., and Jiang, Y. (2022). Structural mechanism of allosteric activation of TRPML1 by PI(3,5)P2 and rapamycin. Proc. Natl. Acad. Sci. U. S. A. *119*, e2120404119. https://doi.org/10.1073/pnas.2120404119.
447. Shen, C., Zhang, Y., Cui, W., Zhao, Y., Sheng, D., Teng, X., Shao, M., Ichikawa, M., Wang, J., and Hattori, M. (2023). Structural insights into the allosteric inhibition of P2X4 receptors. Nat. Commun. *14*, 6437. https://doi.org/10.1038/s41467-023-42164-y.

9 Supplementary Information

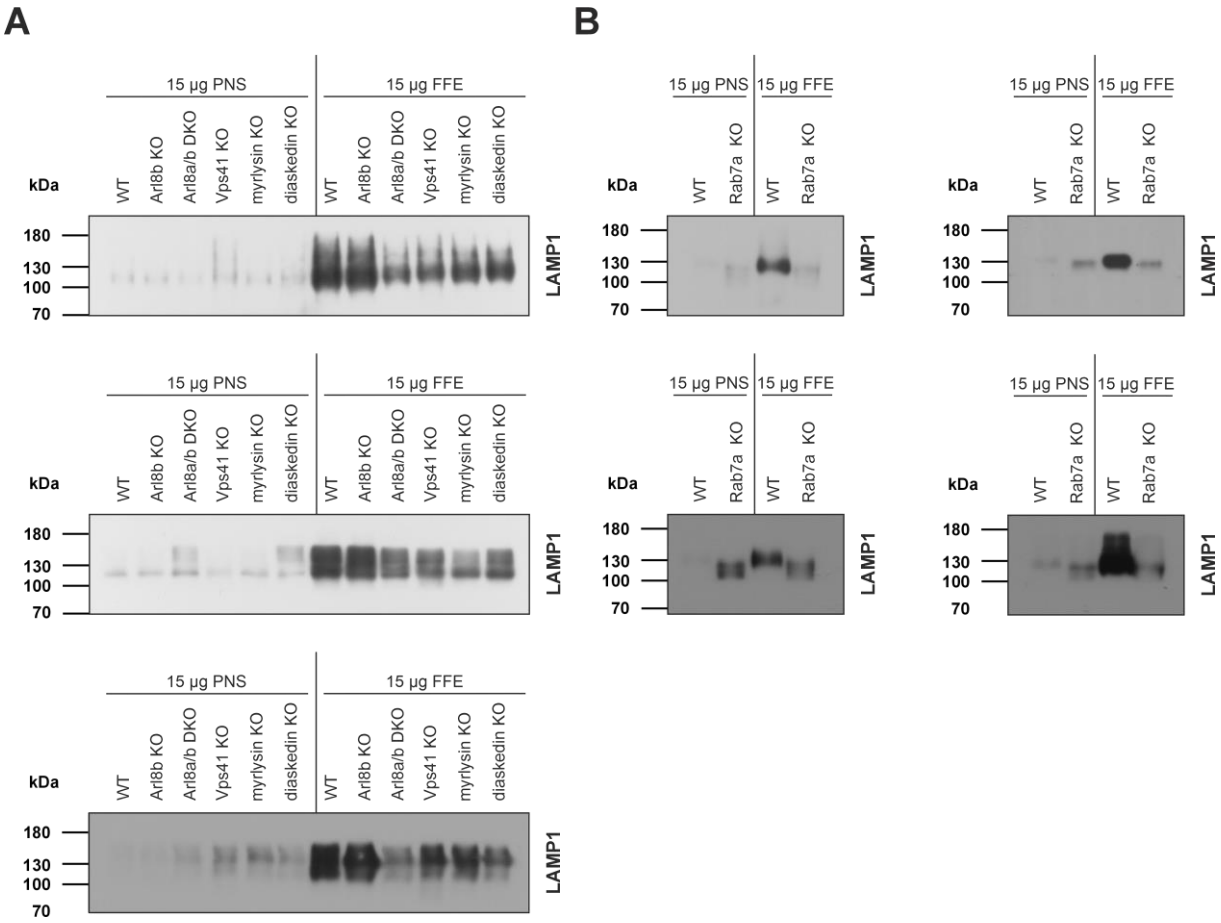

Supp. Figure 1: LAMP1 levels in FFEs from Rab7a, Arl8a/b, Vps41, myrlysin and diaskedin KO cells are reduced compared to WT FFEs. WT and Rab7a, Arl8b, Arl8a/b, Vps41, myrlysin, and diaskedin KO HeLa cells were treated as depicted in Figure 4 A. 15 µg of the harvested PNS and FFE fractions were separated by SDS-PAGE and LAMP1 detected via immunoblotting.

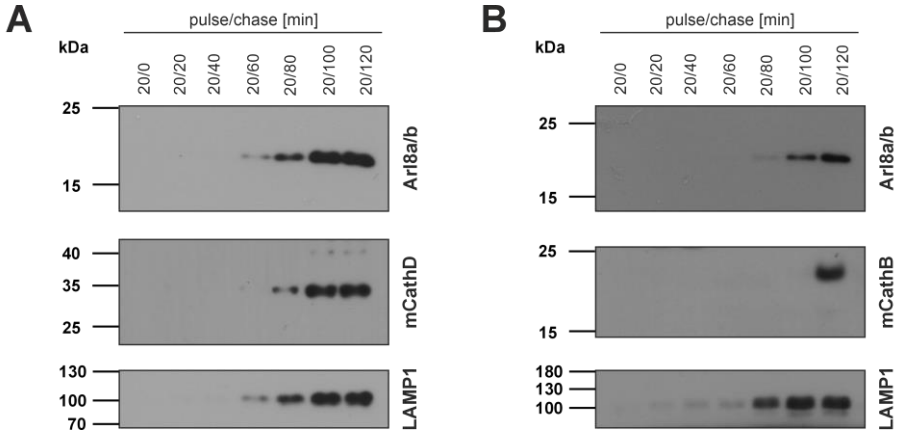

Supp. Figure 2: Rab7a and Vps41 are recruited to FFEs before Arl8a/b, lyspersin, and LAMP1. (A, B) Immunoblots of FFEs purified from WT HeLa cells after 20'/ (0, 20, 40, 60, 80, 100, 120)' min pulse/chase protocol. Purification of FFEs was carried out as shown in Figure 4 A. Blots were analysed for presence of Arl8, LAMP1 (A, B), mCath D (A), or mCath B (B).

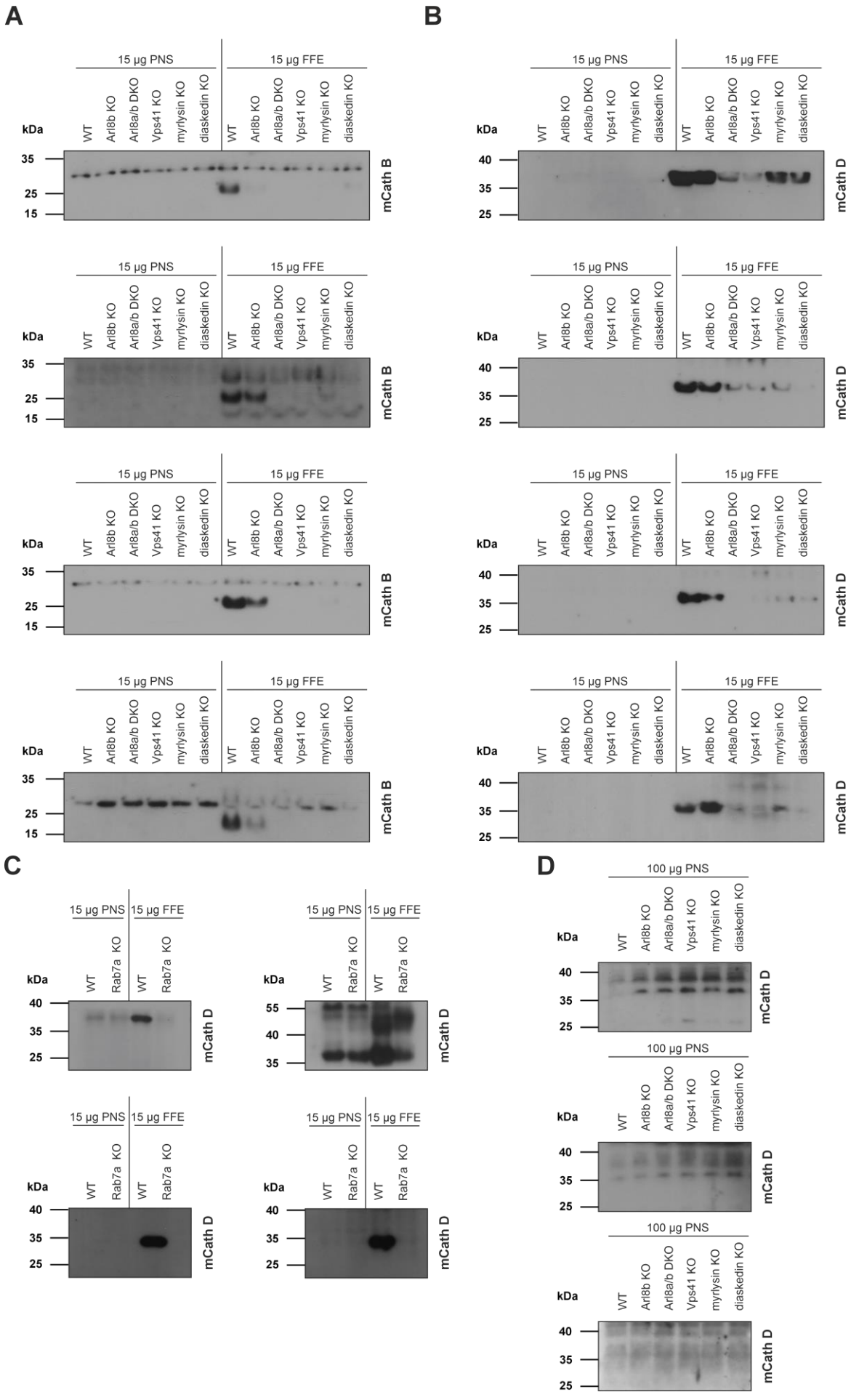
A
B
C
D
15 µg PNS
15 µg FFE
100 µg PNS
kDa
WT
Arl8b KO
Arl8a/b DKO
Vps41 KO
myrlysin KO
diaskedin KO
Rab7a KO
mCath B
mCath D

Supp. Figure 3: Delivery of FF to mCath B and D containing compartments is impaired in KO cells. (**A-C**) FFEs and PNSs from WT, Rab7a, Arl8b, Arl8a/b, Vps41, myrlysin and diaskedin KO cells were prepared as shown in Figure 4 A. 15 µg of either PNS or FFEs were separated by molecular weight via SDS-PAGE and analysed for (**A**) mCath B and (**B+C**) mCath D by immunoblotting [10]. Immunoblots of mCath B (**A**) and mCath D [10] (**B**) are shown for Arl8b, Arl8a/b, Vps41, myrlysin and diaskedin KO cells, as well as mCath D abundance [10] for (**C**) Rab7a KO and their respective WTs. Quantitative data is presented as means + SD (n=4). Values were normalized to the WT FFE sample. **(D**) Immunoblots of 100 µg PNS, analysed for mCath D abundance and quantification for WT, Arl8b, Arl8a/b, Vps41, myrlysin, diaskedin KO cells (n=3).

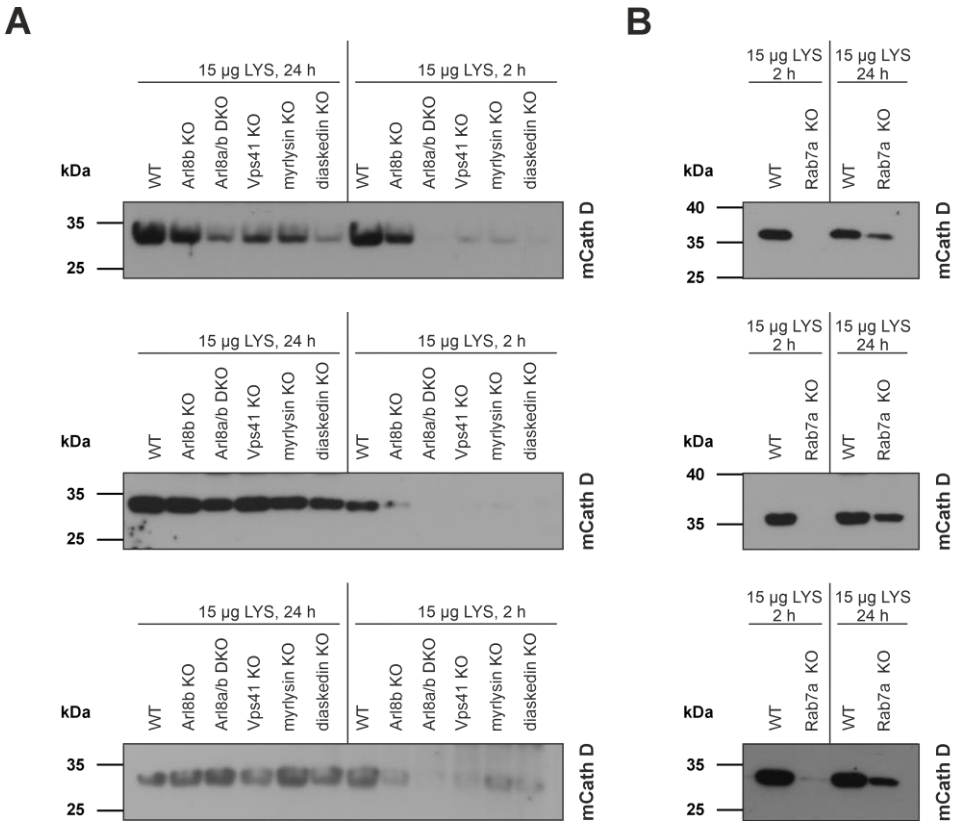

Supp. Figure 4: FF delivery to LE/LYS is significantly delayed in Arl8, Vps41, myrlysin, diaskedin, and Rab7a KO-cells. Immunoblots of 15 µg FFEs, purified after either 2 h or 24 h chase from (**A**) Arl8b, Arl8a/b, Vps41, myrlysin, diaskedin, (**B**) Rab7a KO and their respective WT controls. Samples were harvested as shown in Figure 4 A, separated by weight via SDS-PAGE, and analysed for mCath D with immunoblotting. The immunoblots shown were used for quantification [10].

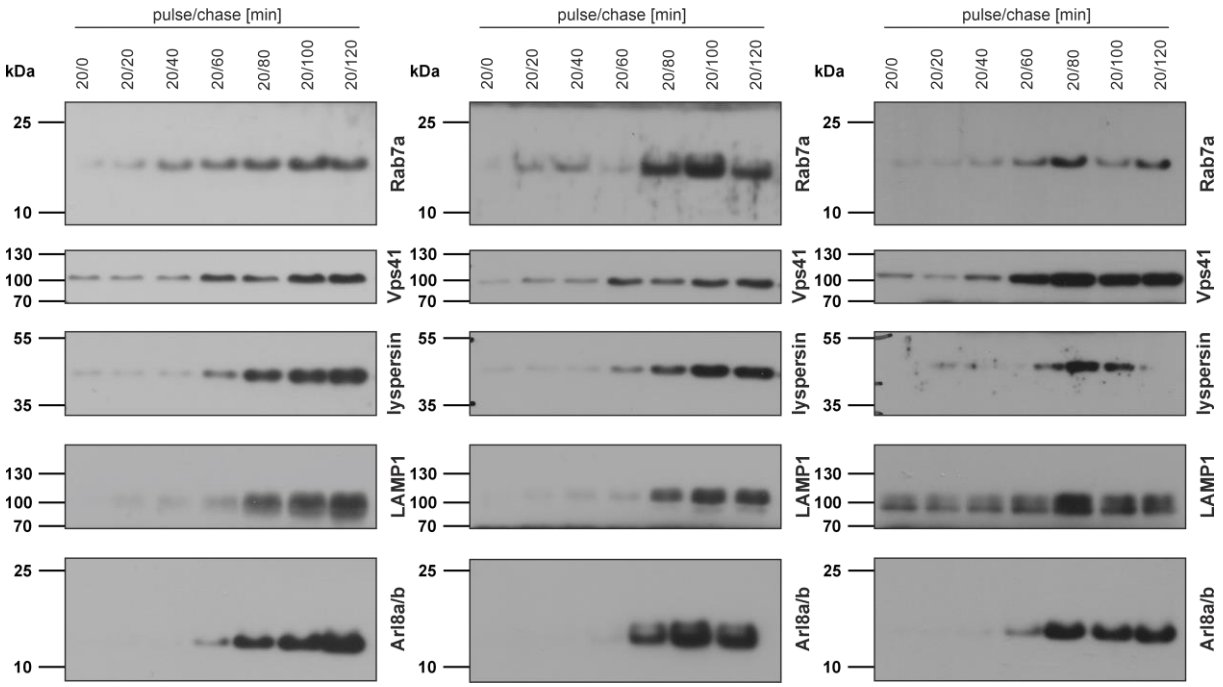

Supp. Figure 5: Rab7a and Vps41 are recruited to FFEs before Arl8a/b, lyspersin, and LAMP1. (**A**) Immunoblots of FFEs purified from WT HeLa cells after 20'/ (0, 20, 40, 60, 80, 100, 120)' min pulse/chase protocol. Purification of FFEs was carried out as shown in Figure 4 A. Blots were analysed for presence of Rab7a, Vps41, lyspersin, Arl8a/b and LAMP1 and used for quantification[10].

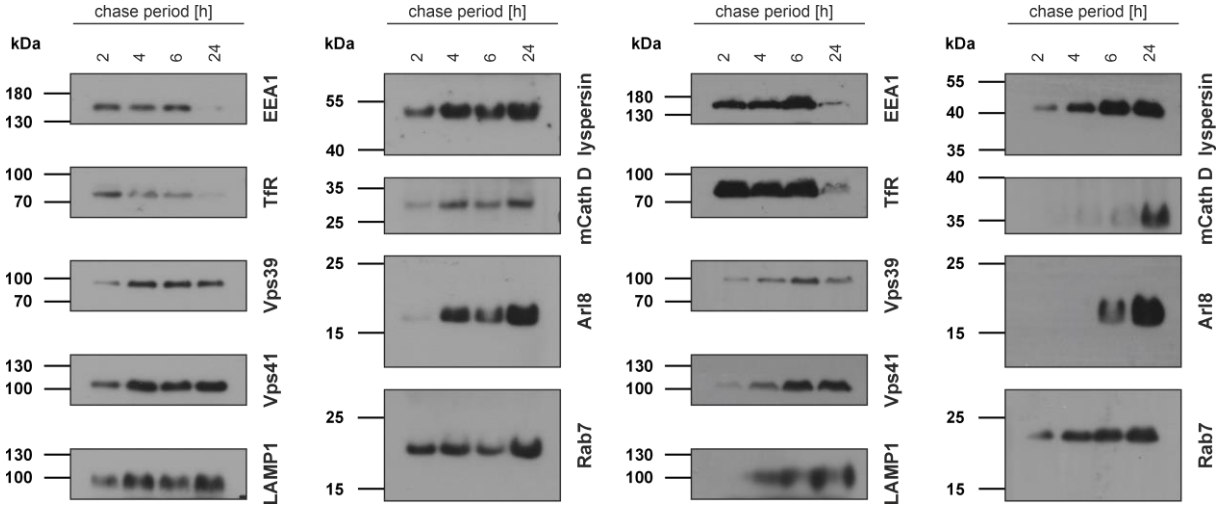

Supp. Figure 6: Early endocytic marker proteins are present on FF-endosomes for long periods of time. WT HeLa cells were pulsed with DMEM/FF for 30 min. Excess FF was removed by washing the cells with PBS twice. Endocytic compartments were allowed to mature within 2, 4, 6 or 24 h of chase period before FFEs were harvested as depicted in Figure 4 A. FFEs were analysed for EEA1, TfR, HOPS subunits Vps39 and 41, LAMP1, lyspersin (BORC), mCath D, Arl8a/b and Rab7a (n=2) [10]

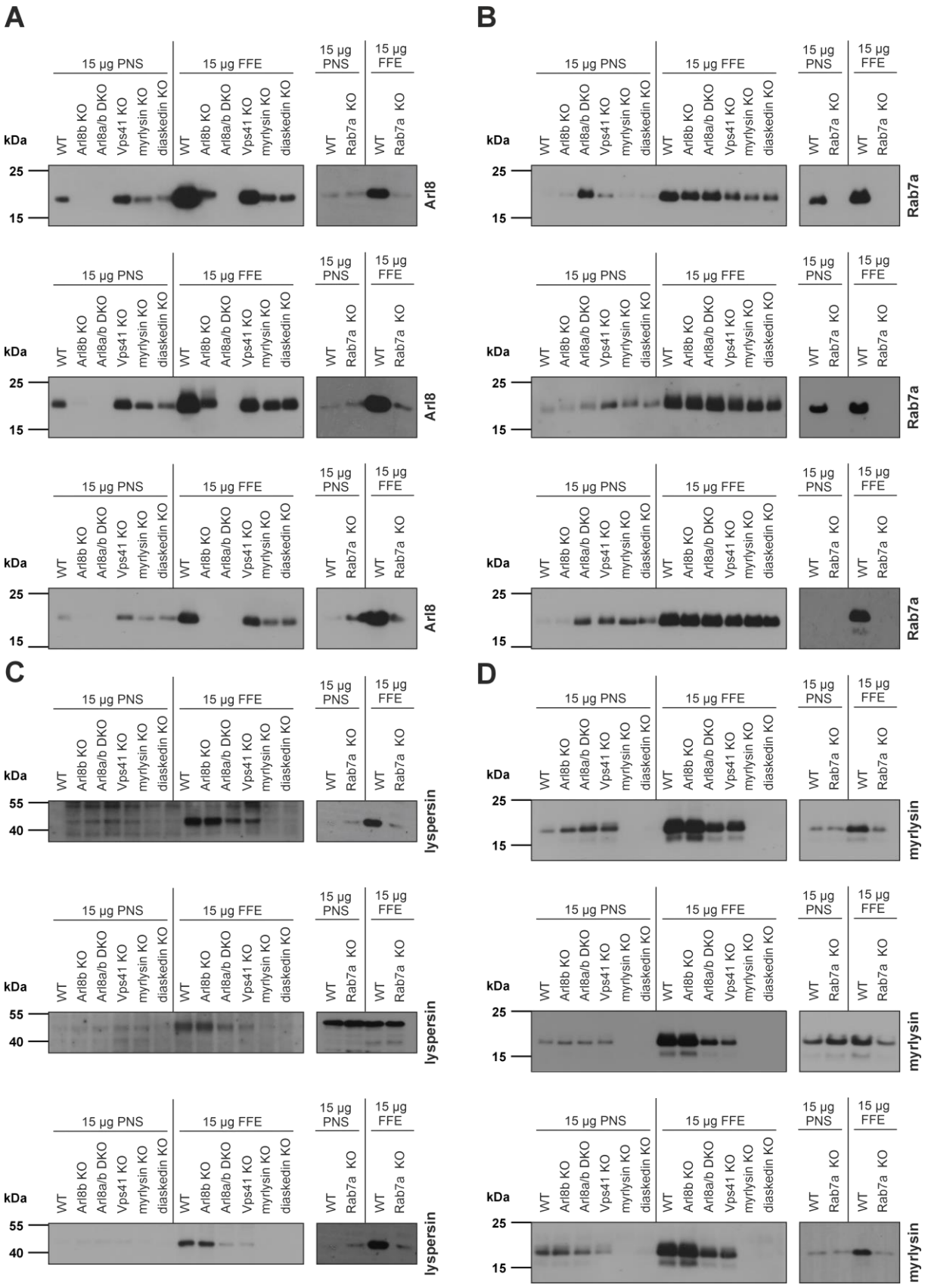

Supp. Figure 7: Vps41 and Rab7a are needed for acquisition of Arl8. (**A-D**) PNS and FFEs from Rab7a, Arl8b, Arl8a/b, Vps41, myrlysin, and diaskedin KOs, together with their respective WT controls, were collected after a standard 30'/120' pulse/ chase protocol (Figure 4 A). Samples of both fractions were prepared for SDS-PAGE and subsequent immunoblotting. 15 µg of protein per sample were analysed for (**A**) Arl8a/b, (**B**) Rab7a, (**C**) lyspersin and (**D**) myrlysin (n=3) (c.f. [10]).

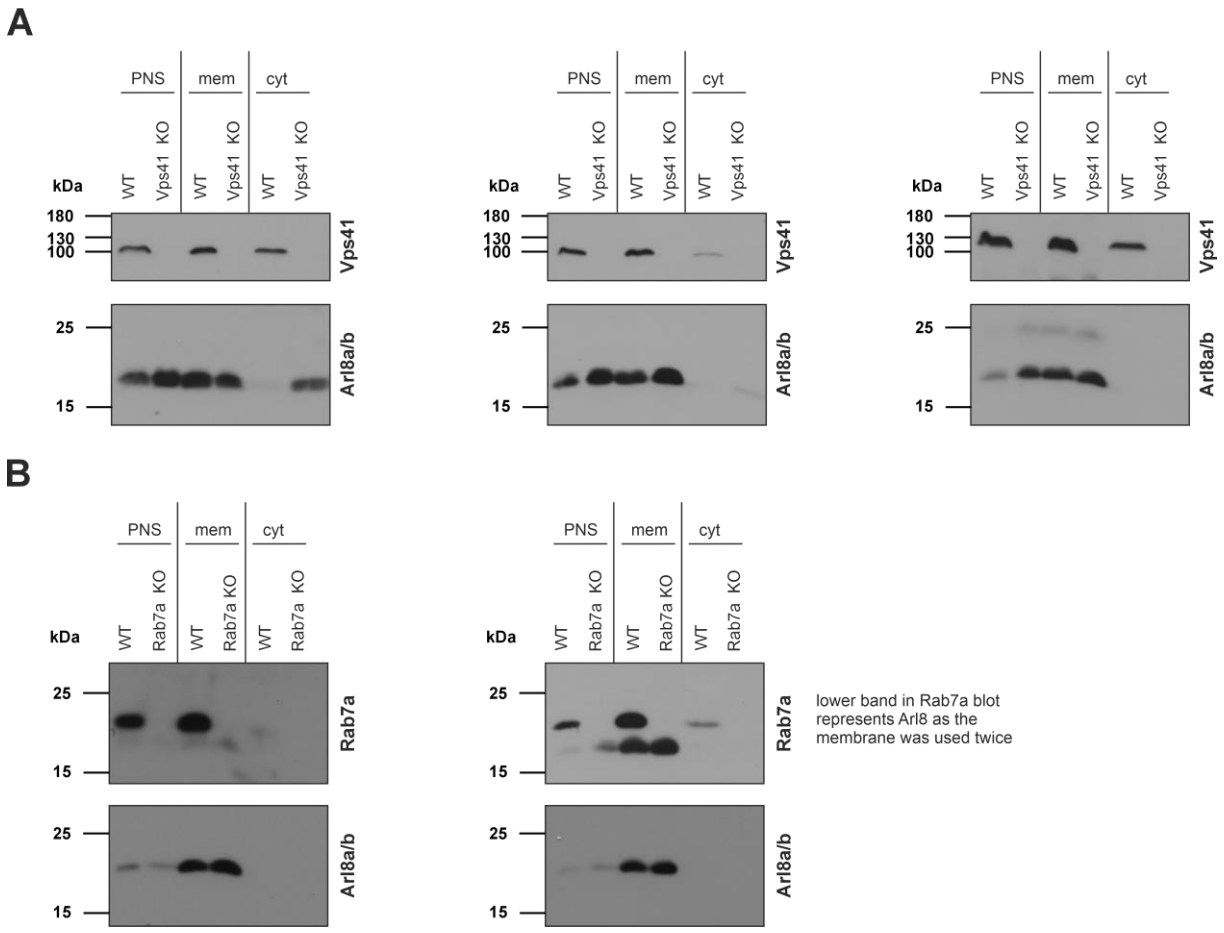

Supp. Figure 8: Arl8 is not displaced from FFE membranes in Rab7a or Vps41 KO cells. Immunoblots from PNS, intracellular membrane (mem) and cytosolic (cyt) fraction derived from (**A**) Vps41 or (**B**) Rab7a KO cells and their respective parental WT cell lines. 120 µg of PNS fractions for each detected POI were separated into cytosolic and membrane fractions by ultracentrifugation (186,000°rcf, 60 min, 4 °C). Cytosolic proteins were precipitated from the supernatant with TCA at 4 °C overnight. The precipitated proteins were sedimented, neutralised with Tris-base, and prepared for SDS-PAGE. 60 µg of PNS and 120 µg of mem and cyt samples (pro rata) were used. The samples were analysed for (**A**) Vps41 (n=3) (**B**) Rab7a (n=2) and Arl8 via immunoblotting [10].

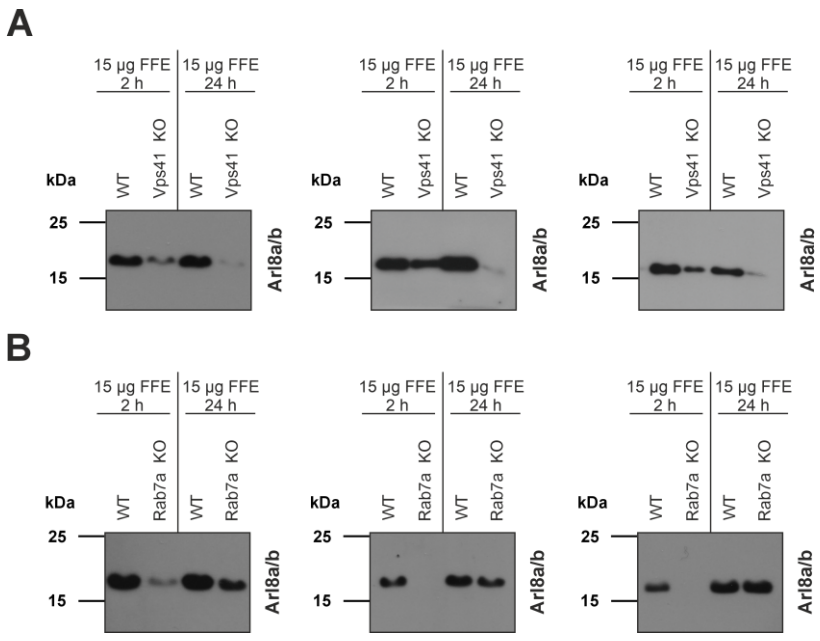

Supp. Figure 9: After 24 h of incubation, Arl8 accumulates on FFEs from Rab7a KO cells but not on FFEs from Vps41 KO cells. FFEs were purified after either 2 h or 24 h of chase from (**A**) Vps41 or (**B**) Rab7a KO cells and their respective parental WT. The samples were prepared for SDS-PAGE and subsequent immunoblotting for Arl8a/b (n=3) [10].

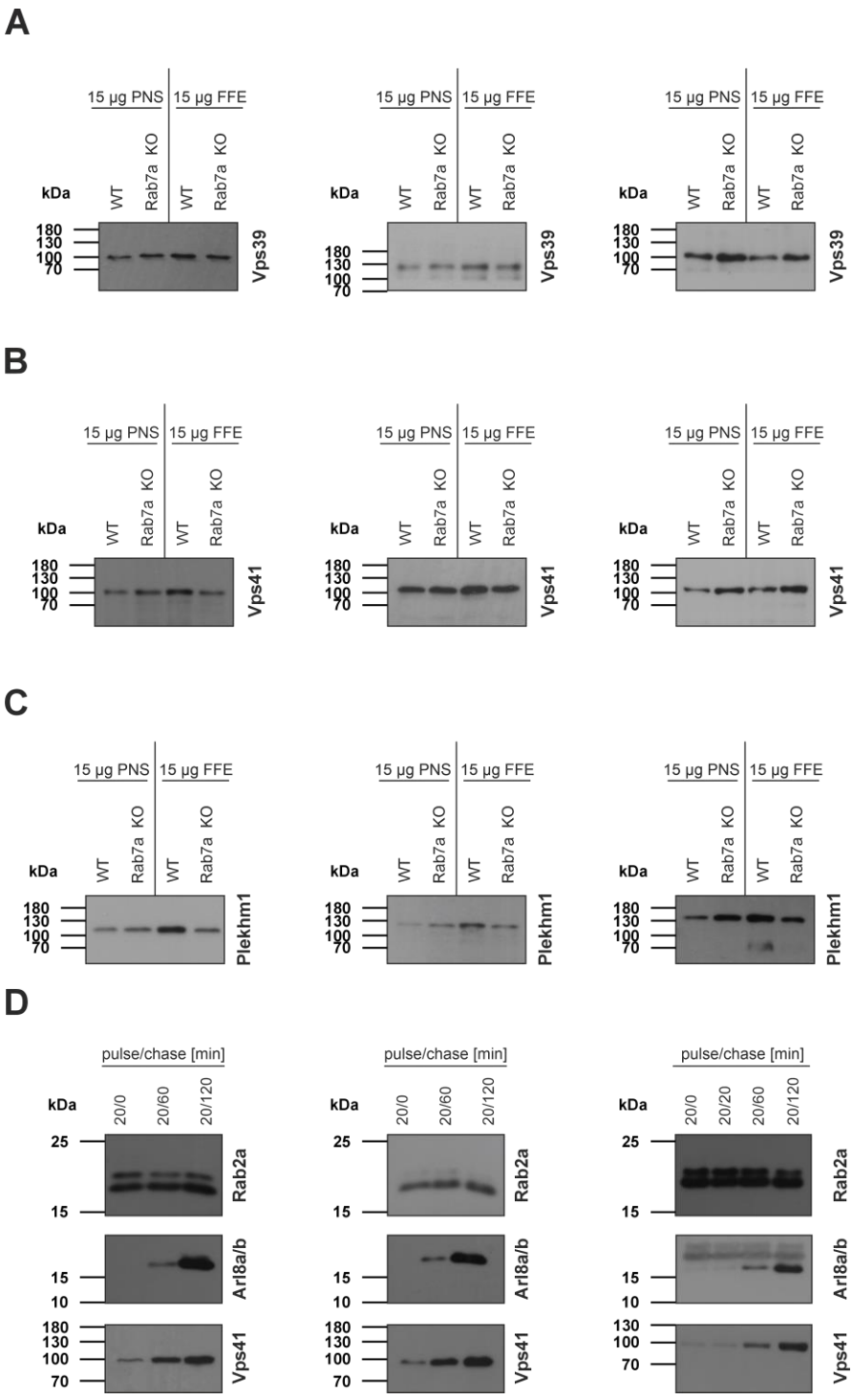

Supp. Figure 10: Rab7a is not involved in anchoring of HOPS to FFE membranes, whereas Rab2a is a possible candidate. (**A-C**) PNS fractions and FFEs were purified from WT and Rab7a KO cells. 15 µg protein per sample were analysed for (**A+B**) Vps39, Vps41 or (**C**) Plekhm1 (n=3) [10]. (**D**) For kinetic assessment if Rab2a was a possible candidate for HOPS recruitment, FFEs from WT HeLa cells were purified after 0, 60 and 120 min of chase after a 20 min pulse period with DMEM/FF. 15µg per sample were analysed for Vps41, Arl8a/b and Rab2a using immunoblotting (n=3) [10].

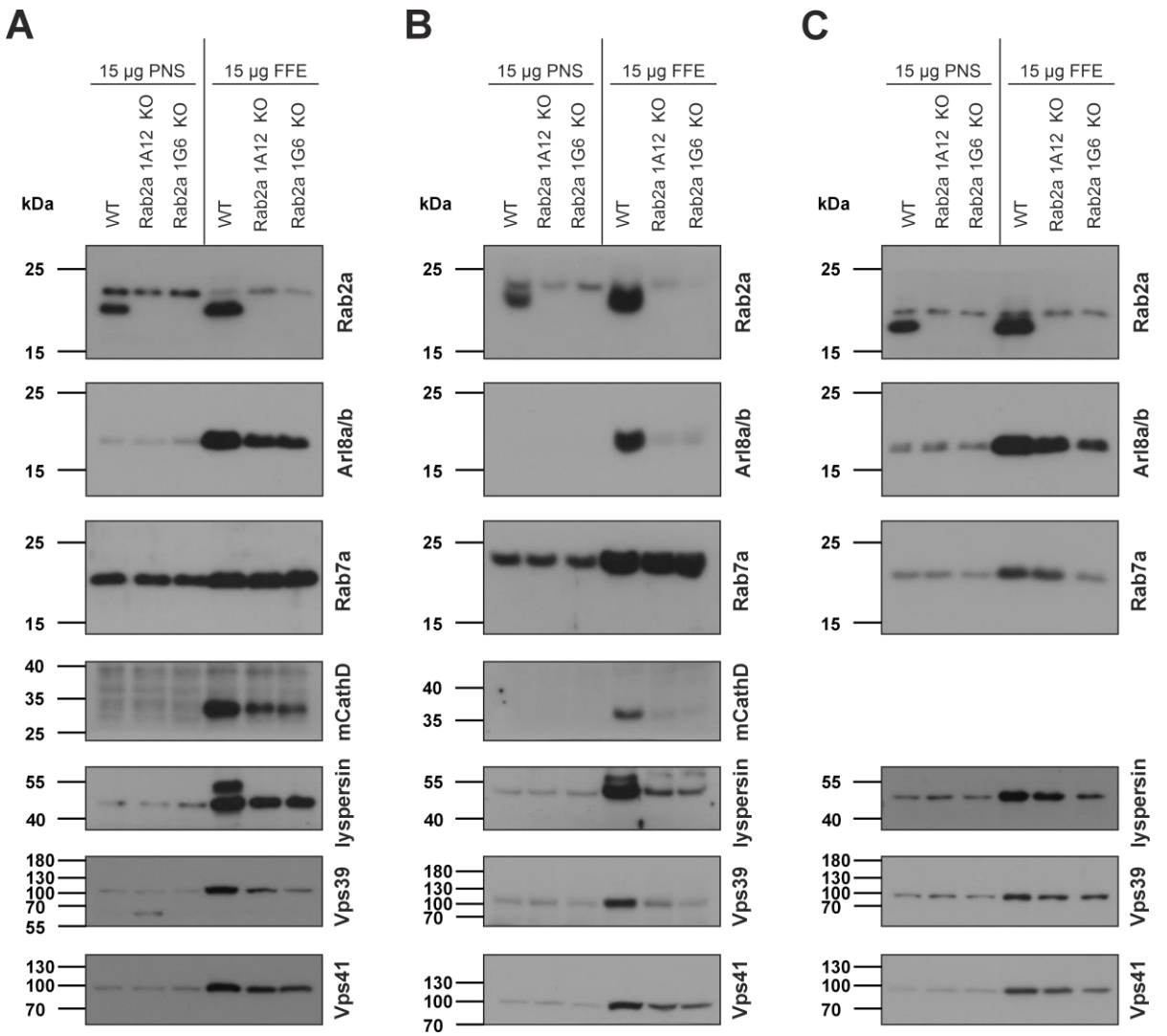

Supp. Figure 11: Vps39 and Vps41 levels are reduced on Rab2a KO (**A-C**) Immunoblots from PNSs and FFEs, purified from WT HeLa cells, 1G9 and 1A12 Rab2a KO clones as shown in Figure 4 A. 15 µg of either PNS or FFEs were separated by SDS-PAGE. Subsequentially, samples were analysed for Rab2a, Arl8a/b, Rab7a, mCath D, lyspersin, Vps39 and Vps41. Immunoblots from three (two in case of mCath D) independent experiments were quantified (n=2).

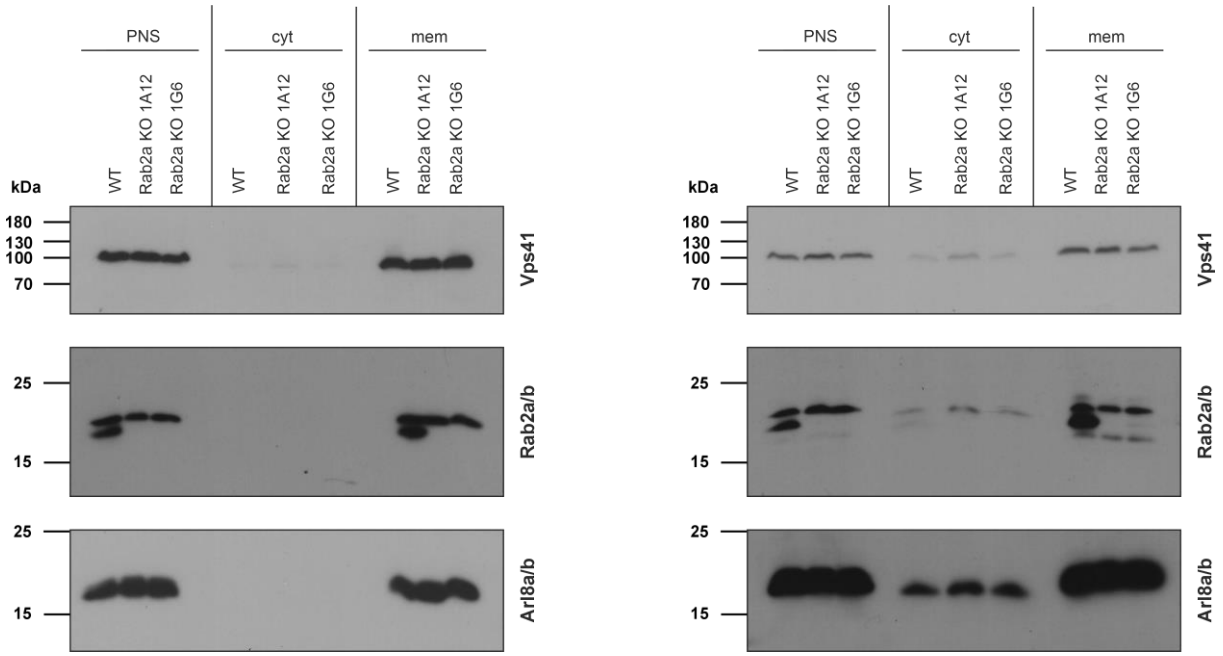

Supp. Figure 12: Rab2a KO does not cause HOPS subunit Vps41 to relocate to the cytosol. Immunoblot from PNS, intracellular membrane (mem) and cytosolic (cyt) fractions derived from either WT HeLa cells, 1G9 or 1A12 Rab2a KO cell lines. 120 µg of PNS fractions for each detected POI were separated into cytosolic and membrane fractions by ultracentrifugation (186,000°rcf, 60 min, 4 °C). Membrane fractions were dissolved in 2 x Laemmli-buffer and stored at -20 °C until use. Cytosolic proteins were precipitated from the supernatant with TCA at 4 °C overnight. The precipitated proteins were sedimented, neutralized with Tris-base and prepared for SDS-PAGE. 60 µg of PNS and 120 µg of mem and cyt samples (pro rata) were used. The samples were analysed for Vps41, Rab2a and Arl8 via immunoblotting (n=2). The yielded blots were not quantified.

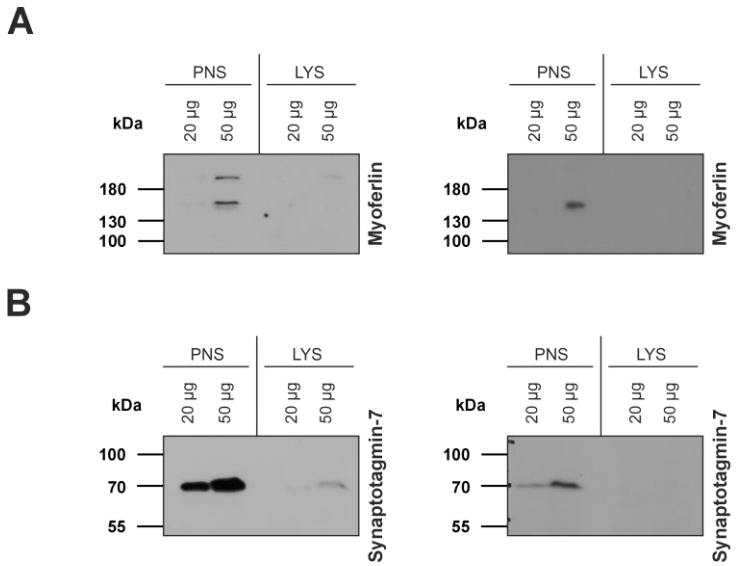

Supp. Figure 13: Neither Syt-7 nor myoferlin are present on J774E LYS. J774E macrophages were pulsed with DMEM/FF for 30 min. Excess FF was removed by washing, and endocytic compartments were allowed to mature within a 120 min chase period. LYS were purified from cell homogenates with a magnetic rack and processed for SDS-PAGE. A sample of PNS was set aside on ice beforehand. 20 or 50 µg of PNS or LYS preparations were separated via SDS-PAGE and analysed for (**A**) myoferlin and (**B**) Syt-7 with immunoblotting. A representative blot is shown (n=2) [2].

10 Abbreviations

AA	arachidonic acid	LYS	lysosome
$AACOCF_3$	arachidonic acid trifluoromethyl ketone	M6PR	mannose-6-phosphate receptor
ADA	N-(2-Acetamido)-iminodiacetic acid	mem	membrane
Anx	Annexin	MES	4-morpholineethanesulfonic acid
AT	ambient temperature	Mon1a/ Ccz1	monensin sensitivity 1a/calcium caffeine zinc sensitivity 1
ATP	adenosine triphosphate	MR	MagicRed
BAPTA	1,2-bis (2-aminophenoxy) ethane-N ,N ,N -tetraacetate	MTC	multi subunit tethering complex
BORC	BLOC one-related complex	MTOC	microtubule organising centre
BSA	bovine serum albumin	MVB	multivesicular body
CaFu	calcium fusion	NC	nitro cellulose
CATCHR	Complexes Associated with Tethering Containing Helical Rods	NCX	Na^+/Ca^{2+} exchanger
CCP	clathrin-coated pit	NEM	N-ethylmaleimide
CCV	clathrin-coated vesicle	NSF	NEM-sensitive factor
CME	clathrin-mediated endocytosis	ORP1L	oxysterol-binding protein-related protein 1L
CORVET	class C core vacuole/endosome tethering	PAMP	pathogen-associated molecular pattern
$cPLA_2$	cytosolic phospholipase A_2	PBS	phosphate buffered saline
CV	cortical vesicle	PCR	Polymerase Chain Reaction
cyt	cytosolic proteins	PenStrep	penicillin/streptomycin
DMEM	Dulbecco's Modified Eagle Medium	PH	pleckstrin homology
ECP	*E. coli*-containing phagosomes	PIC	protease inhibitor cocktail
ECV	endosomal carrier vesicle	PIP	phosphatidylinositol phosphate
EDAC	N-(3-dimethyl-aminopropyl)-N'-ethylcarbodiimide hydrochloride	Plekhm1	pleckstrin homology domain-containing protein family member 1
EDAC	N-(3-Dimethylaminopropyl)-N'-ethylcarbodiimide	PM	plasma membrane
EE	early endosome	PMCA	plasma membrane Ca^{2+} ATPase
EEA1	early endosome antigen 1	PNS	post nuclear supernatant
ELYS	endolysosome	PNS	post nuclear supernatant
ER	endoplasmic reticulum	POI	protein of interest
ESCRT	endosomal sorting complexes required for transport	PRR	pattern recognition receptor
FBS	fetal bovine serum	RE	recycling endosome
FF	ferrofluid	RILP	Rab-interacting lysosomal protein
FFA	free fatty acid	SDS	sodium dodecyl sulfate

FFE	ferrofluid endosome	SE	sorting endosome
GAP	GTPase-activating protein	SERCA	sarcoplasmic/ ER Ca^{2+} ATPase
GDI	guanine dissociation inhibitor	SM	Sec1/Munc18
GEF	guanine nucleotide exchange factor	SNAP	soluble N-ethylmaleimide-sensitive factor Attachment Protein
GTP	guanosine triphosphate	SNARE	Soluble *N*-ethylmaleimide-sensitive factor attachment protein receptors
HEPES	4-(2-hydroxyethyl)-1-piperazineethanesulfonic acid	SOAR	STIM-Orai activating region
HOPS	homotypic fusion and vacuolar protein sorting	StaFu	standard fusion
HRP	horseradish peroxidase	STIM	stromal interaction molecule
ILV	intraluminal vesicle	Syt	synaptotagmin
IPTG	isopropyl-beta-D-thiogalactopyranoside	TAE buffer	Tris acetate EDTA buffer
KD	knockdown	Tf	Transferrin
KO	knockout	TfR	Transferrin Receptor
LAMP	lysosome associated membrane protein	TGN	*trans*-Golgi network
LBP	latex bead phagosome	TMD	transmembrane domain
LE	late endosome	TPC	two-pore channel
LPC12	1-lauroyl-2-hydroxy-sn-glycero-3-phosphocholine	TRIS	Tris(hydroxymethyl)-aminomethan
LPL	lysophospholipid	TRP	transient receptor potential
LT	LysoTracker Red	TRPML	TRP mucolipin
		WT	wild type

List of Publications

Schleinitz, A., Pöttgen, L.-A., Keren-Kaplan, T., Pu, J., Saftig, P., Bonifacino, J.S., Haas, A., and Jeschke, A. (2023). Consecutive functions of small GTPases guide HOPS-mediated tethering of late endosomes and lysosomes. Cell Rep. *42*, 111969. https://doi.org/10.1016/j.celrep.2022.111969.

Becker, J., Schleinitz, A., Hermsen, C., Rappold, S., Saftig, P., Jeschke, A., and Haas, A. (2023). Rab GTPase regulation of phagosome–lysosome fusion is bypassed in the presence of micromolar Ca2+. J. Cell Sci. *136*, jcs260806. https://doi.org/10.1242/jcs.260806.

Danksagung

Mein besonderer Dank gilt meinem Doktorvater Prof. Dr. Albert Haas dafür, dass ich in seinem Labor an meinem Promotionsthema forschen und meine Dissertation erstellen durfte. Vielen Dank für die gute Betreuung, den lehrreichen fachlichen Austausch und dein stets offenes Ohr.

Ich möchte auch Prof. Dr. Dieter Fürst dafür danken, dass er die Rolle des Zweitgutachters übernimmt.

Mein herzlicher Dank gilt auch Prof. Dr. Susanne Schoch McGovern und Prof. Dr. Oliver Gruß für die Mitbeurteilung meiner Arbeit.

Auch möchte ich der DFG danken, die die Mittel für dieses Projekt bereitgestellt hat.

Ganz besonders möchte ich zudem den Mitgliedern der AG Haas danken. Dabei gilt mein besonderer Dank Dr. Andreas Jeschke, der mir nicht nur jederzeit mit Rat zur Seite stand, sondern auch stets zu Scherzen aufgelegt war. Weiterhin möchte ich mich für die exzellente technische Betreuung durch Alexandra Jünger-Leif bedanken. Zuletzt möchte ich mich noch bei meinen Kollegen Lara-Alina Pöttgen, Thomas Haubenthal und Marvin Aßent (gehört ja quasi zur AG) für die großartige Arbeitsatmosphäre, die stetige Hilfsbereitschaft und die vielen lustigen Momente bedanken!

Ich möchte mich auch bei meinem Partner Valentin Hadrich für die grammatikalische Korrektur meiner Arbeit und die Unterstützung während der Promotionszeit bedanken. Auch gilt mein Dank Michael Schwarz, für die ausgiebigen Diskussionen und das Korrekturlesen meiner Arbeit.

Zuletzt möchte ich meinen Eltern für die großartige Unterstützung danken. Ohne euch hätte ich meine akademischen Ziele nie erreichen können!